Development of a fast x-ray detector

T. R. Ariyaratne

How to cite:

Ariyaratne, T. R. (1978) Development of a fast x-ray detector. Doctoral thesis, Durham University.

DEVELOPMENT OF A FAST X-RAY DETECTOR

by

T. R. ARIYARATNE, B.Sc.

A thesis submitted to the University of Durham
for the Degree of Doctor of Philosophy.

Being an account of the work carried out at the
University of Durham during the period October 1975
to September 1978.

ABSTRACT

This thesis describes the development of a gas scintillation drift counter as a high counting rate X-ray detector. The new device is a modified version of the gas scintillation counter which is capable of working in a digital mode at a quite high rate without producing space charge effects.

A gas scintillation drift counter has been built to investigate its behaviour using a gas mixture of argon and nitrogen. Scintillation and transport properties of the gas mixture have been studied using an Am^{241} α-particle source and a (Fe^{55}) 5.9 keV radioactive X-ray source in order to obtain optimum relative compositions of argon and nitrogen. The effects of various operating parameters on the energy resolution of the counter and the characteristics of output pulses have been extensively studied. When deciding on the counter parameters and operating conditions, a special emphasis has been placed on conditions which produce a minimum of space charge around the anode, and small pulse-widths.

Pulse response, gain variations with counting rate and stability of the RCA 8575 photomultiplier used to detect scintillation light have been investigated using a light emitting diode pulser, a constant light source and primary scintillation pulses from 6.9 keV X-rays. An increase in the amplitude of output pulses and a change in the dynode potentials with pulsing rate have been observed when operating the phototube with a resistive potential distribution network attached to its dynodes. These variations have been successfully eliminated by stabilising the dynode potentials using emitter follower configurations.

An energy resolution of 30% has been obtained using 5.9 keV X-rays with a gas amplification factor of about 20. Tests which have been done using cobalt K_α X-rays reveal that the resolving time of the counter system increases with the anode voltage and for a fixed discrimination level of 25 mV it varies from 43 ns at the anode voltage of 2600 V to 67 ns at 3000 V. An energy resolution of 40% has been obtained with cobalt K_α X-rays at a counting rate of 6 MHz and with a gas amplification factor of 15. The characteristics of the scintillation pulses are found to be degraded with increasing intensity of the X-ray beam because of coincident events. However, a counting rate of 9.5 MHz has been achieved with this counter at the expense of its energy resolution.

CONTENTS

Page

CHAPTER FOUR Cont'd

Page

CHAPTER SIX

CHAPTER ONE

INTRODUCTION

With the advent of high intensity radiation sources, the particle detection technology has advanced considerably. New particle detectors have been invented and remarkable improvements have been made in data acquisition methods. Fast detectors with qualities such as good energy and spatial resolution and nano second electronics have been the obvious choices in most high energy applications. One such application which requires detectors with such qualities is the newly developed synchrotron radiation research. Synchrotron radiation is emitted when an electron or positron experiences a radial acceleration. The characteristics of the radiation emitted from the latest electron storage rings show that the emission is white and mainly confined to the X-ray and vacuum ultraviolet (VUV) regions. The intensity of these radiations is a few orders of magnitudes higher than that emitted by the most powerful X-ray machines and they have no competitors in the VUV region. A typical intensity spectrum of the synchrotron radiation emitted by a modern storage ring is shown in figure 1. Most of the synchrotron radiation work, for example investigation of'extended X-ray fine structure' (EXAFS) and researches on biological materials require high rate counting devices with reasonable energy resolution. However, the statistical nature of the occurrence of interaction events makes the realisation of the above requirements more and more difficult at high flux rates. Hence a fast detector with a very short output pulse width is required to meet their demands.

1.1 CLASSIFICATION OF PHOTON COUNTERS

The conditions under which ionizing events fail to be recorded depend on the characteristics of the counter and in this respect photon

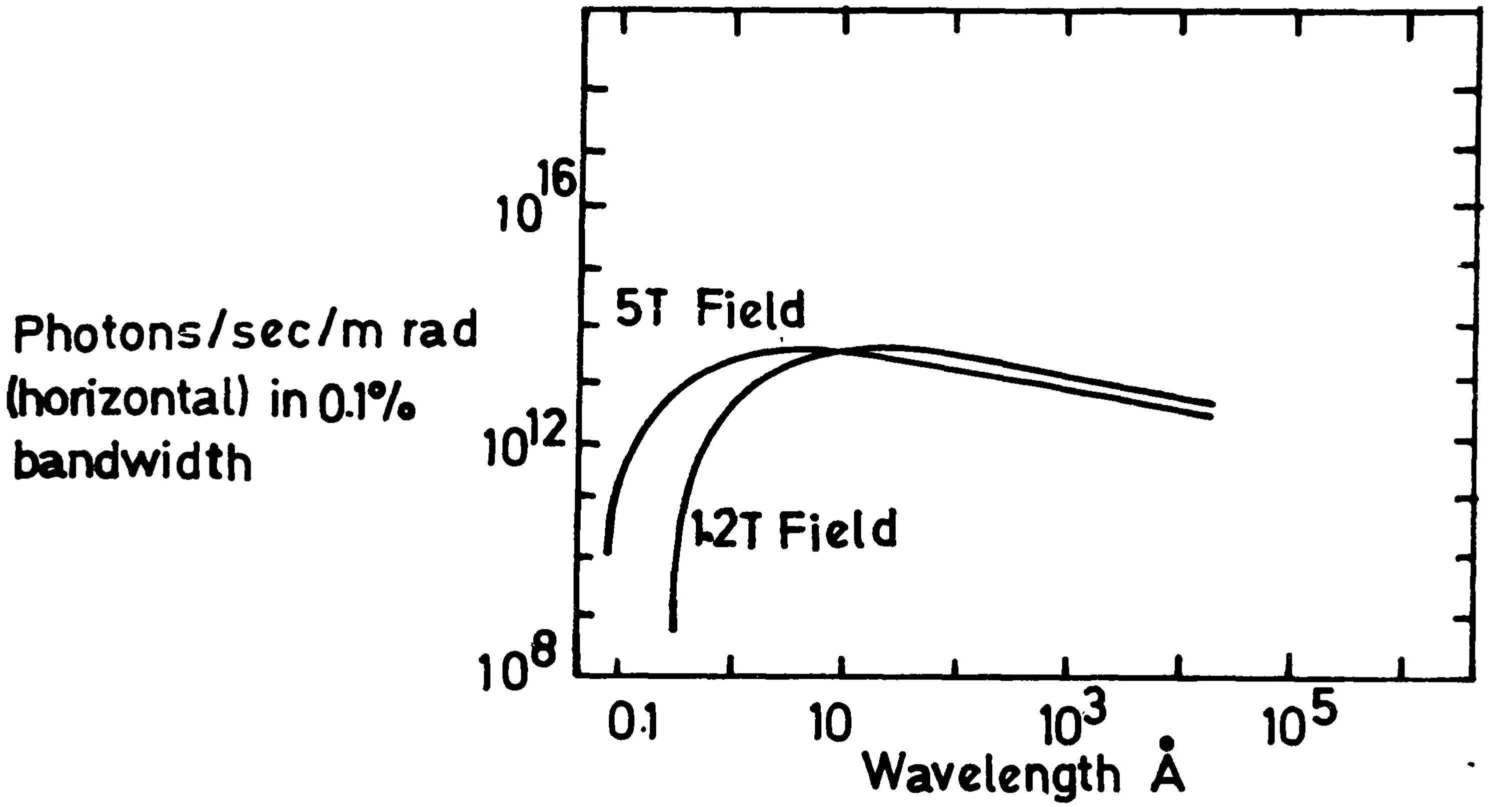

FIG. 1 The calculated spectra produced by a 2 GeV, 1A electron beam from the storage ring dipole magnets and from a 5.0 T transverse wiggler

counting systems can be broadly divided into two major categories. The first of the two types is the paralyzable counter which is unable to provide a second output pulse unless there is a time interval, ρ, called the dead time of the counter after an initial event. Examples of paralyzable counters are Geiger-Muller counters and flash tube detectors. The second type is the non-paralyzable counter. With contrast to the former type it does not exhibit complete paralysis.

Examples of this type are scintillation counters, proportional counters and ionisation chambers. However, the performance of proportional counters at high rate deviates slightly from this non-paralyzable behaviour due to the formation of space charge around the anode wire. This effect will be described later in this chapter.

1.2 PROPORTIONAL COUNTERS AT HIGH COUNT-RATE

Perhaps at first sight, the choice one would make out of the non-paralyzable detectors for high rate soft X-ray counting and energy measurements would be the proportional counter. After the pioneering work of Charpak(2) and collaborators at CERN and by a large number of other groups all over the world the proportional chamber has become one of the fastest detectors used in high energy physics experiments.

The proportional counter consists essentially of a cylindrical cathode or two parallel cathode planes and a very thin anode wire at the centre, see Fig.(2). Ionizing particles traversing the counter produce electron - ion pairs in the gas. A strong positive potential applied to the anode wire accelerates the electrons to produce avalanche multiplications around the wire. All the free electrons thus created are collected at the anode during a very short period and they produce a fast current signal at the detector output. In the proportional region of the counter, the

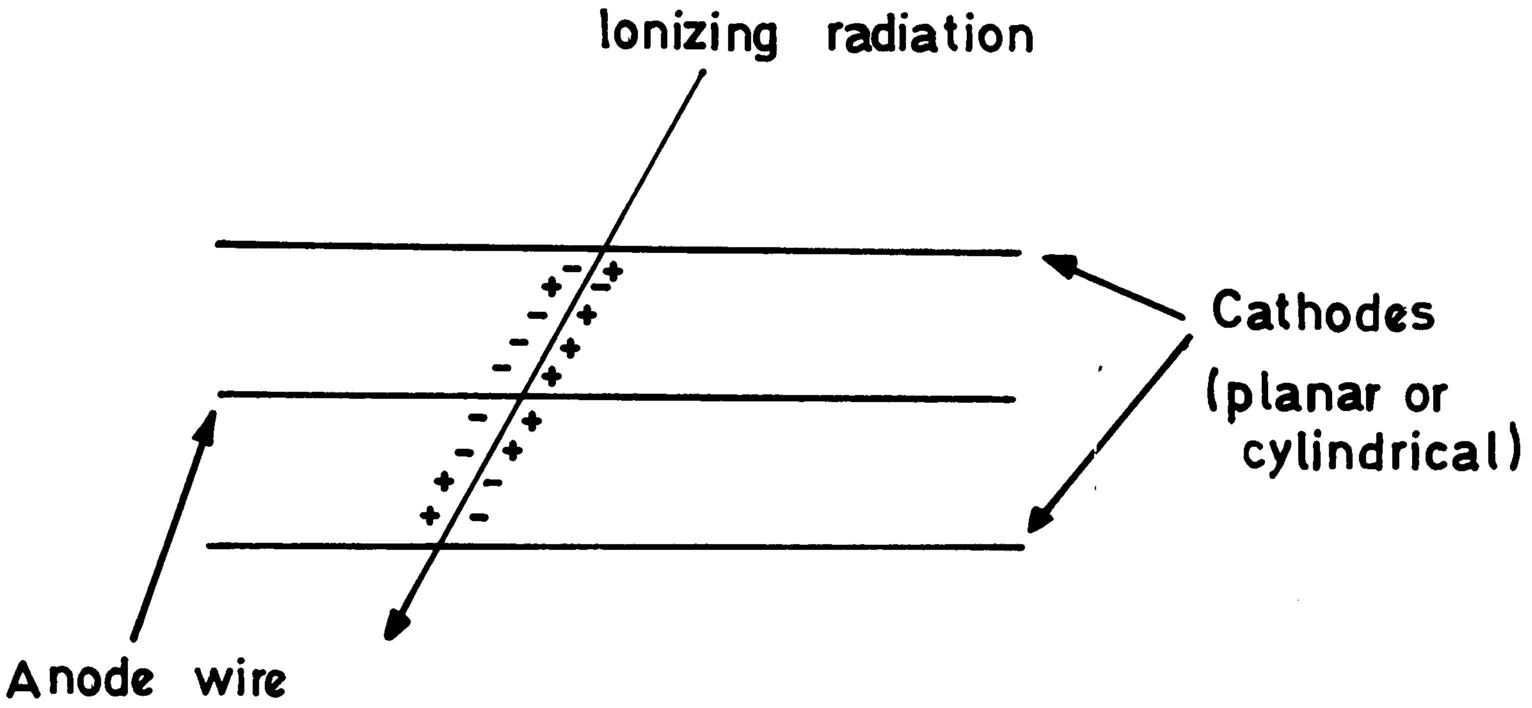

FIG. 2 Section through proportional counter

voltage signal is proportional to the ionisation deposited by the incoming particle. However it has been observed(3) that the output pulse from a cylindrical proportional chamber ceases to be strictly proportional to the initial ionisation when the absolute value of the output charge exceeds some critical value, Q, which corresponds to losing $\sim 10^8$ eV in the gas of the counter if there were no charge amplification. It is clear from this result that the avalanche multiplication in proportional counters imposes a limit to the radiation handling capacity of the counter. This effect can be understood as being due to the formation of space charge around the anode wire by the slow moving positive ions which reduce the local electric field around the wire. This effect not only degrades the energy resolution of the detector at high flux rates, but also reduces the amplitudes of the output pulses with the rate. Figure 3 shows the reduction of pulse heights of 5.9 keV X-rays with counting rate in a drift proportional chamber(4), for several anode potentials.

The drop in pulse height with counting rate also has a dependence(5) on the energy of the incident X-rays. This effect has been demonstrated(6) by using 5.9 keV and 6.9 keV X-rays and is shown in Figure 4. All these factors clearly suggest not only that conventional proportional counters are incapable of handling large flux rates, but also indicates that the ability of gaseous counters to operate at high count rates mainly depends on suppression of the space charge formation inside the counter.

1.3 GAS SCINTILLATION PROPORTIONAL COUNTERS

One of the remarkable achievements in gaseous detector technology is the gas scintillation proportional counter (GSPC). Apart from its other attractive properties as a high rate counter the GSPC provides an alternative solution to space charge problems in conventional proportional counters. The basic operation of the gas scintillation proportional counter

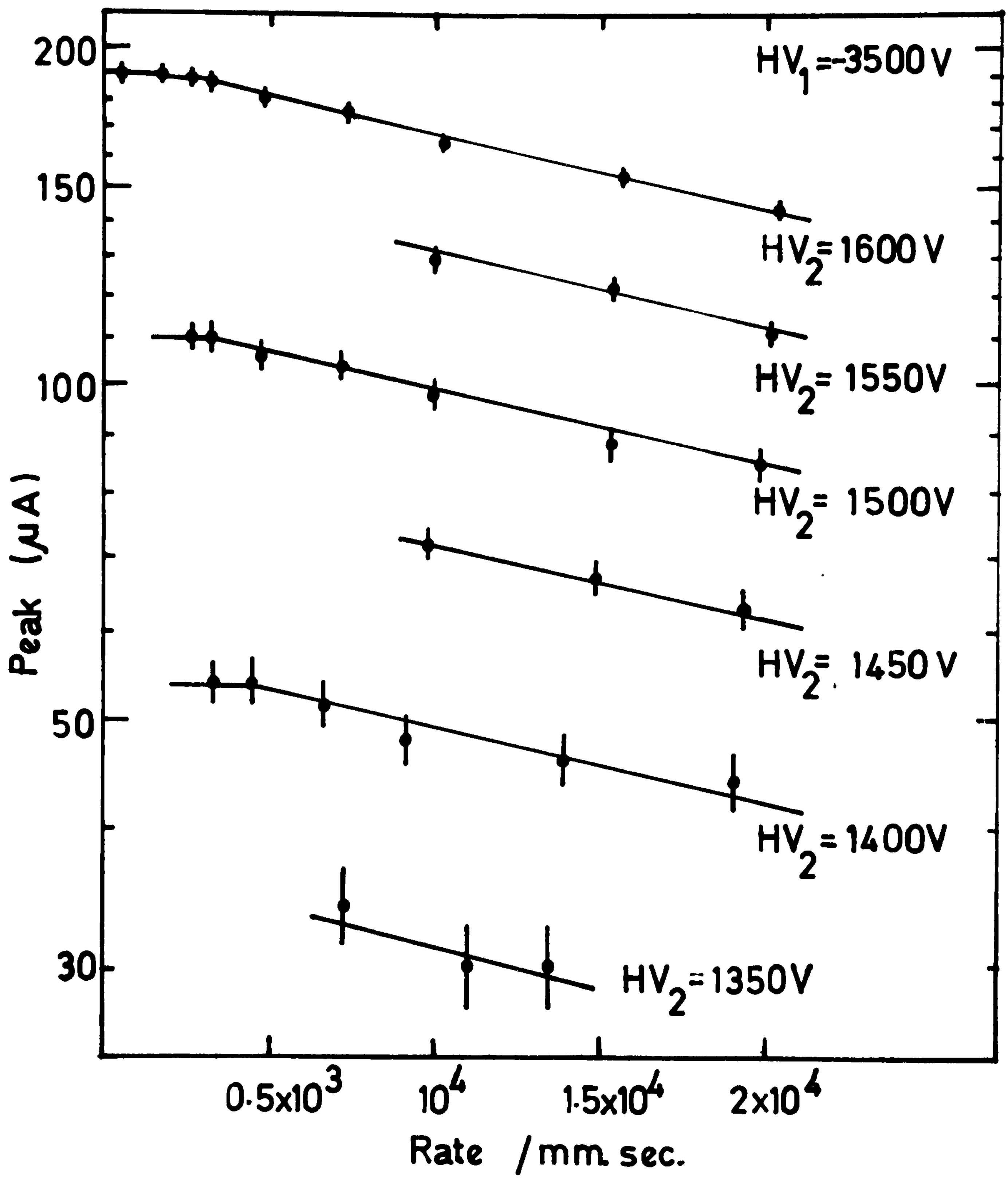

FIG.3 Rate dependence of the peak current on 5.9 keV X-rays in a drift proportional chamber, for several anodic potentials

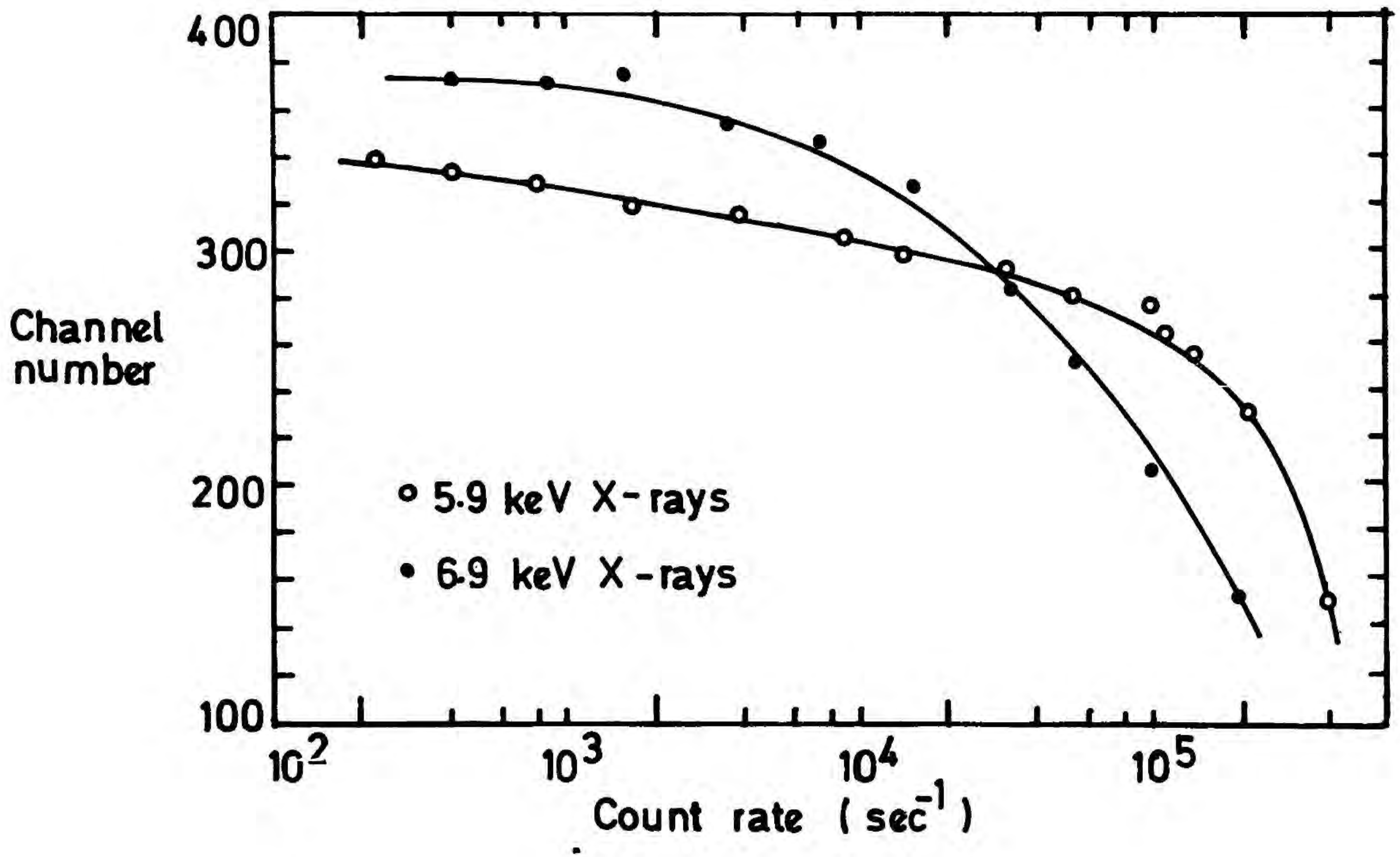

FIG.4 Variation of pulse height as a function of count rate for 5.9 and 6.9 keV X-rays.

is such that when a photon is photoelectrically absorbed in a gas the resulting free electrons are drifted towards a high field region where they acquire enough kinetic energy to excite gas atoms. The field strength is kept below the limit at which charge amplification occurs. The excited gas atoms in the high field region emit photons through radiative de-excitation, these being mainly in the VUV region and observed with a photomultiplier. A schematic diagram of a GSPC is shown in Figure 1. of Chapter three. An anode in the form of a wire is used to produce the high field region. The development of such a counter as a fast X-ray detector is the object of the work described in this thesis.

1.4 EVOLUTION OF THE GSPC

Passage of ionizing radiation through a gas results in the ionization and excitation of its molecules. The excited molecules dissipate their energy either by collisional, by internal quenching processes or by emission of photons in the visible or ultraviolet region. Such luminescence emission is a well known phenomenon. The early studies on luminescence radiation goes way back to the year 1903 when Sir William and Lady Huggins reported their work on emission the spectrum of light from an α-particle emitter, Po^{210}, using spectrometers and photographic techniques. Although a few other authors$^{(8-10)}$ have studied similar types of spectra, the second phase of the work was not reported until the advent of sensitive photomultipliers. In 1949 Auderbert and Lormeau$^{(11)}$, and in 1951 Grun and Schopper$^{(12)}$ employed photomultipliers to investigate quantitatively the emission of transient light pulses during a passage of α-particles through nitrogen and other gases. Similar studies have been reported by A Ward$^{(13)}$. Their results indicated that the light yield from nitrogen and argon is about 100 times greater than that from other gases such as hydrogen, oxygen and carbon dioxide. They also observed a drop in the luminescence emissions with increasing pressure in all gases which they studied.

Another major step towards the development of the GSPC was reported by Koch$^{(14-15)}$ in 1958 and 1960. She studied the influence of a uniform electric field on the luminescence of xenon at atmospheric pressure excited by 4.7 MeV α-particles. The scintillation emission was observed with a quartz window photomultiplier. She found a major light amplification effect ; that is an increase in the scintillation pulse height with increase in the applied electric field. Koch's results of the multiplication coefficient as a function of the electric field are shown in Figure 5. The shape of the scintillation pulses are shown in Figure 6. It is seen that the amplified light pulse consists of two components:

(a) A prompt primary component with rise time <20nS

(b) A secondary component delayed by a time $t_D \sim$ 5-10μ sec relative to the prompt component.

These effects were observed to occur even when the applied electric field was insufficient to produce charge multiplication. Koch proposed that the secondary component was due to the electrons liberated by the α-particle acquiring sufficient energy under the influence of the field to excite, but not to ionize, the atoms of the gas. The secondary component was thus attributed to excitation of the gas by electrons accelerated by the field. This phenomenon has been confirmed by Conde and Policarpo$^{(16)}$ using a counter similar to the cylindrical proportional counter, and a photomultiplier.

The real breakthrough in the developemnt of gas scintillation proportional counter in its present form came with the work by the Portuguese group$^{(17-19)}$ headed by Policarpo. In order to optimise the detection of the emitted light, they made a systematic study of the parameters such as

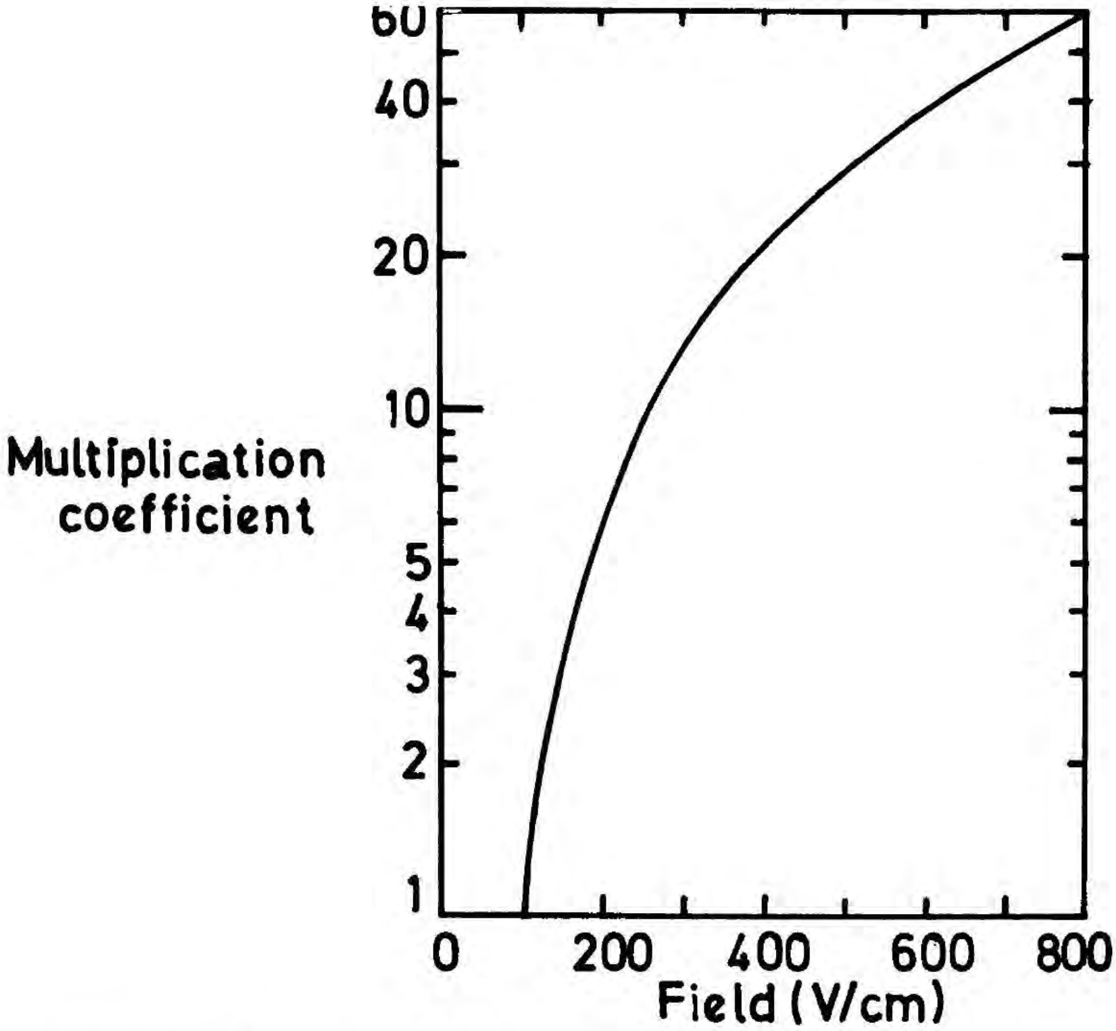

FIG.5 Influence of a uniform electric fied on the scintillation intensity of xenon excited by 4·7 MeV α-particles

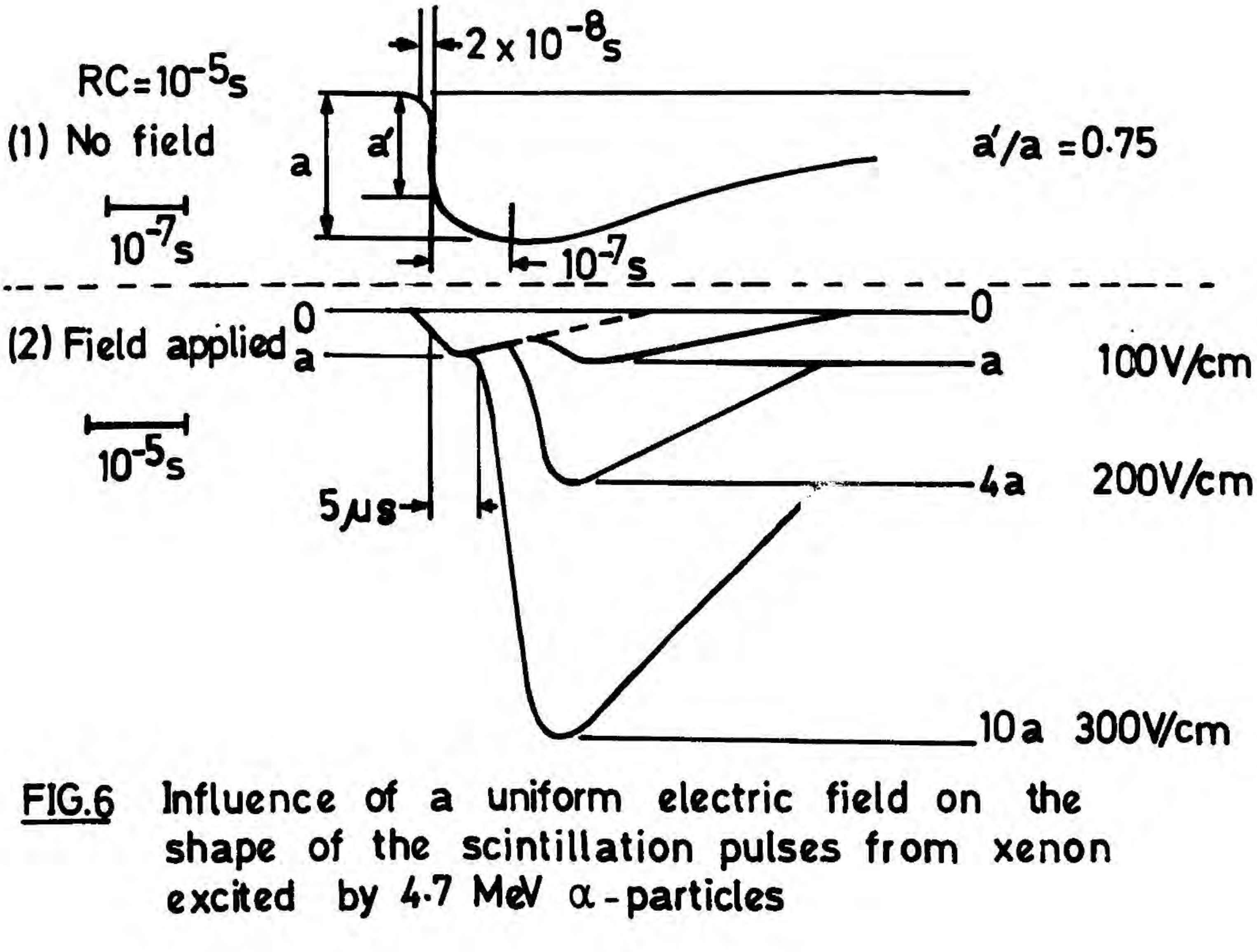

FIG.6 Influence of a uniform electric field on the shape of the scintillation pulses from xenon excited by 4·7 MeV α-particles

gas mixtures, excitation fields, different counter geometries and wavelength shifters which shift the wavelength of the emitted light to the range in which the photomultiplier has its maximum sensitivity,and finally they reached a stage where they could see a considerable light output without any charge amplification in the gas. The major outcome of their work can be summarised as follows.

(1) The amount of light output per unit energy loss is about one hundred times higher than in a NaI(Tl) crystal.

(2) The improvements in statistical fluctuations due to the lack of charge amplification process leads to a better energy resolution than in proportional counters. The authors obtained 8.5% (fwhm) for 5.9 keV X-rays instead of the more usual 15% with charge amplification.

A series of further developments on chambers with different geometries such as with a low field drift space and a region of light amplification$^{(20)}$ and chambers similar to Charpak type proportional and drift chambers$^{(21-22)}$ demonstrate the geometrical flexibility of the GSPC. To find a suitable gas or gas mixtures which can be used in a GSPC, various combinations of Xe, Ar, He, Kr, isobutane, N_2, CH_4, CO, CO_2, and O_2 have been investigated by several workers$^{(22-27)}$. In particular Thiess and Miley$^{(27)}$ extensively studied the optical line and band emission from both atomic and molecular states in a gas scintillation proportional counter using pure He, Ne and Ar, mixtures of these three gases and also with small additives of H_2, N_2, O_2, CO, Kr, and Xe.

While considerable work$^{(28-30)}$ has been done to explain the behaviour of a cylindrical proportional counter (charge amplification), the light production mechanism in a GSPC has so far not been properly analysed. Most of the studies on light amplification processes around the anode were made by using wavelength shifters and photomultipliers of different spectral windows. Thus the results obtained merely present a qualitative understanding of the interaction mechanism, in fact the detected signal was several steps away from the initial stages of interaction of the ionizing radiation with the gas. The first attempt to explain the optical emission in the gas scintillation counter was by Policarpo et al(23) who investigated the optical transitions in the Ar + N_2 scintillation proportional counter, employing a set of optical filters between the photo tube and the counter.

1.5 PRESENT APPLICATIONS OF GSPC

In the field of particle detection, a unique possibility is offered by the gas scintillation counter (GSC). It is the identification of particles according to the ionization loss. Even in the very high energy range ($E >> 2m_oC^2$), while $\frac{dE}{dx}$ for other scintillators changes slightly, a significant increase in $\frac{dE}{dx}$ can be seen with the gas scintillators(31). The $\frac{dE}{dx}$ curve for a krypton filled gas scintillation counter is shown in Figure 7.

The GSPC is still in its development stages. So far most of its applications have been confined to nuclear physics experiments. The use of the gas scintillation counter as a two dimensional X-ray imaging device has been reported by Paul Gorenstein(32). Its ability to reject background events in a space environment and its energy resolution for soft X-rays are already being considered for applications in X-ray astronomy(33) and space experiments(34). It is also worth mentioning that although it has promising features as a high rate counter, so far a little attention has been paid to this fact by other workers except Charpak(22), who has demonstrated its X-ray photon counting ability up to $2 \times 10^6/\text{sec}/\text{mm}^2$. Instead of an ordinary GSPC Charpak has used a gas scintillation drift chamber (GSDC) in his studies. It is a development of the GSPC and the only difference between two types is that in the GSDC an additional electric field is applied to increase the

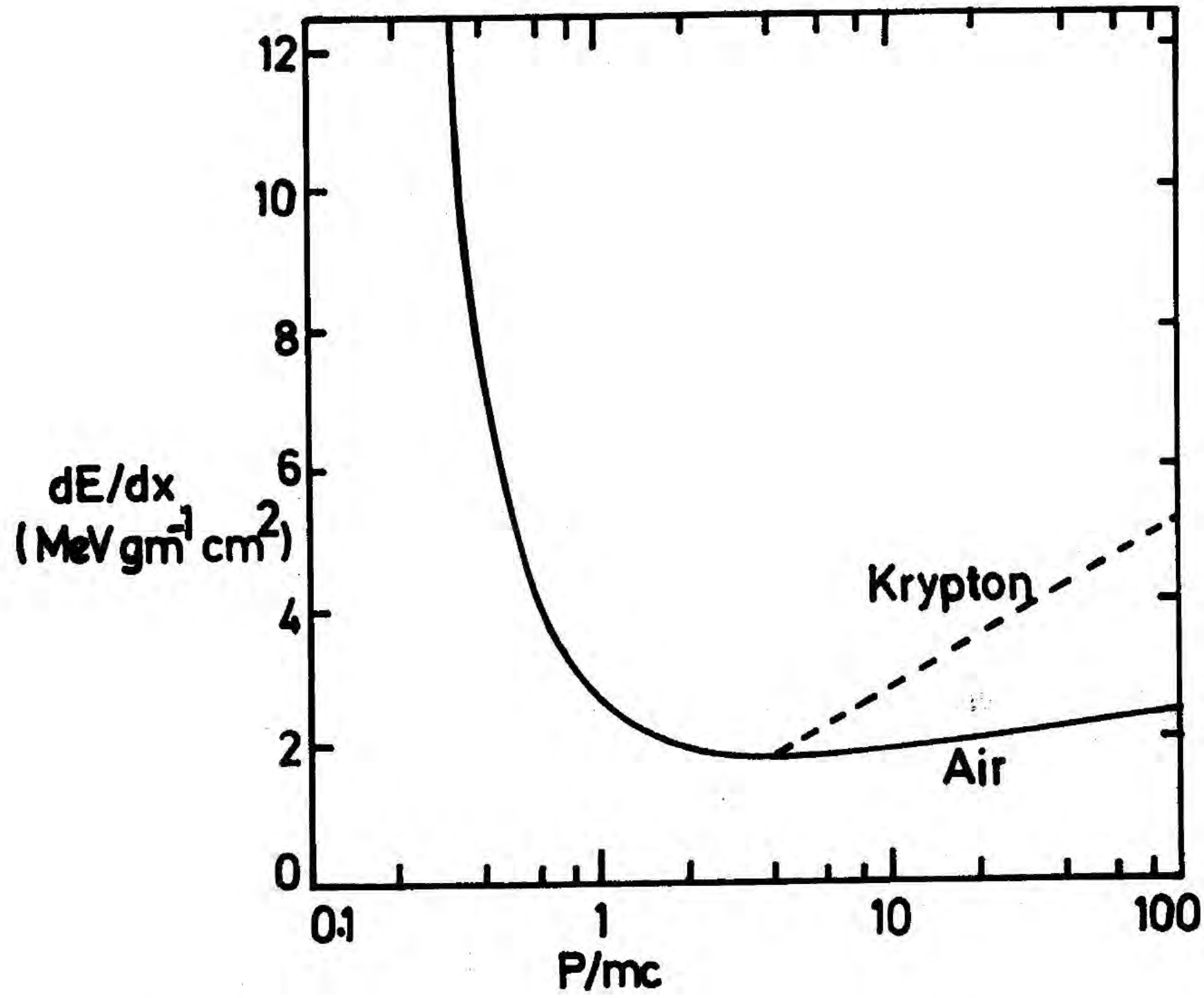

FIG.7 dE/dx versus P/mc in gas.

field in the regions which are away from the anode wire. This field is created in the chamber by applying a negatively increasing potential to the cathode wires, starting from the wires above and below the anode wire. Although the principles of operations of the GSDC are the same as those of GSPC, this device has an added advantage that the X-rays converted away from the anode wire are drifted quickly towards the wire and produce much shorter pulses than those in a GSPC. A detailed description of this device including the application of a drift field will be presented in Chapter three.

1.6 THE GSDC AS A HIGH RATE COUNTER

In fast X-ray counting the gaseous scintillation counter has a number of advantages over other counters. Firstly gas scintillators are among the fastest of the scintillator materials. The optical coupling of the output together with other excellent properties such as very high gain, low output noise level and very fast response, of the photomultiplier make the GSDC extremely low noise and operational in noisy (electrical) environments. The low noise level of a gaseous counter is an important factor which allows the counter to operate at low pulse heights (i.e. low space charge levels) and thereby to reach high count rates. Another remarkable property of the gas scintillation proportional counter is that the pulse shape and rise time are independent of the counter capacitance. This is extremely useful when building large area detectors.

The competitors to GSDC's in fast X-ray spectroscopy are scintillation counters, semiconductor detectors and proportional counters. The ionization chamber, although it seems to be the only counter that can cope with extremely high count rates, suffers two major drawbacks, in X-ray spectroscopy. They are the lack of energy resolution and failure to provide a digital output.

Compared to the gaseous detectors, the energy resolution of scintillation counter for X-rays is generally poor (300 eV per photoelectron at the photo cathode of a photomultiplier versus 30 eV per ion-electron pair where relative energy resolution is proportional to $(\text{signal})^{-\frac{1}{2}}$. Furthermore the organic, plastic and liquid scintillators which are the only suitable scintillators for fast work have relatively low luminous efficiency in the X-ray region. On the otherhand for a given energy loss the amount of light produced by the gas scintillators in secondary scintillation process is two order of magnitude larger than that produced by NaI (Tℓ) which is the most efficient scintillator among the solid and liquid scintillator families.

The semiconductor detectors,however, still retains its position as the detector with best energy resolution (∿3 eV per electron-hole pair). Apart from its excellent energy resolution, semiconductor detectors have a number of other advantages such as fast rise times (10 ns), insensitivity of pulse height to counting rate, windowless operation and linear response for a wide range of energies. But the ~~scintillation~~ semiconductor detector is generally unattractive for high intensity X-ray spectroscopic studies due to two major disadvantages.

(1) It is liable to radiation damage. The lithium drifted detectors are especially radiation damage sensitive because of their low internal fields and consequent short trapping lengths.

(2) The slow rise times of large area detectors. The rise time is determined by the depletion layer capacitance and the resistance of the detector.

$$C_{depl} = \frac{KA}{4\pi W}$$

A- Junction area

K- Dielectric constant

W- Depletion layer thickness.

1.7 PRESENT WORK

This thesis describes the development of the gas scintillationdrift proportional counter as a high rate counter. The investigations were mainly aimed at the following objectives :

(i) Minimization of the secondary light pulse width.

(ii) Optimization of the secondary light production and obtaining a modest value for the energy resolution which change as little as possible with count rate (for X-rays).

The width of the secondary scintillation pulse is determined by the scintillation properties of the gas and the time taken by the primary electrons to drift across the light producing region. The properties of gas scintillators indicate that the addition of small quantities of molecular gases to pure atomic (noble) gases greatly reduces the width of the scintillation pulse. It was apparent from data available on gas scintillators that an argon-nitrogen mixture possessed the attractive features of a 'fast' gas scintillator. The general properties of gas scintillators and the factors which led to choose argon-nitrogen mixture for this study will be discussed in the next chapter. The principles of operation of GSPC will also be discussed in a later chapter.

The properties of gas mixtures have been studied in order to find a suitable composition which yields a high secondary scintillation output with small pulse width. The basic properties of the GSDC including output pulses and the effect of the anode wire diameter on the counter performance have also been investigated to obtain the optimum counter parameters.

The photomultiplier plays an important role in this work. Its performance was tested at high rate using a light emitting diode pulser. It was clear from the data available on the performance of photomultipliers (PM) that the PM gain was a function of the count rate because of the variations of dynode potentials supplied by ordinary resistive potential distribution networks with count rate. This effect has been investigated and the potential distribution network was modified to stabilise the gain. Finally the system has been tested with radioactive X-ray sources and an X-ray machine. The results of these investigations will be described in appropriate chapters. The electronics used in the data acquisition will also be described.

1. V. P.Suller and D.J.Thompson, Nucl.Instr. and Meth. 152 (1978) 1.

2. G.Charpak, R.Bouclier and T.Bressani, Nucl.Instr.and Meth. 62 (1968) 235.

3. G.C.Hanna, D.H.W.Kirkwood and B.Pontecorvo, Phys. Rev. 75 (1949)985.

4. A.Breskin, G.Charpak, F.Sauli, M.Atkinson and G.Schultz, Nucl. Instr. and Meth. 124 (1975) 189.

5. H.W.Hendricks, Rev. Sci. Instr. 40 (1969) 1216.

6. Internal Report, NI-77-13, Durham University.

7. William Huggins, Sir, and Huggins, Lady,
Proc. Roy. Soc. A 72 (1903) 196, 409.
Proc. Roy. Soc. A 77 (1906) 130.

8. R.Pohl, Jb. Radioakat. Elektronik 4 (1907) 100.

9. H.Greinacher, Z Phys. 47 (1928) 344.

10. E.K.Michailova, Wiener. Ber. 143 (1934) 15.

11. R.Auderbert and S.Lormeau, C R Aced. Sci., Paris 228 (1949) 318.

12. A.E.Grün and E.Schopper, Z. Naturf. 6a (1951) 698.

13. A.Ward, Proc. Phys. Soc. A67 (1954) 841.

14. L.Koch, Nuclear Electronics Proc. Symp. Paris (Vienna: I.A.E.A) 1 (1958) 151.

15. L.Koch, Thesis, University of Paris (1960).

16. C.A.N. Conde and A.J.P.L.Policarpo, Diploma Report, University of Manchester (Unpublished) (1960).

17. C.A.N.Conde and A.J.P.L.Policarpo, Nucl. Instr. and Meth. 53 (1967) 7.

18. A.J.P.L.Policarpo, C.A.N.Conde and M.A.F.Alves, Nucl. Instr. and Meth. 58 (1968) 15.

19. A.J.P.L.Policarpo, M.A.F.Alves, M.C.M.dos Santos and M.J.T.Carvalho, Nucl. Instr. and Meth. 102 (1972) 337.

20. P.E.Palmer and L.A.Brady, Nucl. Instr. and Meth. 116 (1974) 587.

21. G.Charpak, S.Majewski and F.Sauli, Nucl. Instr. and Meth. 126 (1975) 38.

22. G.Charpak, S.Majewski and F.Sauli, IEEE. Trans. Nucl. Sci. NS-23 (1976) 202.

23. A.J.P.L.Policarpo, M.A.F.Alves and C.A.N.Conde, Nucl. Instr. and Meth. 55 (1967) 105.

24. A.J.P.L.Policarpo and M.A.F.Alves, Nucl. Instr. and Meth. 58 (1968) 151.

25. C.A.N.Conde, A.J.P.L.Policarpo and M.A.F.Alves, IEEE. Trans Nucl. Sci. NS-15 (1968) 84.

26. H.Tornow, H.Huck, H.J.Kober and G.Martens, Nucl. Instr. and Meth. 133 (1976) 435.

27. P.E.Thiess and G.H.Miley, IEEE. Trans. Nucl. Sci. NS-21 (1974) 125.

28. H.W.Hendricks, Nucl. Instr. and Meth. 106 (1973) 579.

29. J. Sanada and Y Fujita, Nucl. Instr. and Meth. 131 (1975) 469.

30. J. Planinic, Nucl. Instr. and Meth. 136 (1976) 165.

31. D.M.Ritson, Techniques of high energy physics, Vol 5, Interscience Publishers, New York (1961), page 332.

32. P.Gorenstein and K.Topka, IEEE. Trans. Nucl. Sci. NS-24 (1977) 511.

33. R.D.Anderson, L.Karlsson, A.Peacock and B.G.Taylor, Astron. Astrophys. 53 (1976) 309.

34. R.D.Anderson, E.A.Leimann, A.Peacock and B.G.Taylor, Nucl. Instr. and Meth. 146 (1977) 391.

CHAPTER TWO

SCINTILLATION PROPERTIES OF GAS MIXTURES

2.1 INTRODUCTION

The spectral emission following a passage of ionizing radiation or an electrical discharge through gases has been known for many decades. The investigation of such processes have received increasing interest over the last few years since they seem to be important in the understanding of the atmosphere of our own planetary system. In addition these reactions represent extremely important excitation mechanisms in laser systems such as Ne-He[1] and Ar-N_2[2] and as mentioned in chapter one, they also play an important role in the development of gas scintillation proportional counters. The early studies on gas scintillators revealed the importance of noble gases over other gases. They became very attractive in scintillation studies because of their relatively low energy expenditure per ion pair, high and constant light output per unit energy loss and high absorption coefficient for ionizing radiation. The following discussion is therefore mainly confined to the noble gases and their mixtures with molecular gases.

2.2 SCINTILLATION MECHANISM

At room temperature most of the molecules in a molecular gas occupy the lowest vibrational level of their electronic ground state (level 0 of S_o in Figure 1), and from there the transitions take place upwards on absorption of energy. Once a molecule is in an excited state it can decay to a lower energy state, including the ground state, by three different processes :

(1) Radiationless transitions from one electronic state to another.

(2) Radiative transitions between electronic states.

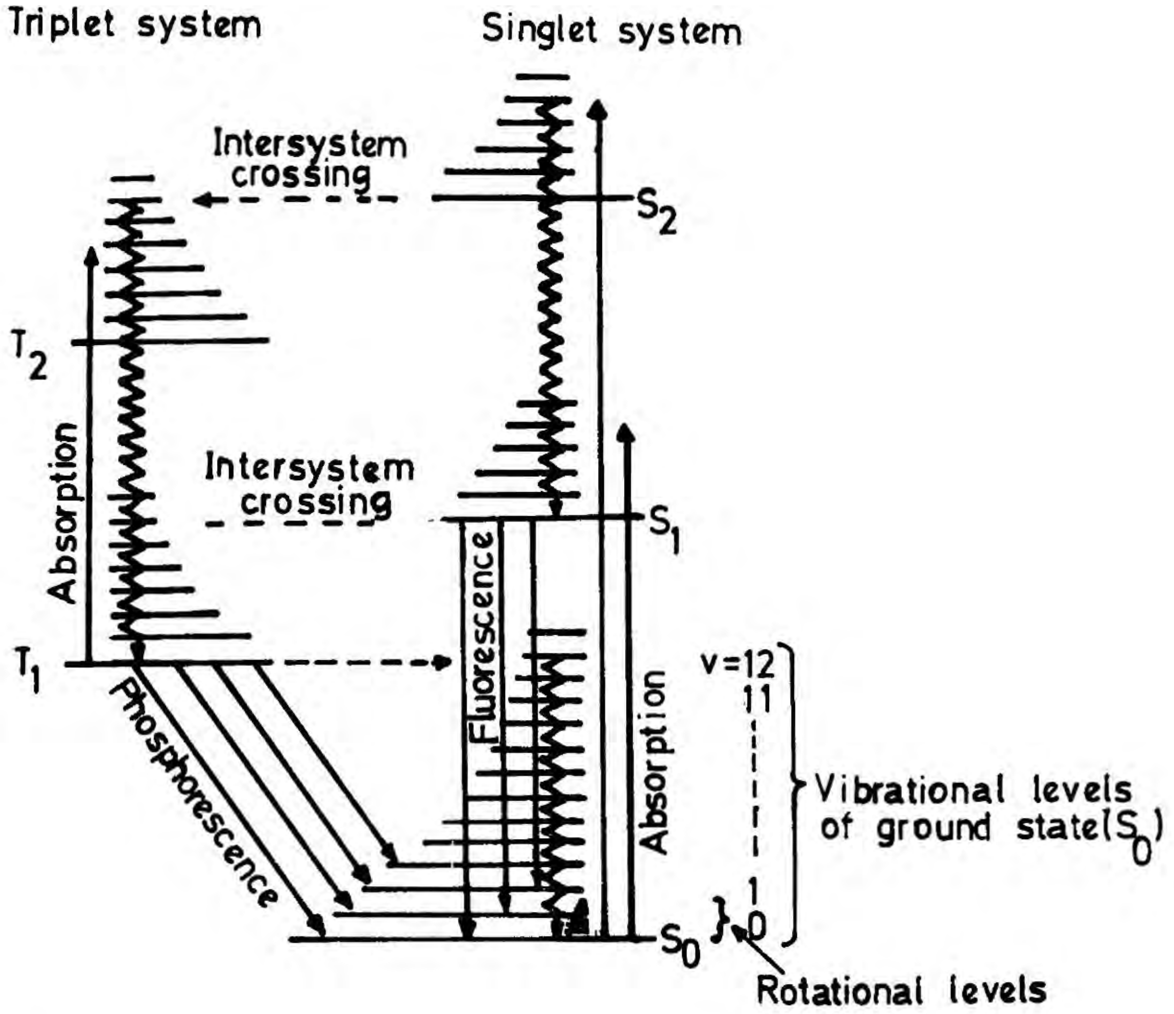

FIG1 Intramolecular transition processes

(3) Electronic energy transfer between molecules.

In most cases, processes 1 and 2 are intramolecular and process 3 is intermolecular. The various intramolecular and intermolecular processes for the dissipation of electronic energy are discussed below.

The dissipation of energy through radiationless transition begins immediately after the excitation process has ended. First the excess vibrational energy is rapidly dissipated to the surrounding medium (within a time of $\sim 10^{-13}$ seconds) and the system is deactivated to the zero vibrational energy level of the excited electronic state. Secondly, if there is any other electronic state whose potential energy function crosses that of the excited electronic state and which has a vibrational level iso-energetic with the zero vibrational energy of the excited state, transfer to the other electronic state occurs. This process, which is known as the internal conversion when the transitions occur between states of the same multiplicity, and otherwise as intersystem crossing, takes place at an extremely rapid rate if the transitions belong to the former type. (The rate constants for singlet - singlet transitions are in the range 10^{11}-10^{13} sec^{-1}).

The deactivation of the excited molecules can proceed through radiative transitions between different energy levels of the molecules. The transitions to higher or lower energy levels are governed by a set of selection rules. In general the life times of the transitions allowed by the selection rules are much shorter (10^{-8}-10^{-9} sec) than those of the forbidden transitions. In the case of noble gases the excited states from which the transitions to the ground state are forbidden have a long life time (μsec) and are called metastable states.

The third process, the energy transfer between molecules, occurs at all but very low pressures, when the radiative life time of the excited molecules is smaller than the time between collisions of the excited molecules with other molecules. These intermolecular collisions are of great importance when the gas has more than one constituent, especially the binary mixtures containing a noble gas and a molecular gas, and they can be categorized as follows :-

(1) Collisional quenching $\overset{*}{A} + B \rightarrow A + B + KE$

(2) Energy transfer $\overset{*}{A} + B \rightarrow A + \overset{*}{B}$

where $\overset{*}{A}$ is an excited atom and A and B are an atom and a molecule in the ground state. The energy balance in quenching processes goes to increase the kinetic energy of the molecules (heat).

The first process quenches the metastable states and some of the radiative transitions (optical states), thus reducing the scintillation efficiency of the system. However, in fast scintillation counting at moderate pressures the first process contributes substantially to reduce the scintillation pulse width,which is one of the main factors limiting the high rate capability of scintillation counters. The second energy transfer process is of great significance when the excited atom $\overset{*}{A}$ is in a metastable state whose energy is almost equal to the energy of one of B's optical states. Under this situation the collisions energy transfer from $\overset{*}{A}$ to B occurs at a considerable rate (resonance) and thereby reduces the metastable concentration in the gas. These processes are additional to the intramolecular processes described earlier, so that the overall rate of decay of an excited state is the sum of the decay rates for the intramolecular and intermolecular processes.

2.3 SCINTILLATION EMISSION SPECTRA OF NOBLE AND MOLECULAR GASES

The spectrum of light emitted during the radiative de-excitation and ionic recombination of noble gases covers a wide range of wavelengths, extending from the visible to the far ultraviolet region of the spectrum. Some of the important energy levels of the noble gases are shown in Fig. 2.

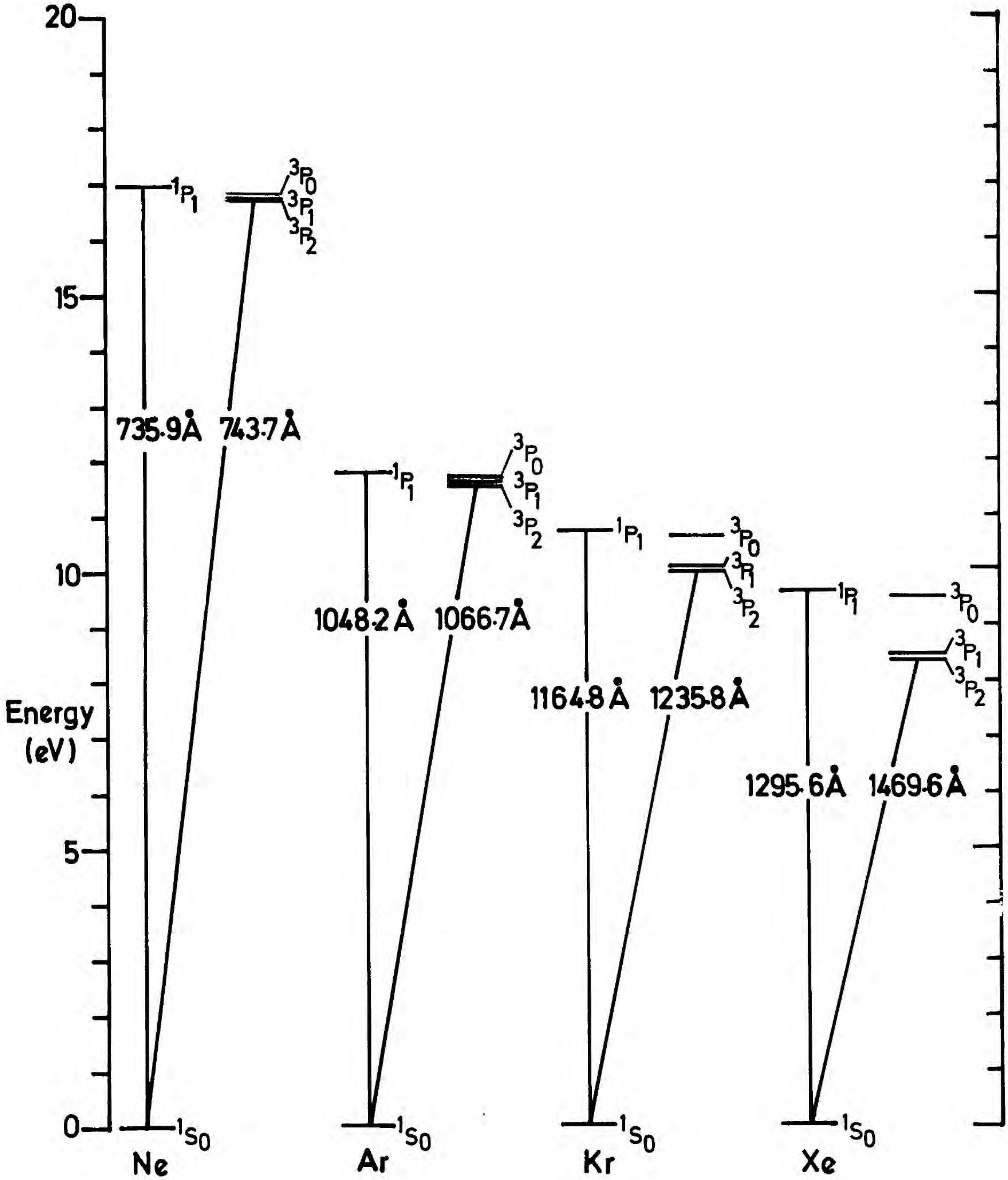

FIG. 2 Some important energy levels in the noble gases

Of these levels, the $3P_2$ and $3P_o$ levels have the longest radiative life time, since the transition from these levels to the ground state $_1S$, are forbidden both by the rules $\Delta S = 0$ (which is a rather weak restriction since L-S coupling is weak in the case of heavy atoms) and by $\Delta J = 0 \pm 1$, $J = 0 \not\rightarrow J = 0$. It is also apparent from Fig 2 that most of the scintillation spectrum (resonance radiation) of the noble gases occurs in the far ultra-violet region. At high pressures an emission continuum has also been observed[3] for the noble gases (see Fig. 3). These have been attributed to molecular emission involving transitions from the metastable states to an unstable ground state, e.g.

$$Ar^* + 2Ar \longrightarrow Ar_2^* + A$$

$$Ar_2^* \longrightarrow Ar_2 \text{ (unstable)} + h\nu$$

The rate of formation of these excited molecules increases with pressure and at very high pressures (>5000 Torr) this process will become the main destruction mechanism[4] of the argon metastable states. These excited molecules with unstable ground states are called excimers.

In contrast to the small number of excitation energy levels in the noble gases, the number of levels present in molecular gases is so large that the spectra emitted by these gases merely contain sets of bands which are formed by closely spaced spectral lines. The formation of these lines which are known as rotational and vibrational lines, is a direct consequence of the rotational and vibrational behaviour of the gas molecules.

2.4 THE SCINTILLATION DECAY TIMES

The scintillation decay times of noble gases generally depend on a number of factors, such as the nature of the excited states involved (i.e. whether they are resonant or metastable), the pressure, excimer formation, photon trapping and the impurities present in the gases. However,

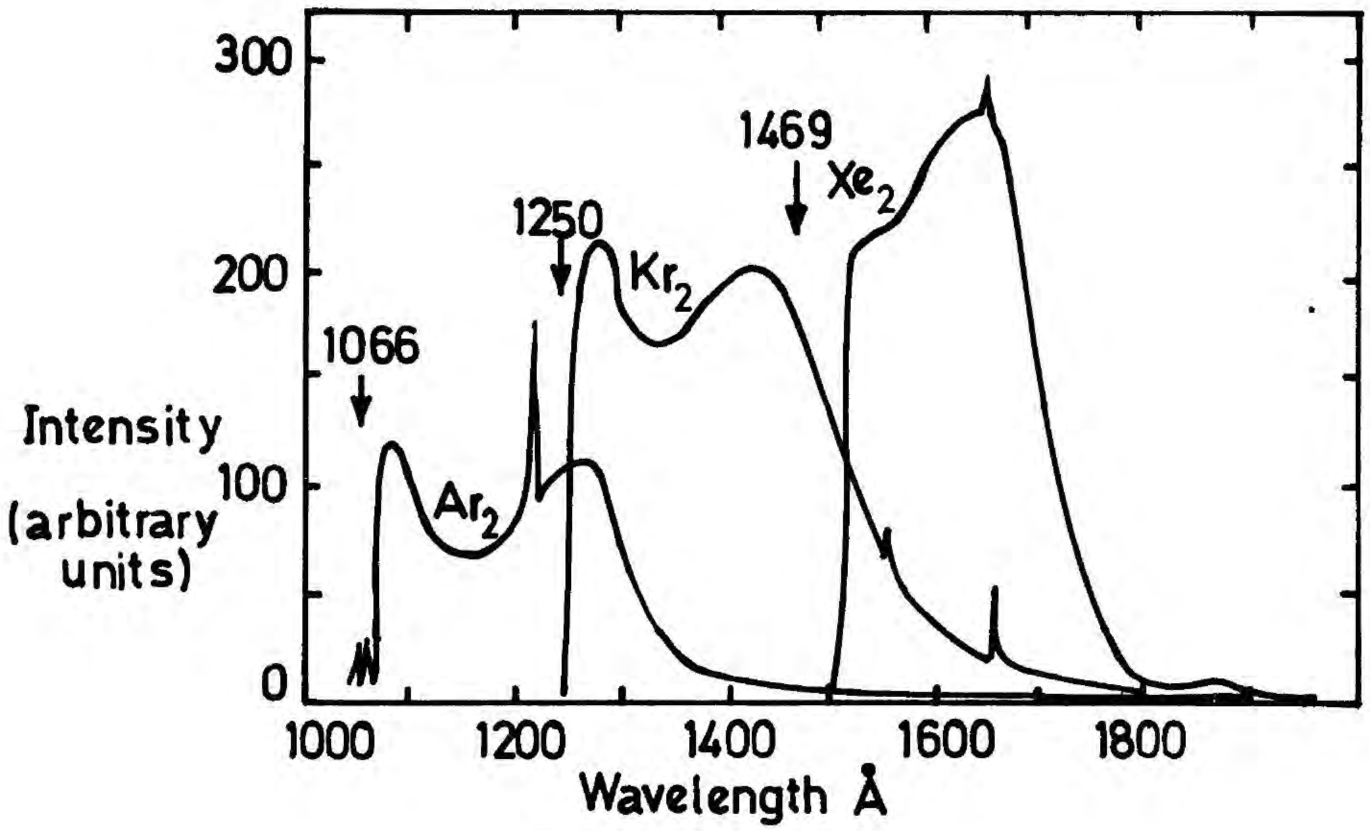

FIG.3 Intensity distribution in continuous spectra of argon, krypton and xenon at 200 Torr

the observed decay time of a scintillation is not only a function of the above mentioned factors but also a function of the measuring instrument. The observed decay times of the resonance states are longer than the natural decay time of the state itself because of the subsequent absorption and re-emission of the photons inside the gas medium before entering the detecting instrument, but even so, these times are much shorter (1-10nS) than the decay times of metastable states (μ sec). On the other hand, the metastable states can decay only through indirect routes such as collisional quenching, formation of excimers and collisions with impurity molecules. Schmidt[5] has studied the decay time of xenon excited by 50 keV electrons as a function of pressure. The behaviour of the decay time was found to be complex. At low pressures ($p<60$ Torr) the emission was mainly characterised by a line emission, while at pressures greater than 60 Torr the main contribution appeared to come from the xenon continuum. Schmidt's results are shown in Fig. 4. The value of the decay time at high pressure extrapolates to ∿9nS at $p = 760$ Torr. The most important effect of increasing pressure is the reduction in the life time of the metastable states. However, this reduction is also accompanied by a reduction in the scintillation efficiency. Schmidt also studied the scintillation decay times of molecular gases such as O_2, N_2, CO_2, and H_2. He found that the decay time of nitrogen was complex due to the presence of two emission components (N_2 second positive and N_2 first negative). The two components have been separated by Anton[6] and his results are shown in Fig. 5. The small scintillation decay time shown in figure is a clear evidence of the quenching ability of nitrogen.

2.5 SCINTILLATION EFFICIENCIES

The practical relative scintillation efficiencies of noble gases have been measured by Northrop[7] et al using a DuMont photomultiplier coated with diphenyl stilbene wavelength shifter. The efficiencies relative to

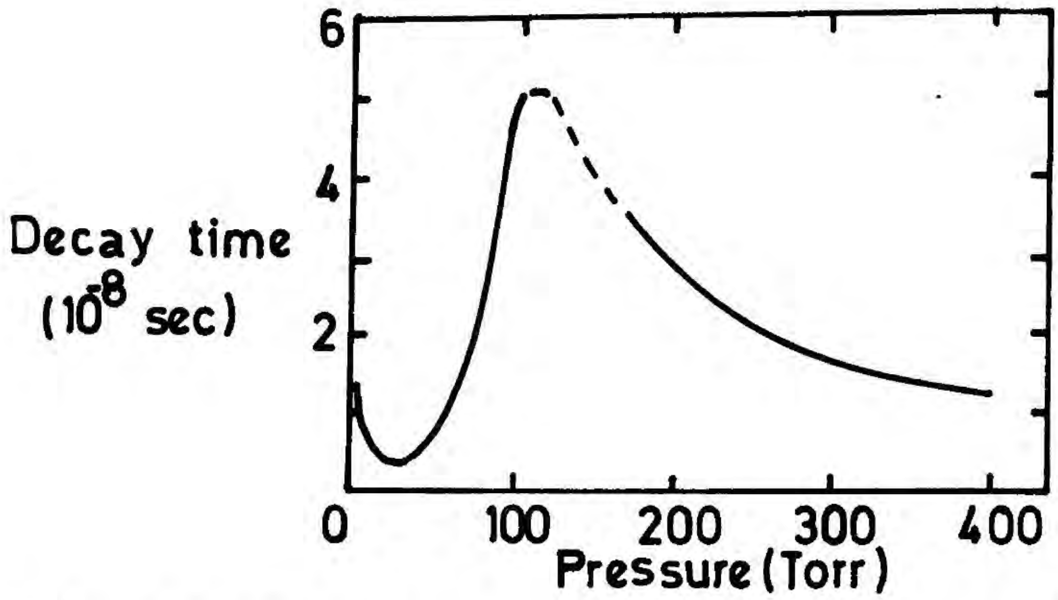

FIG.4 Scintillation decay time of xenon excited by 50 keV electrons as a function of pressure

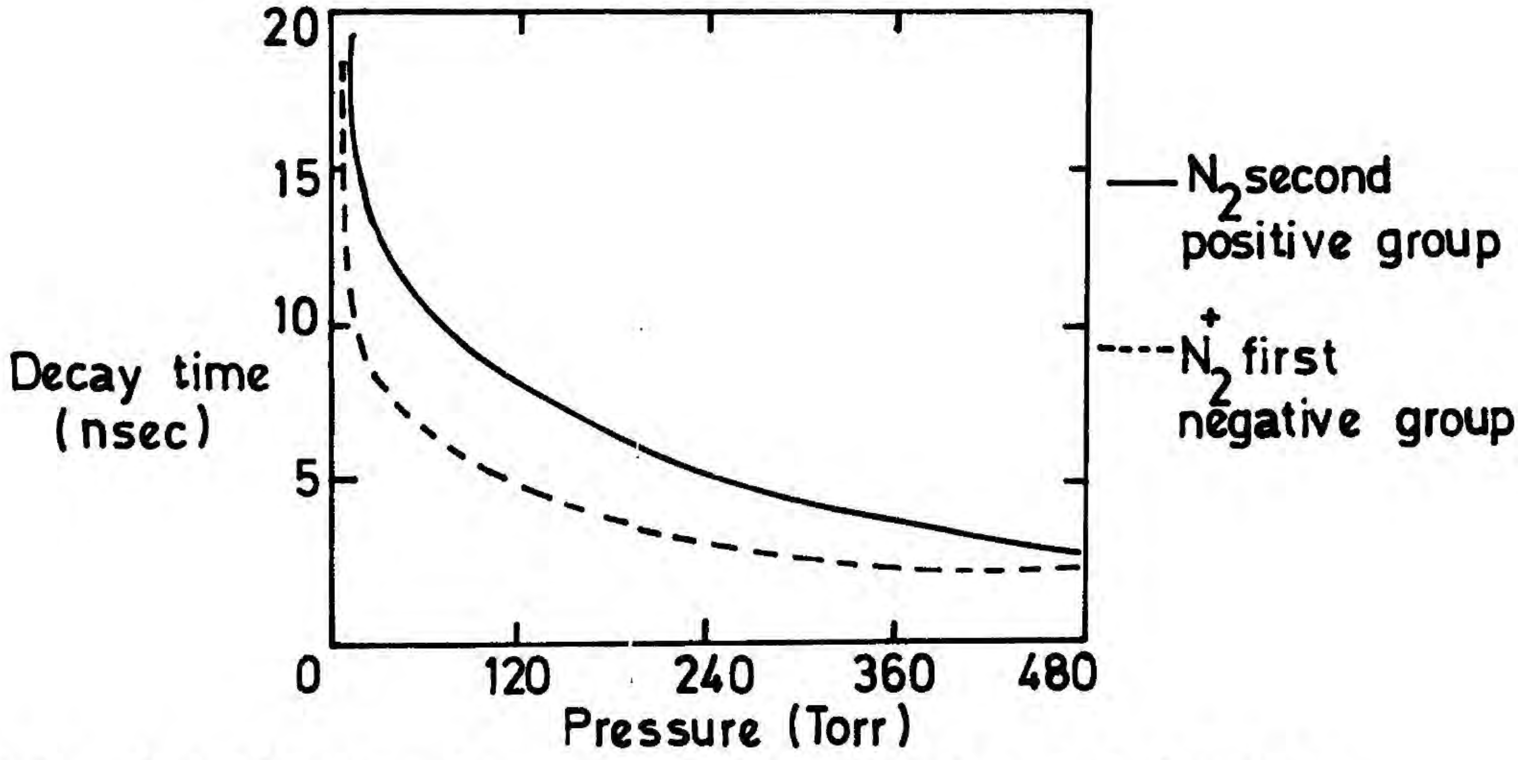

FIG.5 Scintillation decay time of nitrogen as a function of pressure

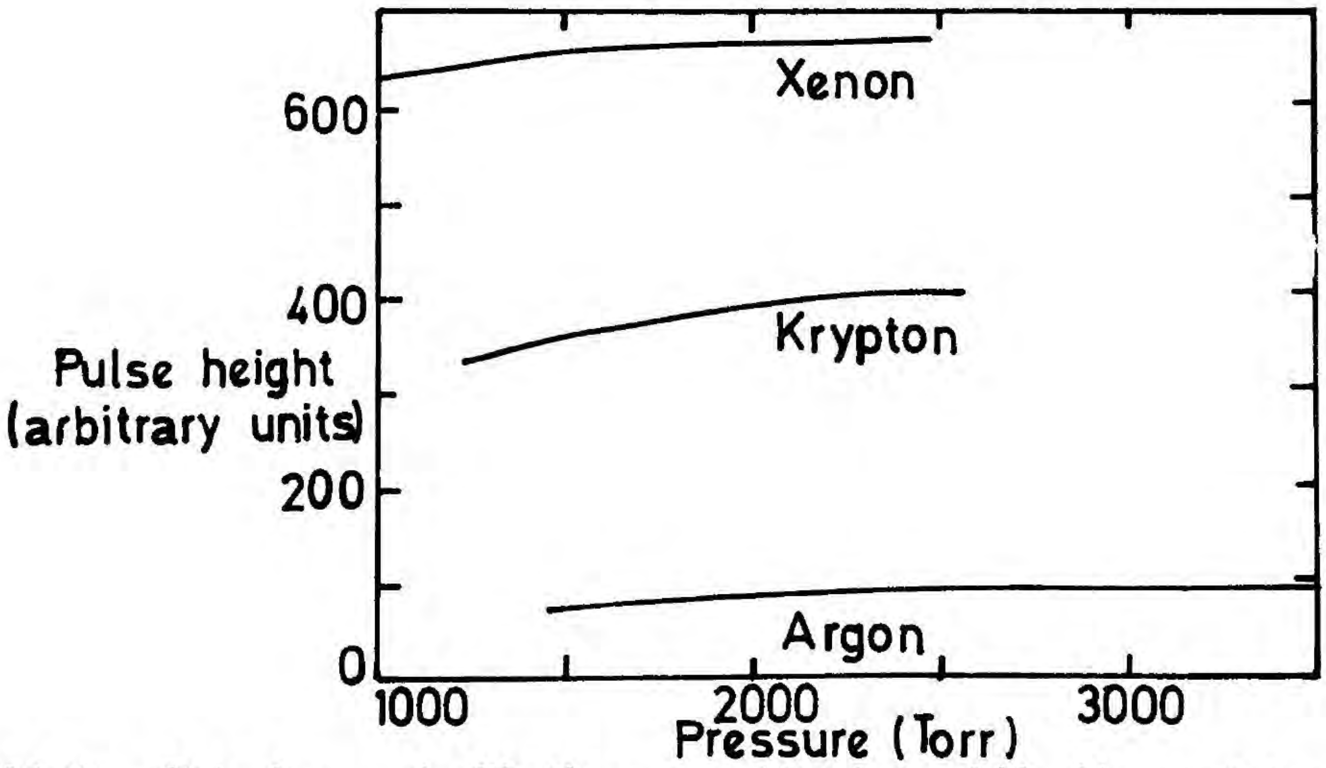

FIG.6 Relative scintillation amplitudes of Xe, Kr and Ar as a function of pressure

xenon are

$$Xe : Kr : A : Ne : He = 1.0 : 0.52 : 0.16 : 0.043 : 0.33.$$

These results are in fair agreement with the relative scintillation efficiencies obtained by Sayres and Wu[8], and some of their results are shown in Fig.6. The mean quantum efficiency of conversion of the primary excited atoms and ions, produced during the interaction of ionising radiation with the gas, into scintillation photons has been computed by Birks[9]. The number of ions and excited atoms produced by a particle of energy E interacting with a noble gas is given by[10]

$$N_i = 0.6 \frac{E}{I}$$

and

$$N_{ex} = 0.4N_i = 0.24\frac{E}{I}$$

where I is the ionization potential.

Thus the total number of primary ions and excited atoms is

$$N_i + N_{ex} = 0.84\frac{E}{I}$$

and these are converted with a mean quantum efficiency $\bar{q}$ into the N scintillation photons, so that

$$N = \bar{q}\,(N_i + N_{ex}) = \frac{0.84\,E\bar{q}}{I} \qquad (2.1)$$

Values for $\bar{q}$ can be estimated using the N/MeV value for anthracene (1.5×10^3)[9] and its relative scintillation efficiency (α N) compared to Xe (see Table 2.2) and other noble gases[7]. Table 2.1 shows the number of ions, excited atoms and photons per MeV (α-particles) and the mean quantum conversion efficiencies for the noble gases. According to Table 2.1, xenon, though expensive, is the most suitable gas to use as a gas scintillator. A much cheaper gas is argon, but its scintillation efficiency is considerably smaller than that of xenon.

The scintillation efficiency of the gases deteriorates due to quenching effects such as collisional quenching and internal quenching. For the noble gases, the latter effect is not important, but the collisional quenching processes reduce the intensity of the line emissions from various optical levels. In the case of molecular gases, however, both effects may be equally important.

Gas	I(eV)	$N_i + N_{ex}$	N	$\bar{q}$
Xenon	12.1	6.9×10^4	10^4	0.14
Krypton	13.9	6.0×10^4	5.2×10^3	0.087
Argon	15.7	5.3×10^4	1.6×10^3	0.03
Neon	21.5	3.9×10^4	4.3×10^2	0.011
Helium	24.5	3.4×10^4	3.3×10^3	0.10

TABLE 2.1 : Number of ions, excited atoms and photons produced per one MeV α-particle, and quantum conversion efficiencies for noble gases

Consider a gas whose molecular number density at pressures p and p_a (p_a = 760 Torr) are N and N_a respectively so that at constant temperature $N = N_a p/_{p_a}$.

Suppose there are n excited states present in the gas at a given time. If $k_f(\mathrm{sec}^{-1})$, $k_i(\mathrm{sec}^{-1})$ and $k_c(\mathrm{cm}^3\ \mathrm{sec}^{-1})$ are the rate constants of fluorescence, internal quenching and collisional quenching, then the quantum efficiency of fluorescence is

$$q = \frac{k_f n}{k_f n + k_i n + k_c N n} = \frac{q_o}{1 + p/_{p'}}$$

where $p' = \frac{(k_f + k_i)\, p_a}{k_c\, N_a}$ and $q_o = \frac{k_f}{k_f + k_i}$

If the efficiency of the primary excitation of a gas by a charged particle is independent of the pressure (which is expected to be so since the efficiency of primary ionization is independent of the pressure, i.e. the energy expenditure per ion-pair produced is independent of p), then the scintillation efficiency s will vary with p as

$$s = \frac{s_o}{1 + \frac{p}{p'}} \qquad (2.2)$$

Equation 2.2 clearly indicates a drop in the scintillation efficiency with increasing pressure.

2.6 WAVELENGTH SHIFTERS

The bulk of the emission spectra of noble gases being in the far ultra violet region imposes the requirement of a wavelength shifter in order to obtain reasonable signals from the detecting photomultiplier. In fast scintillation counting it is necessary that the photoluminescence decay time of the wavelength shifter be as fast as that of the gas itself. The wavelength shifter must also have a high photoluminescence quantum efficiency up to the far ultra violet region. Various materials have frequently been used for this purpose, especially organic substances such as p-quaterphenyl and diphenylstilbene. Wavelength shifters are generally deposited on the window between the gas and the phototube by vacuum evaporation techniques. The importance of using wavelength shifters when observing the emission spectrum of noble gases was demonstrated by Sayres and Wu[8] who reported the relative pulse heights with and without p-quaterphenyl wavelength shifter for both glass and quartz photomultipliers. Their results are reproduced in Table 2.2.

Gas	Optimum pressure (psi)	Glass Photomultiplier		Quartz Photomultiplier	
		without QP	with QP	without QP	with QP
Xenon	6	6	105	88	145
Krypton	8	<3	50	-	83
Argon	10	<3	15	11	28
Helium	45	9	38	14	40
CsI(Tl) (1 mm thick)		160			
Anthracene (3 mm thick)		22			

TABLE 2.2: Relative scintillation pulse heights of various gas, fluorescent converter and photomultiplier combinations (Po^{210} α-particles)

The comparison of pulse heights obtained with and without the wavelength shifter on quartz window photomultiplier which is sensitive to wavelengths greater than 2000 Å, shows that most of the emission occurs at wavelengths less than 2000 Å. It further indicates that the use of a glass window photomultiplier with a proper wavelength shifter is much more effective than the use of quartz window photomultiplier to view scintillations from the noble gases.

Some of the scintillation characteristics of fast organic materials are given in Table 2.3. The quantum efficiencies given are normalized against anthracene. The luminescence decay curves corresponding to these materials are found to be exponential, but in some cases slow components appear[11] at the tail end of the pulse. Table 2.4a gives the relative practical scintillation efficiencies observed by Northrop[15] for various combinations of noble gas scintillators and wavelength shifters. A Du Mont 6292 photomultiplier coated with ∿30 $\mu g\ cm^{-2}$ of wavelength shifter and an α-particle source to excite the gas atoms were used for the measurements. The values presented are normalized to the xenon-diphenylstilbene combination which gives about the same light output as α-particles on NaI (Tℓ). Table 2.4b, which has been obtained by normalizing the first two columns of Table 2.4a against the values in the last column for each wavelength shifter, shows that the relative amount of light obtained from different gases are practically independent of the nature of the wavelength shifter used. It further indicates that the values obtained with a given converter correspond to the number of scintillation photons emitted by different gases.

2.7 SCINTILLATION PROPERTIES OF GAS MIXTURES

Northrop and Gursky[7] have compared the relative scintillation efficiencies of binary noble gas mixtures excited by U^{234} α-particles using a Du Mont 6292 photomultiplier coated with diphenylstilbene. The light output as a function of the fractional pressure of the heavier gas in the mixture for various gas mixtures is shown in Fig.7. All the light outputs are normalized to that of pure xenon. The authors interpret the observed minima in the results in terms of Biondi's[16] results on recombination coefficients of atomic and molecular ions. These indicate that the atomic

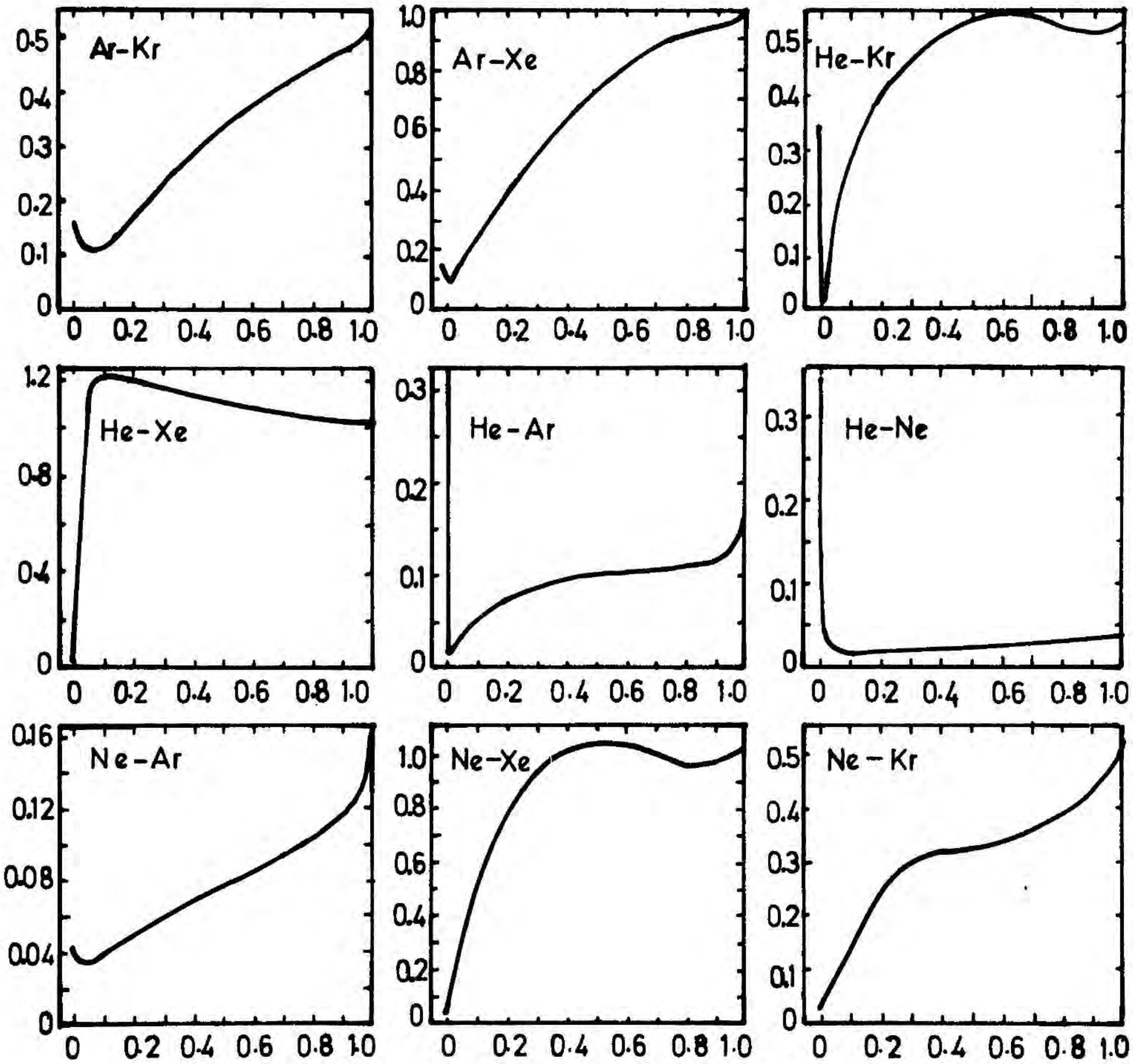

FIG.7 Scintillation light output of binary noble gas mixtures for U^{234} particles. (The ordinates have been normalized to the light obtained from pure xenon. The abscissas are the fraction by pressure of the heavier gas in the mixture.)

Material	Decay time ns	Photo fluorescence efficiency (normalised to anthracene)	Range of the Emission Spectrum (A^o)	Ref
Trans-stilbene	6	0.8	3650 - 4700	11
p-terphenyl	5.5	0.8	3750 - 4800	12
Diphenylacetylene	4.9	0.8	3550 - 4400	12
p-quartenphenyl	4.5 - 7	1	3400 - 5400	13
1,4 Diphenylbutadene	4.1	-	4000 - 5600	14

TABLE 2.3 : Some important properties of organic scintillator materials

Gas / Fluorescent converter	Argon	Krypton	Xenon
p-Quaterphenyl (QP)	-	0.247	0.438
Diphenylstilbene (DPS)	0.202	0.567	1.000
TPB	0.144	0.356	0.699
POPOP	0.071	0.172	0.366
POPOP + DPS	0.066	0.170	0.337
α NPO	0.037	0.090	0.176

TABLE 2.4a :

Gas / Fluorescent converter	Argon	Krypton	Xenon
p-Quaterphenyl (QP)	-	0.563	1
Diphenylstilbene (DPS)	0.202	0.567	1
TPB	0.206	0.509	1
POPOP	0.193	0.467	1
POPOP + DPS	0.196	0.504	1
α NPO	0.210	0.511	1

TABLE 2.4b :

TABLE 2.4 : Relative efficiencies of combinations of noble gases and fluorescent converters.

ion recombination coefficient is at least a factor of 10^3 smaller than the molecular ion coefficient. The addition of small amount of heavier atomic gas to the lighter gas results in a charge transfer between lighter atomic ions and heavier gas atoms, since the heavier gas has a lower ionization potential. Thus the formation of lighter molecular ions which subsequently combine with electrons and produce photons on dissociation, decreases and thereby causes a reduction in the light output. The low concentration of heavier gas atoms inhibits the formation of heavy molecular ions.

The addition of molecular gases to a noble gas causes dramatic changes in the noble gas spectrum. Strickler and Arakawa[17] have studied the emission spectrum of argon on the addition of a second gas such as O_2, CH_4, Kr, CO_2, N_2 and Ne. In all cases except Ne, and to some extent in Ne, there was a rapid decrease in intensity of the continuum with the addition of the first 1% or 2% of the second gas. With the addition of krypton, a gradual increase in intensity of the krypton continuum between 2000 Å - 4000 Å at the expense of the argon continuum was also observed. Fig. 8 shows the quenching of argon emission with the addition of nitrogen and Fig.9 represents the emission spectrum of a mixture of argon with 0.1% nitrogen from 1600 Å to 4300 Å. It indicates that the addition of nitrogen quenches the emission of argon in the region between 1500 Å and 3000 Å and produces the emission of a line spectrum (2nd positive band) between 3000 Å and 4200 Å. However, the results from recent experiments[3] show that the main argon continuum occurs at much smaller wavelengths (1070 Å - 1400 Å) in contrast to the values quoted (1600 Å - 3000 Å) by Strickler and Arakawa.

The maximum intensity of the second positive emission band in nitrogen occurs at a nitrogen concentration of about 3%. With further addition of nitrogen, the intensity of the second positive group begins to decrease and

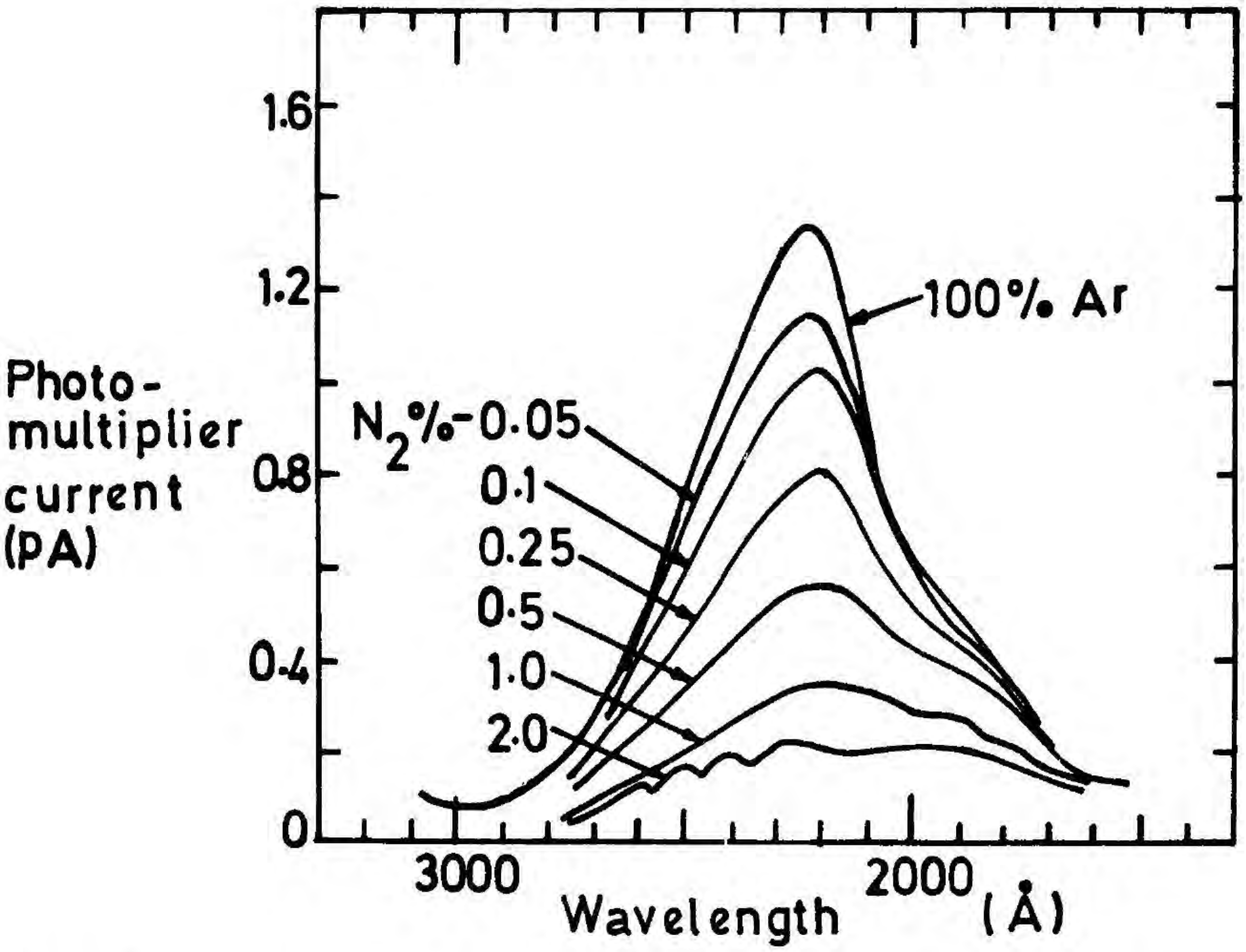

FIG. 8 Intensity of argon continuum for different nitrogen concentrations.

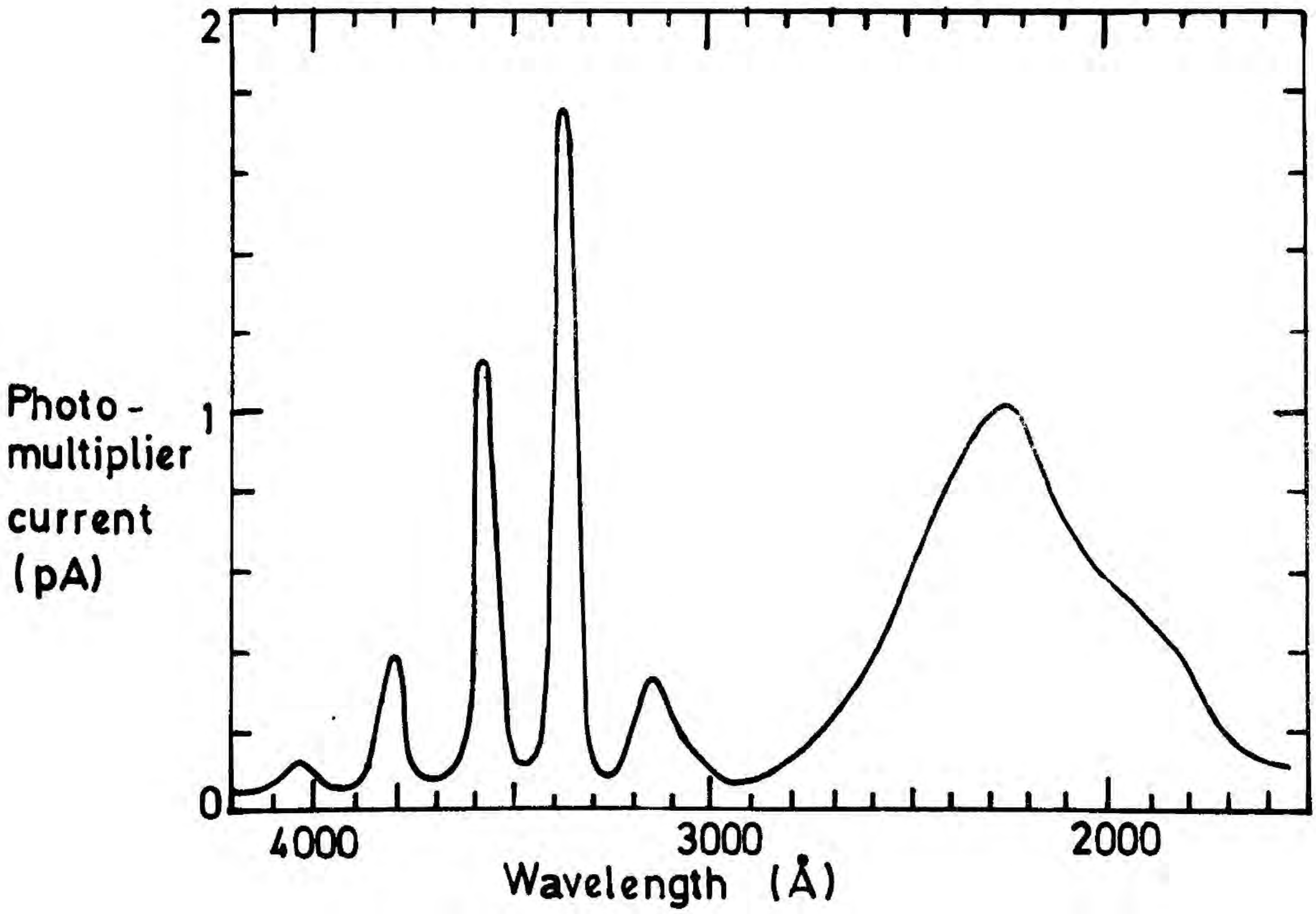

FIG. 9 Emission spectrum for a gas mixture containing 99.9% argon and 0.1% nitrogen.

a new set of lines starts to appear in the wavelength region 2200 Å-2600 Å. The intensity of nitrogen bands at high concentration of nitrogen are shown in Fig.10. Grün and Schopper[18] have measured the practical light output of argon-nitrogen mixtures at p = 585 Torr and 20° C as a function of nitrogen concentration and obtained a similar behaviour, (see Fig.11). The drop in light output at high nitrogen concentration is mainly due to the collisional quenching processes.

2.8 SECONDARY SCINTILLATION PROCESS IN GAS MIXTURES

The passage of ionizing radiation through a gas results in excitation and ionisation of its atoms, and the subsequent de-excitation of atoms and recombination of ions produce a light pulse with a fast leading edge (known as primary scintillation pulse). However, before recombination the electrons originally produced during the ionisation process can be accelerated under an electric field to gain energy and produce more excitation in the medium. In the context of scintillation proportional counter technology, the scintillation produced by these 'secondary excited atoms' are called secondary scintillations.

For a given electric field the intensity of the secondary scintillation output depends on the number of electrons which have energies above the threshold for direct excitation of the atoms in the gas. This number is not only a function of the electric field but also a function of the gas mixture since it depends on the inelastic cross-section of electrons in each constituent of the mixture. The comparison of pulse heights (scintillation efficiencies) of different gas mixtures or the same gas mixture with different concentrations of its constituents is therefore not straight forward as in the case of primary scintillation. This fact can be demonstrated from the results obtained by Policarpo[19] et al on Ar-Xe and He-Xe gas mixtures. The results, which they have obtained with a cylindrical scintillation counter with a 125 μm

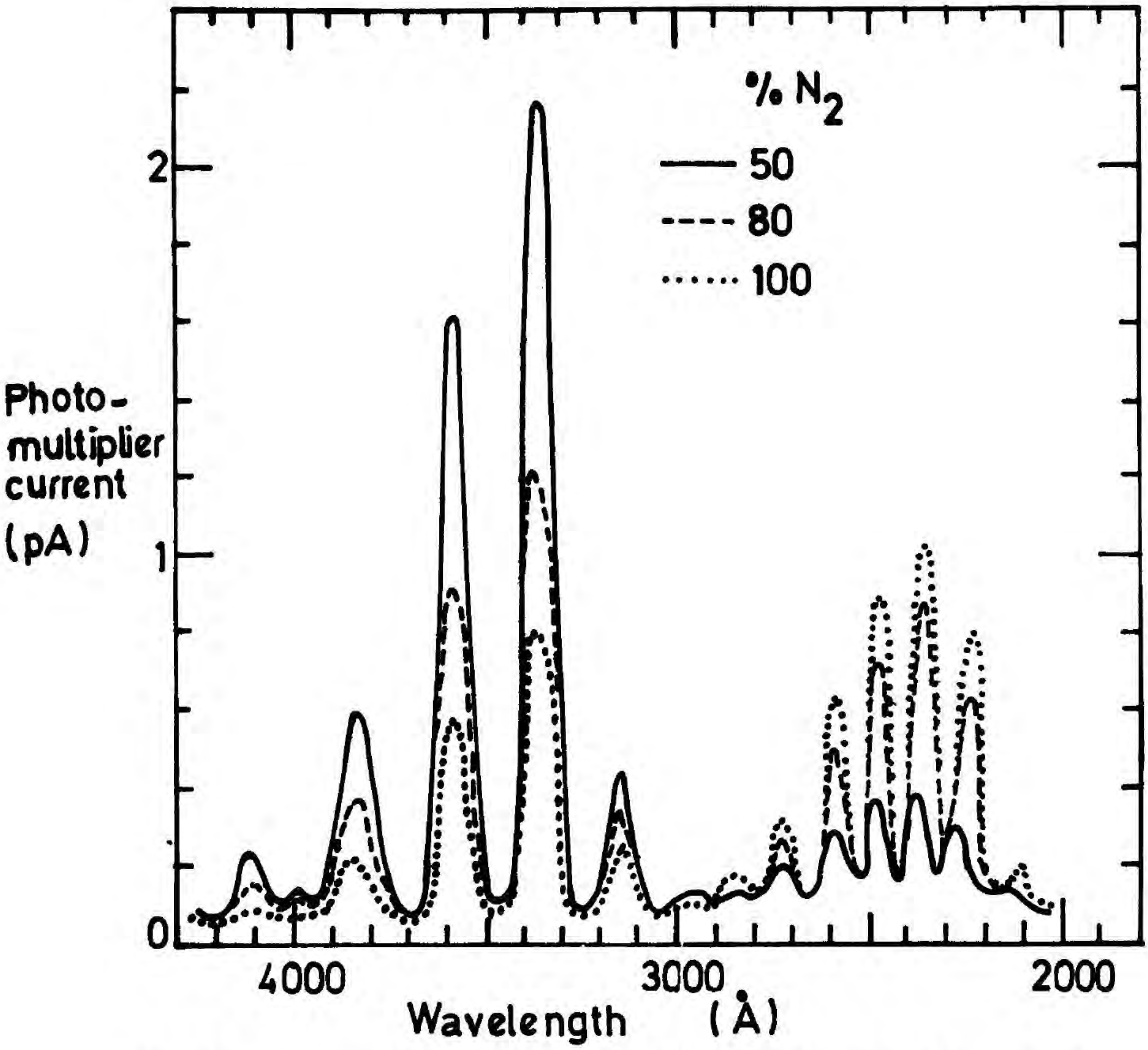

FIG.10 Spectrum of Ar-N_2 mixtures for high concentrations of nitrogen

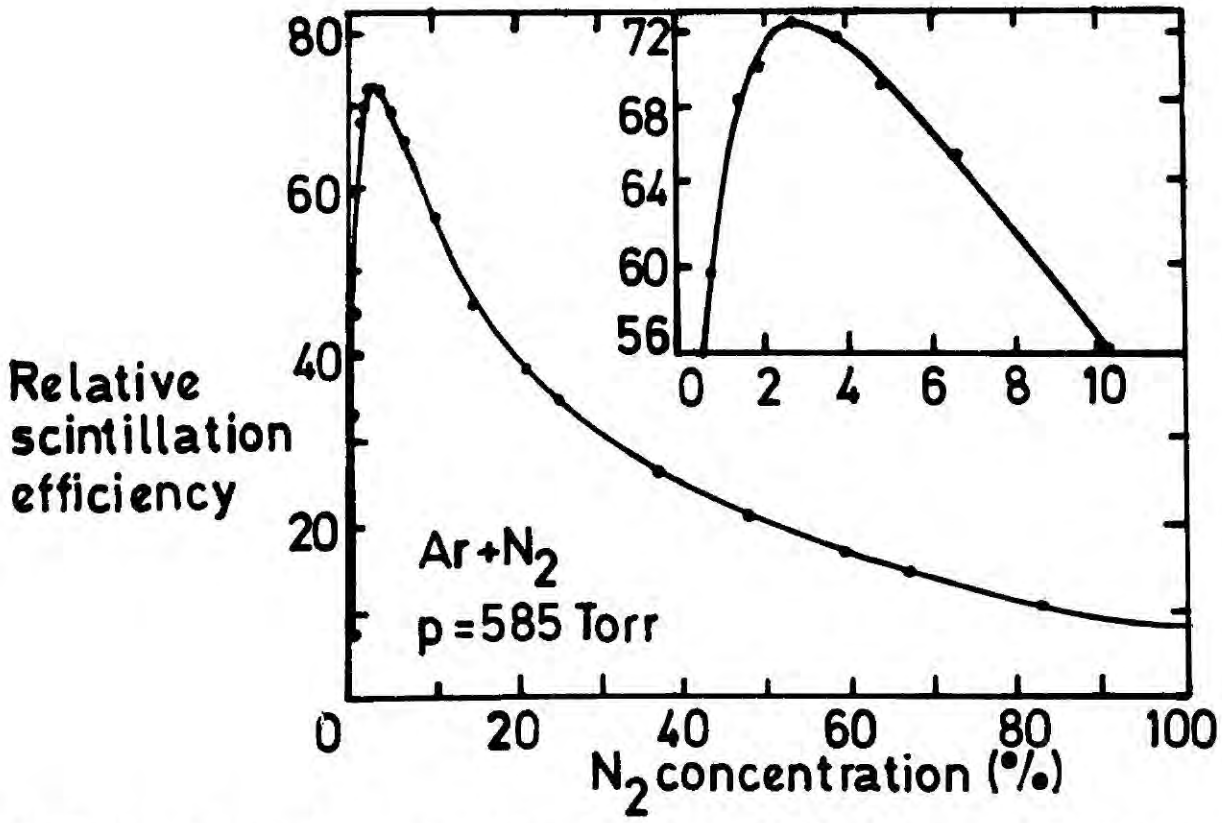

FIG.11 Relative practical scintillation efficiency of Ar−N_2 mixtures as a function of N_2 molar concentration, at p=585 Torr

diameter central anode wire, are shown in Fig. 12. The light output from an Ar-5% Xe mixture is about an order of magnitude greater than that from pure argon. They obtained an even larger practical light output with a He-42.5% Xe mixture although it appears that for a given voltage the practical light output from this mixture is less than that from Ar-5% Xe. This is due to them being able to attain much higher anode voltages with He-42.5% Xe mixture than with Ar-5% Xe mixture before the production of spurious light due to electrons originating from the cathode surface.

The spectral composition of the secondary scintillation is almost identical to that of the primary scintillation since both processes involve the same excitation processes. This fact has been tested by Policarpo et al[20] with $Ar-N_2$ gas mixture using a cylindrical G.S.P.C. with a thick (250 μm diam) anode wire. The work of Strickler and Arakawa[17] concerning the primary scintillation of the same mixture shows that the addition of nitrogen to argon quenches the argon emission with the formation of two main nitrogen lines at 3380 Å and 3580 Å. The Policarpo group employed two optical filters A and B with short wavelength cutoffs at λ_A=3250 Å and λ_B= 3800 Å , in order to measure the intensity of these two lines for several values of the anode voltage and nitrogen concentration. Fig.13a shows the optical transmission properties of their detector system and Fig.13b shows the variation with anode voltage of the ratio 'r' of the pulse height of the secondary light obtained with filters A and B to the secondary pulse height with no filters for several argon-nitrogen mixtures. For filter A, the pulse amplitudes are corrected for absorption effects. Fig.13b shows that for nitrogen concentrations $\gtrsim$ 0.8% the ratio r is practically independent of the anode voltage and nitrogen concentration. It is clear from these results that for nitrogen concentrations $\gtrsim$1%, 80% of the secondary emission from the argon-nitrogen mixture occurs at wavelengths > 3250 Å , and since the transmission from B is only ~14% for nitrogen concentrations > 0.15%, the major part of the emission spectrum should be

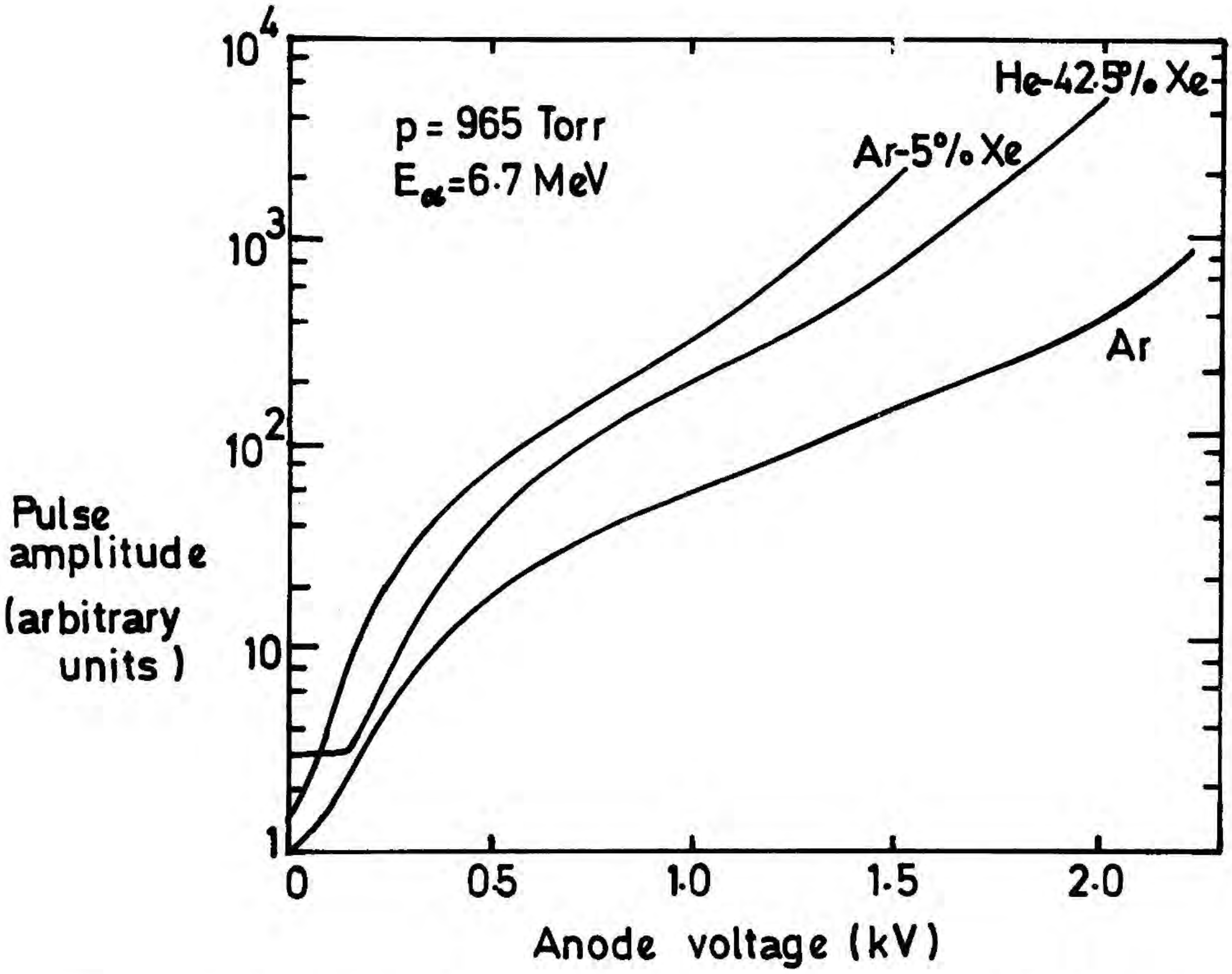

FIG.12 Pulse amplitude vs anode voltage for pure argon and the mixtures Ar-5% Xe and He-42·5% Xe (PS counter with p-quaterphenyl)

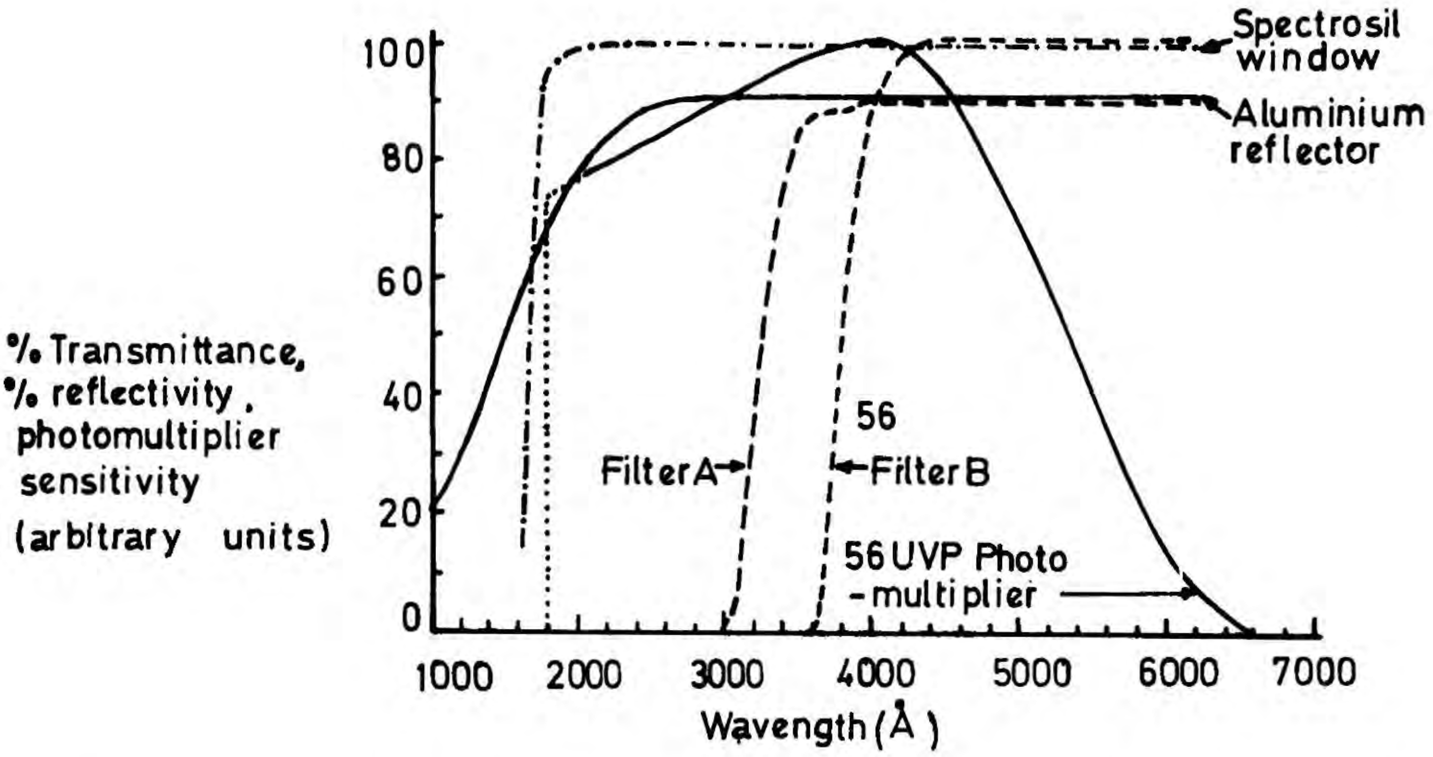

FIG 13a Transmission curves of counter window and filters A and B Reflectivity curve of aluminium and spectral sensitivity of 56 UVP photomultiplier.

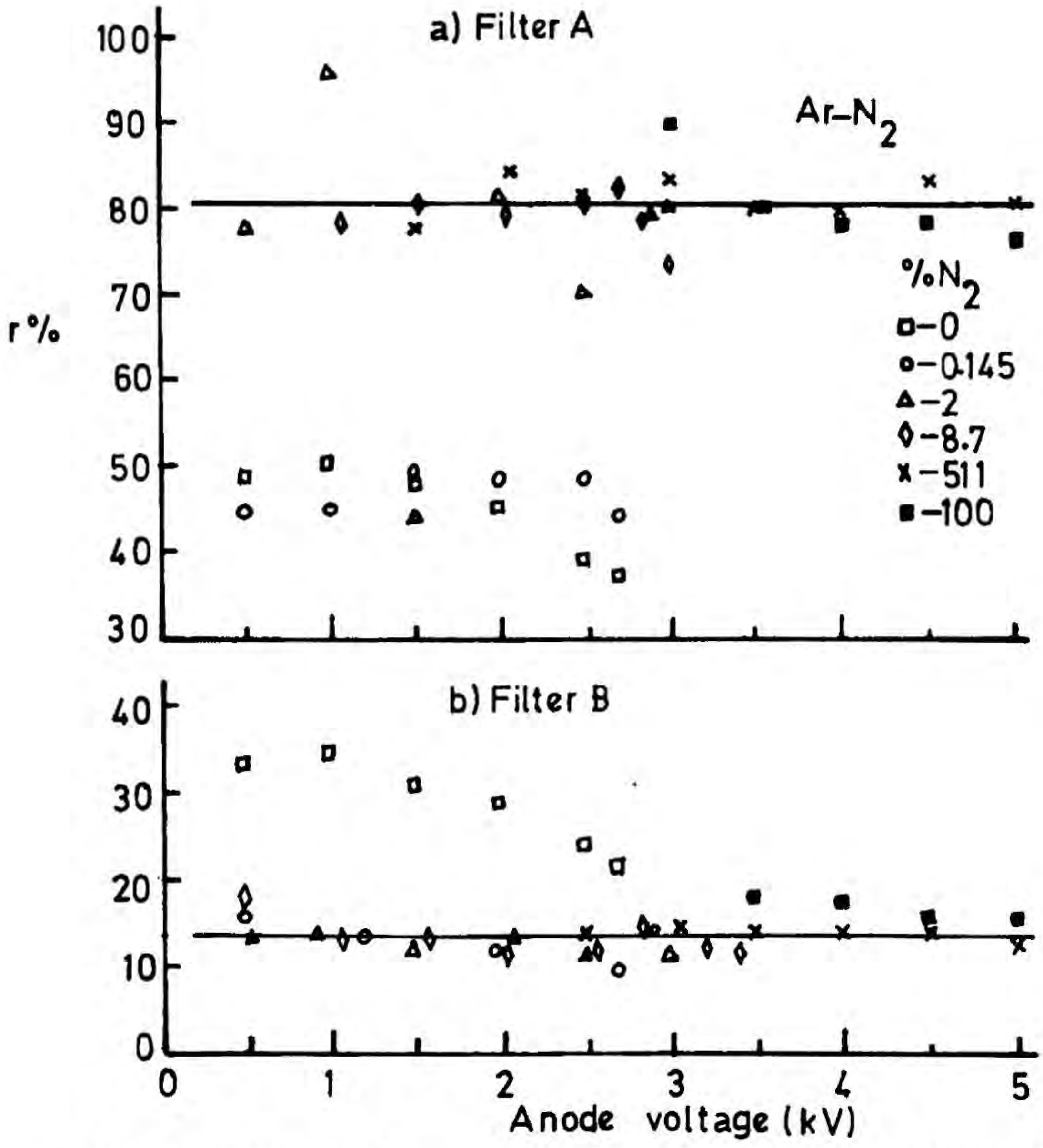

FIG.13b a. Ratio r of the pulse amplitude of the secondary light with λ > 3250 Å to the total secondary pulse amplitude, vs anode voltage; b. The same for λ > 3800 Å.

within the band 3250 Å - 3800 Å.

As a gas scintillator an argon-nitrogen gas mixture has a number of advantages over other gas mixtures.

(1) It is a cheap gas mixture and can be used with flow type detectors.

(2) Nitrogen is a good metastable quenching gas and it re-emits some of the energy originally absorbed from the metastable states ,as photons.

(3) The main emission is in the visible region and therefore relatively less expensive pyrex window photomultipliers can be used to detect the scintillation light,(see Fig.14). The disadvantages of Ar-N_2 gas mixtures over other gas mixtures are the relatively low light output per unit energy loss and low absorption coefficient for ionising radiation compared to xenon and krypton. Despite these disadvantages an argon-nitrogen gas mixture has been chosen as the counter gas since the work described in this thesis employs a flow type counter.

2.9 THE ELECTRON IMPACT EXCITATION OF ARGON-NITROGEN

The formation of secondary scintillation around the anode wire of a scintillation counter is a consequence of the electron impact excitation of gas molecules. Some of the important energy levels of the argon-nitrogen system are shown in Fig.15. The $^3p_1$ and $^1p_1$ states of argon are resonance states, while the ^3p_o and $^3p_2$ states are metastable states. It has been shown[17,20] that both the primary and secondary scintillations emitted by argon-nitrogen gas mixture mainly belong to the second positive group of the nitrogen emission spectrum, which occurs as a result of the deactivation of nitrogen molecules in the C $^3\pi_u$ state to the B $^3\pi_g$ state. It is also important to note that out of all the emission bands shown in Fig.15 only the wavelength range of the second positive band falls within the spectral sensitive region of pyrex window photomultipliers.

The experimental values of the electron impact excitation cross-

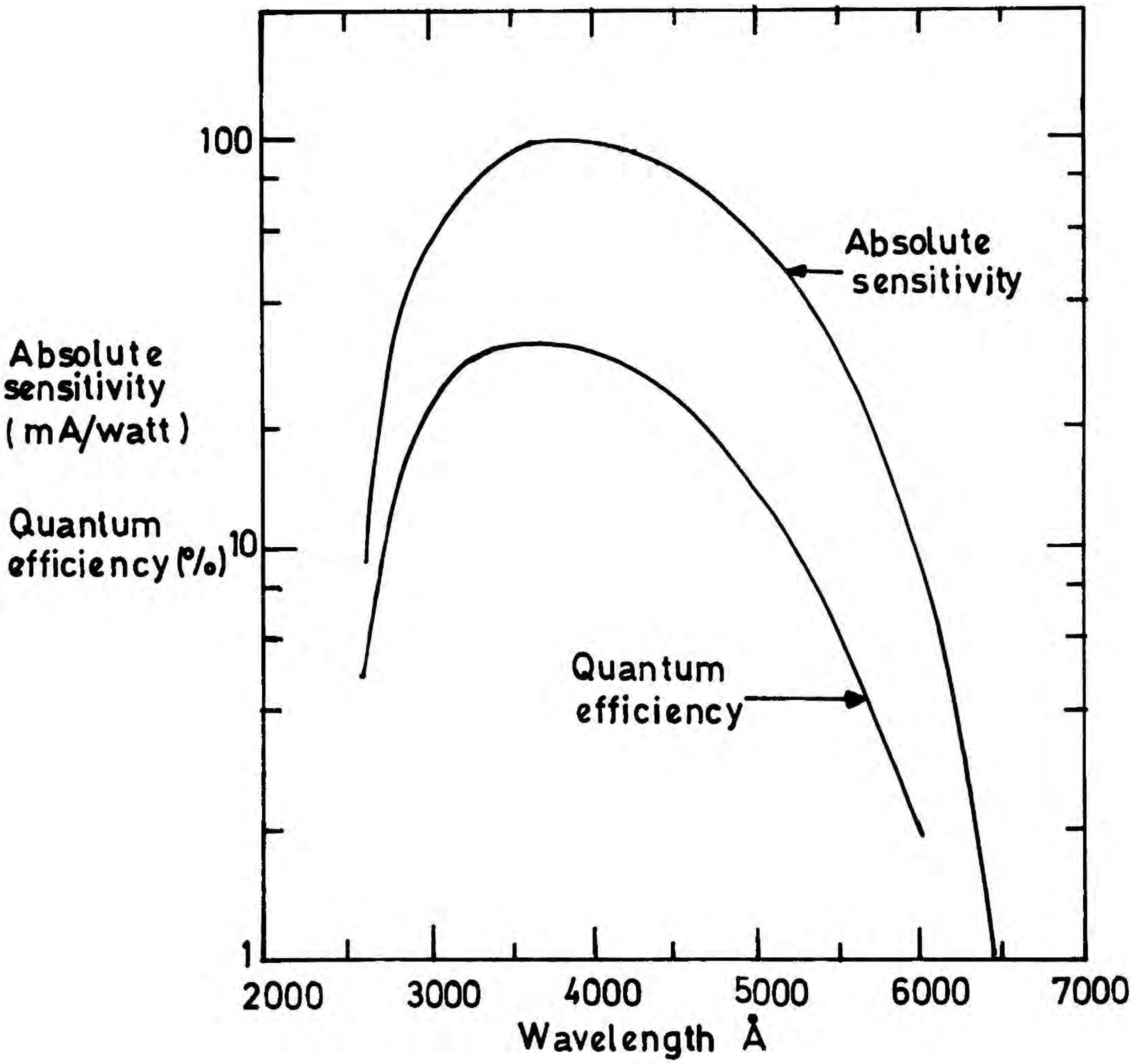

FIG.14 Photocathode spectral response characteristics of an RCA 8575 phototube.

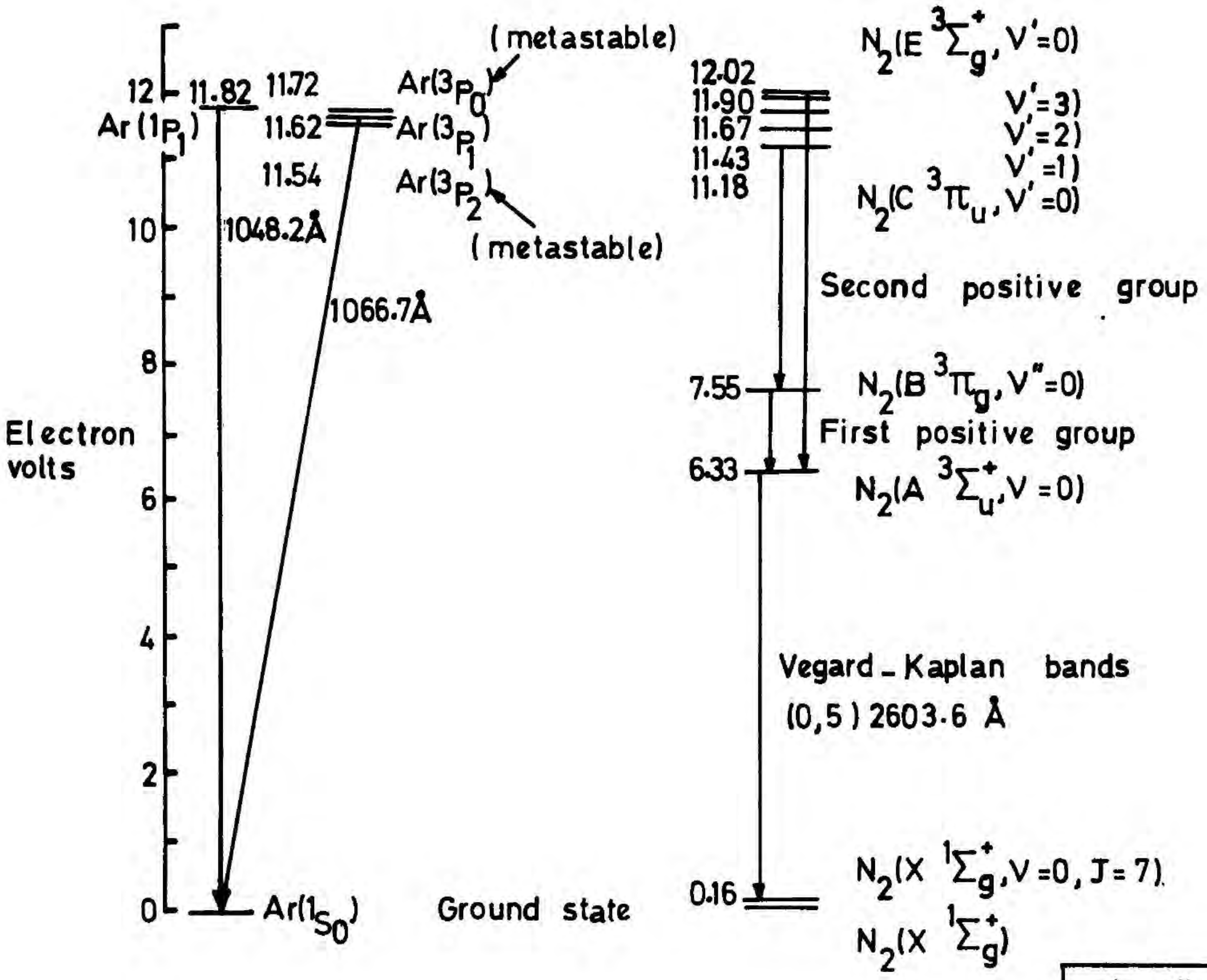

V'→V"	λ(Å)
(0→0)	3371
(0→1)	3577
(2→1)	3136
(3→1)	2964

FIG. 15 Some important energy levels of the argon – nitrogen system.

section for the 3p metastable states of argon[21] and the $C^3\pi_u$ state of nitrogen[22] show that for electron energies above 12 eV the cross-section values for argon are greater than that for nitrogen. For example, at 13 eV $\sigma_{Ar} \simeq 2\,\sigma_{N2} \simeq 0.6\ \text{Å}^2$ and at 16 eV $\sigma_{Ar} \simeq 6\sigma_{N2} \simeq 1.8\ \text{Å}^2$. The electron impact excitation also results in ${}^1P_1$ and ${}^3P_1$ argon resonance states,but with less efficiency, since the excitation cross-section[23] for these processes is smaller (0.14 Å^2) than that for metastable formation. It is therefore clear from the above cross-section values that as far as the formation of excited states by direct electron impact is concerned the formation of metastable states and resonance states in argon is much more likely than that of the "C" state ($C\ {}^3\pi_u$) of nitrogen, especially when the percentage of nitrogen in the mixture is small.

At low pressures it has been established[24-28] that the metastable states of argon transfer their energies by collision to the ground state nitrogen molecules to form the 'C' state of nitrogen.

$$Ar^*\left({}^3P_{2,0}\right) + N_2\left(X\,{}^1\Sigma_g^+\ ,\ \nu' = 0\right) \longrightarrow Ar(1S_0) + N_2^*\left(C\ {}^3\pi_u\ \ \nu' = 1\text{-}3\right) \quad (2.3)$$

This process is efficient (resonant) in argon-nitrogen mixtures since the metastable levels of argon are almost isoenergetic with the nitrogen 'C' state level. The collisional energy transfer from ${}^1P_1$ and ${}^3P_1$ argon resonance states to the ground state of nitrogen is small because of their small life times[29]. ($\tau_{{}^1P_1} = 0.24$nS, $\tau_{{}^3P_1} = 9.5$nS). The ${}^1P_1$ contribution is generally ruled out also, due to the violation of the Wigner Spin conservation rule during the transition. However Chen et al[30] have recently suggested a possible mechanism for collisional energy transfer from ${}^1P_1$ to nitrogen on the basis of the fact that the L-S coupling scheme does not apply rigorously to argon on account of it being a heavy atom.

At high pressures, apart from collisional energy transfer processes, the collisional quenching reactions play a major part in the destruction of argon metastable states. In general the main channels through which the dissipation of energy of the metastables occur are, (a) the formation of argon excimers (Ar_2^*), (b) collision of metastable atoms with the walls of the container and other objects present inside the container (in the case of the G.S.P.C. the only collision object is the anode wire and therefore this factor can be neglected), and (c) the collision of metastable atoms with nitrogen molecules to form products[26] other than the $C\ {}^3\pi_u$ state. The collision of metastable state argon atoms with ground state argon atoms causes two changes in the metastable population ; (1) the formation of excimers and thereby causing a reduction in the population, (2) overpopulation of the lowest metastable state (${}^3P_2$) [Collisional deactivations from neighbouring excited states (${}^3P_1 \rightarrow {}^3P_2$ and ${}^3P_0 \rightarrow {}^3P_2$)][30,31]. The contribution from collisions between argon excimers and ground state nitrogen molecules to the 'C' state of nitrogen is expected to be small, since the energy of the vibrational zero energy level of the triplet argon excimer[32] state is less than the energy of the 'C' state of nitrogen.

2.10 DEACTIVATION OF THE $C\ {}^3\pi_u$ STATE OF NITROGEN

As mentioned earlier in this chapter, the second positive emission of nitrogen occurs as a result of the radiative transitions between the $C\ {}^3\pi_u$ and $B\ {}^3\pi_g$ states. The radiative life time of the $C\ {}^3\pi_u$ state is generally short (τ_c = 39.6 + 2 nS)[33], since $C\ {}^3\pi_u \rightarrow B\ {}^3\pi_g$ is a strongly allowed transition. At low pressures the de-excitation of the 'C' state of nitrogen is mainly governed by radiative transitions. At high pressures ($p \sim 760$ Torr) the collisional quenching processes open more pathways through which the deactivation of the 'C' state of nitrogen can occur. The important collisional quenching mechanisms to be considered here are the collisions of the 'C' state nitrogen molecules with ground state argon atoms and nitrogen molecules. The collisions between excited 'C' state nitrogen and ground state nitrogen molecules have been studied by Millet et al[34] and Calo et al[35] and they have proposed the following mechanisms as possible quenching processes.

(1) electronic quenching

$$C\ ^3\pi_u + x\ ^1\Sigma_g^+\ (\nu' = o) \longrightarrow B\ ^3\pi_g + {}^1\Sigma_g^+\ (\nu' > o) \qquad (2.4)$$

(2) vibrational relaxation.

There is not much literature available on the $Ar\text{-}N_2(C)^3\pi_u$ quenching process except on the possible products of the reaction[36] and the rate of the process. All the important reactions subsequent to the excitation by primary electrons around the anode wire can be listed as follows :

The rate constant for each process is also given against the reaction.

Reaction	Rate Constant	Ref.	
$Ar^* + N_2 \xrightarrow{k_1} N_2(C) + Ar$	$6 \times 10^{-12}\ cm^3.sec^{-1}$	38	(2.5)
$Ar^* + N_2 \xrightarrow{k_2}$ Other products mainly $N_2(B) + Ar$	$3 \times 10^{-11}\ cm.^3sec^{-1}$	26,27,37	(2.6)
$Ar^* + 2Ar \xrightarrow{k_3} Ar_2^* + Ar$	$6 \times 10^{-33}\ cm^6.sec^{-1}$	31	(2.7)
$N_2(C) \xrightarrow{k_4} N_2(B) + h\nu$	$2.5 \times 10^7\ sec^{-1}$	33	(2.8)
$N_2(C) + N_2 \xrightarrow{k_5}$ Other products mainly $N_2(B) + N_2$	$1.15 \times 10^{-11}\ cm.^3sec^{-1}$	34	(2.9)
$N_2(C) + Ar \xrightarrow{k_6}$ Other products mainly $N_2(B) + Ar$	$5.6 \times 10^{-13}\ cm.^3sec^{-1}$	36	(2.10)

where Ar^* represents the Argon metastable states

Ar_2^* " " " excimer state

$N_2(C)$ " " $C\ ^3\pi_u$ state of nitrogen

$N_2(B)$ " " $B\ ^3\pi_g$ " "

and k^s represent the rate constants.

2.11 THE EFFECT OF QUENCHING PROCESSES ON THE SCINTILLATION PULSE

One of the main factors which determines the ultimate rate in fast scintillation counting is the width of the scintillation pulse. Pure noble gases, as used in the early work on the scintillation counters, are not suitable for fast counting work since the metastable states have life times of the order of microseconds, giving rise to pile-up problems at high rate. In order to make the noble gases 'fast' in scintillation counting studies, the long lived metastable states should be destroyed and this could be done by adding molecular gases to the noble gases. The addition of nitrogen to argon serves this purpose with some added advantages mentioned earlier in this chapter. The addition of nitrogen to argon reduces the life times of all the excited states present in argon as well as in nitrogen itself through various de-excitation processes described in the previous section. The overall effect of these processes can be seen as a reduction in the width as well as the amplitude of the scintillation output. The dependence of the life time of a given excited state on various decay channels can be investigated by studying the total transition rate from that state. Furthermore, the dependence of life times of excited states on the pressure and the composition of the gas mixture (argon-nitrogen) can also be predicted from these studies since the transition rates are a function of the relative concentrations of the constituents of the mixture.

Suppose $\left[Ar\right]$ and $\left[N_2\right]$ represent the number density of molecules (cm^{-3}) present in an argon-nitrogen mixture whose relative composition is known, and let $\left[Ar^*\right]$ be the concentration of metastable states of argon at a given time.

The overall decay rate of the argon metastable states at any time can be written as the sum of the individual decay rate of the processes represented by equations (2.5), (2.6) and (2.7).

$$\frac{d}{dt}\left[Ar^*\right] = k_1\left[N_2\right]\left[Ar^*\right] + k_2\left[N_2\right]\left[Ar^*\right] + k_3\left[Ar\right]^2\left[Ar^*\right]$$

$$= K\left[Ar^*\right] \qquad (2.11)$$

where K is the overall decay constant.

Since the life time of the metastable state is $\frac{1}{K}$ (= $\tau_{metastable}$) then from equation (2.11),

$$\tau_{metastable} = \frac{1}{k_1\left[N_2\right] + k_2\left[N_2\right] + k_3\left[Ar\right]^2} \qquad (2.12)$$

The variationsof the life time of the metastable states ($\tau_{metastable}$) with the nitrogen concentration and the total pressure of the argon-nitrogen mixture are shown in Figs. 16 and 17. The rapid fall off in life time of the metastable states at small nitrogen concentrations clearly shows the metastable quenching ability of nitrogen. It must be mentioned here that this analysis is only an approximate one since it only deals with the major collision processes.

It can be seen from the above expression for $\tau_{metastable}$ that the last two terms in the denomenator predominate over the first term at high pressures and as a result the scintillation efficiency decreases. This fact is illustrated in Figs. 18a, b, which show the ratio r as a function of pressure (for 10% N_2 mixture) and nitrogen concentration.

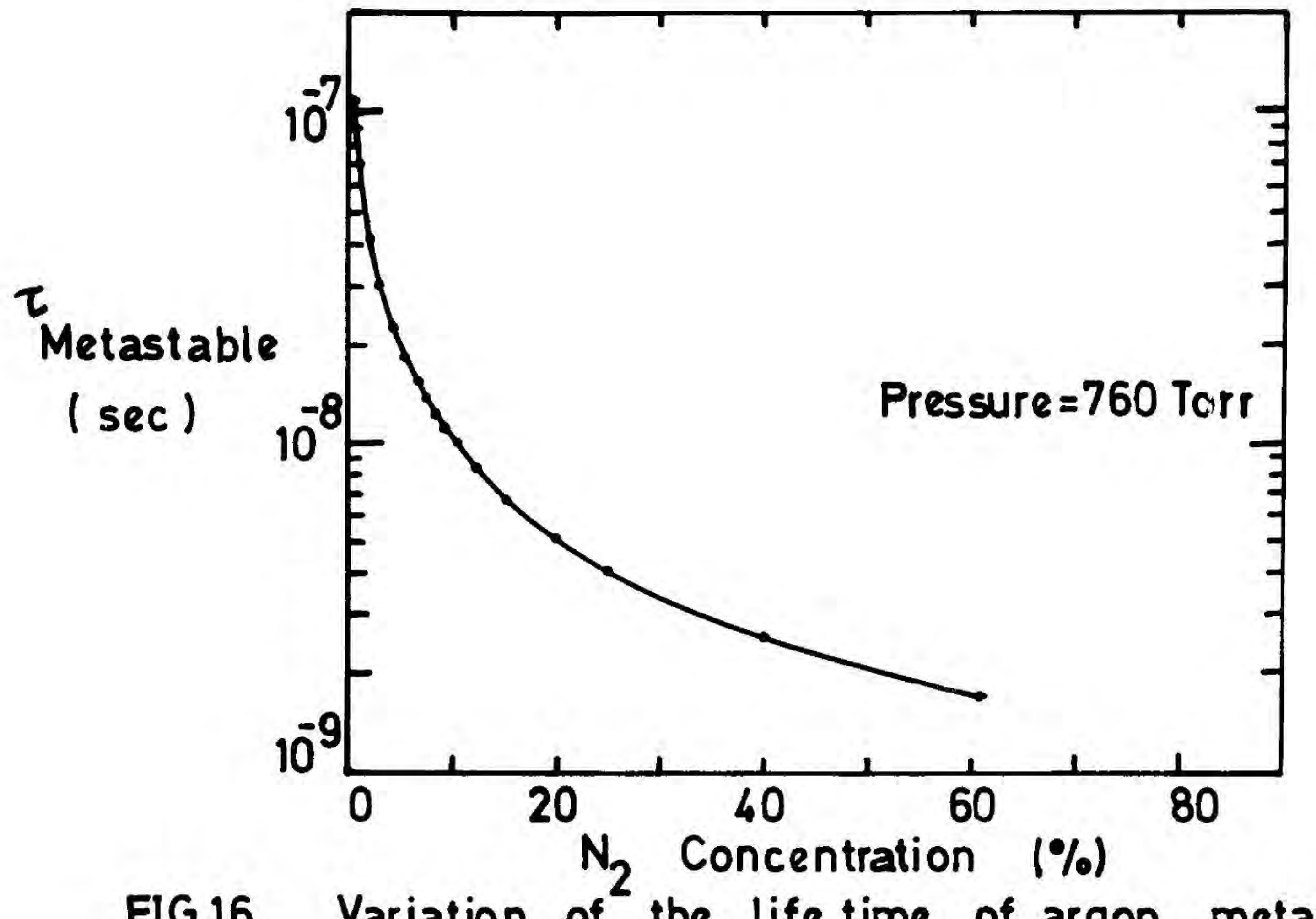

FIG.16 Variation of the life time of argon metastable state ($3P_2$) with N_2 concentration.

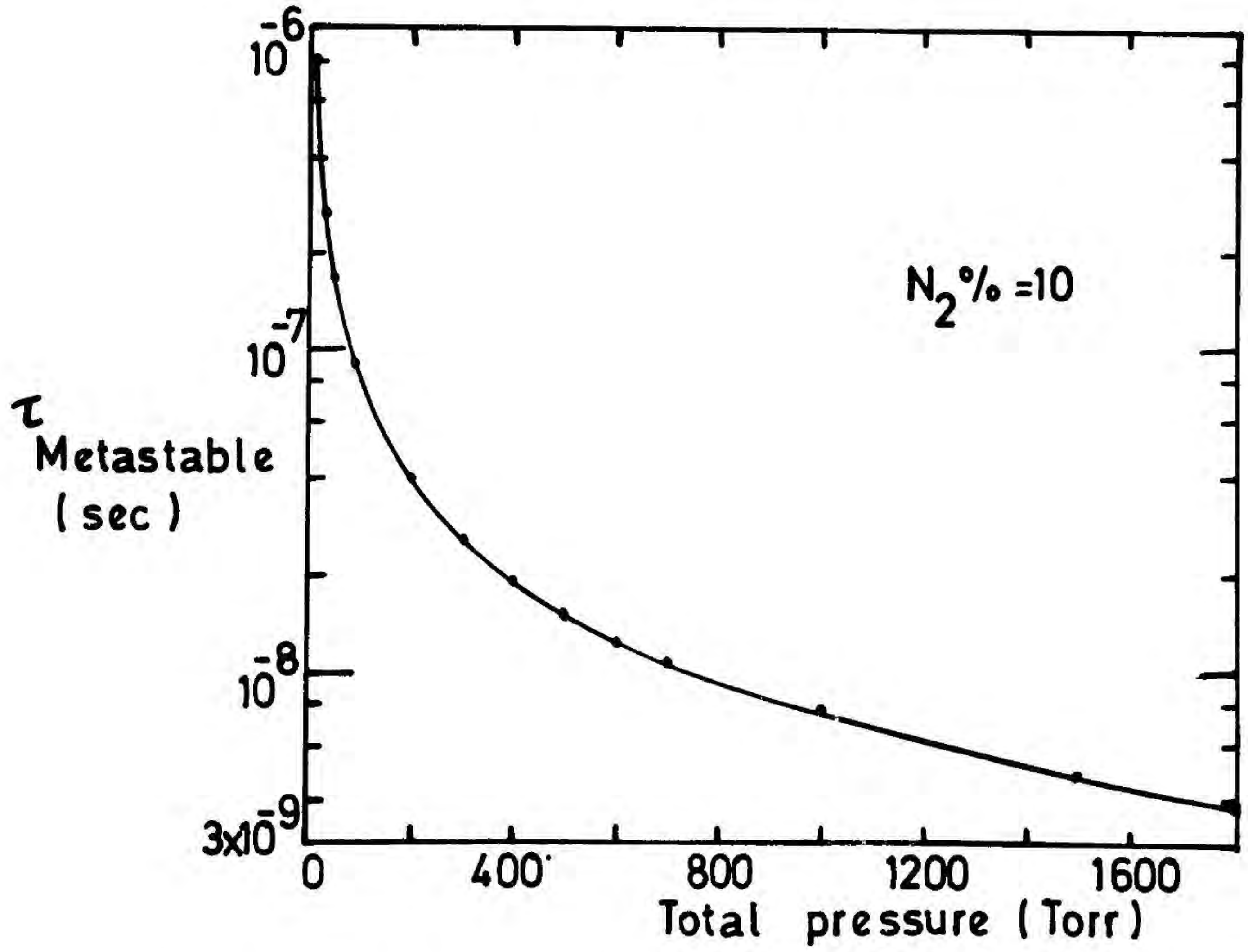

FIG 17 Variation of the life time of argon metastable state ($3P_2$) with total pressure.

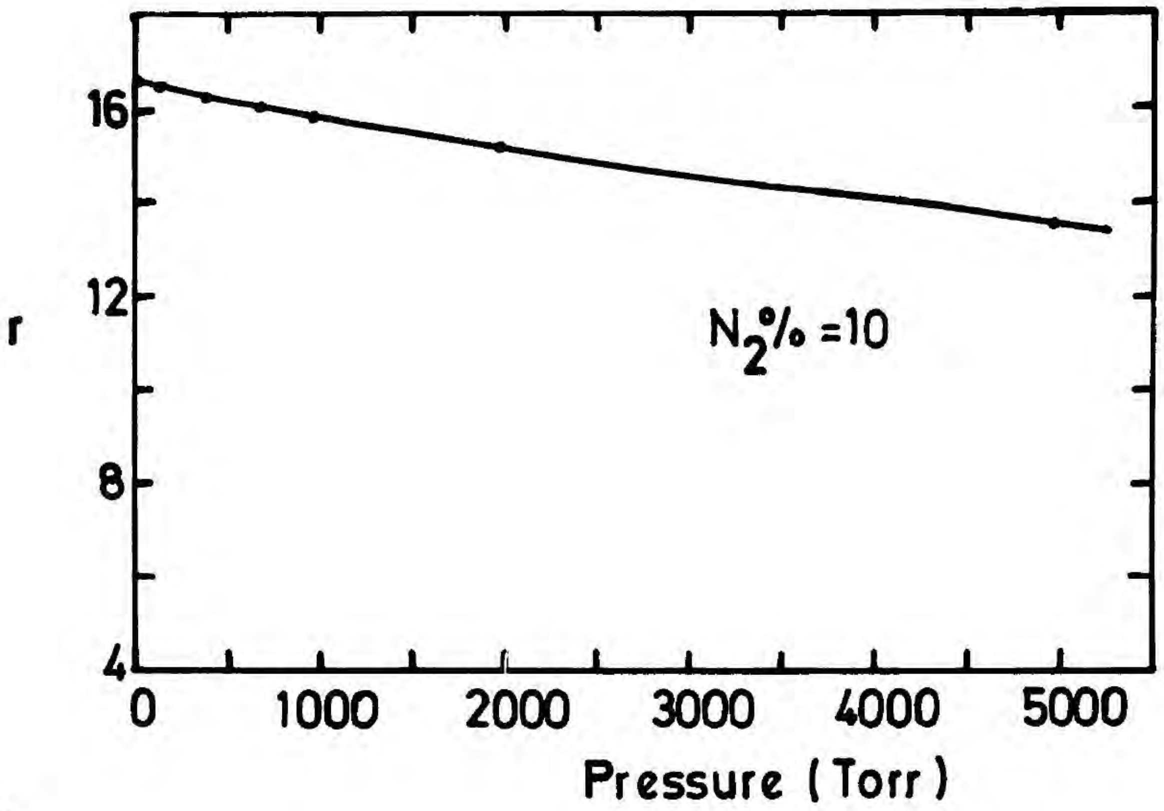

FIG.18 a

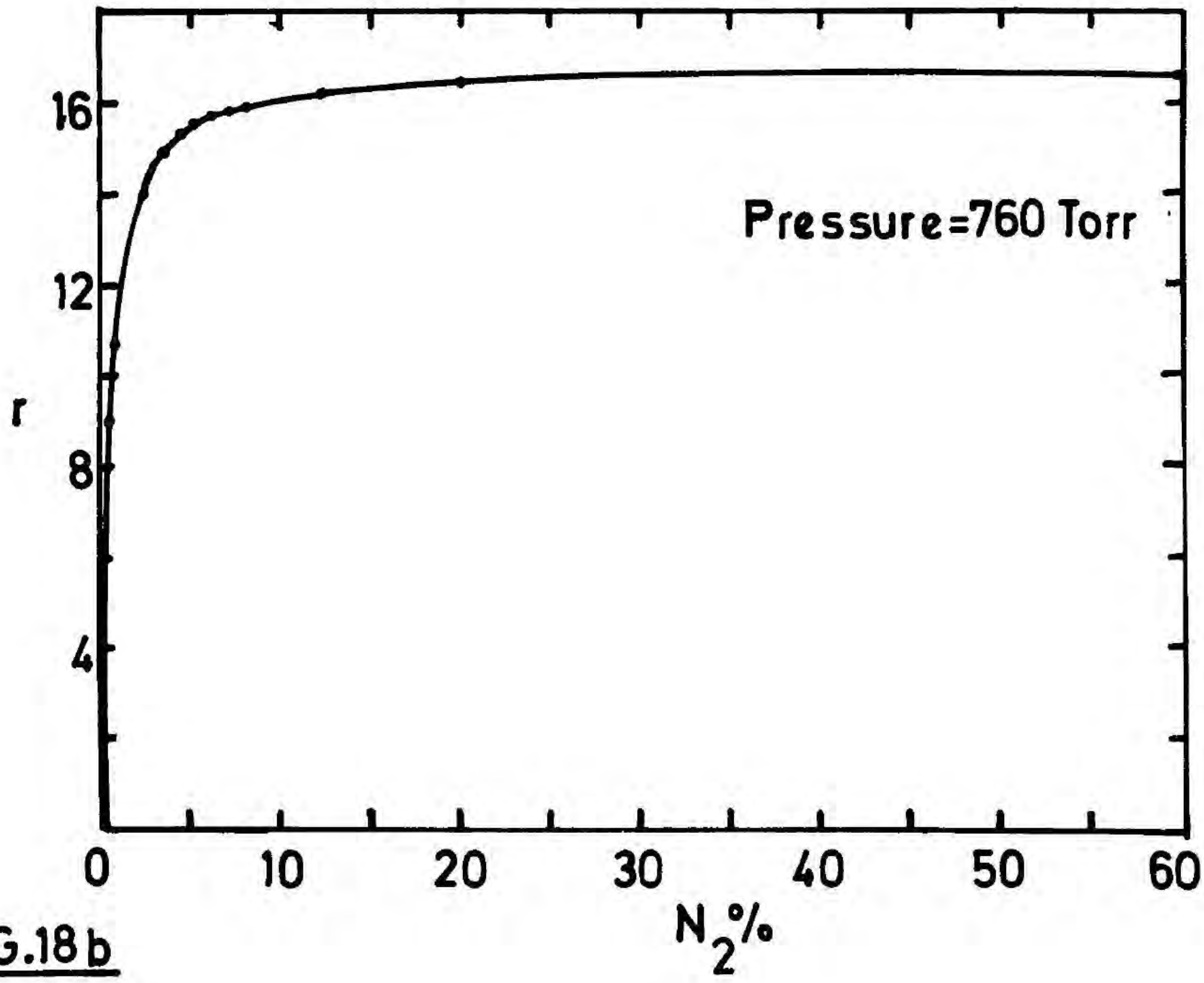

FIG.18 b

FIGS.18 a&b r as a function of total pressure and N_2 concentration in the mixture.

where $r = \dfrac{\text{Rate of } N_2\text{ (C) formation}}{\text{Total Ar}^*\text{ destruction rate}} = \dfrac{k_1\left[N_2\right]}{k_1\left[N_2\right] + k_2\left[N_2\right] + k_3\left[Ar\right]^2}$

Once the long lived metastable states have been quenched, the width of the scintillation pulses become a function of the life time of the $C\ {}^3\pi_u$ state of nitrogen. The life time of the $C\ {}^3\pi_u$ state $\left(\tau\ N_2(C)\right)$ can be derived from the following expression

$$\frac{d}{dt}\left[N_2\ (C)\right] = k_4\left[N_2(C)\right] + k_5\left[N_2\right]\left[N_2(C)\right] + k_6\left[N_2(C)\right]\left[Ar\right]$$

$$= \frac{1}{\tau_{N_2(C)}}\left[N_2(C)\right]$$

$$\therefore \quad \tau_{N_2(C)} = \frac{1}{k_4 + k_5\left[N_2\right] + k_6\left[Ar\right]} \qquad (2.13)$$

It shows that $\tau_{N_2(C)}$ depends only on the quenching rates of nitrogen and argon, and since $k_5 >> k_6$, even a small addition of nitrogen to argon should decrease both the width and the amplitude of the scintillation pulse. The dependence of $\tau_{N_2(C)}$ on the nitrogen concentration and pressure (for 10% N_2 gas mixture) are shown in Figs. 19 and 20.

The above analysis indicates that in fast scintillation counting, if both high rate capability and a good resolution are required, a compromise between the width and the amplitude of the pulse must be made, since the reduction in pulse amplitude due to the collisional quenching processes leads to the deterioration of the energy resolution of the counter. The results obtained in this analysis cannot be related to the actual (physical) scintillation pulses since the time dependence of formation of the scintillation pulses have been excluded in these calculations.

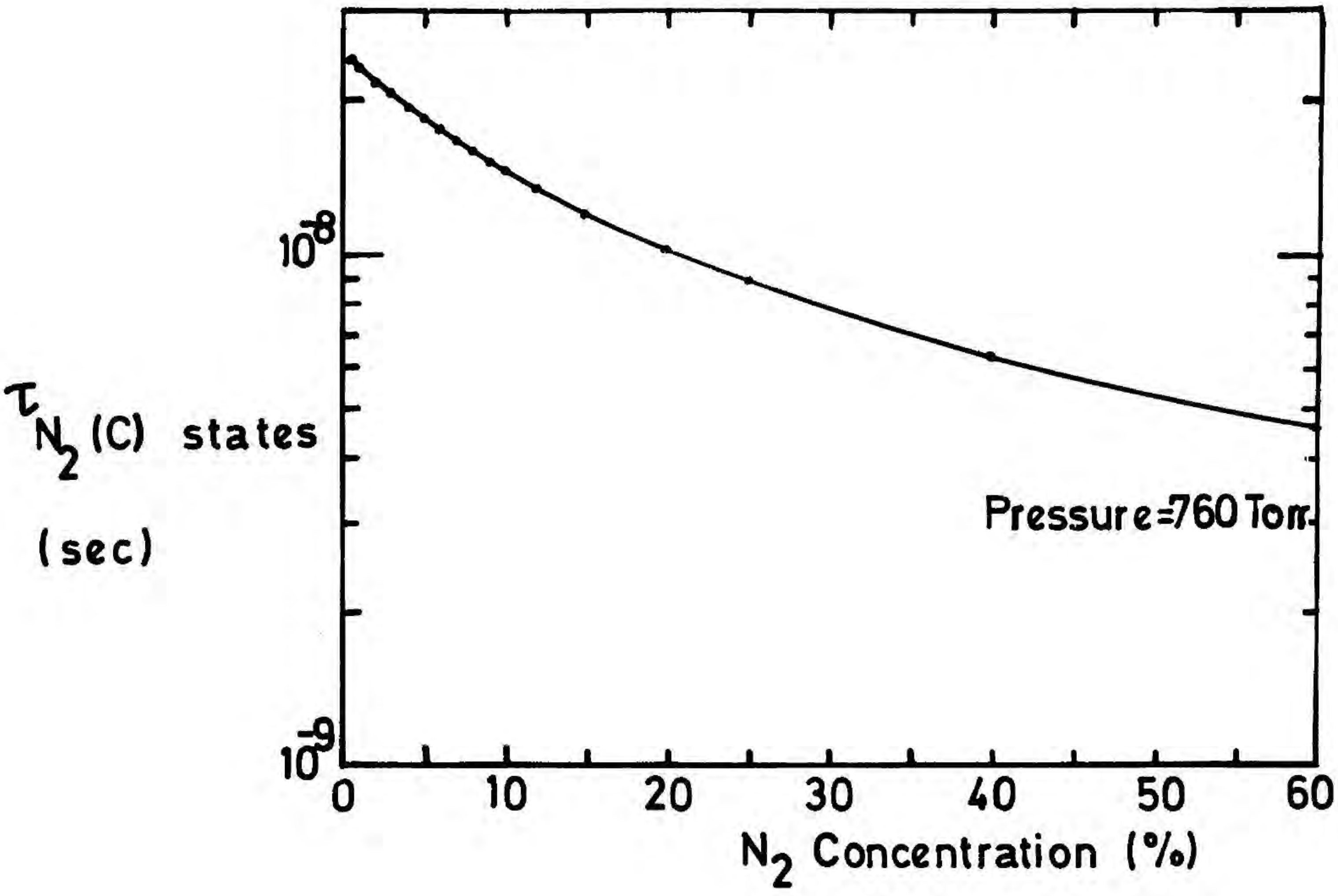

FIG.19

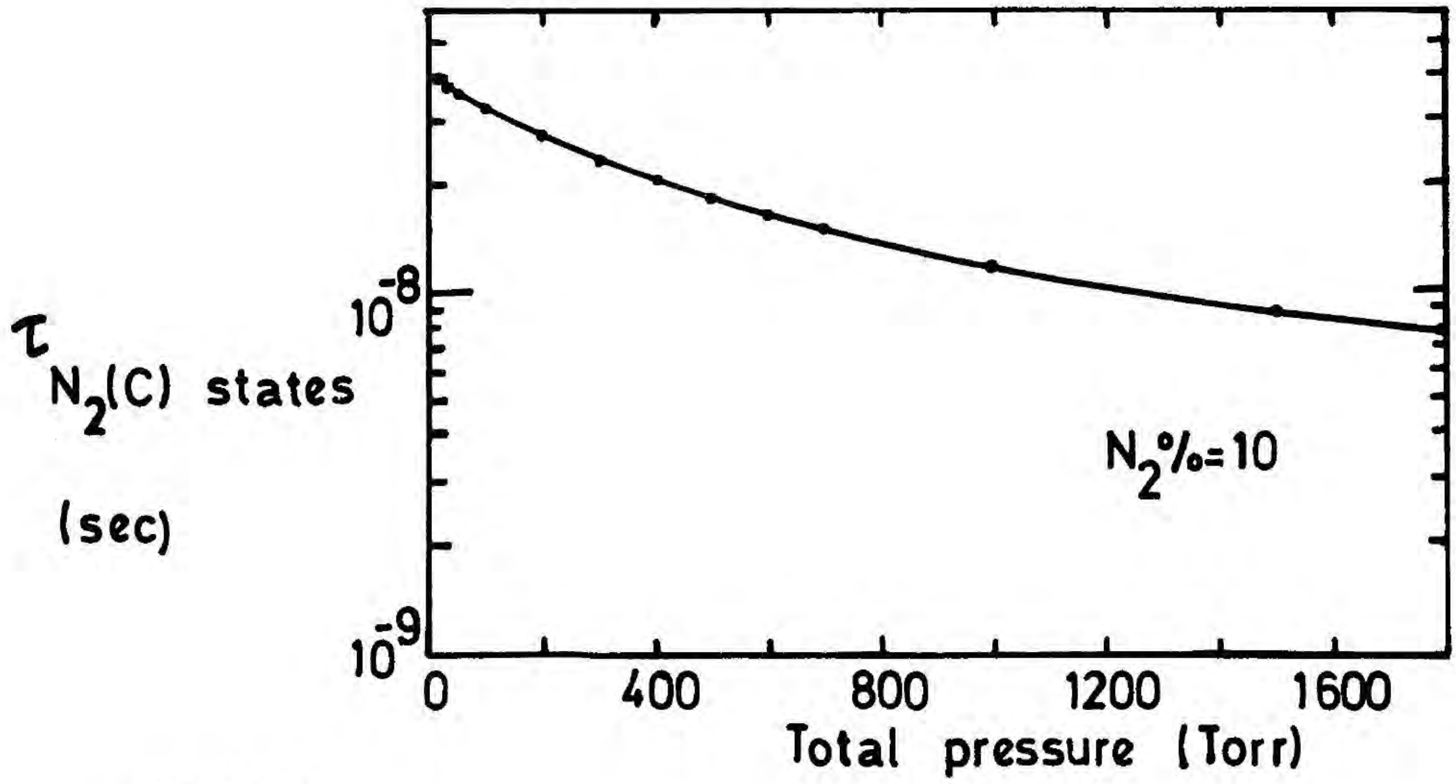

FIG.20

FIGS.19& 20 Variation of life time of the N_2(C) states with N_2concentration and total pressure of the mixture.

Chapter 2 - References

1. O.Svelto and D.C.Hanna, Principles of Lasers, Plenum Press,1976.
2. S.K.Searles and G.A.Hart, Appl. Phys. Lett. 25 (1974) 79.
3. P.G.Wilkinson, Can. J. Phys. 45 (1967) 1715.
4. S.K.Searles, Appl. Phys. Lett. 25 (1974) 735.
5. K.Schmidt, Z. Naturforsch, 11a (1956) 1023.
6. J.B.Birks, The Theory and Practice of Scintillation Counting, Pergamon Press,London, (1964) p 578.
7. J.A.Northrop, and J.C.Gursky, Nucl. Instr. and Meth. 3 (1958) 207.
8. A.Sayres and C.S.Wu, Rev. Sci. Instr. 28 (1957) 758.
9. J.B.Birks, The Theory and Practice of Scintillation Counting, Pergamon Press, London, (1964) p 596.
10. R.L.Platzman, Intern. J Appl.Radn. Isotopes 10 (1961) 116.
11. J.B.Birks, T.A.King, I.H.Munro, Proc. Phys. Soc. 80 (1962) 355.
12. T.D.S.Hamilton, Proc. Phys. Soc. B70 (1957) 144.
13. S.H.Liebson, M.E.Bishop and J.O.Elliot, Phys. Rev. 80 (1950) 907.
14. R.K.Swank and W.L.Buck, Rev. Sci. Instr. 26 (1955) 15.
15. J.A.Northrop, Rev. Sci. Instr. 29 (1958) 437.
16. M.A.Biondi, Phys. Rev. 83 (1951) 1078.
17. T.D.Strickler and E.T.Arakawa, J. Chem. Phys. 41 (1964) 1783
18. A.E.Grün and E.Schopper, Z Naturforsch 9a (1964) 134.
19. A.J.P.L.Policarpo, C.A.N.Conde, M.A.F.Alves, Nucl. Instr. & Meth. 58 (1968) 151.
20. A.J.P.L.Policarpo, M.A.F.Alves and C.A.N.Conde, Nucl. Instr. and Meth. 55 (1967) 105.
21. C.R.Lloyd, E.Weigold, P.J.O.Teubner and S.T.Hood, J. Phys. B Atom. Molec. Phys. 5 (1972) 1712.
22. D.C.Cartwright, S.Trajmar, A.Chutjian and W.Williams, Phys. Rev. A16 (1977) 1041.

23. C.R.Lloyd, P.J.O.Teubner, E.Weigold, S.T.Hood, J. Phys. B. 5 (1972) L44.

24. D.H.Stedman and D.W.Setser, J. Chem Phys. 52 (1970) 3957.

25. E.S.Fishburn, J. Chem. Phys. 47 (1967) 58.

26. D.W.Setser and D.H.Stedman, J. Chem.Phys. 53 (1970) 1004.

27. L.G.Piper, J.E.Velazco and D.W.Setser, J. Chem. Phys. 59 (1973) 3323.

28. M.Touzeau and D Pagnon, Chem. Phys. Lett. 53 (1978) 355.

29. E.Ellis and N.D.Twiddy, J. Phys. B (Atom.Molec.Phys.) 2 (1969) 1366.

30. C.J.Chapman, A.J.Masson and R.P. Wayne, Mol. Phys. 23 (1972) 979.

31. J. Le Calve and M.Bourene, J. Chem. Phys. 58 (1973) 1446.

32. Y.Tanaka and K.Yoshino, J. Chem. Phys. 53 (1970) 2012.

33. A.W.Johnson and R.G.Fowler, J. Chem. Phys. 53 (1970) 65.

34. P.Millet, Y.Salerrero, H.Brunet, J. Galy, D.Blanc, and J.L.Teyssier, J.Chem. Phys. 58 (1973) 5839.

35. J.M.Calo and R.C.Axtmann, J. Chem. Phys. 54 (1971) 1332.

36. V. Puech, F.Collier and P.Cottin, J. Chem. Phys. 67 (1977) 2887.

37. J.R.McNeely, G.S.Hurst, E.B.Wagner, and M.G.Pyane, J. Chem. Phys. 63 (1975) 2717.

38. S.K.Searles, and G.A.Hart, Appl. Phys. Lett. 28 (1976) 384.

CHAPTER THREE

CONSTRUCTION AND OPERATION OF GAS SCINTILLATION DRIFT COUNTERS

3.1 INTRODUCTION

It is appropriate in this chapter to provide a detailed account of the design considerations and the construction techniques used in building a high rate gas scintillation drift counter. This will also include some of the mechanical, electrical and optical properties of the system. The geometrical design of the counter does not involve any specific requirements such as fitting to a beam line or to a large experimental system since it has been built entirely for laboratory tests. However, it was perfectly compatible for use with the X-ray machines in Durham.

In order to provide a comprehensive background knowledge, the latter part of this chapter is mainly devoted to a description of the principles of operation of the scintillation drift chamber and some factors affecting its performance at high rate. Some properties of the counter are also given at the end of the chapter.

3.2 DESIGN CONSIDERATIONS

Basically the gas scintillation counter is a combination of a conventional proportional counter and a photomultiplier. In this study, instead of a cylindrical proportional counter, it was decided to use a planar wire counter largely because this type of counter including the drift counter has already been extensively studied at Durham, and also because of some other advantages which will be described later in this section.

A schematic diagram of a gas scintillation counter is shown

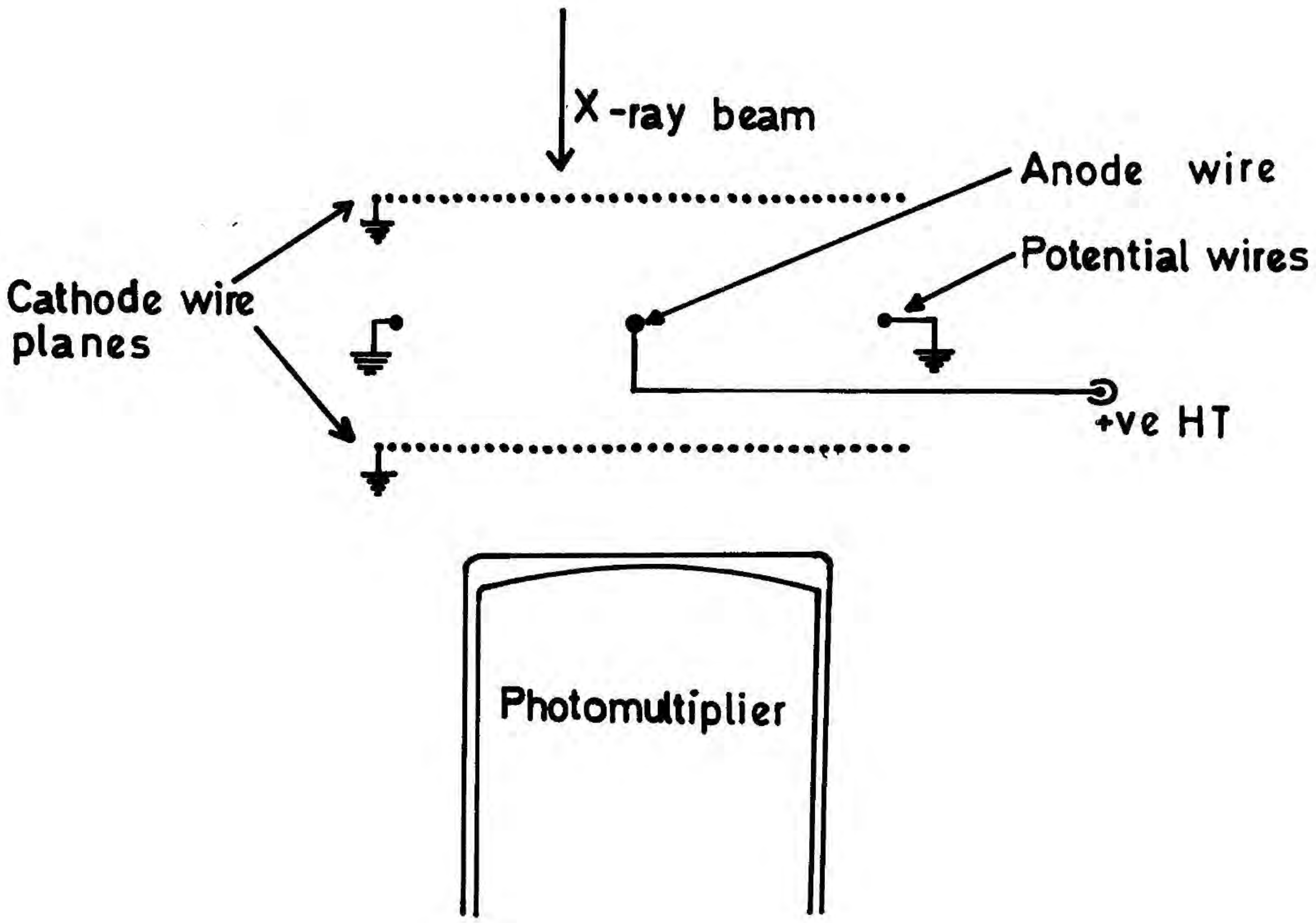

FIG.1 Section through gas scintillation proportional chamber.

in Fig.1. The only difference between the conventional proportional counter and the proportional counter used in the scintillation mode is that the diameter of the anode wire used in the latter type is much larger than that of the former. The large diameter anode wires are used in scintillation counters simply to obtain large excitation regions with minimum ionization around the wire. The electric field around the anode wire of a cylindrical proportional counter as a function of the distance from the centre of the wire for different wire diameters is shown in Fig.2. The anode potential and the cathode radius of this hypothetical counter are 2000 V and 7 mm. It is clear from Fig.2 that large diameter wires can create electric fields which are just sufficient to produce secondary excitations of atoms over a substantial region without producing much ionizations. This is to be contrasted with small diameter wires where a very high field, sufficient to produce ionization,occurs. However, extremely large diameter wires are not suitable for high rate counters since their wide excitation regions result in wide pulse widths.

One of the most important requirements which should be fulfilled in the secondary light production process is the localisation of the excitation process to a very small region on the anode wire. This ensures that the same light collection efficiency exists for all the X-ray photons converted in the chamber irrespective of their position of conversion.

If the path of the X-ray beam is very close to the anode wire as shown in Fig.3, the light collection efficiency of the counter strongly depends on the point of conversion of the X-ray photons in the gas medium. This is due to the fact that the primary electrons produced by the photons converted in the upper half of the counter drift towards the top half of the anode wire surface which obscures the photocathode of the photomultiplier and prevents the secondary light reaching the photocathode.

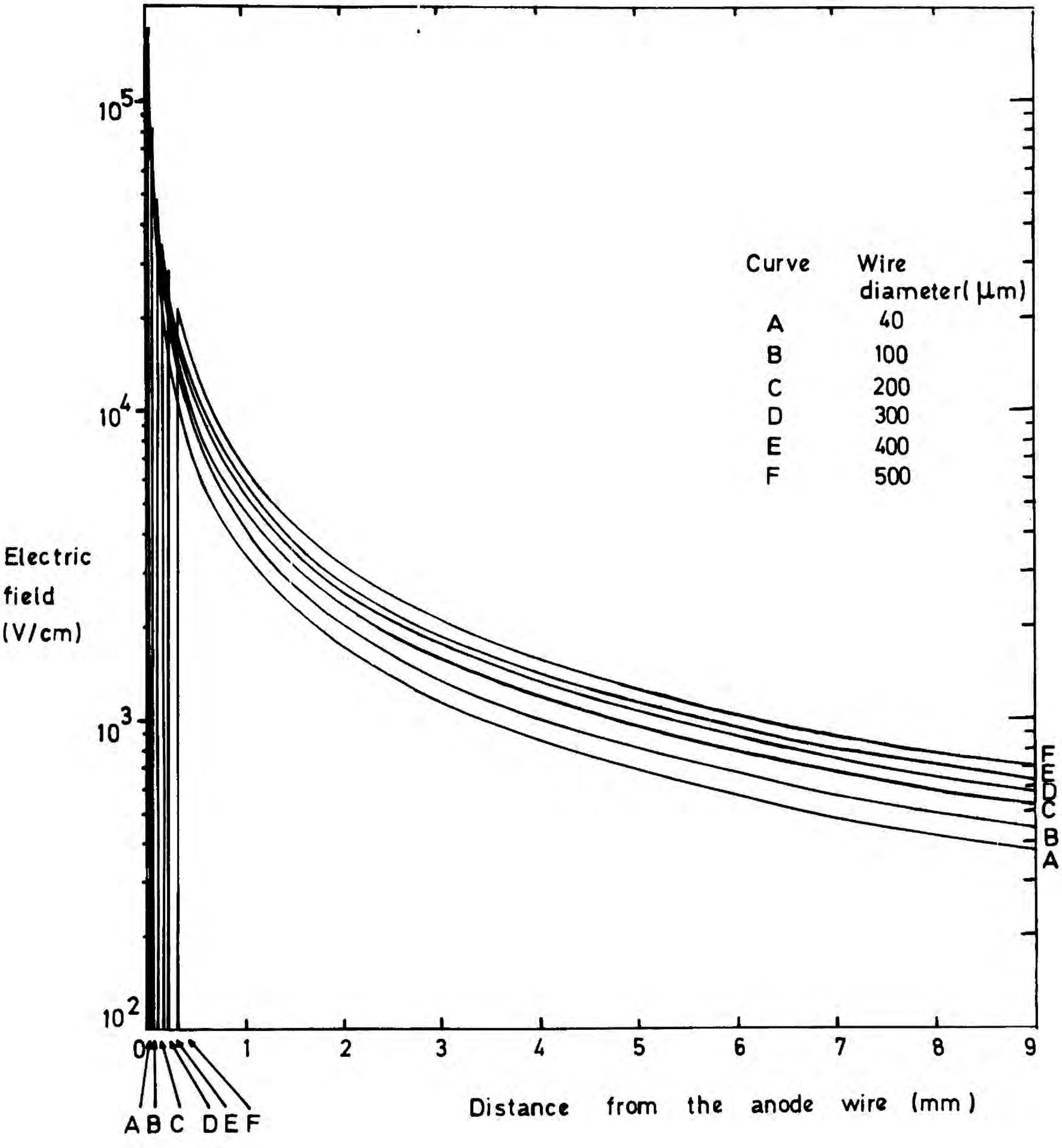

FIG. 2 Electric field around the anode wire of a cylindrical proportional chamber.

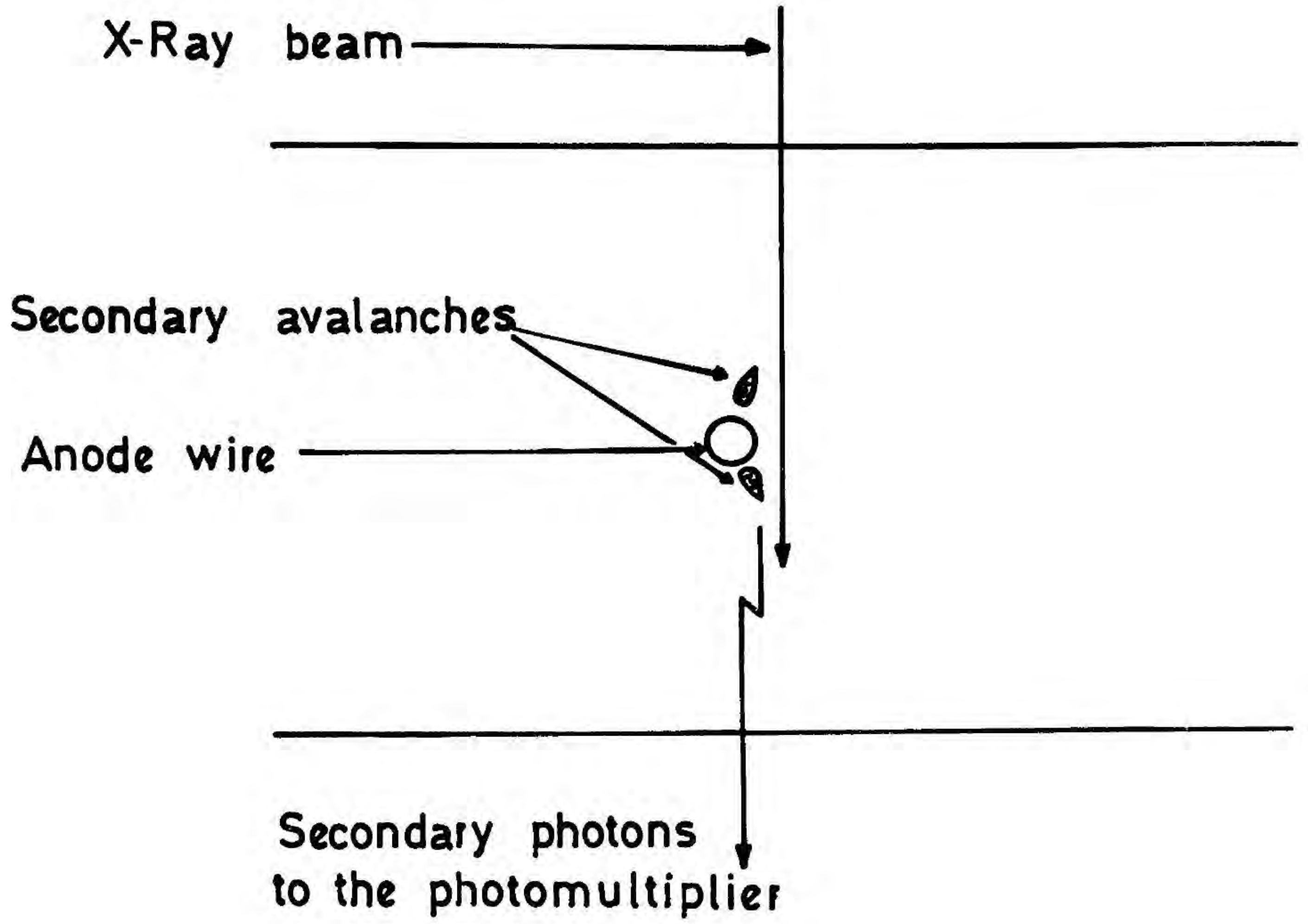

FIG.3 Passage of the X-ray beam close to the anode wire.

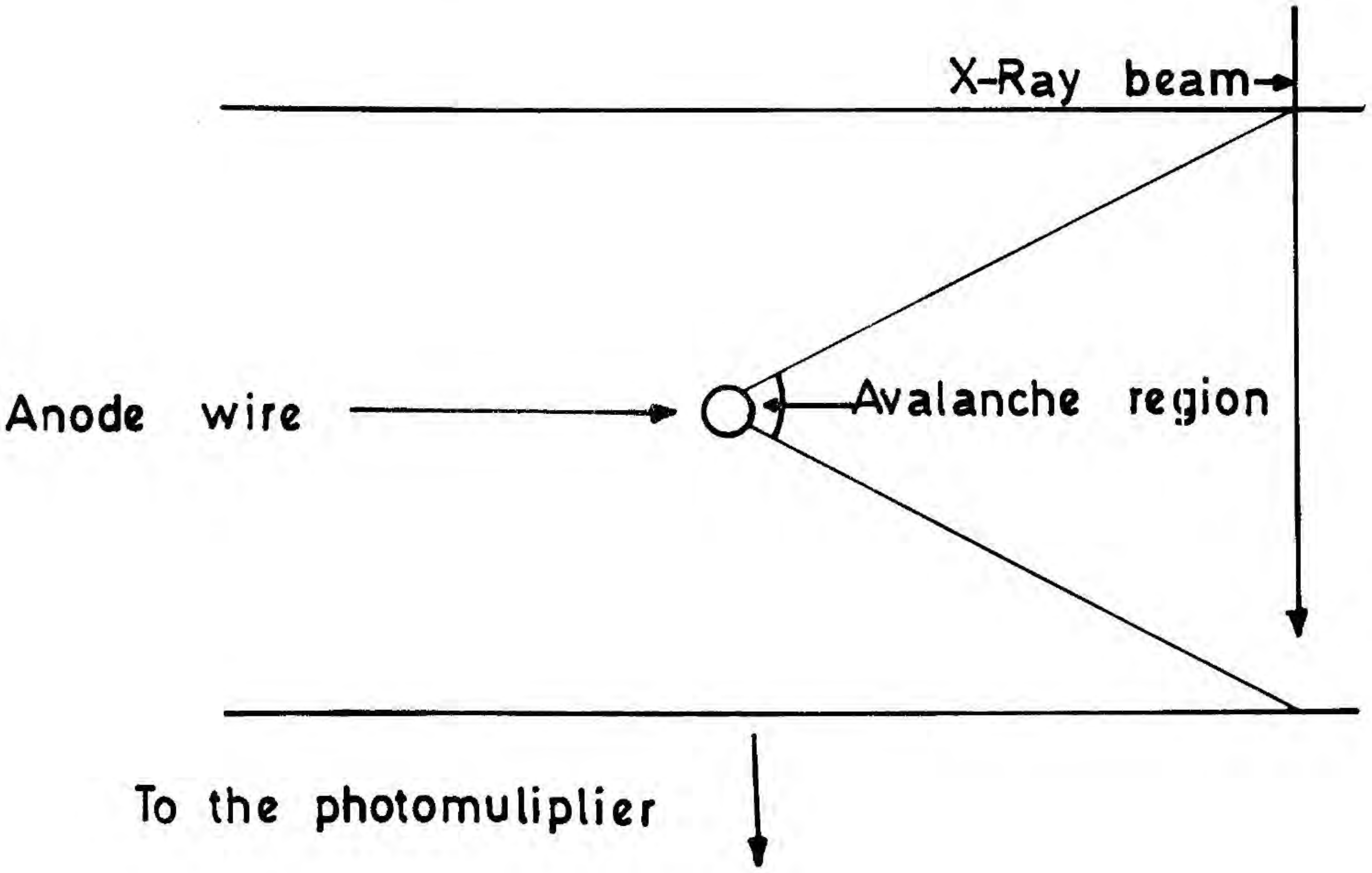

FIG.5 Passage of the X-ray beam away from the anode wire.

This effect is significant as the light is essentially produced near the wire, within a region with dimensions comparable to the diameter of the wire. The secondary light reaching the photocathode under this situation is only the light reflected from the window and the walls of the counter. On the other hand most of the light produced by X-rays converted in the lower half can reach the photocathode and produce bigger pulses than those due to the upper half since in this case the secondary excitations take place close to the lower half of the anode wire surface.

This effect has been observed by Policarpo(1) et al who obtained a light pulse height spectrum with two peaks for a single peak on the charge pulse spectrum. They managed to cut down the smaller light peak to 2% of the larger peak by reducing the reflected component of the secondary light reaching the photomultiplier. This method should reduce the efficiency of the system, however, as it counts the X-rays converted only in the lower half of the counter. We also observed a similar behaviour (see Fig.4a) with a proportional scintillation counter used in the preliminary tests(2), but we were able to obtain a single peak in two ways ; either by shifting the X-ray beam away from the anode wire, (see Fig.5) or by applying a potential of appropriate polarity to one of the cathode planes to change the electric field in one side of the wire to compensate the light loss due to shadowing of the photocathode. The second method is however not suitable since it modifies the radial field around the anode wire. An added disadvantage in allowing an X-ray beam close to the anode wire is that in this case the light production in the top and bottom halves of the anode wire is susceptible to any slight asymmetry in the anode wire position in the direction normal to the cathode planes. On the other hand, when the path of the beam is not

FIG. 4a Double peak formed by a G.S.P.C for monoenergetic X-rays.

FIG. 4b Pulses from a G.S.P.C (without additional drift field).

FIG. 4c Same pulses after adding a drift field of 500 V/cm.

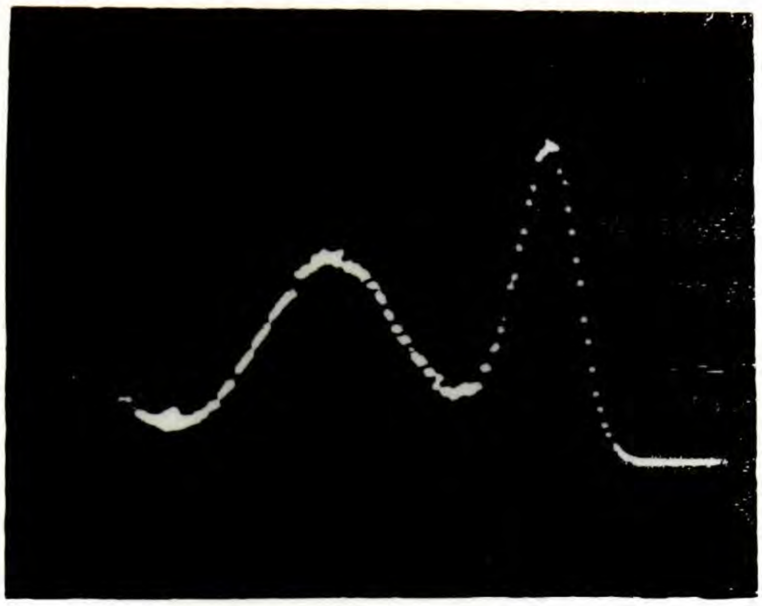

FIG. 4a

Horizontal: 20 ns/div

Vertical: 50 mV/div

FIG. 4b

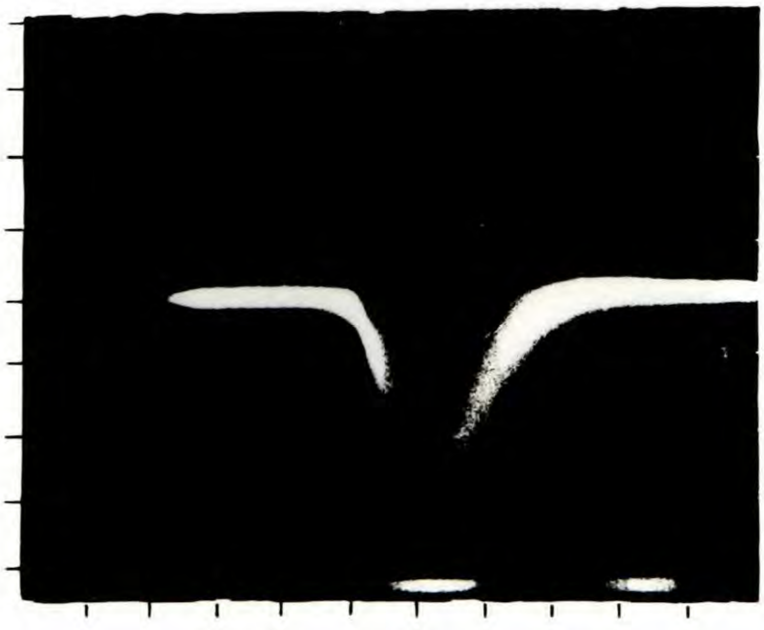

Horizontal: 20 ns/div

Vertical 50 mV/div

FIG. 4c

close to the anode wire as shown in Fig.5, the secondary light production is confined to a small region on one side of the anode wire and therefore a reasonably constant light collection efficiency can be expected for all the X-ray photons converted in the counter irrespective of their position of conversion.

In such a system, however, the weak electric field in the region where conversion of X-rays takes place results in long electron collection times giving rise to long light pulses due to the diffusion effect, (see Fig.4b). This is obviously an undesirable feature for a high rate counter. This system can be improved by employing an additional adjustable drift field towards the anode wire without making appreciable modification on the original electric field around the wire (see Fig.4c). According to this idea first put forward by Charpak$^{(3)}$ et al, the cathode planes consist of wires parallel to the anode wire and held at increasingly negative potentials starting from zero at the wires directly above and below the anode wire. The effect of this modification on a conventional wire proportional chamber is shown in Fig.6. Curve A shows the electric field across the proportional chamber as a function of the distance (r) from the anode wire and curve B represents the resultant field when the cathode wires are connected to the increasingly negative potentials to produce a drift field. In this case the potential wires are also connected to the maximum negative cathode potential. Curve C shows the same resultant field without the potential wires. The distance from the anode to the cathode plane and to the potential wires of this hypothetical chamber are 6 mm and 24 mm respectively. It is clear from these curves that the drift field inside a drift chamber is much higher than that inside a proportional chamber especially for large r where the drift field is mainly determined by the applied drift voltage. Because

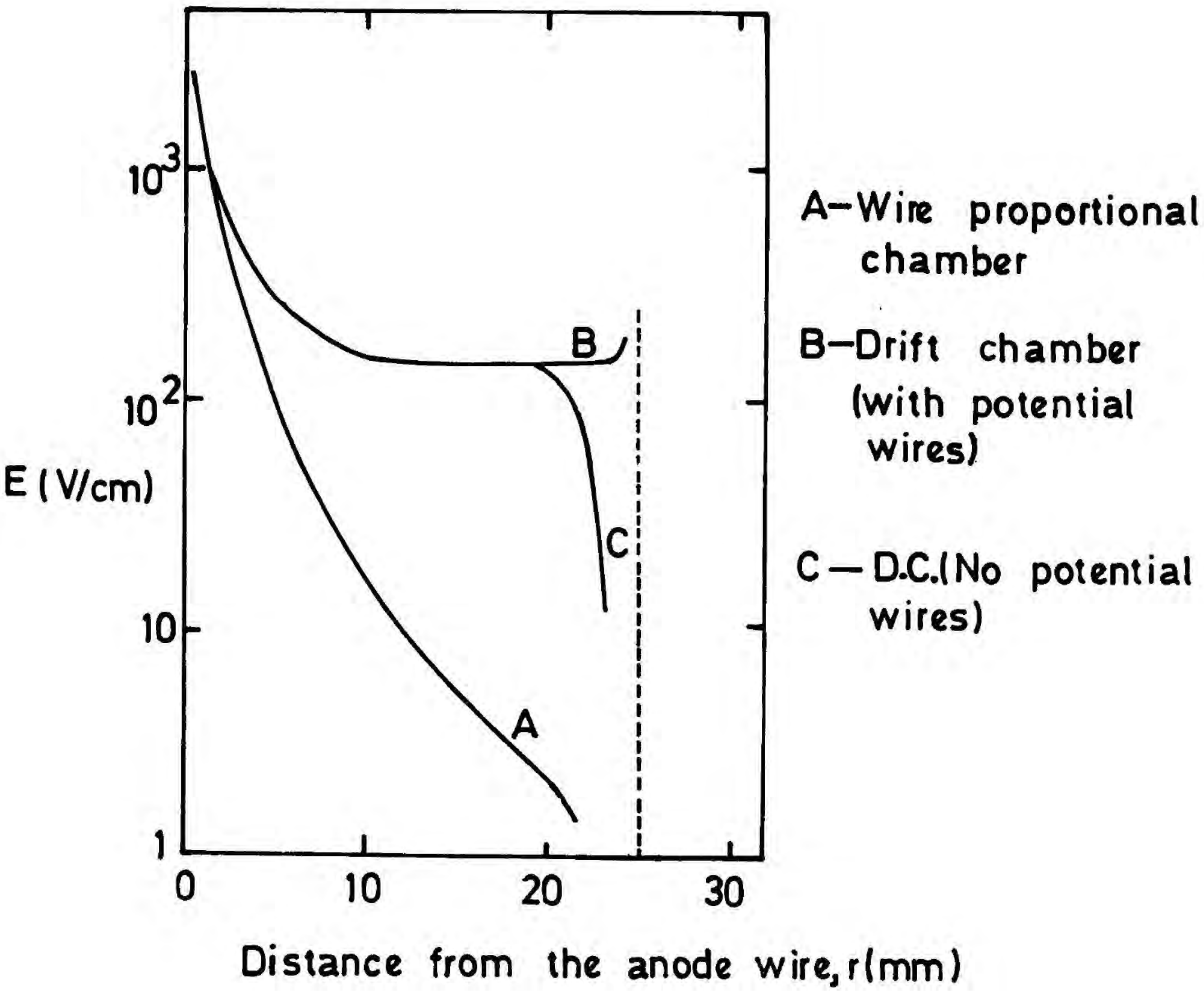

FIG. 6 Electric field variations inside the wire chambers.

of these advantages, it was decided to develop a gas scintillation drift counter (G.S.D.C.) as a high rate counter.

3.2.1 Counter Design

The techniques and most of the materials employed during the design of the chamber are similar to those used in building ordinary drift chambers. Fig.7 shows a section through the counter parallel to the direction of the incident beam and it is very similar to the system used by Charpak(4) et al. The photomultiplier is placed a few centimeters away from the anode wire so that its axis passes through the region where secondary excitations takes place. Two cathode planes of the chamber are electrically shielded by two earthed planes placed equidistant from the cathode planes, the one close to the photomultiplier being a wire mesh.

An R.C.A.8575 pyrex window photomultiplier was used to detect scintillation pulses. A dynode potential distribution network designed at the Daresbury Nuclear Physics Laboratory was used for preliminary testings of the counter. It is a resistive network recommended(5) for high current (fast) applications. Photomultipliers with conventional resistive potential divider networks are generally not suitable for work involving pulse height measurements at high rate (high tube currents) since the dynode potentials and hence the gains(6) of the photomultipliers change with the tube current. This distribution network was later replaced by a stabilised potential divider. The stabilisation of the dynode potentials were done by means of emitter follower circuits and a detailed description of the design and performance of such a potential distribution network will be given in Chapter five. All the tests except one (the drift velocity measurements which do not require any pulse height measurements) were done with the new potential divider.

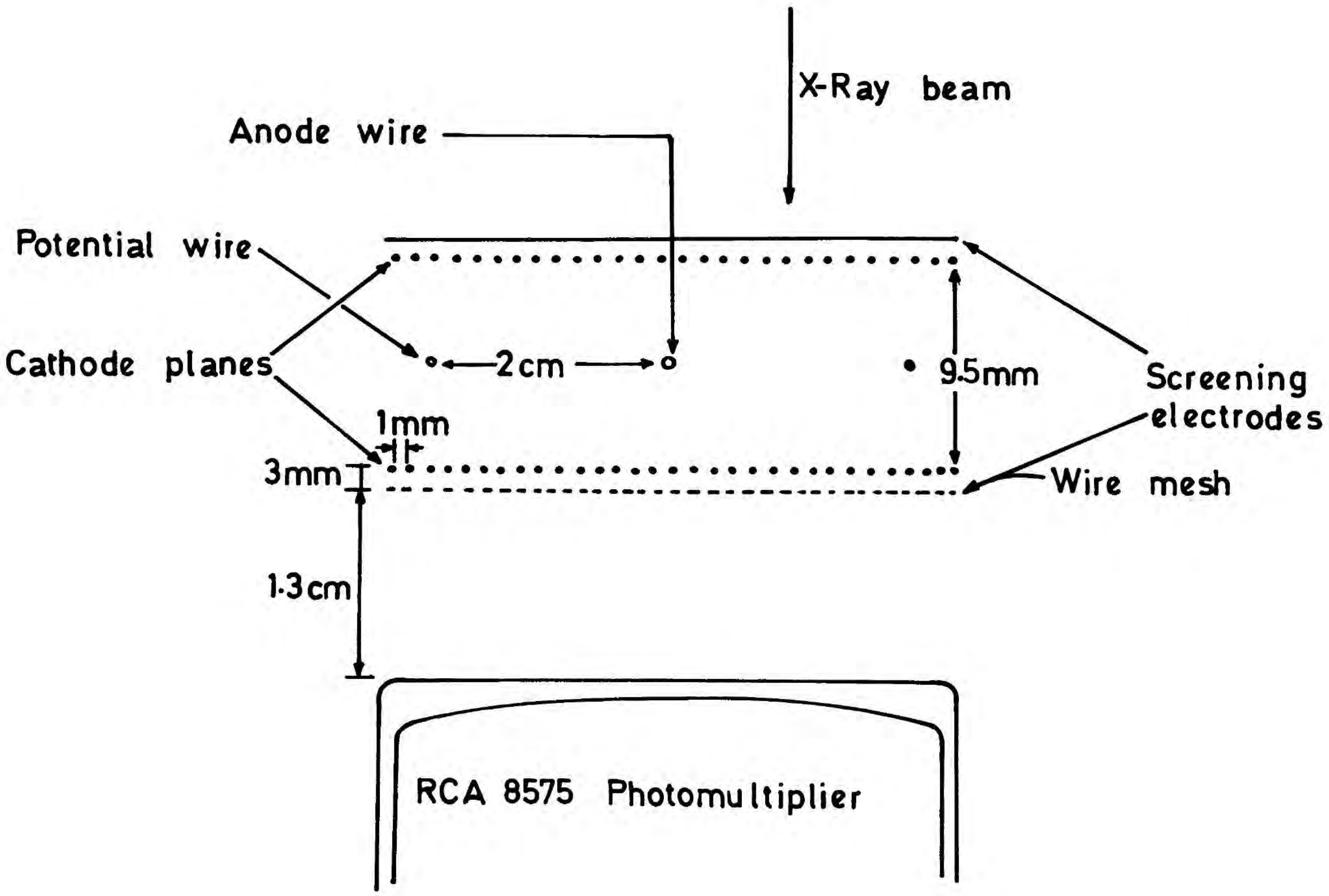

FIG. 7 Section through G.S.D.C.

3.2.2 Wire Plane Configuration

The two cathode planes which provide the necessary lateral drift field are made from 120 μm diameter copper-beryllium wires with 1 mm spacing. Symmetrically placed between the cathode planes is a thick nickel anode wire. The diameters of the anode wire used by various authors are spread over a large range ; for example, Policarpo(7) et al used 125-250 μm diameter wires while Charpak(4) et al's choice was 500 μm. It was decided to use a 410 μm diameter wire for this work ; the factors which determined this diameter for the anode wire will be described in Chapter four.

On either side of the anode wire is a potential wire (200 μm diameter, Nickel) which maintains the uniformity of the drift field right up to the end of the drift cell. The earthed screening electrode (wire mesh) close to the photomultiplier is made from 120 μm diameter copper/beryllium wires and its transparency is 78%.

3.2.3 Drift Chamber Dimensions

Perhaps the most important dimension of the chamber is the thickness of its active volume. This thickness must be large enough to absorb adequate amounts of X-ray photons to obtain the necessary count rates. The large thicknesses, however, create problems in the operation of drift chambers because increasing the gap between the cathode planes increases the voltages required to produce adequate secondary pulse amplitudes and the drift fields must be also increased. As a result the secondary avalanches are very likely to be produced especially between the cathode planes and the earthed screening electrodes since this gap is generally kept small to reduce the intensity loss of the incident beam before entering the active region of the chamber. Table 3.1 shows all the dimensions and other parameters of the system.

Table 3.1

Inside area of cross-section parallel to the electrode planes = $65 \times 145\ \text{mm}^2$

Distance between cathodes = 9.5 mm

Distance between the screening electrode and cathode = 3 mm

Distance between the anode wire and potential wires = 20 mm

Active area of the chamber = $40 \times 145\ \text{mm}^2$

Diameter of the phototube window = 51 mm

The photomultiplier is installed in the system so that its window is in direct contact with the gas medium. A gas gap of 13 mm is allowed between the photomultiplier window and the inner screening electrode in order to reduce the electric field distortions around the photocathode which normally runs at negative potential. However, a large separation between the photo cathode and the anode wire is undesirable since it leads to a poor light collection efficiency.

3.2.4 Construction of the Counter

A vertical cross section of the system parallel to the direction of the incident X-ray beam is shown in Fig.8. The system can be divided into two parts ; the photomultiplier with its housing and the drift chamber.

The phototube was fitted to its 21 pin socket and the relevant dynode pins were connected to the potential distribution network. The network was firmly fixed to a metal disc to which a H.T. Lemo and a BNC feedthrough connector were fitted in order to provide the potential to the distribution network and to obtain the photomultiplier anode output. The photomultiplier tube was protected from stray magnetic fields by

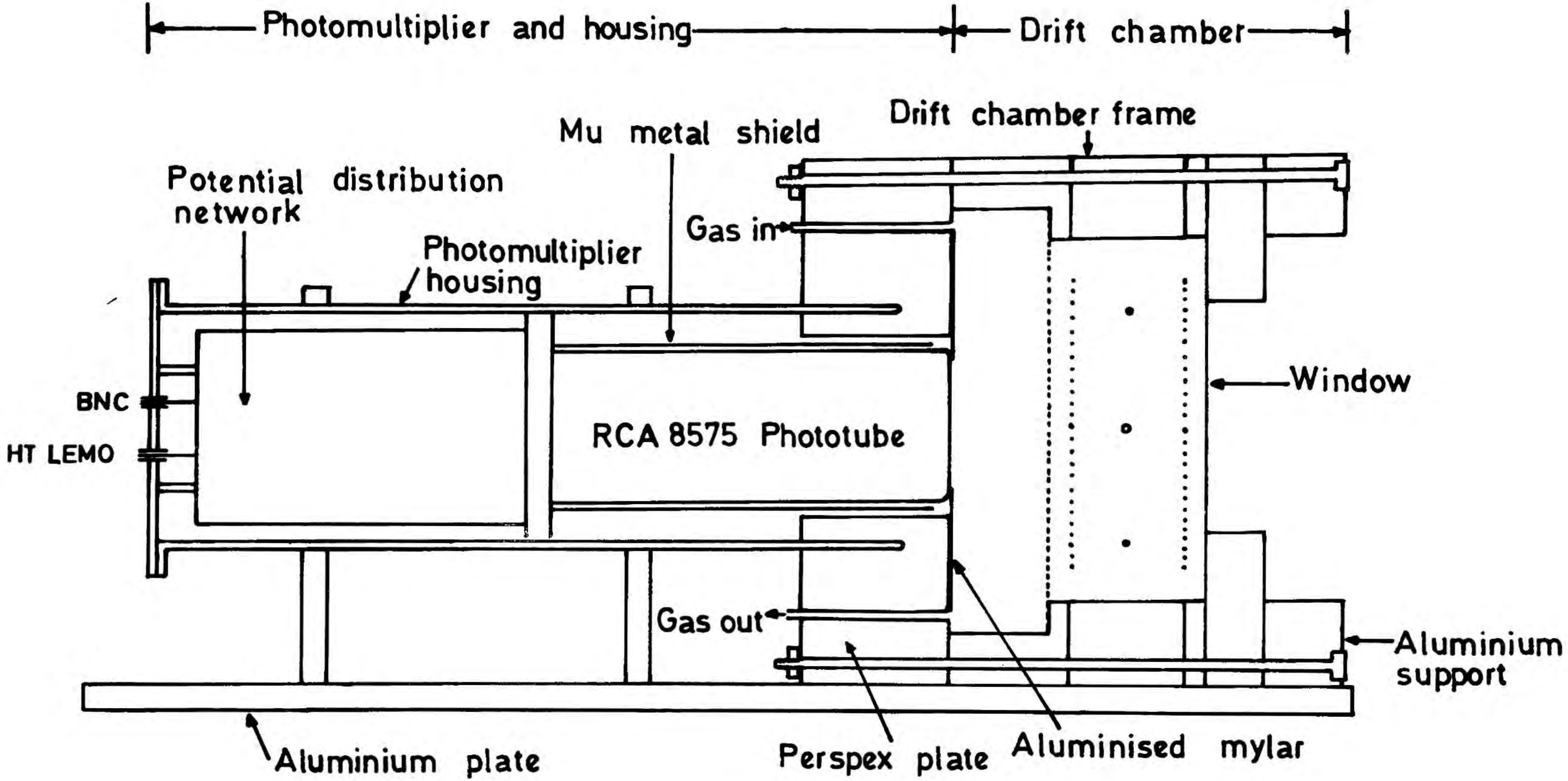

FIG. 8 Section through the counter.

means of a mu-metal shield fitted to the tube socket. The photomultiplier housing was made from a steel tubing one end of which was welded to a small metal annular ring to clamp the photomultiplier tube assembly (metal disc). The other end was fitted to a thick perspex plate with a circular hole concentric with the tube. The diameter of the hole (55 mm) was slightly greater than that of the phototube and the surface dimensions of the perspex plate were identical to those of the drift chamber. The length of the housing was such that when the phototube assembly was inserted into the housing and clamped, the surface of the phototube window just emerged from the hole in the perspex plate. The housing and the perspex plate were fixed to a thick aluminium plate which forms a base to the system. The gas inlet and outlet were also made in this perspex plate.

The drift chamber part consisted of four separate frames all made from perspex. It was decided, however, to make both cathode wire planes and the anode wire plane in a single perspex frame in order to keep the relative positions of the planes fixed when assembling the counter. The three-dimensional view of this frame together with other frames are shown in Fig.9. The three steps were cut in both sides of the frame in order to fix the printed circuit connection boards which consisted of 1 mm copper strips with 2 mm pitch. These were used for cathode, anode and potential wire connections. Two slots were made on either side of the frame in order to make the latter two connections possible from outside. The printed circuit boards were positioned accurately on the steps with reference to one edge of the frame and cemented firmly with araldite. The accurate positioning of the printed circuit boards is important since even a small displacement of top and/or bottom cathode planes relative to the anode wire distorts the electric field around the wire and the lateral

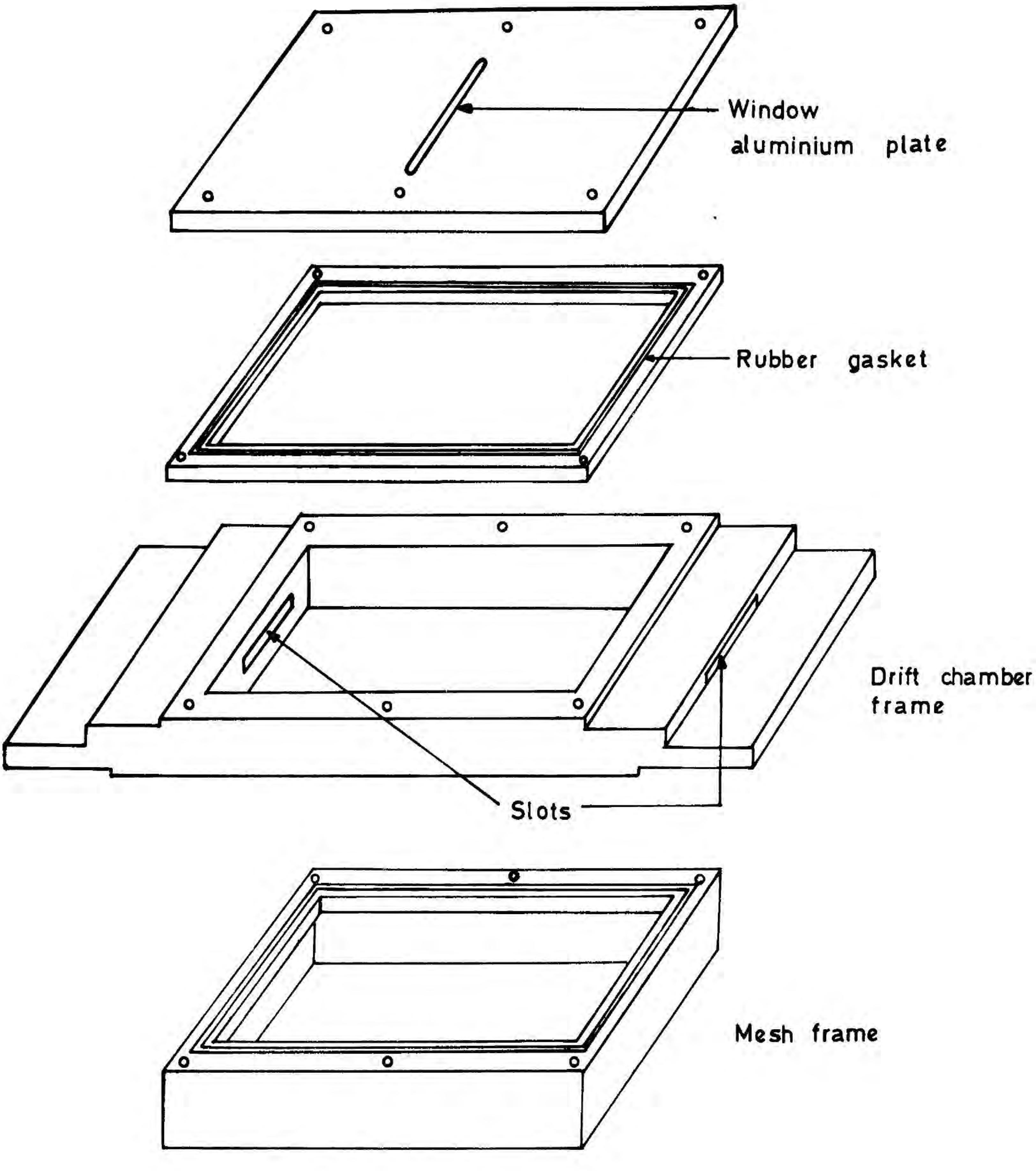

FIG. 9 Three dimentional view of the chamber frames.

drift field. The wires were then soldered to the centre of each strip, and Fig.10 shows a section through the anode wire of the chamber illustrating the wire connections. The slots were then completely filled with silicone rubber to avoid any discharges occurring between the anode wire and the inside surface of the slot when potentials are applied to the anode and the cathode planes. This type of discharge was observed on a previous occasion when operating the chamber without a filling in the slot. The wiring of the mesh was done in a similar manner using printed circuit boards fitted to inside walls of a perspex frame as shown in Fig.10.

The outer screening electrode was an aluminium plate which also served as the window to the chamber. A slot (3 mm x 50 mm) was cut at the middle of the plate to allow X-rays into the chamber. The inside of the plate (side which faces the chamber) was covered with a 50 μm thick aluminised mylar sheet, and the slot with very thin (5 μm) aluminised mylar in order to minimise the absorption and scattering of the incident beam. All the inside walls of the perspex frames except the regions which were close to the H.T. wires were also covered with aluminised mylar for better light reflection.

Aluminium is a good reflector for light in the U V and visible regions. Fig. 11 shows[(8)] its reflectance as a function of wavelength. In order to get the maximum effect of reflection, the aluminised mylar was fixed to the walls with the aluminium side facing the counter.

Before assembling the counter, the gap between the phototube and perspex plate was closed by covering the surface of the perspex plate and the edge of the phototube window up to 1-2 mm from its perimeter with double-sided pressure sensitive tape and an aluminised mylar sheet.

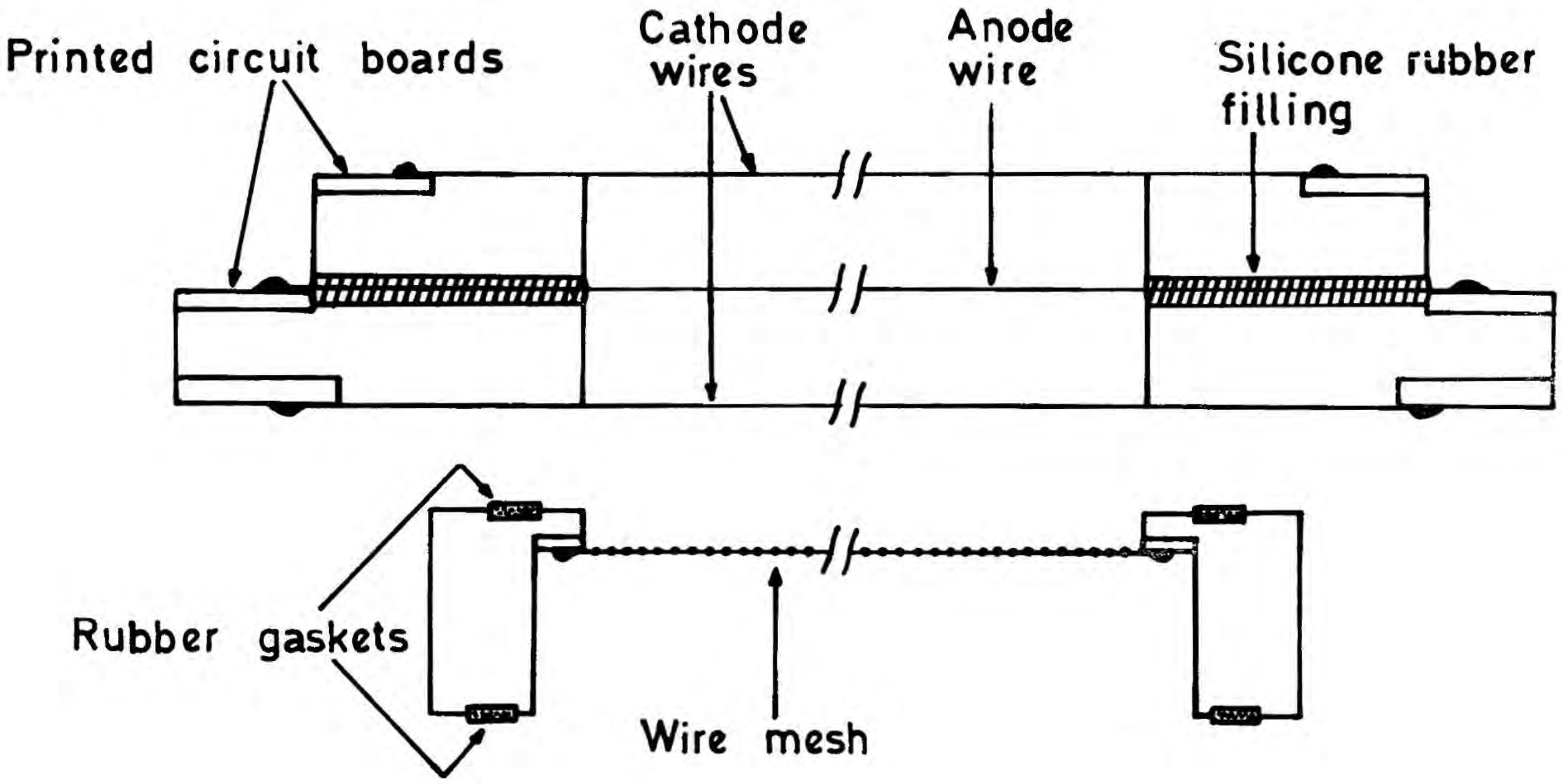

FIG. 10 Section through the drift chamber and mesh frames.

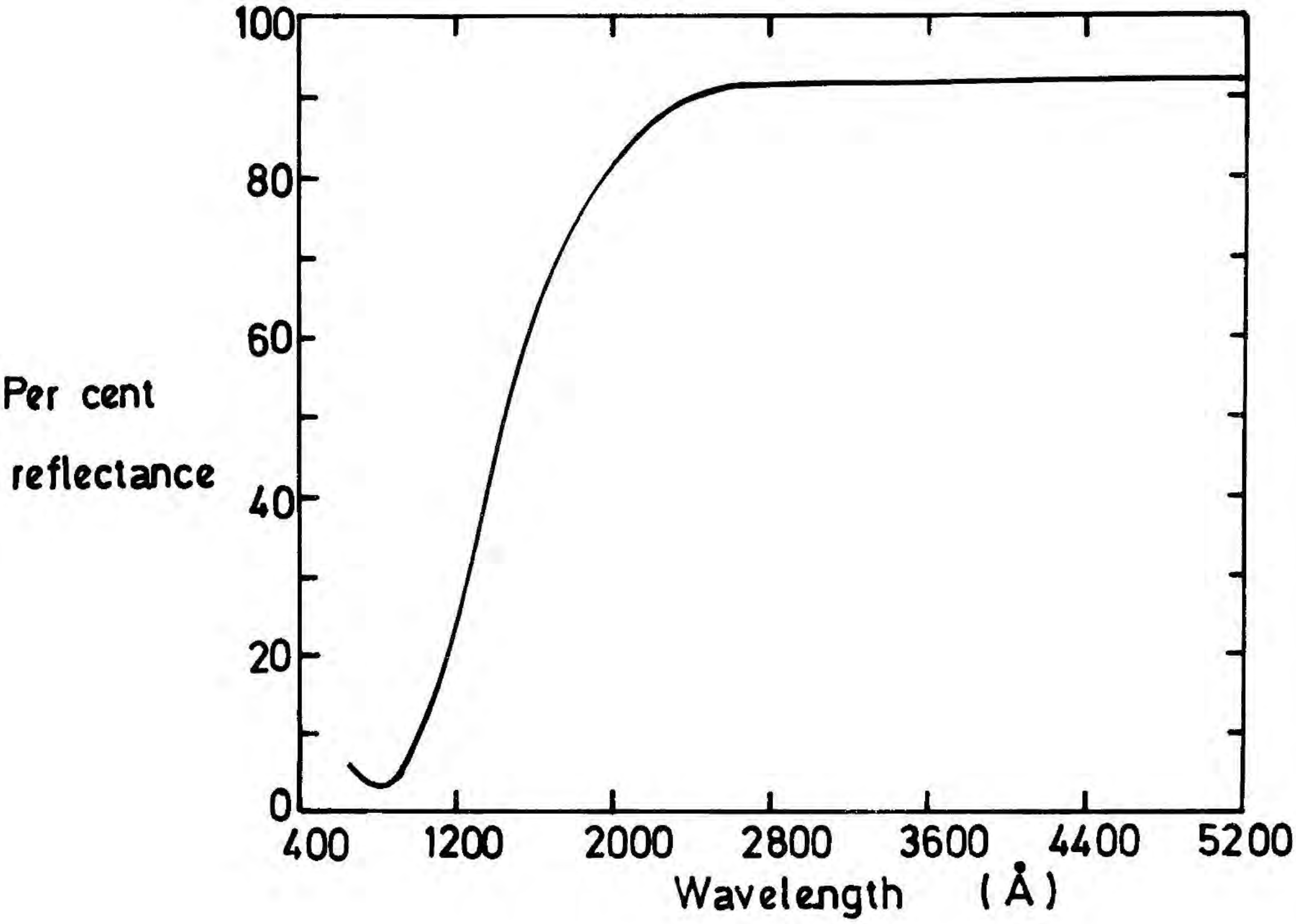

FIG.11 Per cent reflectance of evaporated aluminium film as a function of the wavelength of incident light.

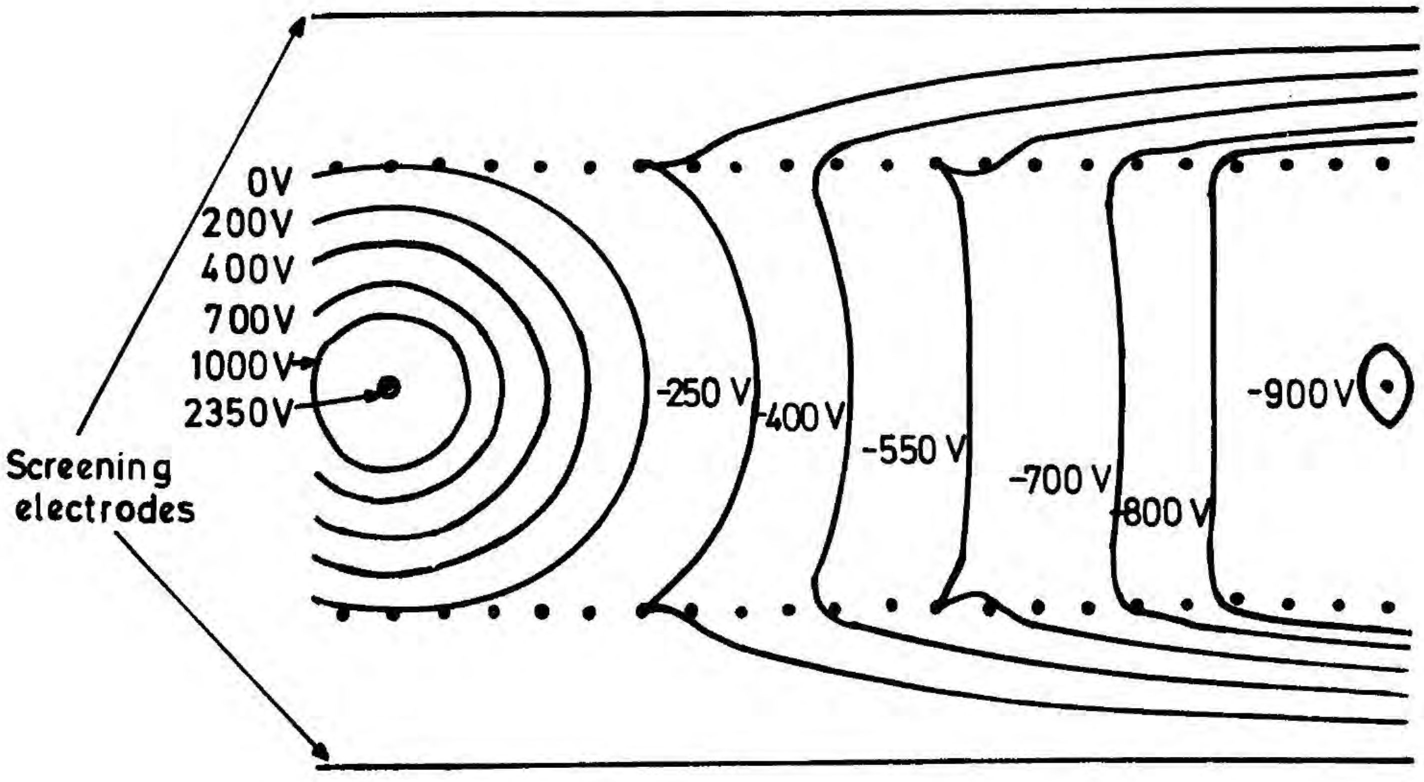

FIG.13 Equipotentials across the G.S.D.C.
(Anode potential =3500 V, applied drift field =500 V/cm).

It is important that the counter must be gas tight once it is assembled. This was achieved by fitting rubber gaskets to surfaces of all the frames except the drift chamber frame as shown in Fig.10. Finally the counter was assembled and clamped with six screws and nuts. A thick aluminium frame was also added to the system to support the perspex frames and increase the rigidity of the system. Fig.12 shows a view of the complete counter. The whole counter was placed in a light tight box and all the connections to the counter were made through the feedthrough connectors.

3.3 APPLICATION OF THE ELECTRIC FIELDS

Two separate H.T. power supplies were used to fix the anode wire potential and to control the lateral drift field. The connections to the wires were made through the printed circuit boards. A 10 MΩ resistor was connected in series with each H.T. supply as a safety precaution. The anode wire was kept at a positive potential while the cathode planes were maintained at negative potentials. A photomultiplier power supply with negative polarity was used to power the photomultiplier.

Electrical connections to the cathode wires and the potential wires were made in the following way.

The cathode wires equidistant from the anode wire in each half cell were connected together. This was done for both cathode planes and one half cell of each cathode plane was connected to a resistive potential ladder in such a way that the two cathode wires right above and below the anode wire are at zero potential and each pair of wires equidistant from the zero potential cathode wires receive negatively increasing potentials in steps up to the maximum potential on the potential wires and also the cathode wires above and below the potential wires. All these connections were made externally by means of ribbon cables.

FIG.12 Photograph of the counter.

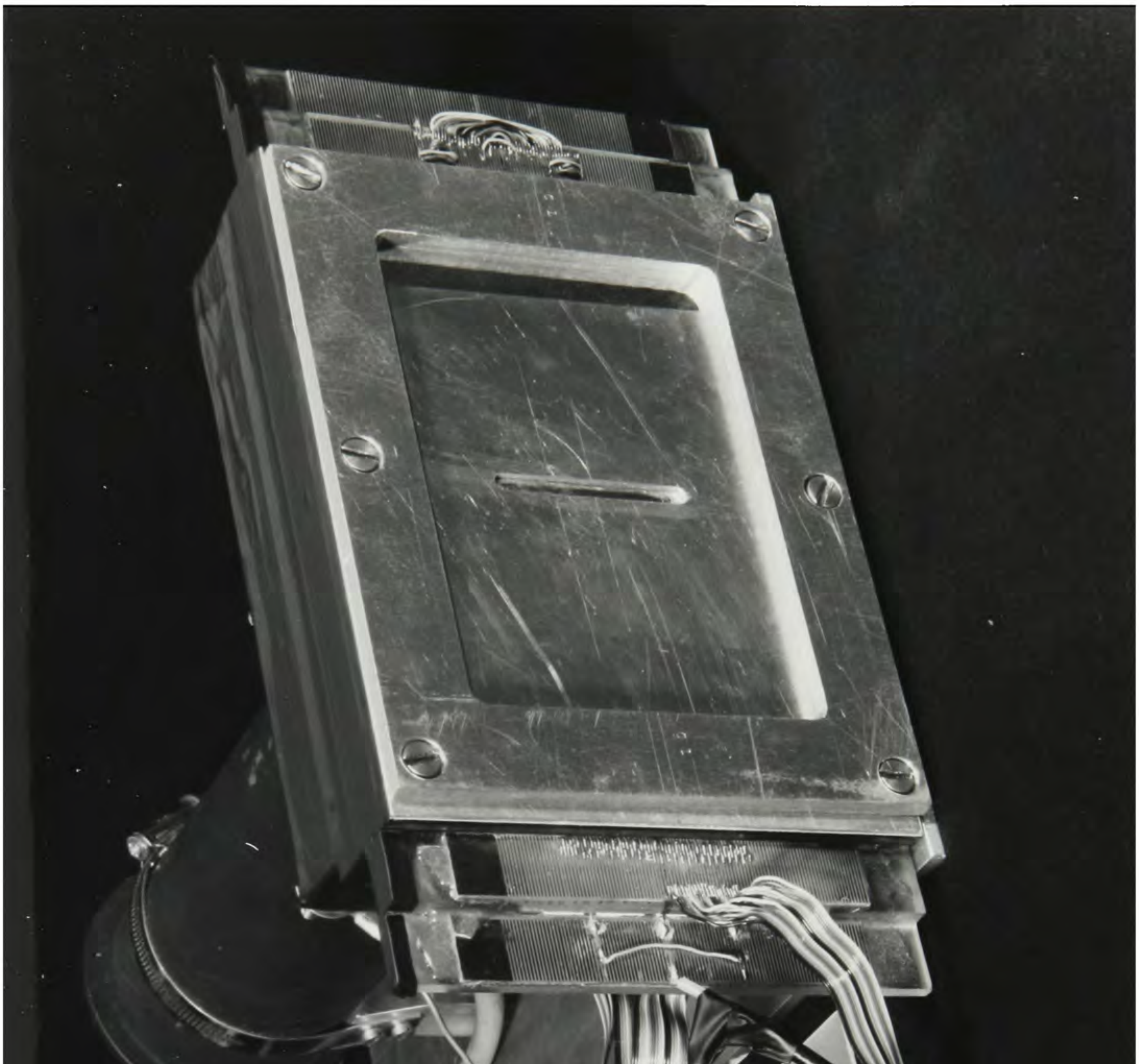

The calculated equipotential lines for a drift chamber with dimensions similar to the one described in the Section 3.3.3 are shown in Fig.13. These calculations were computed by means of a program which uses an iterative technique to solve Poisson's equation for the drift region. The effect of the wire diameters is not included in this calculation. In fact the program assumes zero diameters for all the wires. The drift voltage gradient and the 'anode wire' potential used in the calculation were 500 V/cm and 3500 V respectively. In this case, however, the effect of the diameter of the anode wire can approximately be accounted for by assuming the value of the equipotential whose diameter coincides with that of the anode wire, as the true potential on the anode wire. For example, in order to reproduce the same field as given in Fig.13, a 400 μm diameter wire needs about 2750 V. It is also clear from this figure that as the path of the X-ray beam is moved away from the anode wire, the region through which the secondary excitations take place is also gradually localised to a small region. Fig.14 shows the variation of the electric field across the central plane of the chamber with distance. It can be seen from it that the effect of the anode wire field is large up to a considerable distance from the wire.

3.4 THE GAS MIXING SYSTEM

All the gases used during the course of study were of research grade. According to the manufacturers(9) data the purity of argon and nitrogen were better than 99.9995 % and 99.9995% respectively, and the impurity concentrations (ppm) in both gases were also as follows; CO_2<0.5, CO <1.0, H_2 <2.0, CH_4 <0.5, N_2 <3.0 (for Ar), N_2O <0.1, O_2 <0.5 and water <0.5. Gases were mixed by means of a mixing system. A GEC Elliott flowmeter was used to measure the argon rate of flow and an air flowmeter (4-40 cc/min) was used for the nitrogen. The validity of

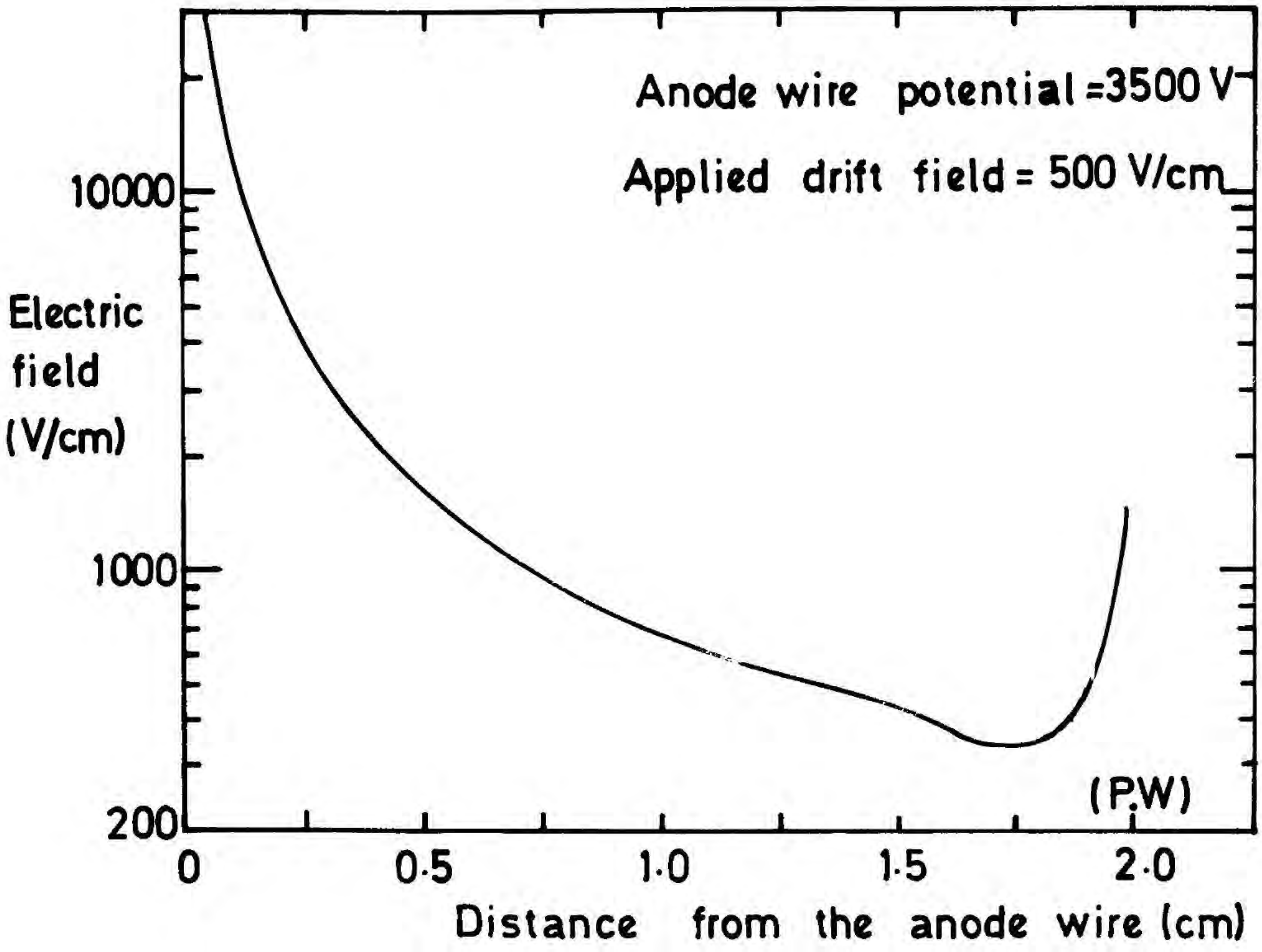

FIG.14 Electric field across the central plane of the G.S.D.C.

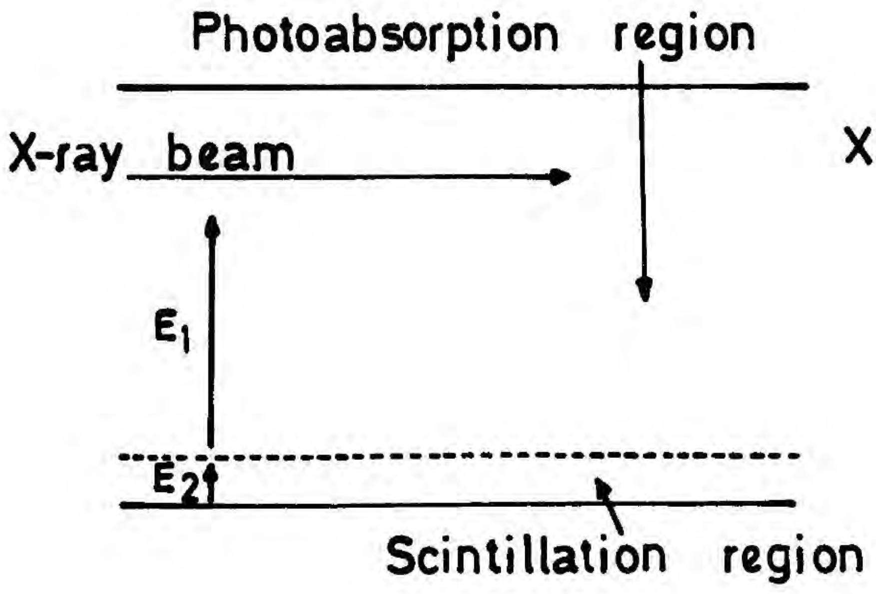

Fig 15 a

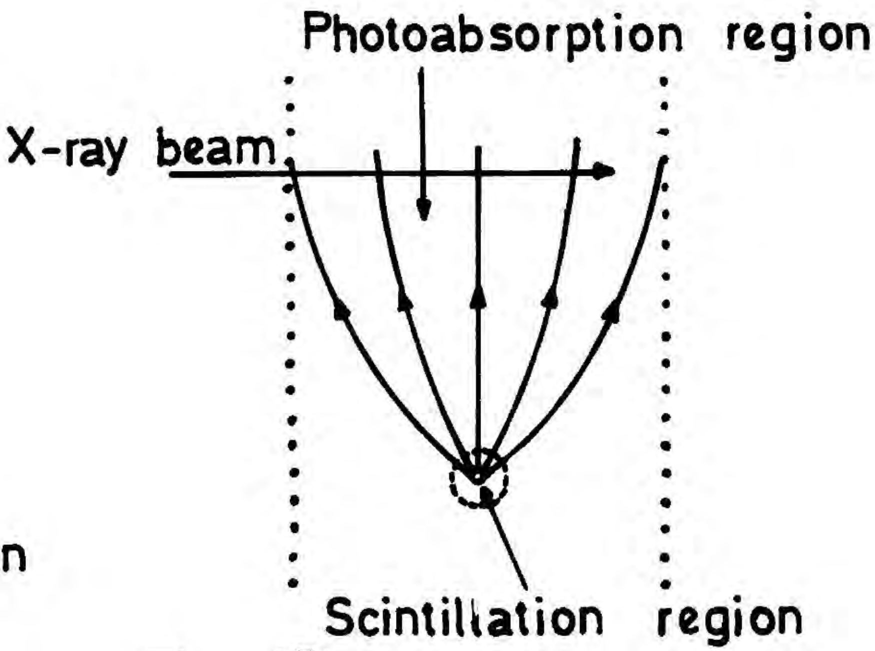

Fig 15b

FIGS. 15a & 15b Schematic diagram of the types of drift chambers illustrating photoabsorption and scintillation regions (E_1 and E_2 are the electric fields in photoabsorption and scintillation regions.

the scale on the air flowmeter for use with nitrogen was checked by calibrating it against an argon flowmeter scale through which the true flow rates of nitrogen were already known$^{(10)}$, and was found to be justified within the errors involved in reading the scales. The mixtures with very low nitrogen percentages were obtained by mixing large quantities of argon with a small quantity of nitrogen (usually 5 cc/min). However, the input flow rate to the counter was always maintained at a constant level by venting a proportion of the gas mixtures direct to the air. According to the manufacturers data the accuracy of the flow meters is within 2%.

3.5 PULSE FORMATION

The absorption of high energy photons (X-rays) in a gas results in the ejection of energetic photo electrons from the gas atoms. These electrons soon dissipate their energy through further excitation and ionisation of gas atoms and the range (R) through which this dissipation takes place is a rapidly varying function ($R \propto E^2$)$^{(11)}$ of the electron kinetic energy (E). For example, the photoelectrons produced from the K shell of argon by 5.9 keV photons have a range of ∿ 60 μm. The primary charge cloud produced by a high energy photon is therefore fairly localised in the gas.

In a GSDC these clouds of electrons drift towards the anode wire under the influence of the electric field and gain sufficient kinetic energy to cause further excitation of gas atoms. However, in practice at the anode wire potentials necessary to produce detectable scintillation signals the primary electrons, when near the anode wire gain sufficient energy to produce ionisation in the gas. Successive ionisation results in an electron multiplication process characterised by the parameter known as Townsend's first ionisation coefficient α. This is defined as the number of secondary electrons produced by an electron when traversing through a distance of 1 cm in the direction of a uniform electric field E.

Suppose N_o is the number of primary electrons produced by a high energy photon interacting with the gas and x_i and x_{ex} $(x_i<x_{ex})$ are the distances from the anode wire (x = o), at which the excitation and the ionisation processes begin then the number of electrons (N_x) present in the electron cloud at a distance x $(x<x_i)$ from the anode wire is given by the equation

$$dN = N_x \, \alpha \, (x) \quad dx \tag{3.1}$$

α is not a constant in this equation but a function of x since the electric field close to the anode wire varies as $\frac{1}{x}$

$$\text{Since} \quad \int_{N_o}^{N_x} \frac{dN}{N_x} = \int_{x}^{x_i} \alpha \, (x) \, dx \tag{3.2}$$

$$\text{Then} \quad N_x = N_o \exp \left[\int_{x}^{x_i} \alpha \, (x) \, dx \right] \tag{3.3}$$

The rate of excitation due to encounters between electrons and gas atoms can be represented by an excitation coefficient ε , analogous to α, ε being the number of excitations per electron per unit distance travelled (1 cm) in the field direction. Hence the total number of excited atoms formed by the electrons when traversing from the point where primary ionisation takes place to the anode wire is

$$N = \sum_{j} \left\{ \int_{a}^{x_i} \varepsilon_j(x) \, N_o \exp \left[\int_{x}^{x_i} \alpha(x) dx \right] dx + \int_{x_i}^{x_{ex}} N_o \varepsilon_j(x) dx \right\} \tag{3.4}$$

where j represents the jth excitation level and 'a' is the diameter of the anode wire.

The second term in the expression accounts for the excitation growth at field strengths below those necessary for ionisation growth. Unlike α the behaviour of ε with electric field has not been established for most of the gas mixtures. Thus the above integral for N cannot easily be evaluated. As mentioned in Chapter two, some of these excited states de-excite through the radiative de-excitation process and the rest transfer their energies to ground state molecules either to form optical states or merely to increase their kinetic energy.

Depending on the light collection efficiency of the counter, a fraction of the photons produced by the de-excitation processes reach the photo cathode of the photomultiplier where they produce a bunch of photoelectrons whose size depends on the conversion efficiency of the photocathode. As a result of successive electron multiplication along the dynode chain, each photoelectron gives rise to a fast narrow electron pulse at the photomultiplier output. However, since all the photoelectrons in the bunch travel down the dynode chain very close to one another, all the electron pulses overlap together to form a single electron pulse at the output.

The width of the output pulse is of prime importance in high rate counters. In a GSPC the duration of the output pulse is determined by a number of factors, such as the width of the single photo electron response of the photomultiplier, the life times of the excited states, the thickness of the scintillation region, the drift velocity of electrons in the gas, the effective diameter of the electron cloud and the diffusion coefficient for electrons in the gas. The output pulse width for a single photoelectron at the cathode of a photomultiplier is very small ($\sim$2-3 ns) for photomultipliers which are normally used in fast scintillation studies. Then in the case of GSDC's where there are uniform electric fields present in both the scintillation and photoabsorption regions (see Fig.15a) the electron cloud of effective diameter D at the end of the photoabsorption region produces a scintillation pulse whose mean pulse width $\bar{t}$ can be written as

$$\bar{t} = \frac{D}{V_d} + \frac{S}{V_s} + \bar{\tau}_R \qquad (3.5)$$

where S is the thickness of the scintillation region, V_d and V_s are the drift velocities of electrons in photoabsorption and scintillation regions respectively and $\bar{\tau}_R$ is the combined decay tine of the excited states involved in the scintillation. In the case of argon-nitrogen gas mixtures the decay times of the argon excited states (mainly the metastable states) and N_2(C) state contribute to τ_R. In a scintillation drift chamber whose scintillation field region is provided by an anode wire (see Fig.15b) the drift velocity of electrons, unless saturated, is not a constant but a function of the distance (x) from the anode wire since the electric field varies as $\frac{1}{x}$. Therefore, V_d and V_s in the above expression have to be modified accordingly in order to obtain an expression for width of the scintillation pulses. It is apparent from the above expression that high drift velocities are necessary to achieve small pulse widths.

3.6 SPACE CHARGE GAIN LIMITATIONS

In general GSDC's are operated at very low electron amplifications around the anode wire and therefore the space charge effects are negligibly small even at considerably high counting rates (10^5 - 10^6 X-ray counts per sec). However, when the rate is further increased the accumulation of slow moving positive ions around the anode wire causes a drop in the local electric field close to the wire, thus reducing the electron amplification factor for subsequent electron pulses. The severity of this effect obviously depends on the amount of electron amplification introduced during the secondary scintillation process.

By applying Poisson's equation to the space charge around the anode wire (radius a) of a cylindrical proportional counter, Hendrick(12) has shown that the effect of the space charge is to reduce the electric field near the anode wire by effectively reducing the anode potential by an amount

$$\Delta V = \frac{\rho e\, b^2}{4\, \varepsilon_o} \tag{3.6}$$

where b is the radius of the outer shell of the counter and ρ is the mean space charge density and is related to the average counting rate $\bar{R}$ by the expression

$$\rho = N_o\, M \frac{p\, \ell n(b/a)}{\mu V 2\pi L} . \bar{R} \tag{3.7}$$

where N_o is the average number of primary electrons per pulse, M is the electron multiplication factor, p is the gas pressure (in atmospheres), V is the applied potential to the anode wire, μ is the mobility of positive ions in the gas mixture and L is the active length of the anode wire. It is clear from these two expressions that the effective anode wire potential $(V - \Delta V)$ drops linearly with the count rate. However, at very high count rates the rate at which the effective anode wire potential drops reduces due to the reduction in M. Since the dependence of the electron multiplication factor on the anode wire potential is exponential, the space charge effect gives rise to an exponential drop in the pulse height at high rates but becomes a less rapidly varying exponential at extremely high rates.

3.7 DIFFUSION OF ELECTRONS

As mentioned in Section 3.6, one of the factors which affects the duration of the scintillation pulse is the diffusion of electrons in the gas. Although the primary ionisation results in the production of a localised cloud of primary electrons, diffusion causes the cloud to enlarge as the electrons drift towards the light producing region where they form a wider scintillation pulse than that which would be produced by an undiffused cloud.

The diffusion is a natural process in which there is a net spatial movement of particles due to a gradient in the concentration of the particles. The diffusive flow takes place in the direction opposite that of this gradient and the flow rate is directly proportional to the magnitude of the gradient. The constant of proportionality is called the diffusion coefficient D. This can be expressed mathematically as

$$J = - D\nabla N \tag{3.8}$$

where J is the net number of particles flowing through unit area normal to the flow direction per second and ∇N is the gradient of the number density of the diffusing particles. This relationship is known as Fick's law of diffusion. In the absence of an electric field this relationship can be applied to electrons diffusing in a gas.

Spreading of a cloud of particles by diffusion through an unbounded gas has been studied by Einstein(13). According to his findings, if a large number of particles N_o, originally located at the origin of a three-dimensional co-ordinate system is released at t = 0 and allowed to diffuse through a gas at uniform pressure, the number density at a distance r from the origin at time t is

$$N = \frac{N_o}{(4\pi Dt)^{3/2}} e^{-r^2/4Dt} \tag{3.9}$$

where D is the diffusion coefficient as before.

The root mean square displacement of the particles from the origin at time t is

$$\sqrt{\overline{r^2}} = \sigma_r = \sqrt{6Dt} \tag{3.10}$$

and in one dimension

$$\sqrt{\overline{x^2}} = \sigma_x = \sqrt{2Dt} \tag{3.11}$$

Huxley and Crompton(14) have recently shown that equation (3.11) is also applicable to a group of electrons that spreads by diffusion as the centroid of the group moves under the influence of an electric field, provided that D is replaced by D_L, the diffusion coefficient in the direction of the electric field. The value of D perpendicular to the direction of electric field however remains unchanged. The difference between D and d_L was first observed by Wagner et al(15) who measured the ratio of diffusion coefficient to mobility of electrons in gases, parallel and orthogonal to the electric field. The mobility (μ) of electrons in a gas is defined as W = μE where W is the drift velocity of electrons in the gas corresponding to an electric field E. The results of Wagner et al for argon and nitrogen are shown in Fig.16.

If during time t, the distance traversed by the centroid of a group of electrons in a gas influenced by an electric field is d then

$$\sigma_x = \sqrt{2\, D_L \frac{d}{W}} \tag{3.12}$$

and

$$\sigma_{orthogonal} = \sqrt{2\, D \frac{d}{W}} \tag{3.13}$$

where $\sigma_{orthogonal}$ is the root mean square displacement of electrons in the direction orthogonal to the electric field. These equations indicate that the factor $\frac{x}{W}$ must be minimised in order to reduce the effect of diffusion. σ_x and $\sigma_{orthogonal}$ for a group of electrons after a 1 cm drift in argon and nitrogen are shown in Fig.17. These curves were derived using equations (3.12) and (3.13) and also using the data in Fig.16. Unfortunately, the curves for argon-nitrogen mixture cannot be calculated due to the lack of experimental results. It is clear from these curves that the diffusion lengths (σ_x and $\sigma_{orthogonal}$) are appreciable even for small drift distances.

3.8 PULSE WIDTH AND HEIGHT MEASUREMENTS

3.8.1 Variation of Pulse Width and Height with Drift Distance

The output pulses from the GSDC were investigated using a fast amplifier (LeCroy 612AM) and a Tektronix 475 (100 MHz) oscilloscope. A collimated Iron 55 X-ray source (5.9 keV, 8 mCi) was used to produce scintillation pulses. An argon-nitrogen mixture (90% - 10%) was constantly passed through the counter. The composition of the gas mixture was decided after a series of tests, a detailed account of which will be presented in Chapter four. The shape of the secondary scintilla-

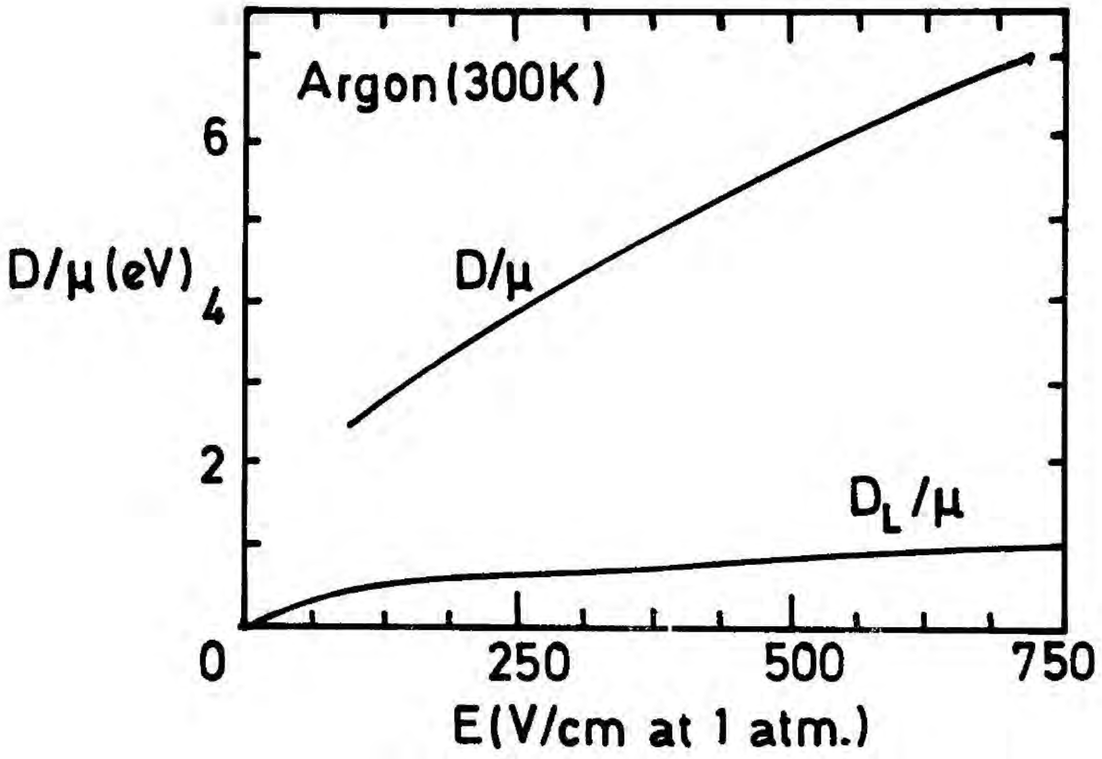

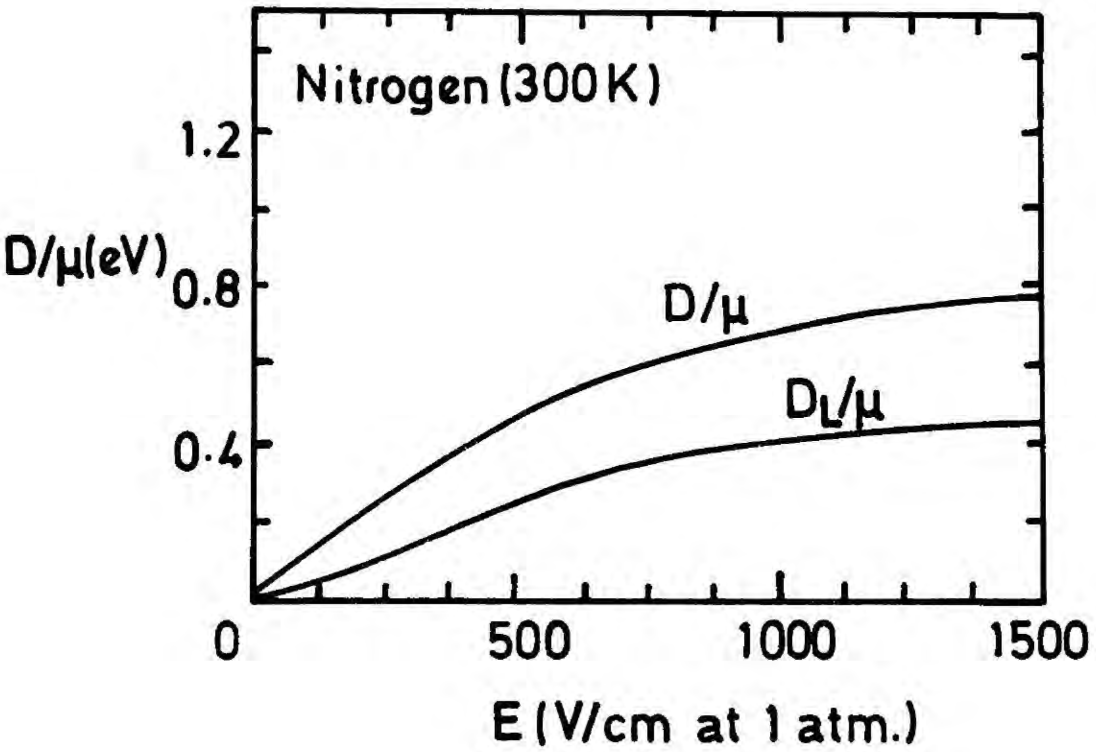

FIG.16 Ratio of diffusion coefficients to mobility, parallel(D_L) and orthogonal(D) to electric field.

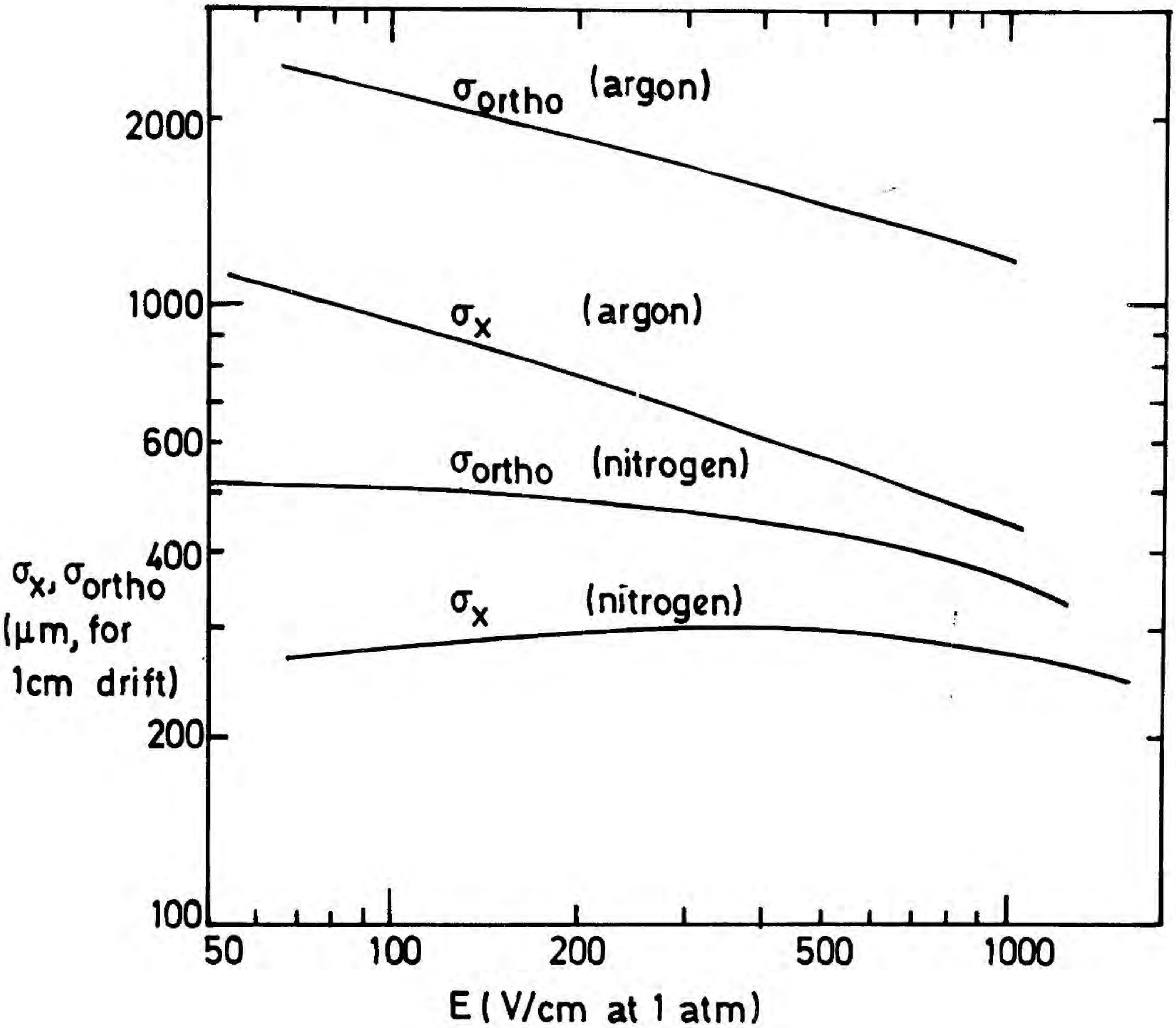

FIG 17 Dependence of the standard deviation of electron diffusion on the electric field for 1cm drift, in argon and nitrogen.

tion pulses from the counter at the photomultiplier output is shown in Fig.18a.

In order to investigate the variation of pulse width and height with drift distance, the X-ray source was moved across the chamber in measured steps and the resulting pulse width and height and also the rise and fall time of the voltage pulses were recorded. The anode wire voltage and the drift field applied for these measurements were 2.8 kV and 500 V/cm respectively. Fig.19 shows the pulse width and the rise and fall times of the pulses as a function of drift distance and Fig.20 shows the variation of pulse height with drift distance. At the same time, voltage pulses from the preamplifier output were fed into a pulse height analyser (Northern Scientific, NS 900) where they were amplified and integrated and then presented as a pulse height spectrum. Fig.20 also shows the peak of the charge (integrated) pulse height spectrum as a function of drift distance. As expected two peaks appeared on the pulse height spectrum when the X-ray beam was within 4mm of the anode wire, (see Section 3.2). As shown in Figs 19 and 20, the width and the amplitude of the voltage pulses vary inversely with the distance of the source from the anode wire, but the charge pulse height remain constant with the drift distance. Smaller pulse widths and large pulse heights observed for smaller drift distances are due to the small amount of diffusion experienced by the primary electron clouds. ~~A similar behaviour has been~~ The opposite phenomenon, ~~noticed~~ observed by Breskin(16) et al working on conventional drift chambers ; they found an increase in the voltage pulse height with drift distance (see Fig.21). They also found a much less pronounced change in the charge pulse height with drift distance. So far a satisfactory explanation has not been found for this phenomenon.

FIG. 18a Secondary scintillation pulses from a G.S.D.C.

FIG. 18b Pulse height spectrum for 5.9 keV X-rays.

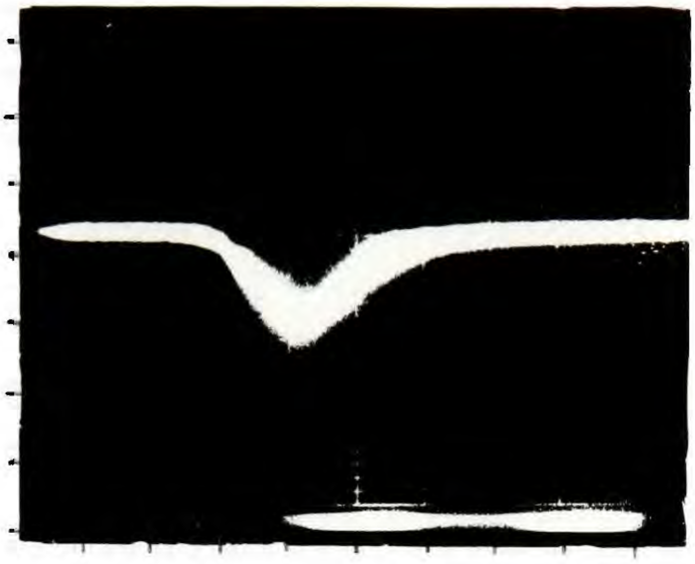

Horizontal. 20 ns/div

Vertical 5 mV/div

FIG. 18a Secondary scintillation pulses from a G.S.D.C

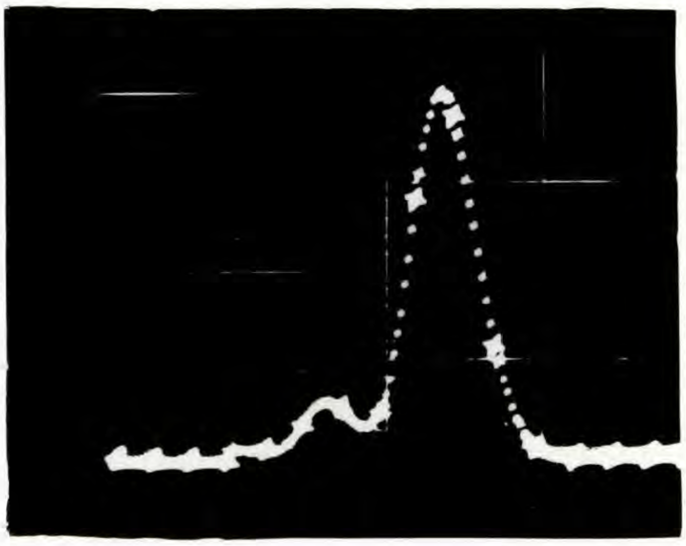

FIG. 18b Pulse height spectrum for 5.9 keV X-rays.

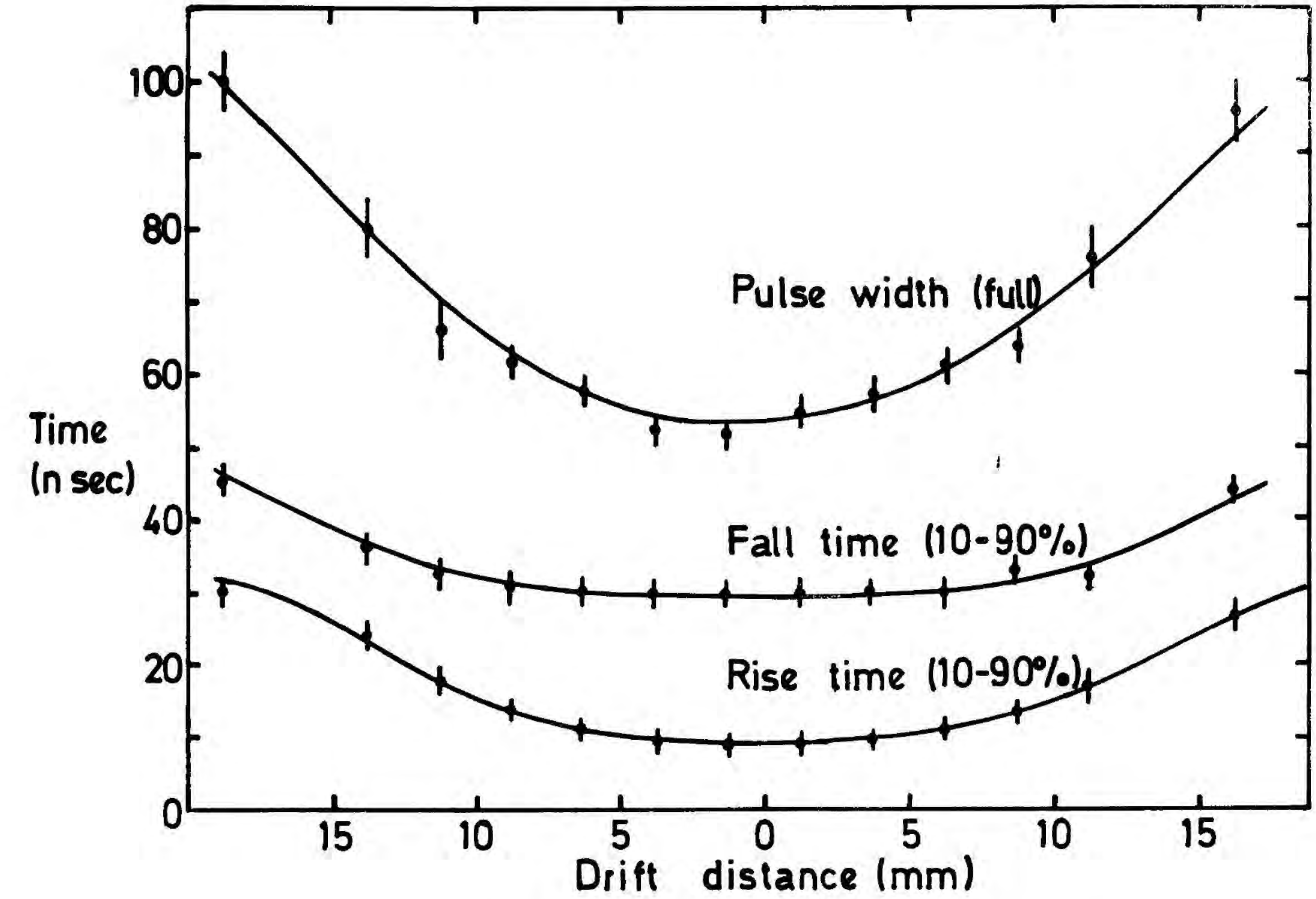

FIG. 19 Width, rise time and fall time of the voltage pulses vs drift distance for 5·9keV X-rays.

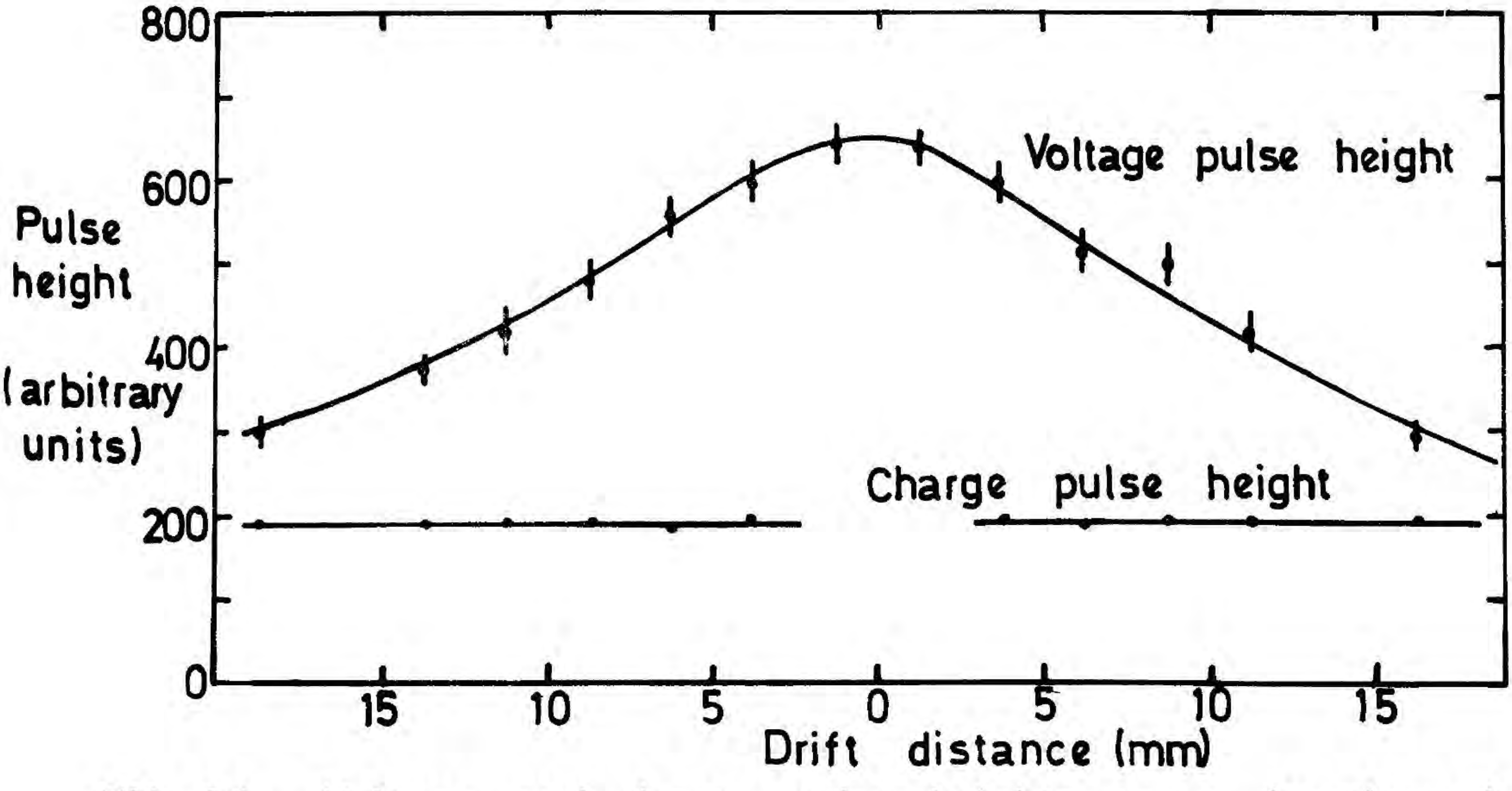

FIG. 20 Voltage and charge pulse heights as a function of drift distance for 5·9keV X-rays.

3.8.2 Variation of Pulse Width and Height with Drift Field

The width and height of the voltage pulses and the peak of the charge pulse height spectrum were measured as a function of the applied field using the same experimental set up described in the preceding section. Fig 22a shows the variation of pulse width with drift field. The width of the pulse was found to decrease with drift field. This can be explained as being due to an increase in the drift velocity of electrons with drift field (see Equation 3.5) and also due to the reduction in the time available for the diffusion processes which enlarge the primary electron cloud. Shown in Fig 22b are the variations of voltage and charge pulse heights with applied drift field. It also shows the variation of charge pulse height obtained from the anode wire as a function of drift field. An Am^{241} α-particle source was used to produce anode pulses whose amplitudes after being amplified were measured on an oscilloscope. It is apparent from Fig.22b that the charge pulse heights vary linearly with the drift field for moderate drift field values. These curves are useful when correlating results obtained with GSPC's to GSDC's with similar dimensions.

3.8.3 Variation of Pulse Height with the Energy of Incident Photons

In general the pulse heights produced by X-rays absorbed in the chamber are proportional to the energy deposited by the X-rays. Although this is true for an ideal GSDC, the results of the Section 3.2 indicate that even if the beam is monoenergetic, it forms two sets of pulse heights when the beam is very close to the anode wire. However, this difficulty can be overcome by shifting the beam away from the anode wire and under this condition respectable energy resolution can be obtained for X-rays by this detector. As an example a pulse height spectrum obtained on the P.H.A. for 5.9 keV X-rays absorbed in the chamber is shown in Fig 18b.

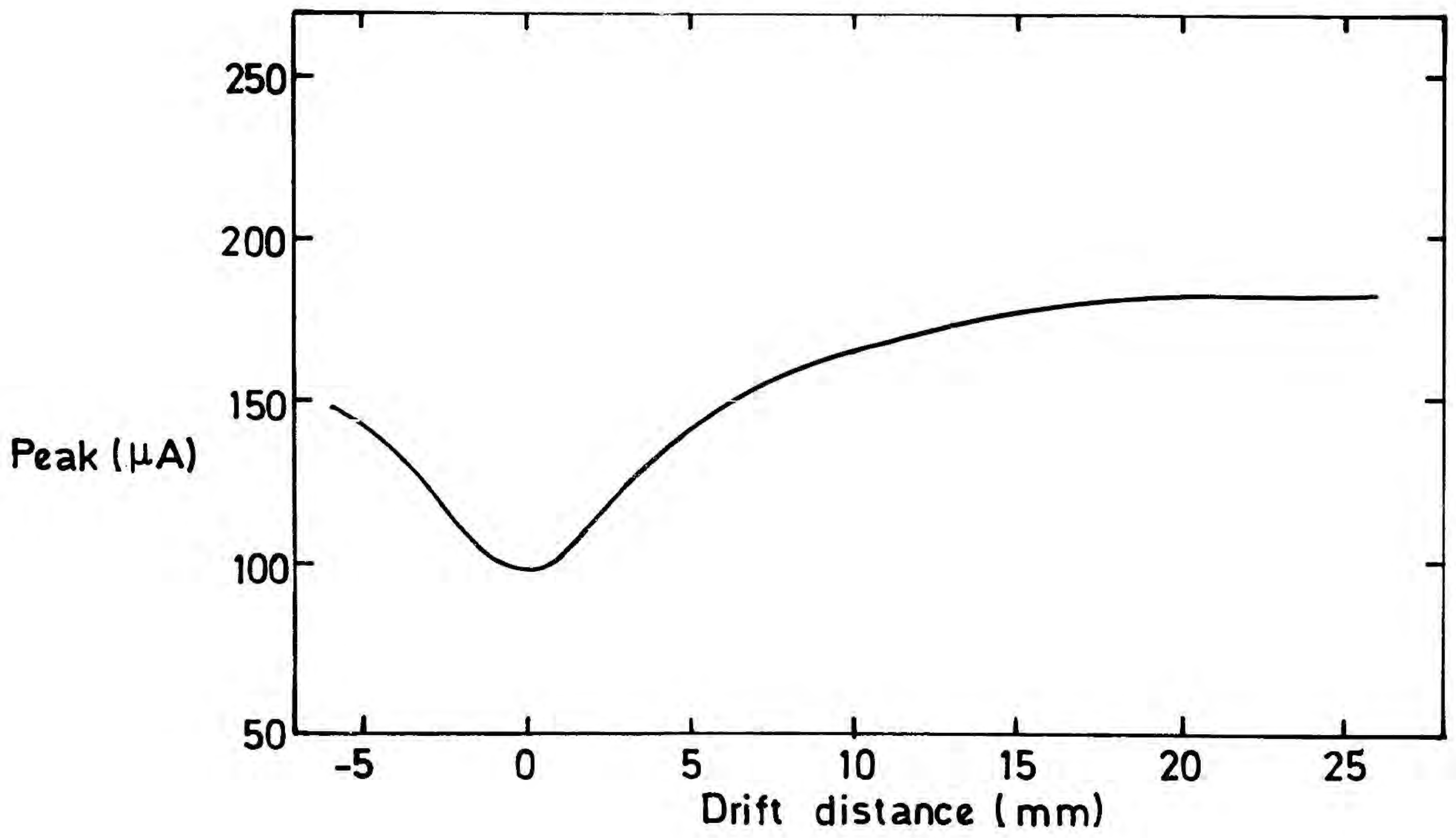

FIG. 21 Pulse height as a function of distance from the anode wire for 5·9 keV X-rays.

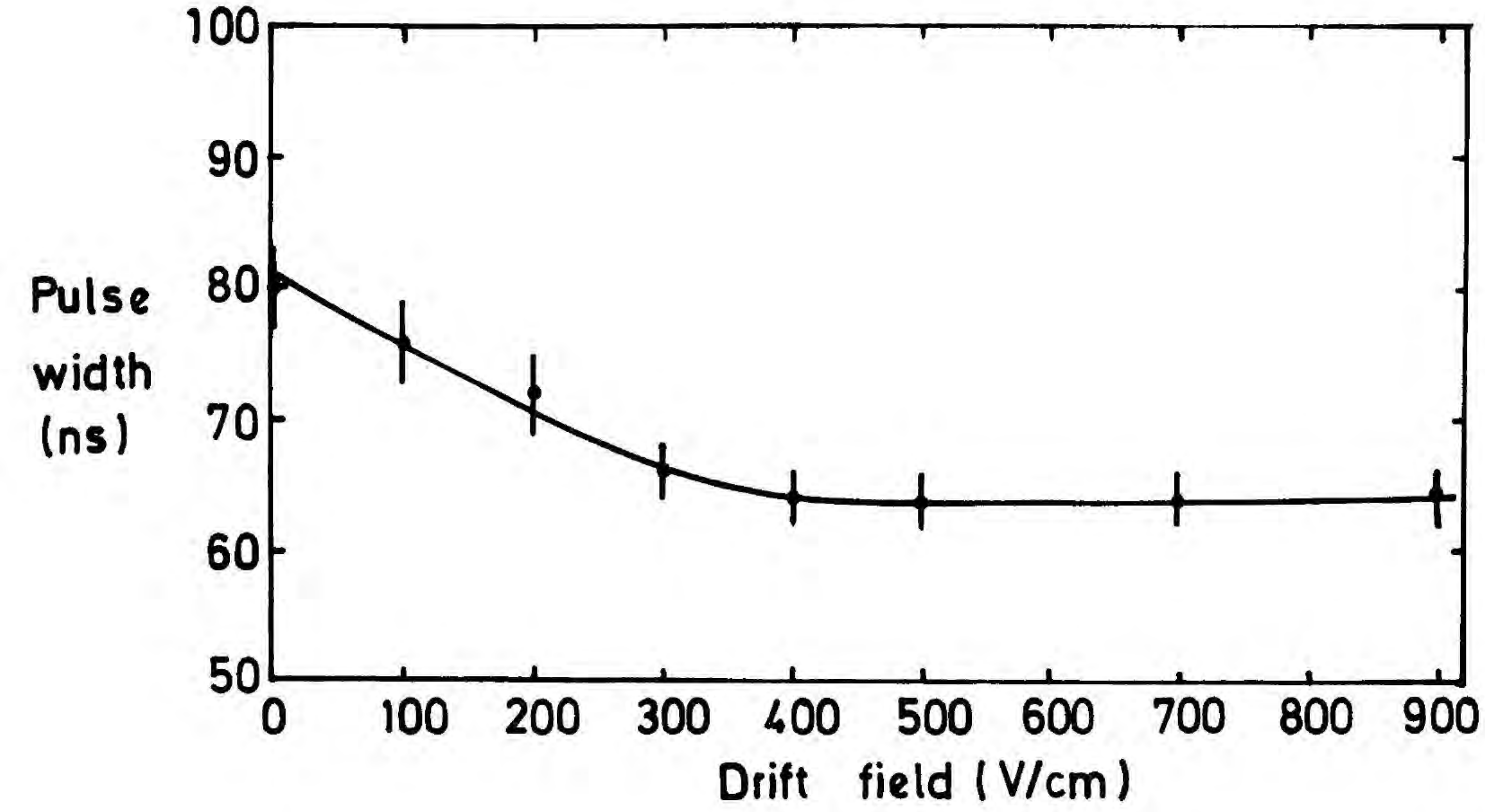

FIG. 22a Variation of the width of scintillation pulses as a function of drift field.

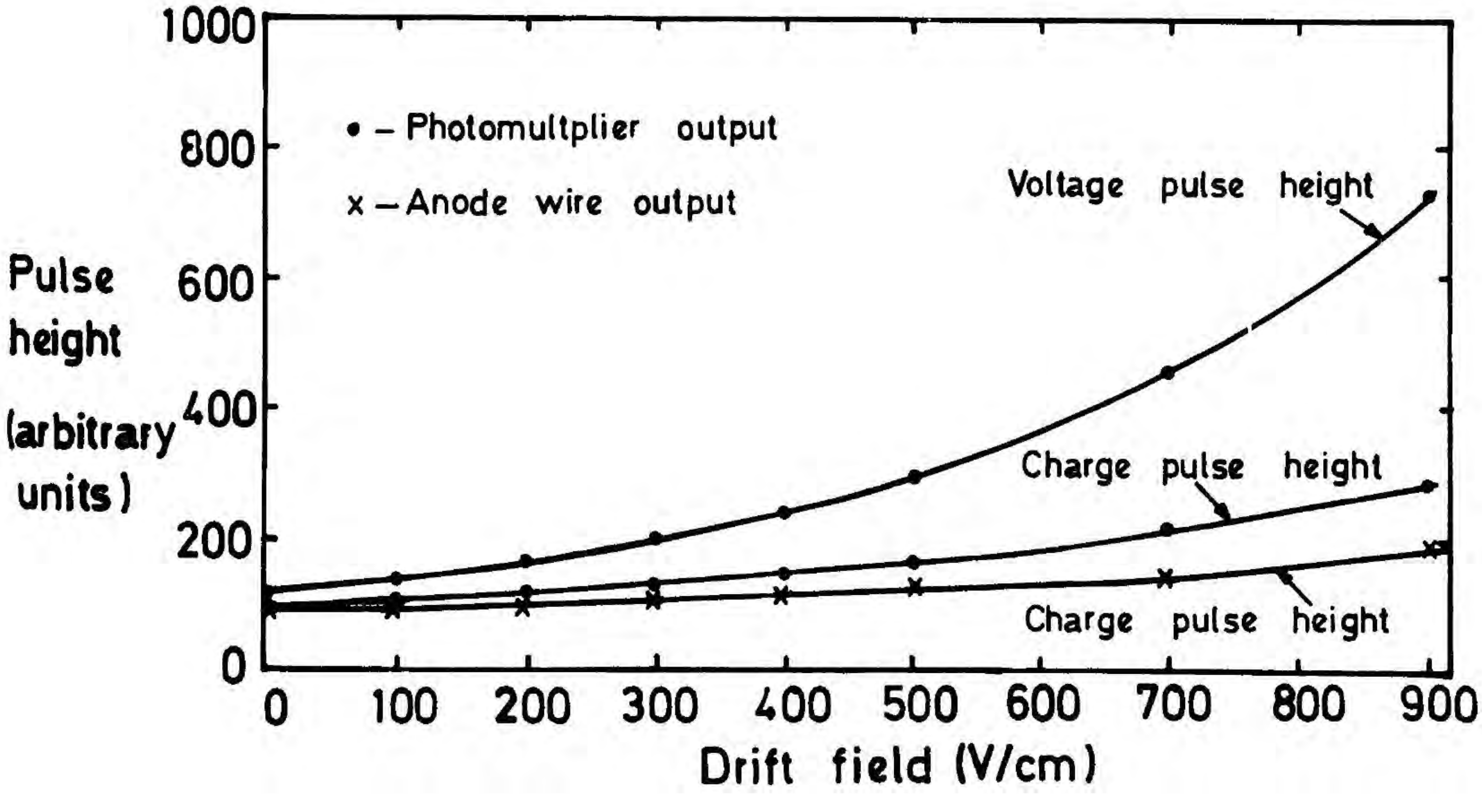

FIG. 22b Variation of charge and voltage pulse heights with drift field.

The main peak is due to the X-rays whose energies are completely absorbed in the active volume of the counter and the escape peak is formed when the photoelectric absorption is followed by an emission of a photon with energy just below the K-edge of argon. These photons have a very long mean free path for absorption and can therefore escape from the active detection volume. The energy of the escape peak is therefore equal to the energy of the incident X-rays less the energy of the argon K-edge.

The linear dependence of the detector pulse height on the energy of the absorbed X-ray photons is extremely important for spectroscopic studies in the X-ray region. This property has been investigated by irradiating the GSDC with X-rays of different energies and noting the peaks of the pulse height spectra on the P.H.A. A (variable energy) X-ray source from the Radio Chemical Centre provided X-rays of six different energies. Fig.23 shows the peak position as a function of the energy of the incident X-rays. According to Fig.23 the counter shows a good linearity at least up to photon energy of 22 keV.

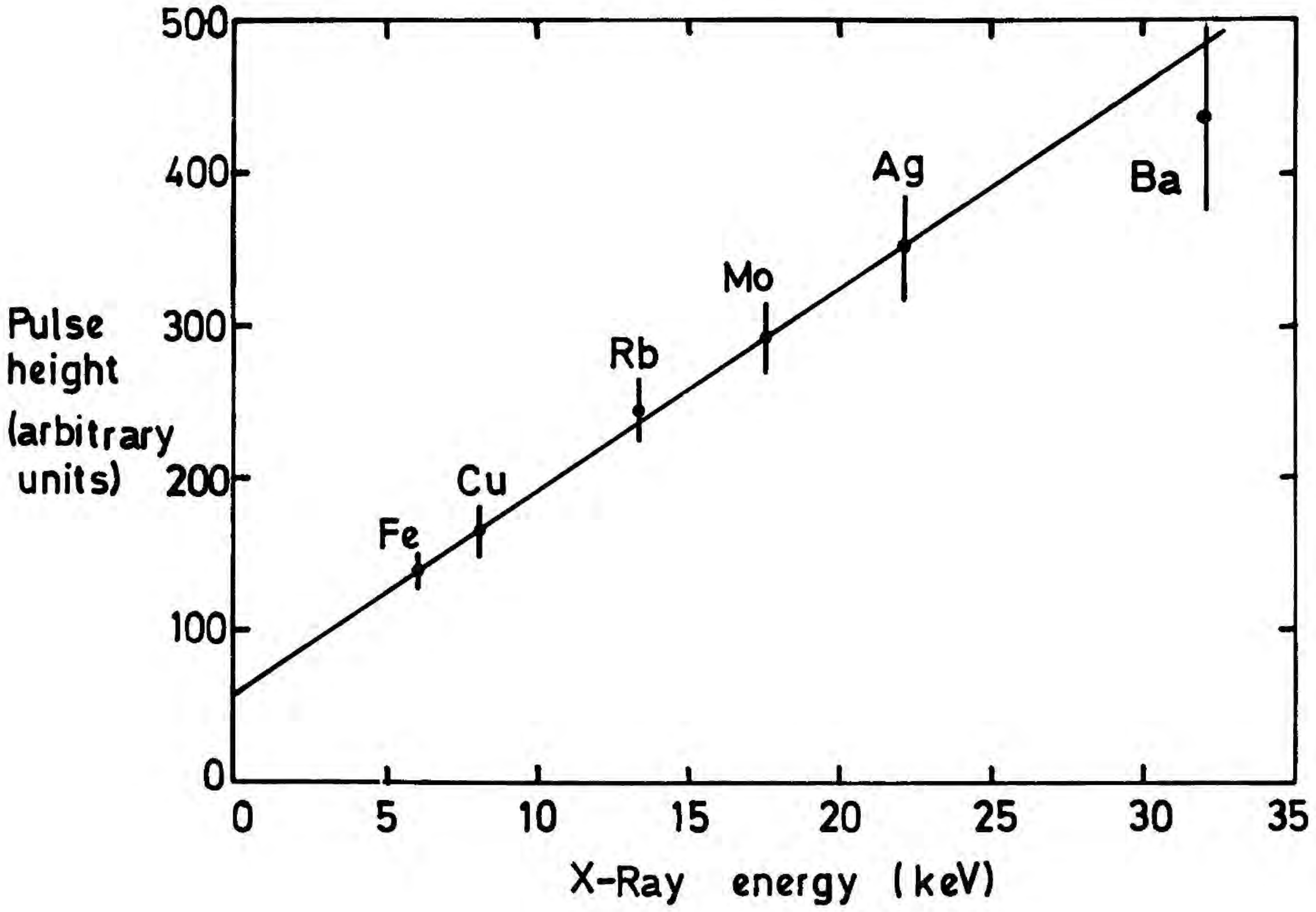

FIG.23 Energy proportionality of the counter.

Chapter 3 - References

1. A.J.P.L.Policarpo, M.A.F.Alves and M.J.T.Carvalho, Nucl.Instr. and Meth. 97 (1971)491.
2. S.S.Al-Dargazelli, T.R.Ariyaratne, J.M.Breare and B.C.Nandi, J. Phys. D: Appl.Phys., 11 (1978) 1773.
3. G.Charpak, F.Sauli and W.Duinker, Nucl. Instr. and Meth. 108 (1973) 413.
4. G.Charpak, S.Majewski and F.Sauli, I.E.E.E. Trans. Nucl. Sci. NS-22 (1976) 202.
5. Instruction Manual for R.C.A. 8575 Phototube.
6. A.K.Gupta, N.Nath, Nucl. Instr. and Meth. 53 (1967) 352, R.D.Connor and M.K.Husain, Nucl. Instr. and Meth, 6 (1960) 337.
7. A.J.P.L.Policarpo, M.A.F.Alves and C.A.N.Conde, Nucl.Instr. and meth., 55 (1967) 105.
8. J.B.Sabine, Phy. Rev. 55 (1939) 1064.
9. Product Catalogue, British Oxygen Company.
10. Rotameter 1100, Gas Calibration Curves, G E C Elliott Process Instrument Section, Croydon (1973).
11. T. J. Harris and E. Mathieson, Nucl.Instr. and Meth. 96 (1971) 397.
12. R.W.Hendricks, Rev.Sci. Instr. 40 (1969) 1216.
13. See, for example, E.W.McDaniel. Collision Phenomena in Ionized Gases, Wiley, New York (1964) Ch.10.
14. L.G.X.Huxley and R.W.Crompton, The Diffusion and Drift of Electrons in Gases, Wiley, New York (1974).
15. E.B.Wagner, F.J.Davis and G.S.Hurst, J.Chem.Phys., 47 (1967)3138.
16. A.Breskin, G.Charpak, F. Sauli, M.Atkinson and G.Schultz, Nucl. Instr. and Meth, 124 (1974) 323.

CHAPTER FOUR

SOME PROPERTIES OF THE ARGON-NITROGEN GAS MIXTURE

4.1 INTRODUCTION

This study investigates some of the useful properties of argon-nitrogen gas mixtures. In particular the study includes measurements of the drift velocity of electrons in the mixture and the secondary light gain which in the context of G.S.D.C. terminology is defined as the ratio of the secondary scintillation light output to the primary scintillation light output. A knowledge of the behaviour of these parameters is of great importance when deciding on the operating conditions which produce the optimum performance of the counter.

4.2 DRIFT VELOCITY MEASUREMENTS

As mentioned in Chapter 3 one of the factors which determines the width of the scintillation pulse is the drift velocity of electrons in the gas mixture. This factor limits the counting rate that can be handled by a gas scintillation drift counter. In addition small drift velocities result in long electron diffusion paths which further increase the width of the scintillation pulse. A high drift velocity is therefore an essential requirement in attaining a high counting rate with GSDC's.

One of the methods recently used(1) to measure the drift velocity of electrons in gas mixtures is to use a plane wire drift chamber in the time of flight mode. In this method a bunch of electrons is formed at a known distance from the anode wire by means of a beam of ionizing radiation and is allowed to drift under a constant electric field towards the anode wire where it produces more electrons through the charge amplification process and forms a fast current signal which can be detected using suitable electronics. The zero time signal which signifies the time of formation of the primary electron bunch, is derived from a solid scintillator placed in the path of the radiation beam and the stop signal from the anode wire. The time interval between the zero time signal and the stop signal gives the drift time and hence the drift velocity. The charge amplification factor which determines the size of the anode signal restricts the use of this method to certain gas mixtures in which the signal amplitudes reach detectable levels before the chamber starts to breakdown. In these types of gas mixtures the ultraviolet photons produced around the anode wire are quickly absorbed by the gas itself and as a consequence a large charge amplification is possible before the production of the secondary avalanches. The above mentioned method is not applicable to gas mixtures in which the photon quenching ability is poor, as the UV photons can extract photoelectrons from the cathode and produce secondary avalanches soon after the primary avalanche. The drift velocity of electrons in such gas mixtures (argon-nitrogen is one example) can be obtained however, by operating the chamber in the scintillation mode under which the probability of forming secondary avalanches is negligible since the operating voltage on the anode wire is low.

In contrast to the conventional drift chamber, the scintillation drift chamber can produce two trigger signals, the first of which occurs due to the primary scintillation of the incoming particle. The primary electrons produced by the incident particle drift towards the anode wire where they produce the secondary scintillation signal. The time duration between the two photomultiplier signals which correspond to primary and secondary scintillations gives the drift time.

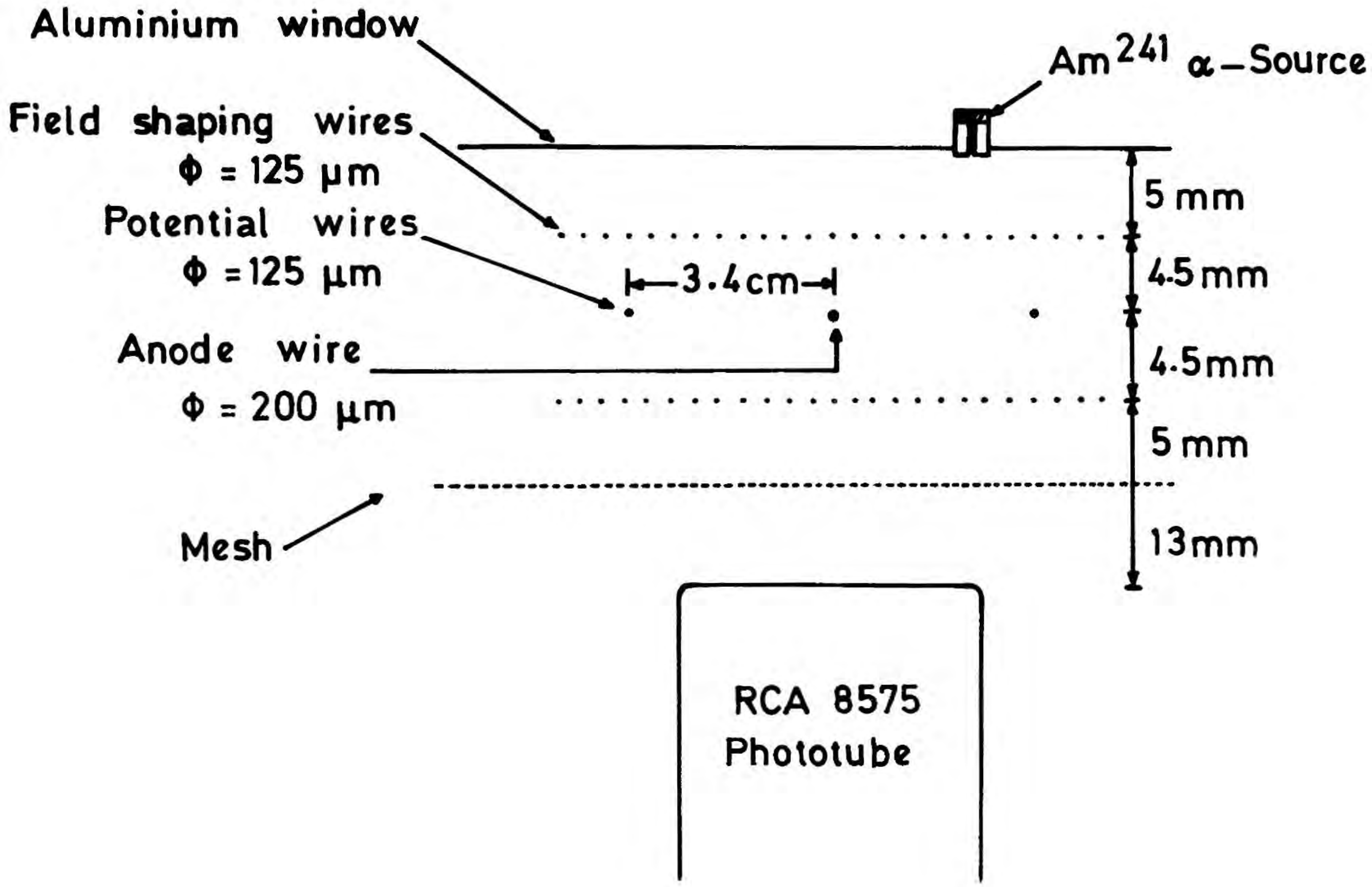

FIG.1 Experimental arrangement for drift velocity measurement.

4.2.1 Experimental Set-up

The experimental arrangement outlined in Fig (1) was used to measure the drift velocity of electrons in the argon-nitrogen mixture. The drift chamber consisted of two wire cathode planes with 2 mm wire spacing, one anode wire and two field wires. The diameters of cathode, field and anode wires were 125 μm, 125 μm and 200 μm respectively. For drift velocity measurements however, a drift chamber with a smaller diameter anode wire is better than one with a larger diameter since for a given anode voltage a more uniform drift field can be obtained with the former. The front window of the chamber was a thick earthed plate of aluminium with a slot cut at the centre and the side facing the photomultiplier tube covered with aluminized mylar to increase the light reflection. The rest of the characteristics of the chamber system are similar to the one described in Chapter three. A collimated radioactive source of α-particles from Am^{241} was placed in the slot and fixed to the aluminized mylar so that the beam direction was normal to the cathode planes. The portion of mylar close to the collimator hole region was removed to increase the range of α-particles in the gas medium and to reduce the multiple coulomb scattering of the beam. The diameter and the thickness of the collimator were 0.5mm and 10 mm and the distance from the beam to the anode wire (drift distance)was measured to be 1.80 ± 0.05 cm.

A block diagram of the timing electronics used is shown in Fig (2). A time to amplitude converter (T.A.C.) and a pulse height analyser (P.H.A) were used to measure the drift time distributions. The T.A.C. works on the principle of charging a capacitor from a highly stable current source during the time interval between the start and the stop signal. The resulting voltage on the capacitor is amplified, shaped and presented at an output socket. The output is then digitised and recorded on the P.H.A.

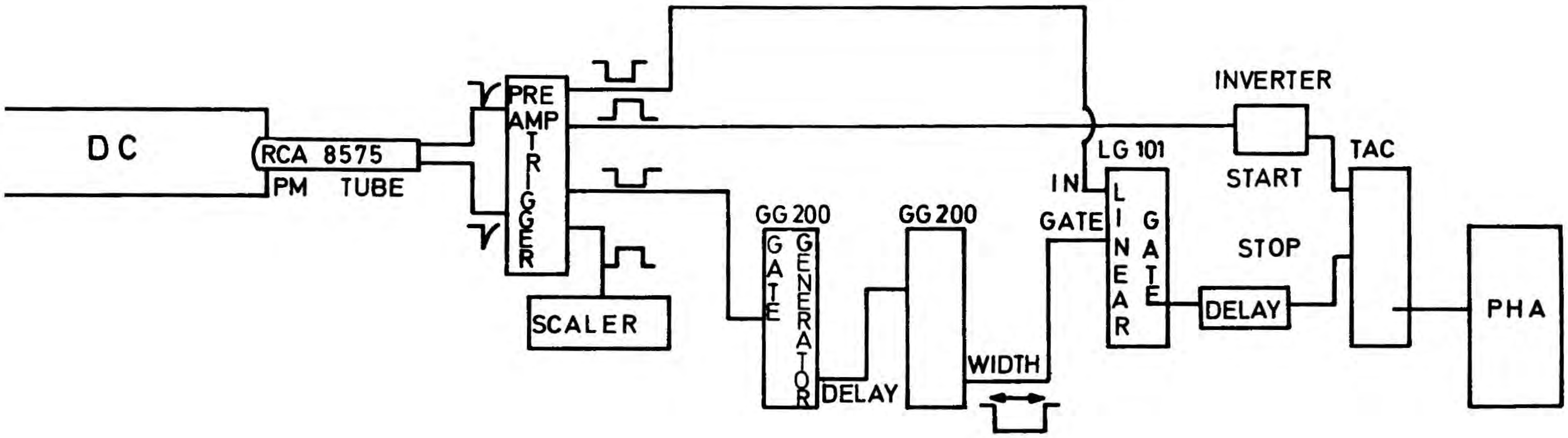

FIG.2 Electronics used to store drift time distribution on a P.H.A.

by means of its built-in analogue to digital converter (A.D.C.).

The output from the photomultiplier was divided into two and converted separately into fast NIM standard signals by means of a C.E.R.N multi-channel preamp-trigger which produced two simultaneous outputs (one inverted) for an input. The primary scintillation signal (a preamp-trigger output) was used to start the T.A.C. To stop the T.A.C. by the secondary scintillation signal, one of the preamp-trigger outputs was fed into a linear gate and another output from the preamp-trigger was used to open the gate for a certain duration, at the time of arrival of the secondary scintillation signal. The gate width and the delay were constantly monitored to ensure that the gate time window always contains the secondary scintillation pulse. Under these conditions the linear gate output provided the necessary stop signal to the T.A.C. In order to shift the drift time distribution to convenient channels on the P.H.A, a known time of extra delay was introduced to the stop signal. The data rate was kept low (< 50 Hz) to avoid false start and stop signals being fed into the T.A.C.

The drift times (channel numbers) were measured at different drift fields and nitrogen concentrations. To investigate the effect of drift distance on drift time, some of the results were repeated for drift distances, d, of 1 cm and 2.5 cm. The channel number corresponding to zero drift time was obtained by irradiating the region around the anode wire with α-particles and noting the lowest channel to be excited. Finally the T.A.C. - P.H.A. system was calibrated by feeding in pulses separated by known delays to the T.A.C. using a pulse generator . The T.A.C. - P.H.A. system was found to be linear throughout the operating range and the system sensitivity was found to be 10 ns/channel. It was observed that the rise time of the secondary scintillation pulses was much larger than that of the primary scintillation pulses. In order to minimise the timewalk arising from this difference, both pulses were discriminated at a lower level (200 μV) to produce the NIM standard signals. It was also found that the amplitude of the photomultiplier output dropped with the nitrogen concentration in the mixture. This reduction was compensated for by adjusting the photomultiplier voltage. The amplitude of the photomultiplier output was maintained at ∿ 6 mV (∿ 3 mV at each preamp-trigger input) throughout the experiment.

4.2.2 Experimental Results

4.2.2 (a) Effect of the Anode Wire Potential on the Drift Time

The collimated α-source was placed at a distance of 1.8 cm from the anode wire. The drift field set by the cathode planes was kept at a fixed value and the drift times of the electrons were measured at different anode wire voltages. This measurement was repeated for different drift fields and different concentrations of nitrogen. The results are shown in Fig (3), which indicate a considerable dependence of drift time on the anode wire potential. This is because the drift velocity of electrons in the argon-nitrogen mixture does not attain saturation within the working range of the drift field, and therefore is affected by the sense wire field. The effect of anode wire potential on the measurement of drift time was minimised by operating the anode wire at the lowest possible potential, which was found to be about 550 V. Furthermore, all the measured drift times have been corrected for anode wire potential effect as follows :

Fig (3) shows that the plot of drift time against anode wire potential is linear on a log-linear graph. The gradients of the plots for different concentrations of nitrogen and different drift fields are found to be nearly the same. To obtain the correction factor, the drift

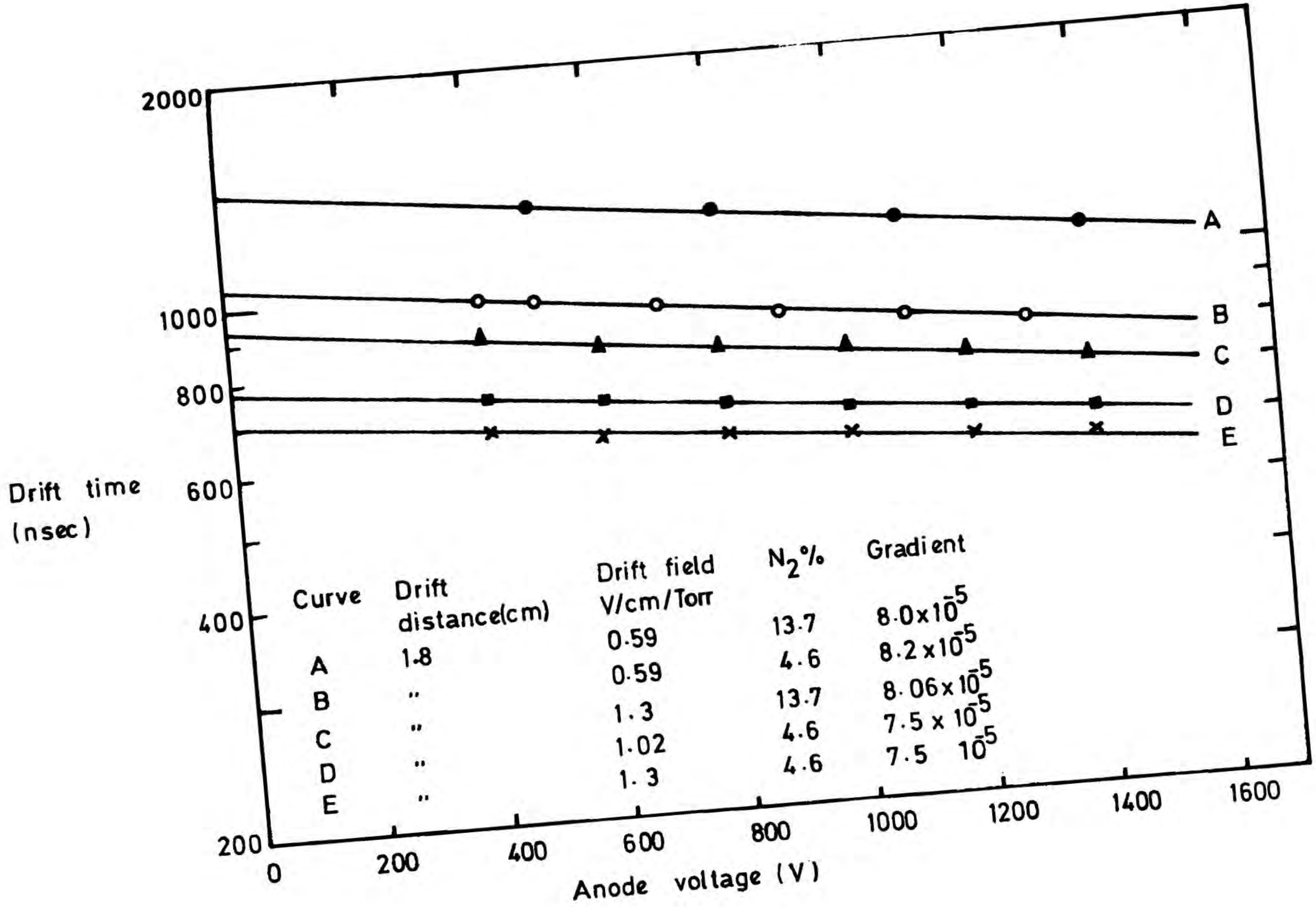

Curve	Drift distance(cm)	Drift field V/cm/Torr	N_2%	Gradient
A	1.8	0.59	13.7	8.0×10^{-5}
B	"	0.59	4.6	8.2×10^{-5}
C	"	1.3	13.7	8.06×10^{-5}
D	"	1.02	4.6	7.5×10^{-5}
E	"	1.3	4.6	$7.5 \ 10^{-5}$

FIG. 3 Dependence of drift time on the anode voltage.

times corresponding to zero anode wire potential were obtained by extrapolating the straight lines to the drift time axis. The correction factor is the ratio of the drift time at zero anode wire potential to that at the potential of 550 V. The correction factors were calculated for different drift fields and concentrations of nitrogen and the mean value of the correction factor so obtained was used to correct all the subsequent measured drift times for the drift distance of 1.8 cm. The error involved in assuming the same correction factor for all the measured drift times is less than 2%. A similar procedure was followed to correct the drift times for the drift distances of 1.0 cm and 2.5 cm. As expected, the correction factors for 2.5 cm and 1.0 cm. were smaller and larger respectively than the value for 1.8 cm. The measured and corrected values of the drift times as a function of the drift fields for two different nitrogen concentrations are shown in Fig (4).

The corrected drift velocities as a function of drift field for different drift distances are shown in Fig (5). The percentage of nitrogen in the mixture for these measurements was 4.6. The curve for the 1.0 cm drift distance is in good agreement with that for 1.8 cm. except at low drift field values where the 1.0 cm values are slightly higher than the 1.8 cm values. The curve for a drift distance of 2.5 cm is lower than the other two ; this is probably due to diffusion effects and the potential dip around the field wire.

4.2.2 (b) Drift Velocity as a Function of Drift Field

Fig (6) shows the corrected drift velocity measured as a function of drift field for different nitrogen concentrations. Data for the drift fields below 0.5 v/cm. Torr are slightly inaccurate due to the slow rise time of the secondary pulse and above that value, the variation of rise time with the drift field was found to be small ($t_r \sim 45$ nS).

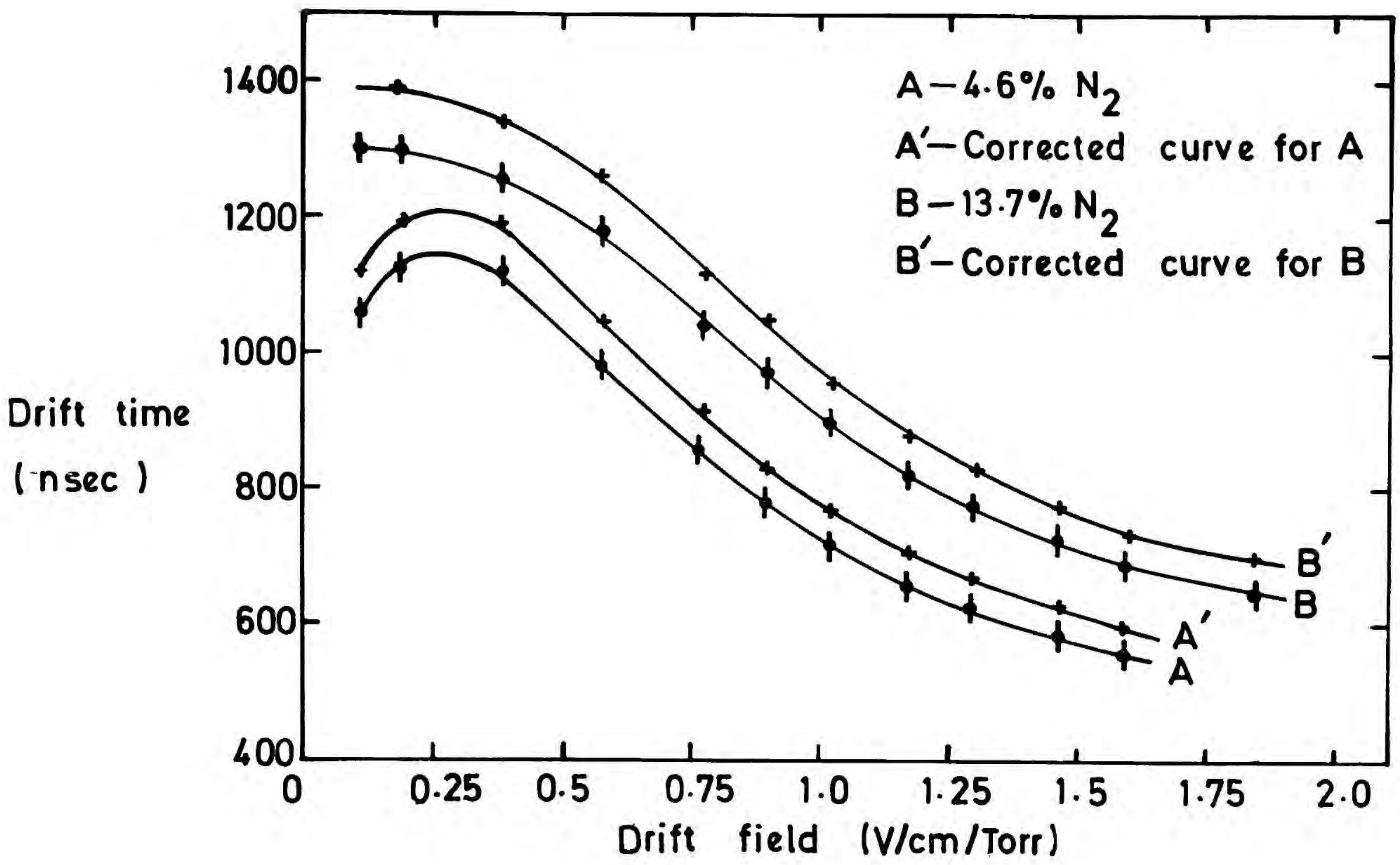

FIG. 4 Corrected drift time versus drift field.

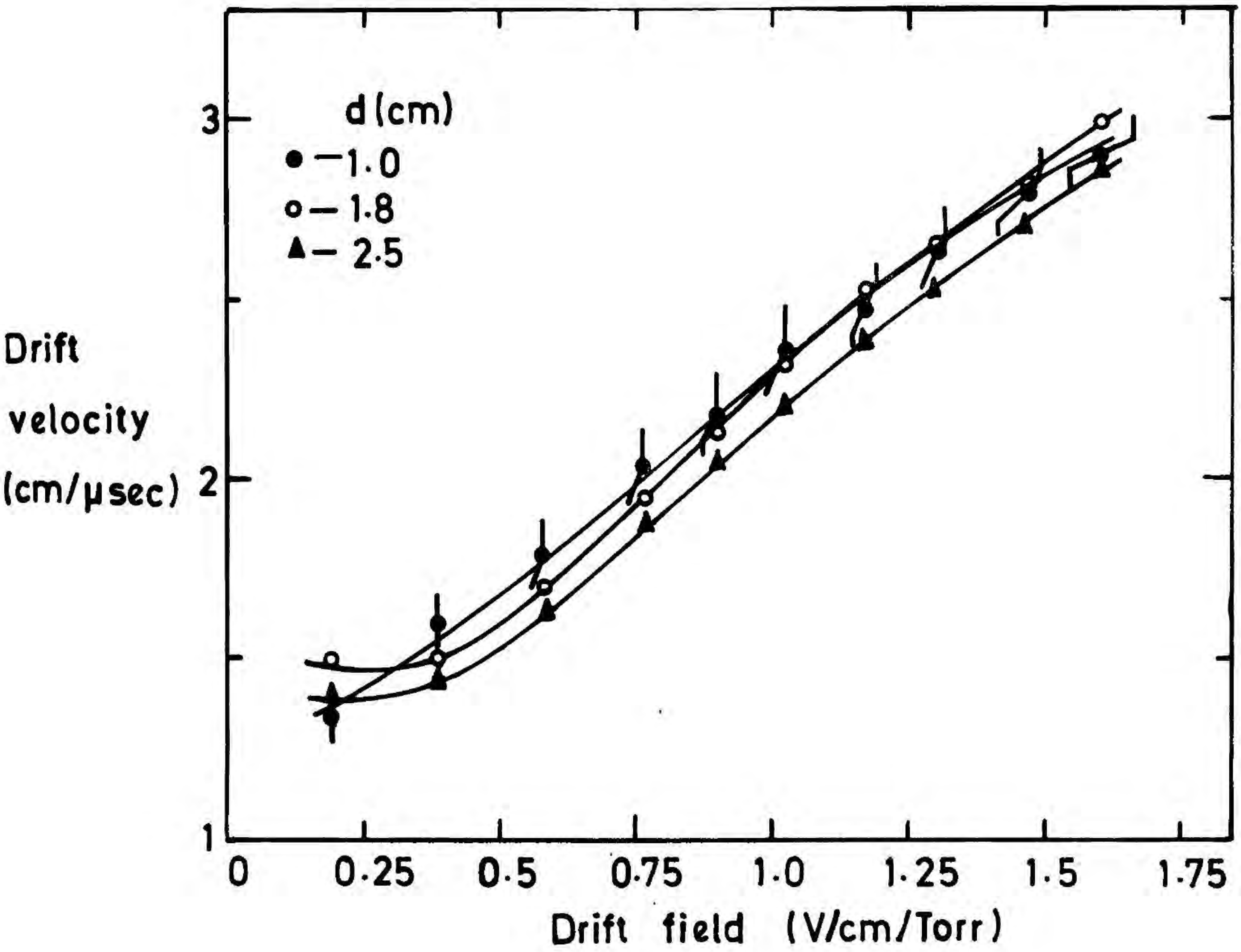

FIG.5 Corrected drift velocity as a function of drift field for different drift distances.

Accuracy of the measurements was estimated to be ∿ 5 per cent. The main feature of these curves is the monotonic increase od drift velocity with the drift field although the curve for smallest nitrogen concentration (1.96%) appears to saturate just outside the maximum drift field that could be obtained with our chamber. The drift velocity results obtained by Colli et al$^{(2)}$ show that both the saturated value of the drift velocity and the drift field at which the saturation occurs increase with the nitrogen concentration, at least for mixtures with small nitrogen concentrations (see Fig (7)). Unfortunately we have not been able to reach saturation velocities with the nitrogen concentrations given in Fig (6) because of electrical discharges across the electrode planes.

4.2.2 (c) Drift Velocity as a Function of Nitrogen Concentration

The drift velocity of electrons in the mixture was measured as a function of nitrogen concentration and the results corresponding to drift fields of 1.02 and 0.59 V/cm. Torr are shown in Fig (8). The drift velocity - nitrogen concentration curve shows a maximum at a nitrogen concentration of about 2.5%. The dotted curves in Fig (8) were calculated from the measured drift velocities in pure argon and nitrogen. The method of calculation is described in Section 4.2.5.

4.2.3 Comparison with Other Results

Most of the measurements of drift velocity of electrons obtained with argon-nitrogen gas mixtures have been measured with small nitrogen concentrations of less than 2%. However, Klema et al$^{(3)}$, using an ionisation chamber, obtained the drift velocity of electrons in a "pre-purified" argon - 10% nitrogen gas mixture as a function of drift field and their results are presented in Fig (9) with the results obtained in the present study for an argon - 10% nitrogen mixture. The drift velocity values corresponding to drift fields above 0.5 V/cm. Torr

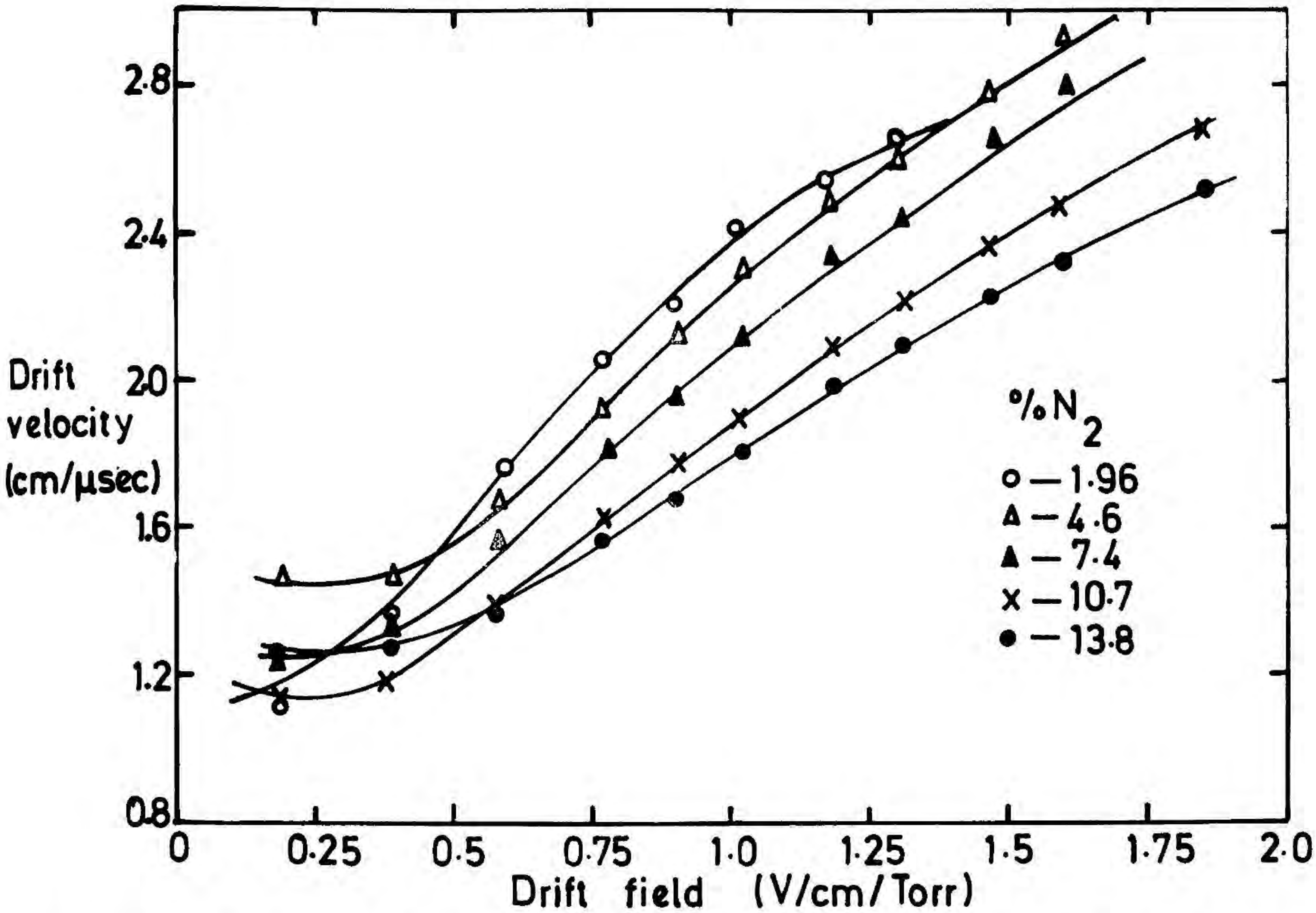

FIG. 6 Drift velocity of electrons in Ar - N_2 mixture as a function of drift field for different nitrogen concentrations.

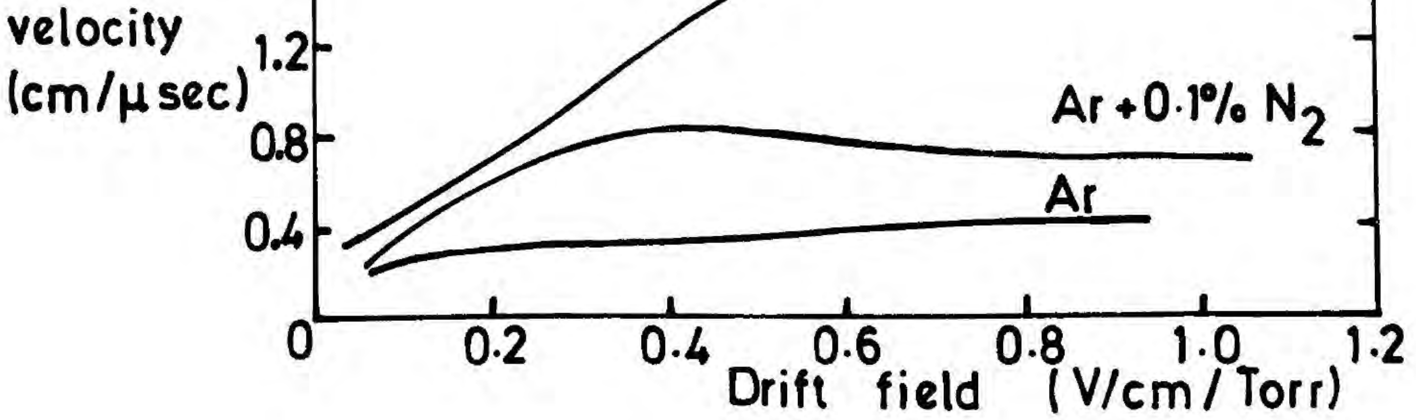

FIG. 7 Drift velocity of electrons in pure argon, and in Ar with small added quantities of N_2.

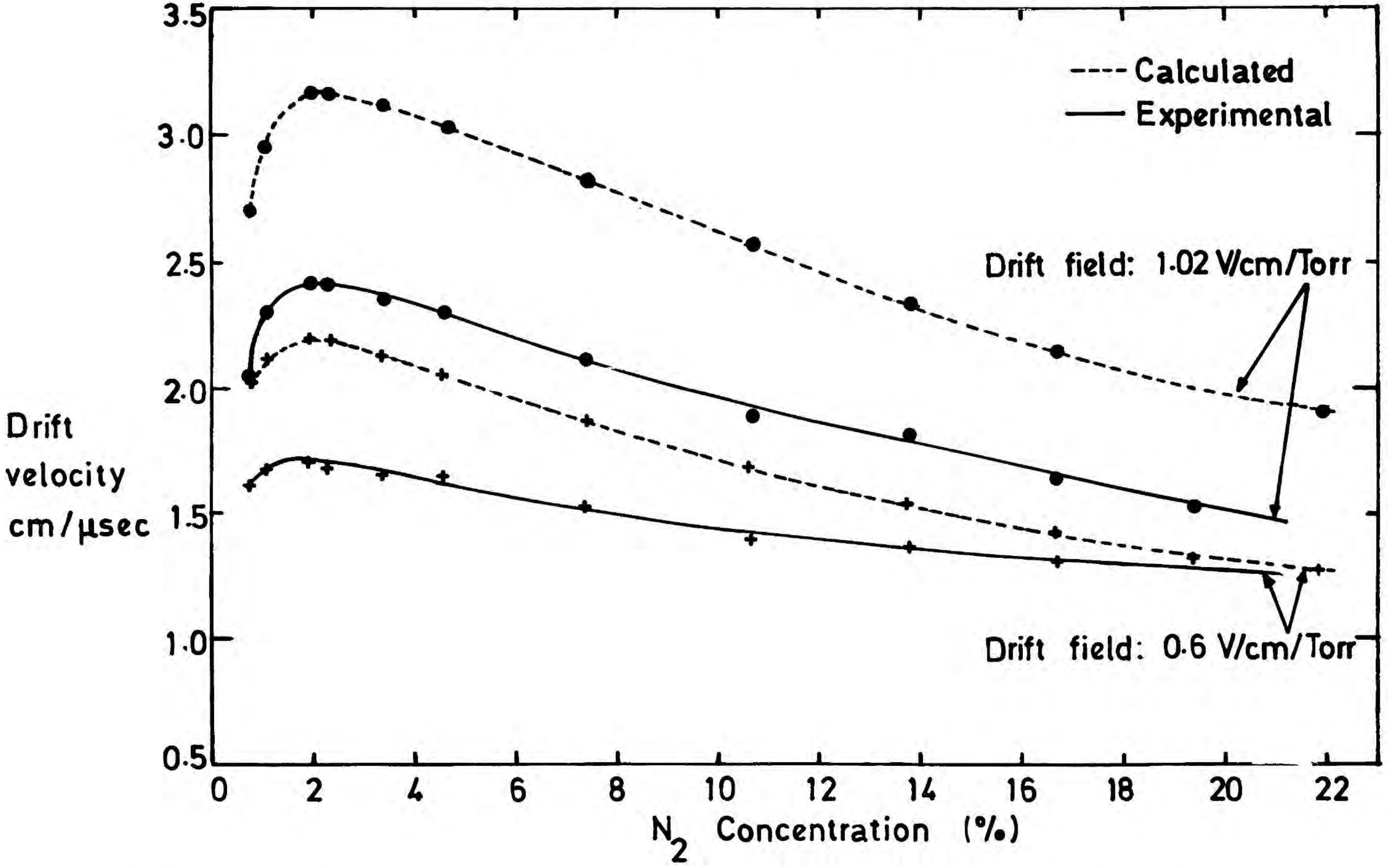

FIG.8 Drift velocity versus nitrogen concentration for two drift fields.

obtained in the present study are in agreement with the values obtained by Klema et al within ten per cent. English and Hanna$^{(3)}$ have also studied the drift velocity of electrons in argon-nitrogen mixtures with large nitrogen concentrations (0-20%), but their work was confined to small drift fields (0-0.6 V/cm.Torr) in which range the results of this study are not very accurate.

4.2.4 Calculation of Drift Velocity for Different Nitrogen Concentrations

English and Hanna$^{(4)}$ suggested an approximate method of calculating the drift velocity of electrons in a mixture of gases from a knowledge of the characteristics of the constituents. A brief description of the method of calculation is given and the drift velocities for the mixture of argon and nitrogen are compared with the experimental results.

If the electron mean free path per torr and the average fractional energy loss by the electron per collision with the constituent gases are known, the same quantities for the mixture of gases are given by

$$\frac{1}{\lambda_M} = (1 - F)/_{\lambda_A} + F/_{\lambda_N} \tag{4.1}$$

$$\eta_M/_{\lambda_M} = (1 - F)\eta_A/_{\lambda_A} + F\eta_N/_{\lambda_N} \tag{4.2}$$

where λ's and η's are the mean free paths per torr and average fractional energy losses per collision respectively. A, N and M refer to pure argon, pure nitrogen and mixture containing a fraction F of nitrogen respectively.

The relation between the drift velocity W, electric field strength E and the agitational velocity U can be written$^{(5)}$ as

$$W = 0.826 \left(\frac{e}{m}\right)\left(\frac{E}{p}\right)\left(\frac{\lambda}{U}M\right) \tag{4.3}$$

where p is the pressure of the gas in Torr and e and m are the charge and mass of the electron respectively. Equation (4.3) merely expresses quantitatively the fact that the drift velocity is proportional to the field strength multiplied by the average time between collisions. The derivation of this equation is given, for example, in Ref (5). The numerical constant which depends on the agitational velocity distribution of electrons is related to the Druyvesteyn distribution. The relation between W and U can also be written as

$$W^2 = 0.413 \quad \eta_M U^2 \tag{4.4}$$

Equation (4.4) can be derived by considering the amount of energy gained by an electron moving under an electric field and the subsequent losses through collisions with molecules, [i.e. for an electron traversing a distance d

$$E\ e\ d = \frac{Up}{\lambda_M} \quad \frac{d}{W} \quad \eta_M \quad m\ U^2/_2$$]

Substituting for W in (4.3) from (4.4) and also substituting the numerical values for e and m, equations (4.3) and (4.4) can be rewritten as

$$E/_p = 4.42 \times 10^{-16} \quad U^2 \ (\eta_M)^{\frac{1}{2}} \ (\lambda_M)^{-1} \tag{4.5}$$

$$W = 0.642\ U\ (\eta_M)^{\frac{1}{2}} \tag{4.6}$$

λ_M and η_M can be calculated as a function of U from equations (4.1) and (4.2), if λ_A, λ_N, η_A and η_N are known functions of U. Thus the values of W and $E/_p$ can be obtained for a particular value of U by

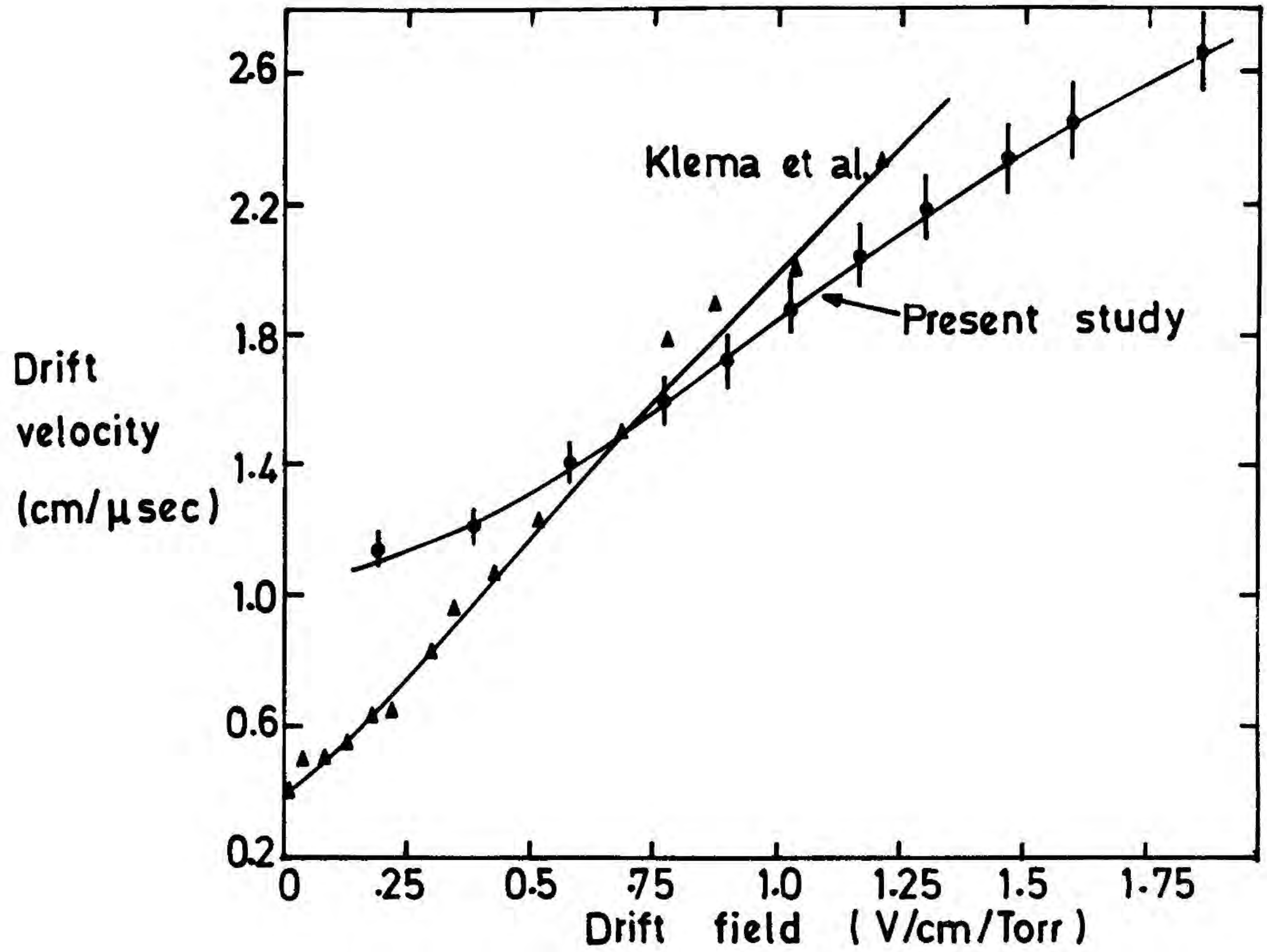

FIG.9 Comparison of drift velocity mesurements for Ar – 10% N_2 mixture.

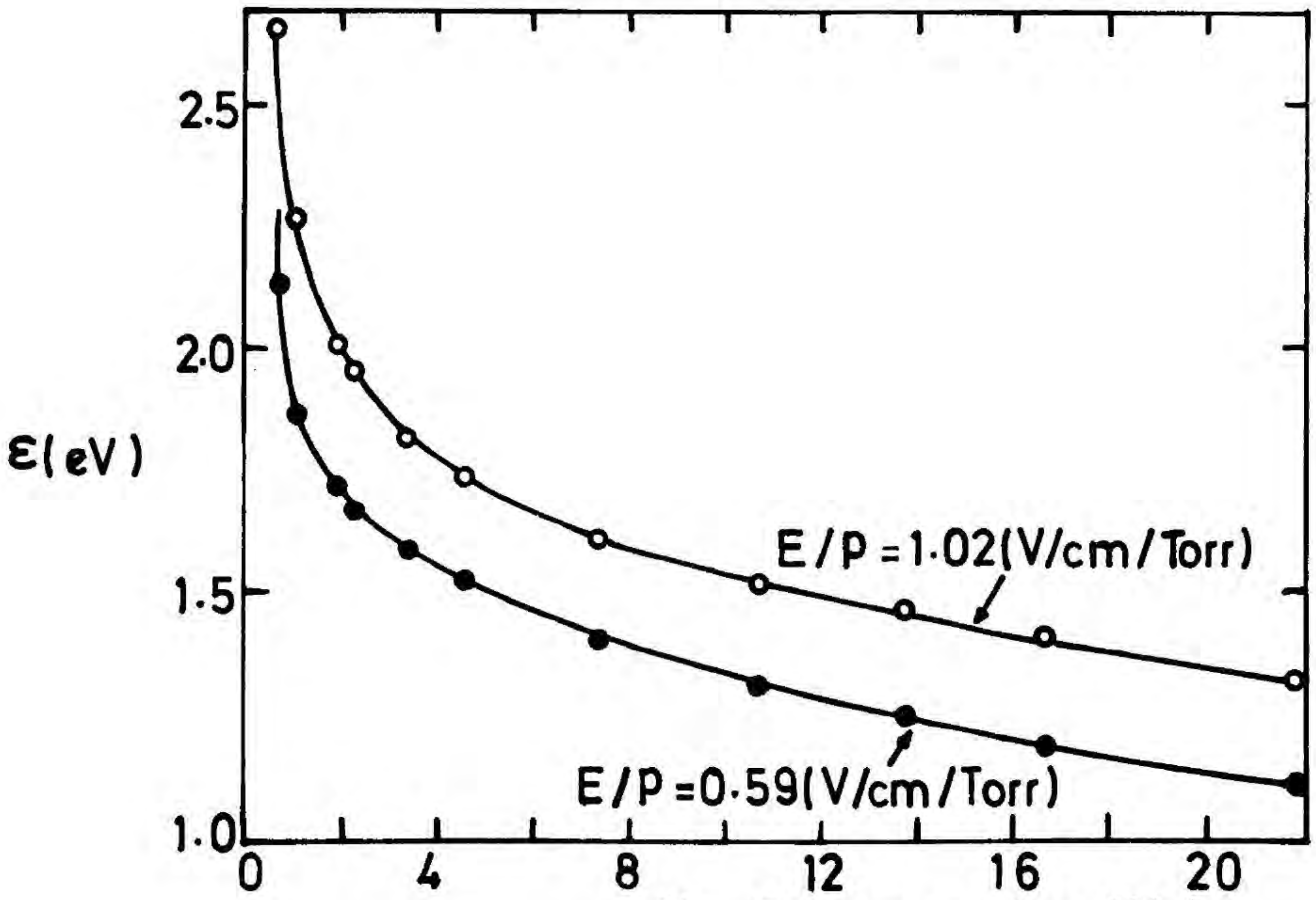

FIG.10 Mean agitational energy of electrons in argon – nitrogen mixture.

substituting λ_M and η_M corresponding to the same U value in equations (4.5) and (4.6).

The mean freepath per torr and the average fractional energy loss of electrons in pure argon and nitrogen have been calculated from the following expressions$^{(6)}$

$$\lambda = 7.38 \times 10^{-9} \frac{W(k)^{\frac{1}{2}}}{E/_p} \qquad (4.7)$$

$$\eta = 2.21 \times 10^{-14} \frac{W^2}{k} \qquad (4.8)$$

where k is the measured value of the Townsend's energy factor which is defined as the ratio of the mean agitational energy of the electrons to the mean thermal energy of gas molecules. In the derivation of relations (4.7) and (4.8) a Druyvesteyn distribution of electrons has been assumed. The drift velocity measurements of Colli and Facchini$^{(2)}$ for pure argon and the drift velocity measurements of Nielson$^{(7)}$ for pure nitrogen have been used to calculate λ_A, η_A, λ_N and η_N. The values of k obtained for nitrogen by Crompton and Sutton$^{(6)}$ and for argon by Townsend and Bailey (as quoted by Townsend$^{(5)}$) have been used.

Following the above procedure the drift velocity as a function of $E/_p$ has been calculated for different concentrations of nitrogen. The drift velocities obtained for $E/_p$ = 0.59 and 1.02 V/cm.Torr have been plotted as a function of nitrogen concentration in Fig (8). The calculated values are found to be consistently higher than the measured values, but the shapes of the calculated curves are very similar to those of the experimental curves. The maxima of the measured drift velocity curves are nearly at the same positions as the calculated drift velocity curves. The disagreement between the calculated and measured values of drift velocity could be due to two reasons.

(1) Since the drift velocity of electrons in pure argon is extremely sensitive to small amounts of impurities, the values of W and also of k obtained by Townsend et al are probably not representative of a pure gas.

(2) Deviation of the actual energy distribution of electrons from the Druyvesteyn distribution law, derived by assuming only elastic collisions between electrons and gas molecules, and mean free paths (α 1/elastic scattering cross-section) between collisions independent of electron energy. This situation is far from reality especially in the case of gas mixtures containing a molecular gas and a noble gas because of the inelastic collisions of electrons with the gas molecules and the complex energy dependent elastic cross-section of electrons in noble gases. It is found that most practical situations can be described however, by assuming either a Druyvesteyn or a Maxwellian distribution of electrons.

The mean agitational energy of electrons E, mean free path per Torr λ_M and the average fractional energy loss per collision η_M are also plotted as a function of nitrogen concentration in Figs (10), (11) and (12) respectively.

The drift velocity maximum obtained with the argon-nitrogen mixture can be explained qualitatively by considering the scattering cross-section curves for pure argon and nitrogen. The momentum transfer cross-section of electrons in pure argon(8) as a function of agitational energy is shown in Fig (13). In general the momentum transfer cross-section, q_m, differs from the total collision cross-

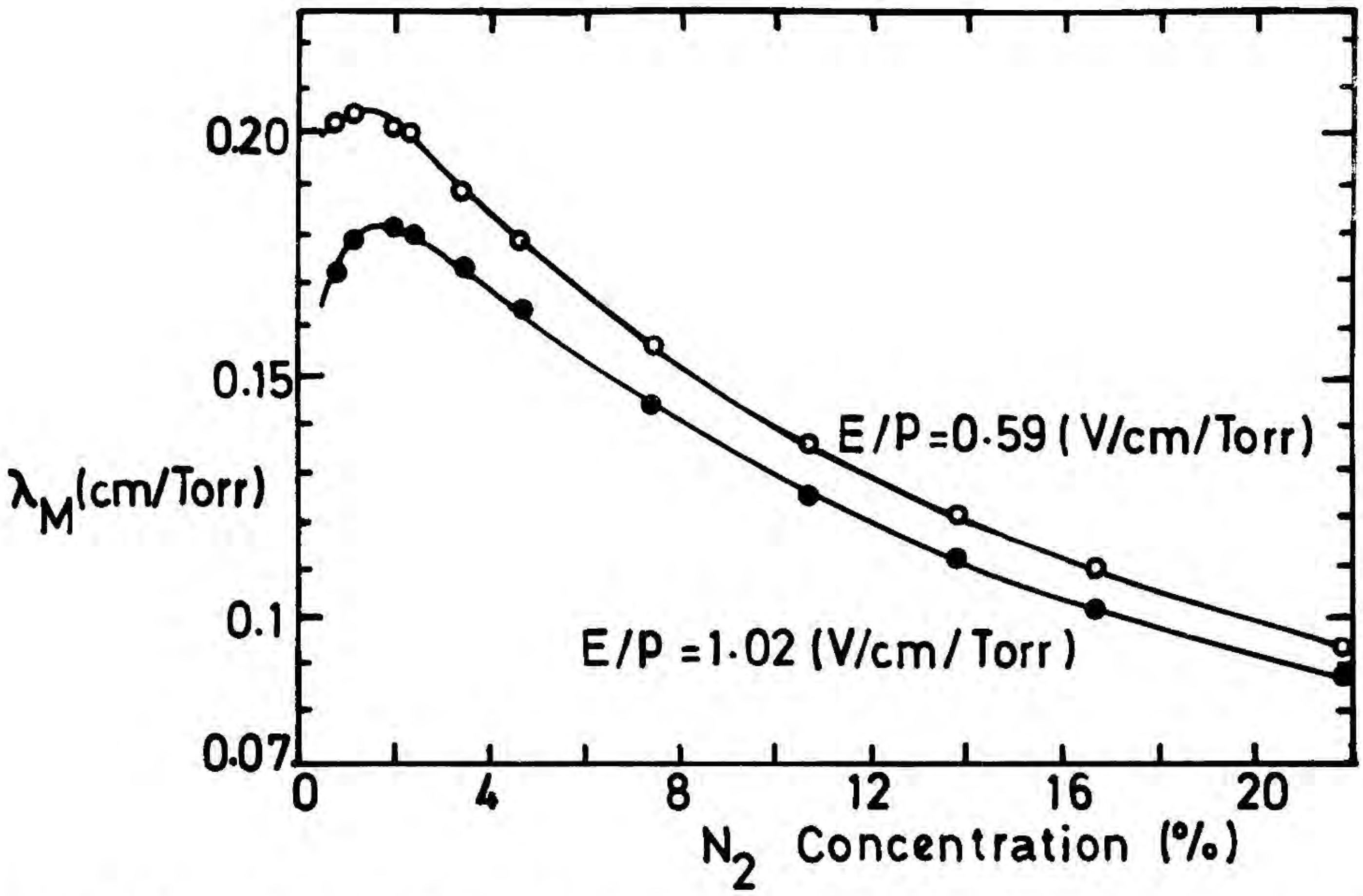

FIG.11 Mean free path of electrons in argon-nitrogen mixture as a function of nitrogen concentration.

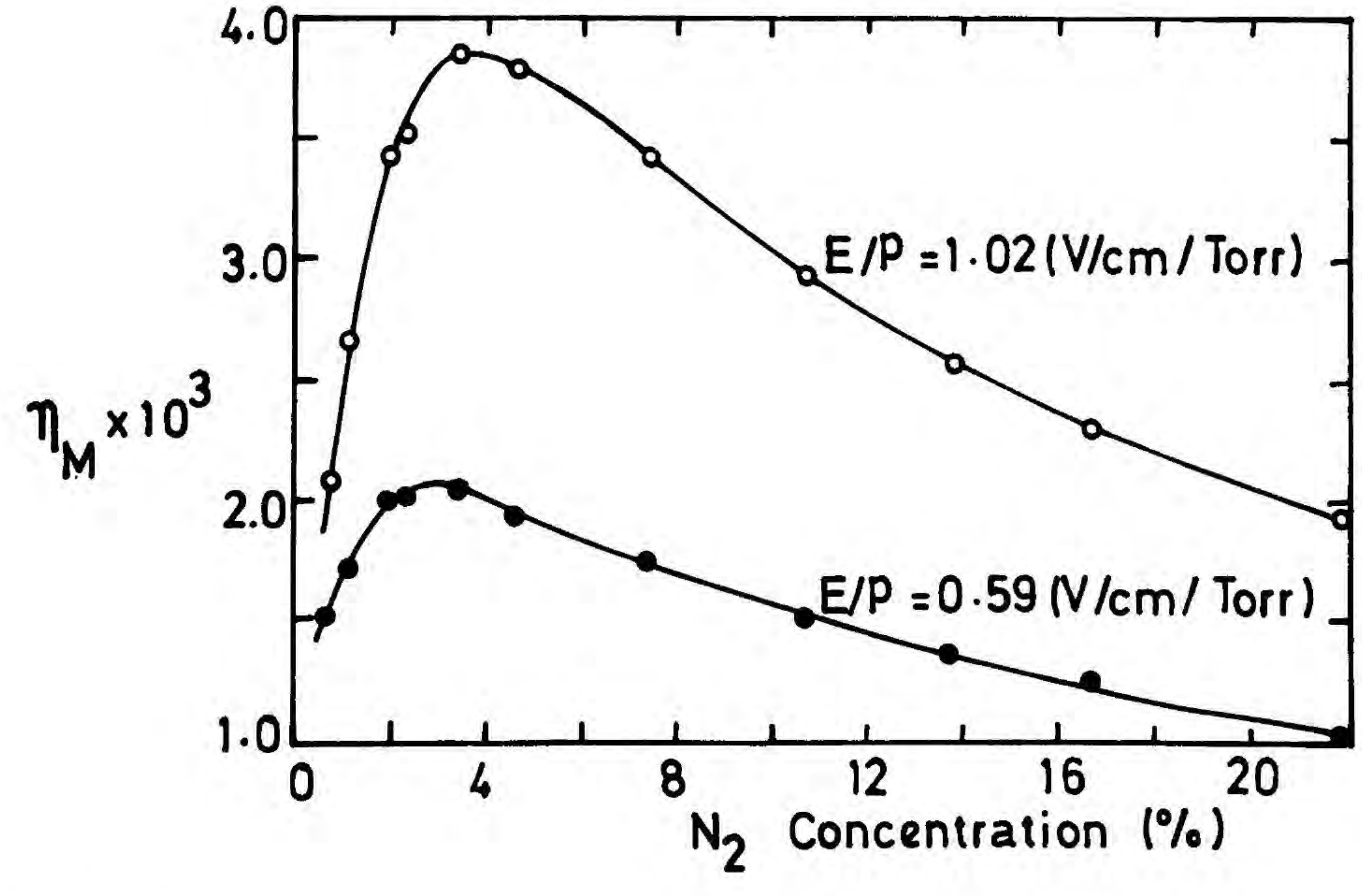

FIG.12 Mean fractional energy loss of electrons in argon-nitrogen mixture as a function of nitrogen concentration.

section q_s since the former value depends on any anisotropic behaviour in the scattering process. For isotropic scattering $q_m = q_s$ and the results of Massey and Burhop$^{(9)}$ show that for electrons the two values agree closely at low electron energies (< 10 eV) and that $q_m > q_s$ at higher energies.

The agitational energy of electrons in pure argon is high even at moderate drift fields, (see Fig (14)) and a small addition (1-2%) of nitrogen to argon causes a rapid fall in the agitational energy of electrons in the latter (see Fig (10)). The change induced by this addition on the electron scattering cross-section curve for pure argon (curve in Fig 13) is negligible however, as the nitrogen concentration in the mixture is very small. The scattering cross-section curve for pure argon can therefore be used to explain the behaviour of argon-nitrogen mixtures whose nitrogen concentration is small compared to argon.

According to the behaviour of the scattering cross-section curve for pure argon, the decrease in agitational energy is accompanied by a reduction in the scattering cross-section of electrons in the mixture and as a result the mean free path ($\alpha \frac{1}{q_s}$) of electrons increases giving rise to a higher drift velocity. Consistent with this argument, Fig (11) shows a sharp increase in the mean free path for collision, λ_M, with the addition of a small percentage of nitrogen. The increase in the fractional energy loss of electrons in this region (see Fig (12)) is mainly due to the inelastic collisions of electrons with nitrogen molecules and is the main reason for the rapid fall in the agitational energy with the addition of nitrogen.

As the percentage of nitrogen in the mixture is increased, the elastic scattering cross-section of electrons in nitrogen begins to

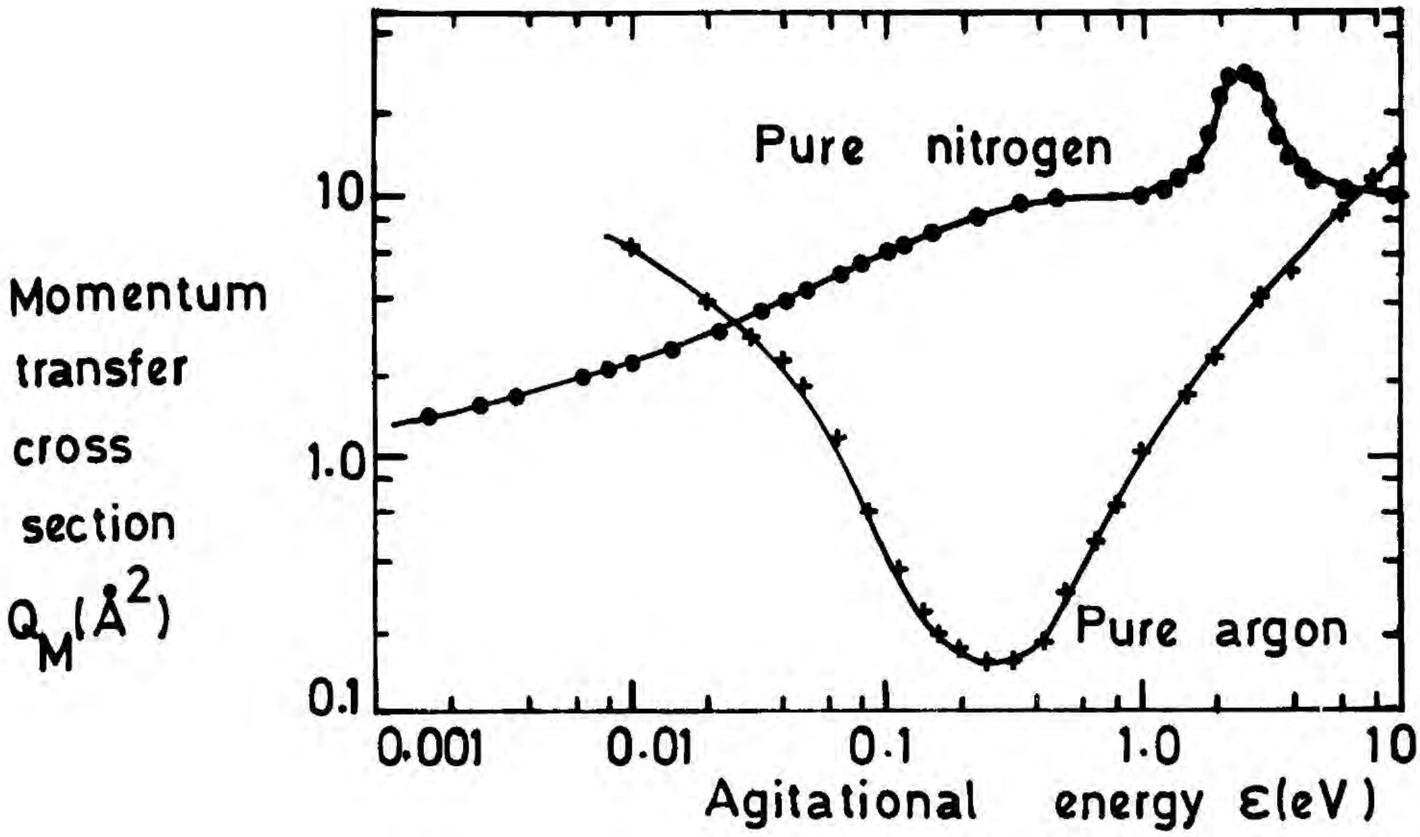

FIG.13 Momentum transfer cross section of electrons in argon and nitrogen as a function of mean agitational energy.

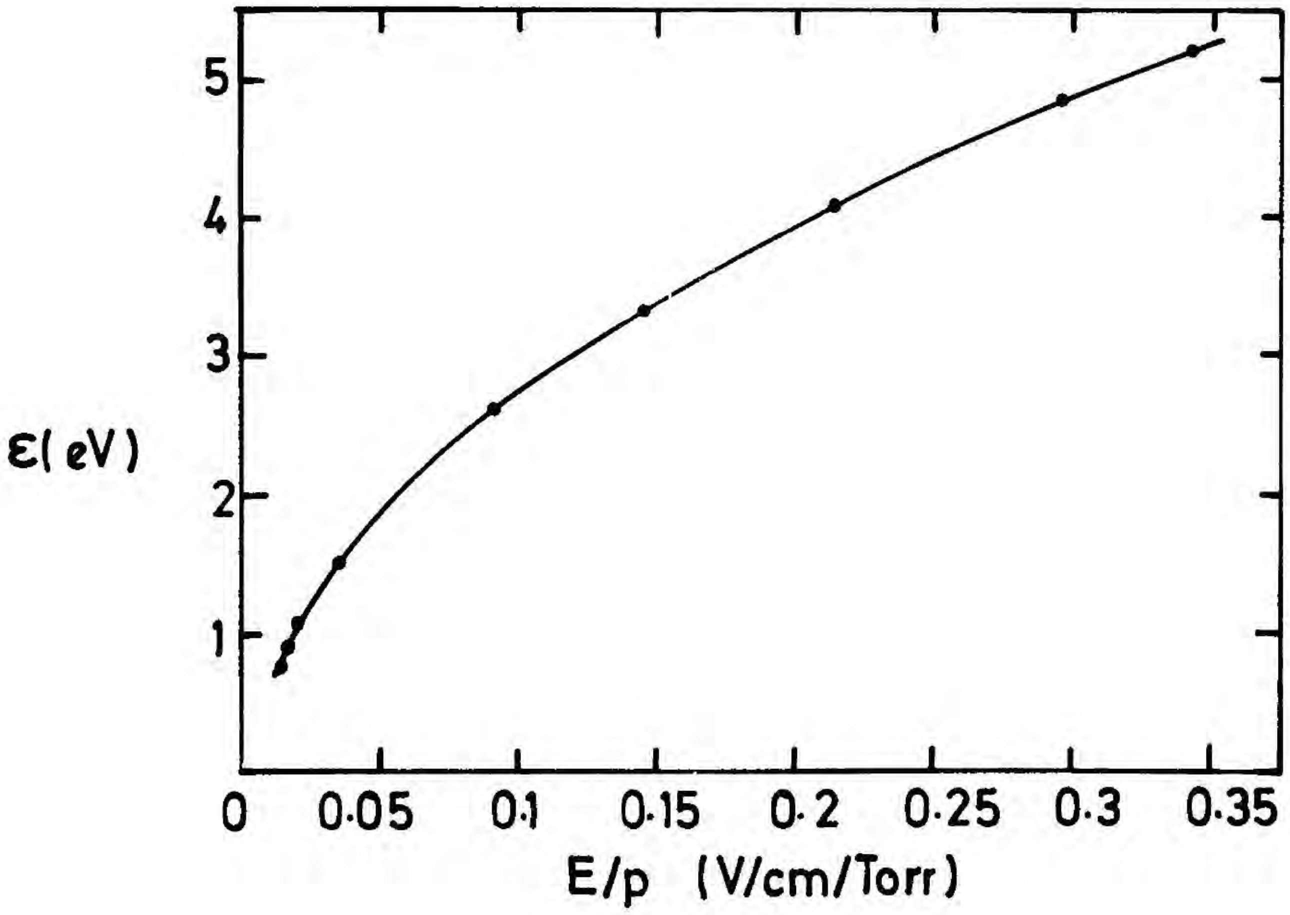

FIG.14 Mean agitational energy of electrons in argon as a function of electric field.

dominate and gradually it fills up the cross-section dip (Ramsauer dip) in the argon cross-section curve, resulting in shorter electron mean free paths for collisions and hence smaller drift velocities. This change over from increase to decrease of drift velocity should take place at a small nitrogen concentration since the electron scattering cross-section in nitrogen$^{(10)}$ is much larger than that in argon for small agitational energies (see Fig (13)).

4.3 SECONDARY SCINTILLATION LIGHT GAIN

The amount of secondary scintillation light emitted per unit energy loss of the incident radiation in a GSDC operating at high rate is of great importance for two reasons :-

(i) If the gas mixture is efficient in producing secondary light, the counter can be operated at low anode voltages to minimize the space charge effects which greatly deteriorate the performance of the counter at high rate.

(ii) The energy resolution of the counter improves with greater light output.

As mentioned in chapter three the production of secondary electron-ion pairs is inevitable during the secondary scintillation process around the anode wire. The light gain is therefore always accompanied by a corresponding charge gain which is defined as the ratio of secondary scintillation charge to the primary charge.

It is obvious that the secondary scintillation light output is a function of nitrogen concentration in the mixture. In order to achieve successful operation of the counter, the percentages of the constituents of the gas mixture must be chosen in such a way that the light output for a fixed charge gain is a maximum. It was with this intention that the light and charge gain in the argon-nitrogen mixture were investigated.

4.3.1 Experimental Arrangement

A planar scintillation proportional chamber was used in these measurements in order to avoid the unnecessary drift voltage and the undesirable gap between the outer cathode plane and the earthed plane. The experimental system is shown in Fig (15). The whole chamber was built from perspex. The two cathode planes and the anodw wire plane were made out of three separate frames in order to have flexibility in thickness of the active volume of the chamber. The outer cathode was a plate of aluminium, the inside of which was covered with aluminised mylar. A small hole was pierced on the plate close to its centre in order to allow radiation into the chamber. The inner cathode plane was made from 120 μm diameter copper-Beryllium wires with 1 mm spacing. A 200 μm diameter nickel wire was used as an anode. On either side of the anode wire there was a potential wire (300 μm diameter) to facilitate the drift of the electrons towards the anode wire. The distance from the anode wire to each cathode plane was 6 mm. The rest of the design of the chamber was identical to the one (GSDC) described in chapter three.

The anode wire was connected to a positive H.T. power supply and both the cathode planes and the potential wires were at earth potential. A collimated source of Am^{241} α-particles (5.486 MeV) was fixed firmly with double sided adhesive tape to the hole in the outer cathode plane to allow α-particles into the chamber without passing through a window material. The charge pulse produced by an X-ray source is not sufficient to be detected but the amount of charge produced by an α-source can be detected easily. The thickness of the collimator was adjusted so that the range of α-particles extends to the inner cathode plane. The range of 5.47 MeV α-particles both in argon and nitrogen at NTP is approximately 4 cm(11).

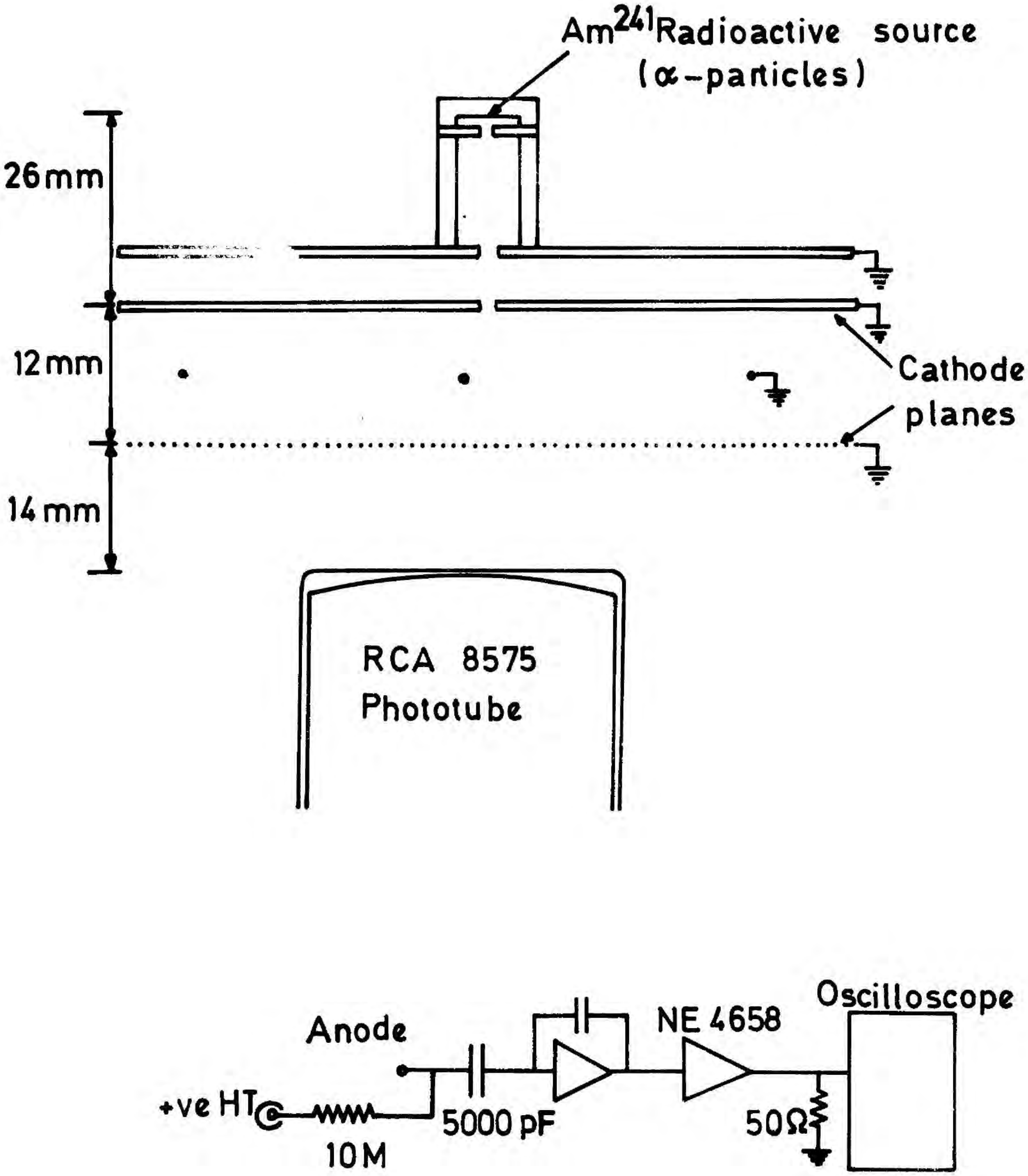

FIG. 15 Experimental arrangement to measure light and charge gains of a G.S.P.C .

The light output from the photomultiplier and the charge output from the anode wire were obtained through a decoupling H.T. ceramic capacitor (5000 pF) and amplified by means of a F.E.T. input charge sensitive amplifier ($T_r \simeq 100$ nS) and a Nuclear Enterprise main amplifier, NE 4658 (with equal integrating and differentiating time constants of 0.8 μ sec). The amplitude of the output (into 50 Ω) was measured on a Tektronix, TEK 475, oscilloscope.

The secondary scintillation pulse height was found to rise sharply with anode voltage and as a result the preamplifier appeared to saturate at relatively low anode wire voltages. In order to avoid such saturations in the system and to obtain measurements over a large range of anode voltages (0 - ∿ 3000 V) the following procedure was adopted.

(i) The photomultiplier was operated at relatively low voltages (900 V - 1100 V).

(ii) An attenuator (attenuation of 1 dB) was inserted between the preamplifier and the photomultiplier output to reduce both primary and secondary scintillation amplitudes to reasonable levels before commencing the measurements.

(iii) The photomultiplier was operated well below its saturation limit and the required dynamic range in the output pulse height was achieved by operating the photomultiplier at a lower voltage for higher anode wire voltages and later normalising all the pulse heights to one photomultiplier voltage.

4.3.2 Results (a) Light Gain

Fig (16) shows the dependence of the secondary light gain on the applied anode Voltage for different nitrogen concentrations. It should be mentioned that the first few values in each curve are not very accurate

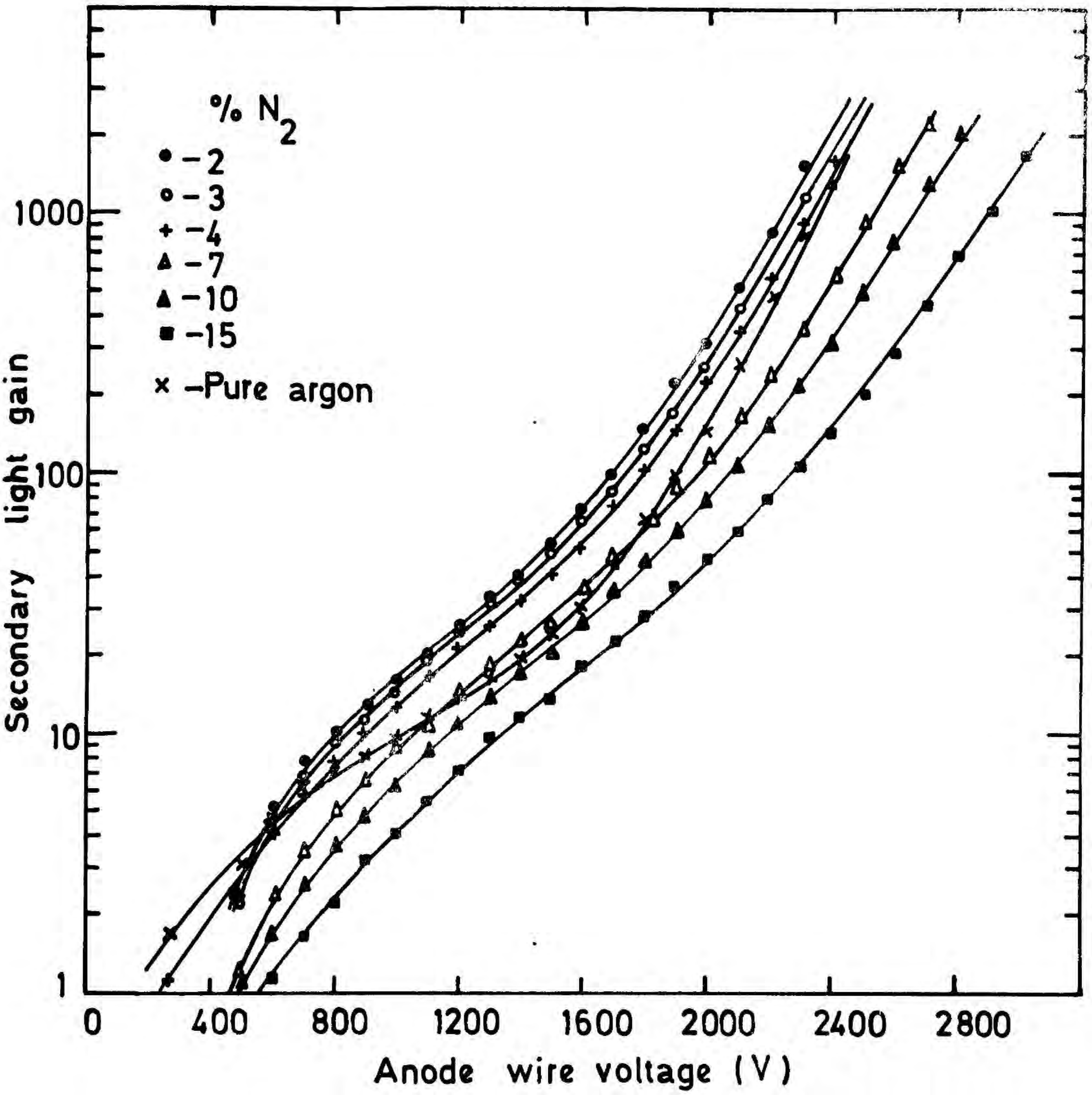

FIG.16 Secondary light gain as a function of anode voltage for different nitrogen concentrations in argon nitrogen mixture.

because of the small secondary light amplitudes.

All the curves show two distinct slopes, one at low anode voltages and the other at high anode voltages, though they can not be distinguished at the middle. These slopes can be attributed to two stages in the light production mechanism ; at low anode voltages the secondary light production is mainly due to the excitations of the gas atoms only by the primary electrons, but at high anode voltages the primary electrons acquire more energy from the electric field and produce more secondaries which then dominate in the light production process. Another feature of these curves to be noted is the drop in the light gain with nitrogen concentration for a fixed anode voltage (2000 V) (see Fig (17)). It can be seen from Fig (17) that the light gain drops with nitrogen concentration with an indication of a maximum at about 1% N_2.

A maximum was also obtained in the secondary light amplitude at 2% nitrogen concentration, (see Fig (18)). The same general behaviour has been observed by Policarpo et al[(12)] working at 1000 Torr. They found the maximum light output for secondary scintillation at a nitrogen concentration of 2.5%. In contrast to the maximum obtained in the light gain curve the maximum in the secondary light output curve near 2% N_2 is entirely due to the lack of sensitivity of the photomultiplier to photons in the far ultraviolet region in which most of the emission from the argon-nitrogen mixture occurs. This is due to insufficiency of nitrogen population which would convert the argon excited states to nitrogen excited states. This has been investigated by Alves et al[(13)] using a photomultiplier and a quartz window coated with p-quaterphenyl wavelength shifter. Their results are shown in Fig (19). The flat response obtained for small nitrogen concentrations is clear evidence of the fact that lack of spectral sensitivity of the detection system creates the light output maximum at 2.5% of nitrogen.

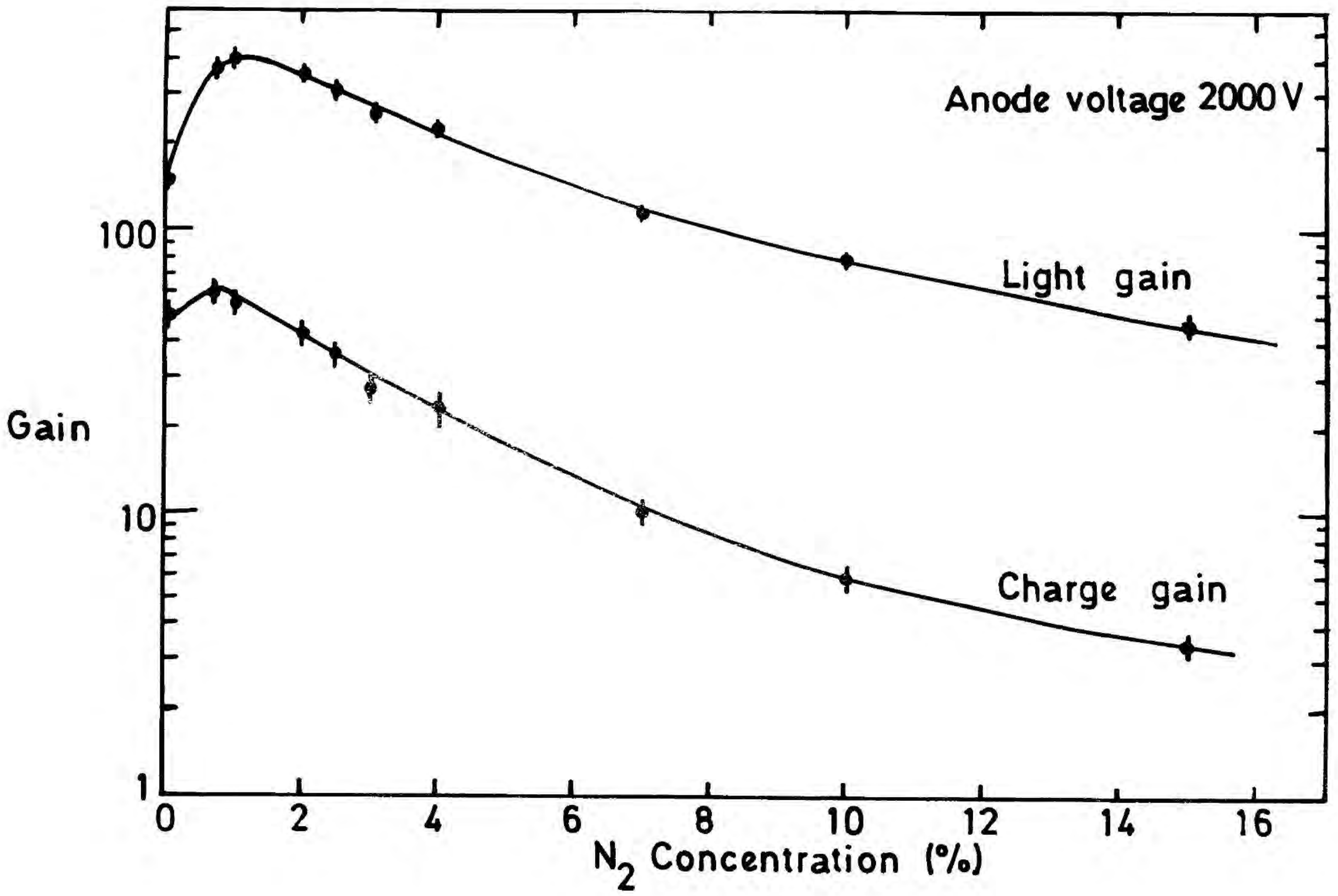

FIG.17 Secondary light and charge gains as a function of nitrogen concentration for a fixed anode voltage.

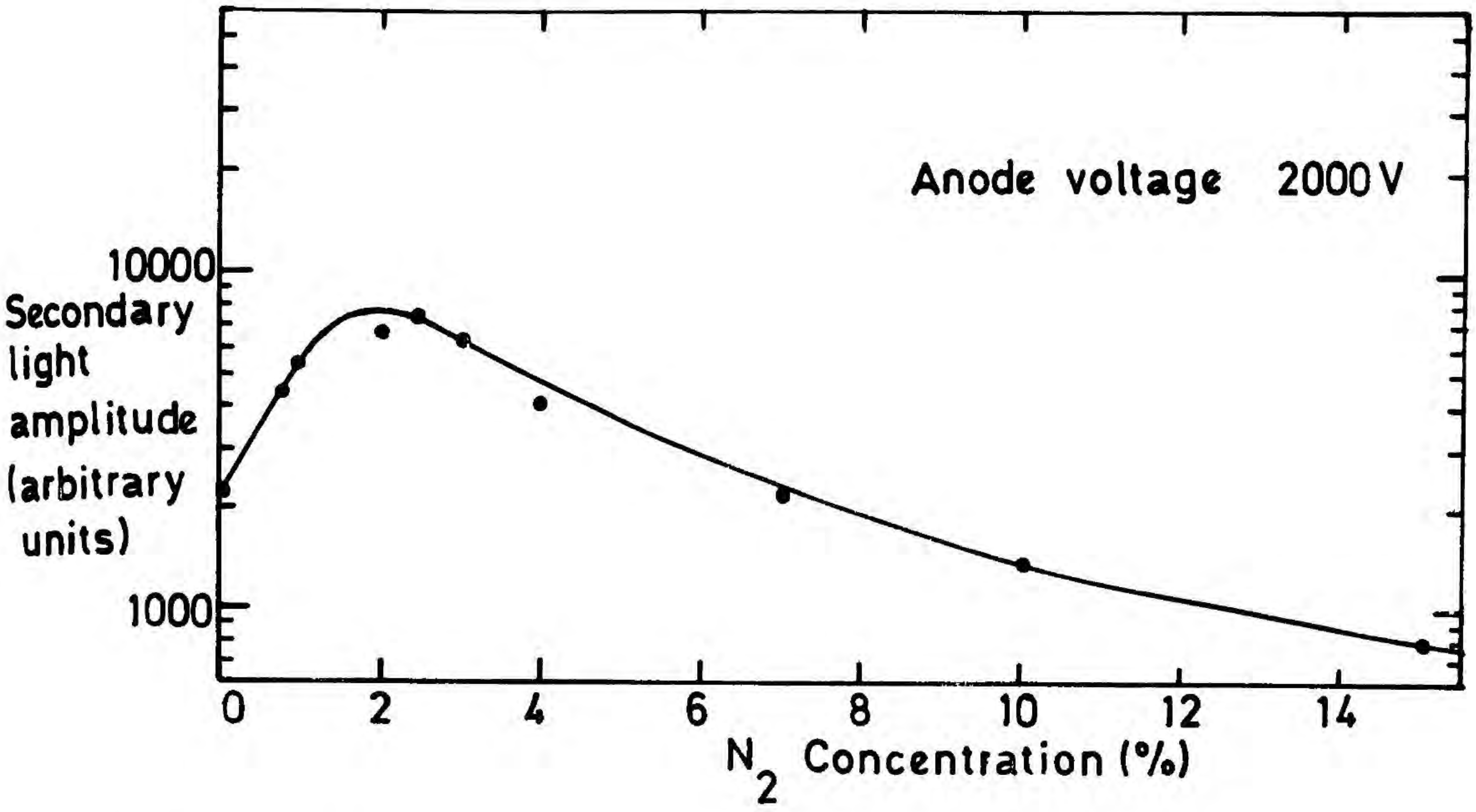

FIG. 18 Amplitude of the secondary light as a function of nitrogen concentration for a fixed anode voltage.

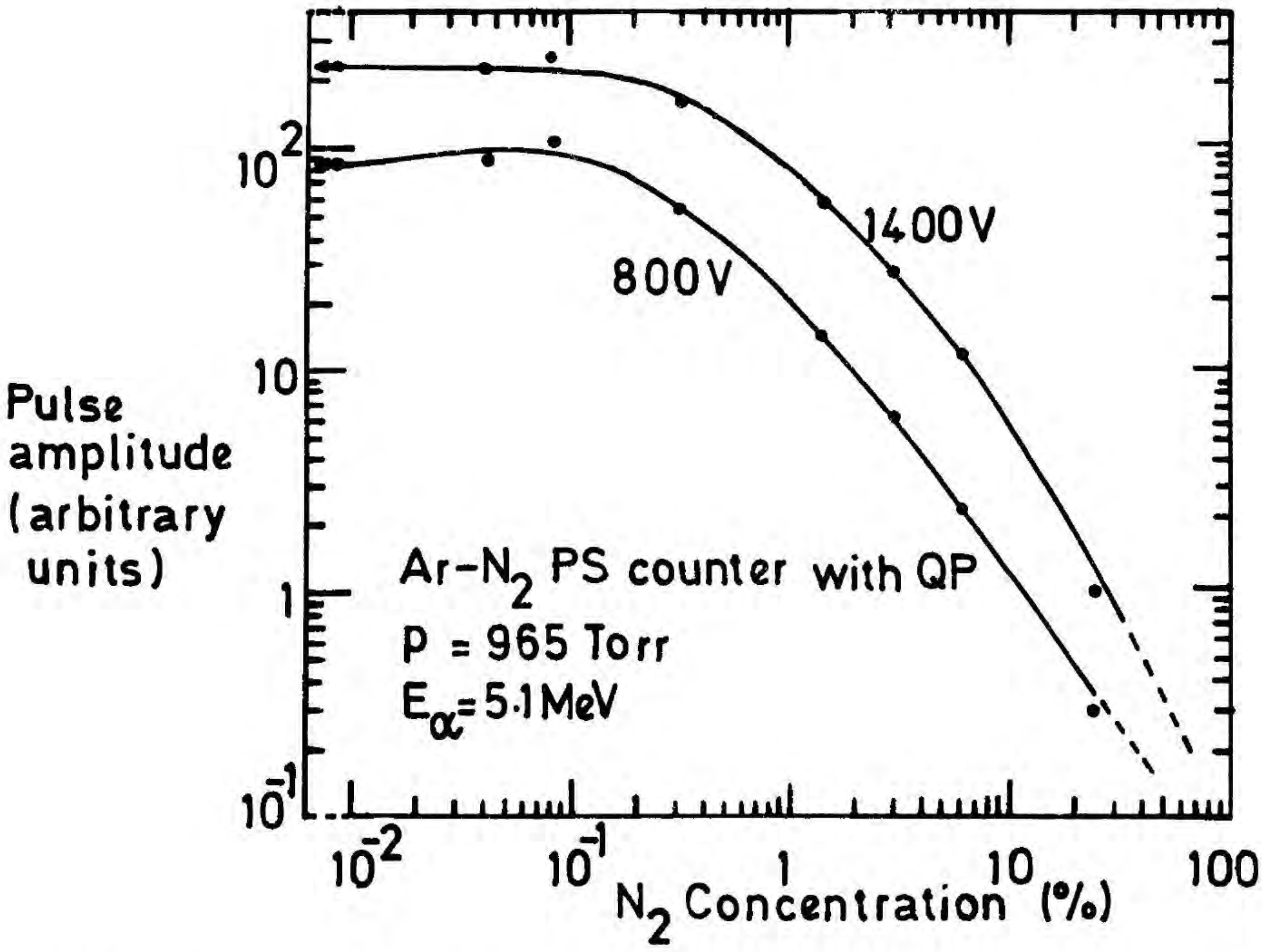

FIG. 19 Variation of pulse amplitude with nitrogen concentration for 800 and 1400 V anode voltage.

(b) Primary Scintillation Light Output

The primary scintillation pulse height was also measured with no voltage applied to the chamber and without an attenuator in the system as a function of nitrogen concentration and the results are shown in Fig (20). They indicate that the maximum primary pulse height for an argon-nitrogen gas mixture at 760 Torr can be obtained with ∿ 8.5% nitrogen concentration. The drop in the light output at small concentrations of nitrogen is again due to the insufficiency of the nitrogen population in the mixture and poor photomultiplier response. The decrease in amplitude at higher concentrations is mainly due to collision quenching processes. In the absence of an electric field Teyssier$^{(14)}$ et al using an UV sensitive photomultiplier (λ = 2200-5000 Å) at p = 450 Torr, obtained a maximum light output for 6% nitrogen concentration. Eggler$^{(15)}$ et al also using a pyrex window photomultiplier and a wavelength shifter, obtained a maximum pulse height for 10% nitrogen concentration at 5000 Torr. The value obtained by Grun and Schopper$^{(16)}$ using a photomultiplier with a perspex window at 585 Torr was 2.5%.

(c) Charge Gain

The amplitude of charge pulses was measured as a function of the anode voltage for the same nitrogen concentration values given in Fig (16) and the gain calculated from the results are shown in Fig (21). For small anode voltages, the charge gain grows less rapidly than light gain and this confirms the fact that at small electric fields the main light production is through the excitation of gas atoms. Large light gain for a small charge gain is obviously an important requirement in high counting rate work since it allows the counter to handle high radiation fluxes without forming a space charge cloud around the anode wire. Fig (17) also represents the charge gain as a function of nitrogen

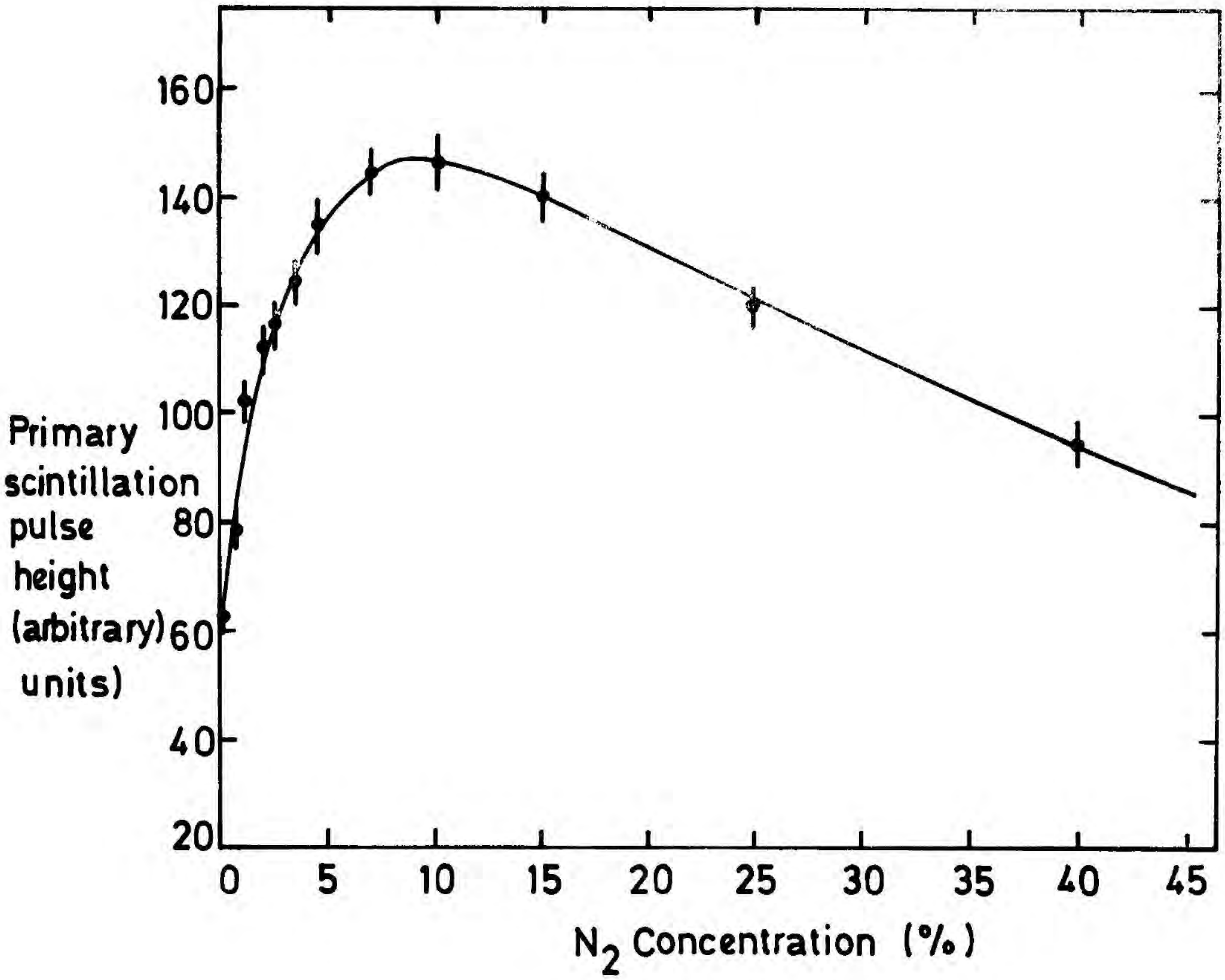

FIG. 20 Amplitude of primary scintillation pulses as a function of nitrogen concentration.

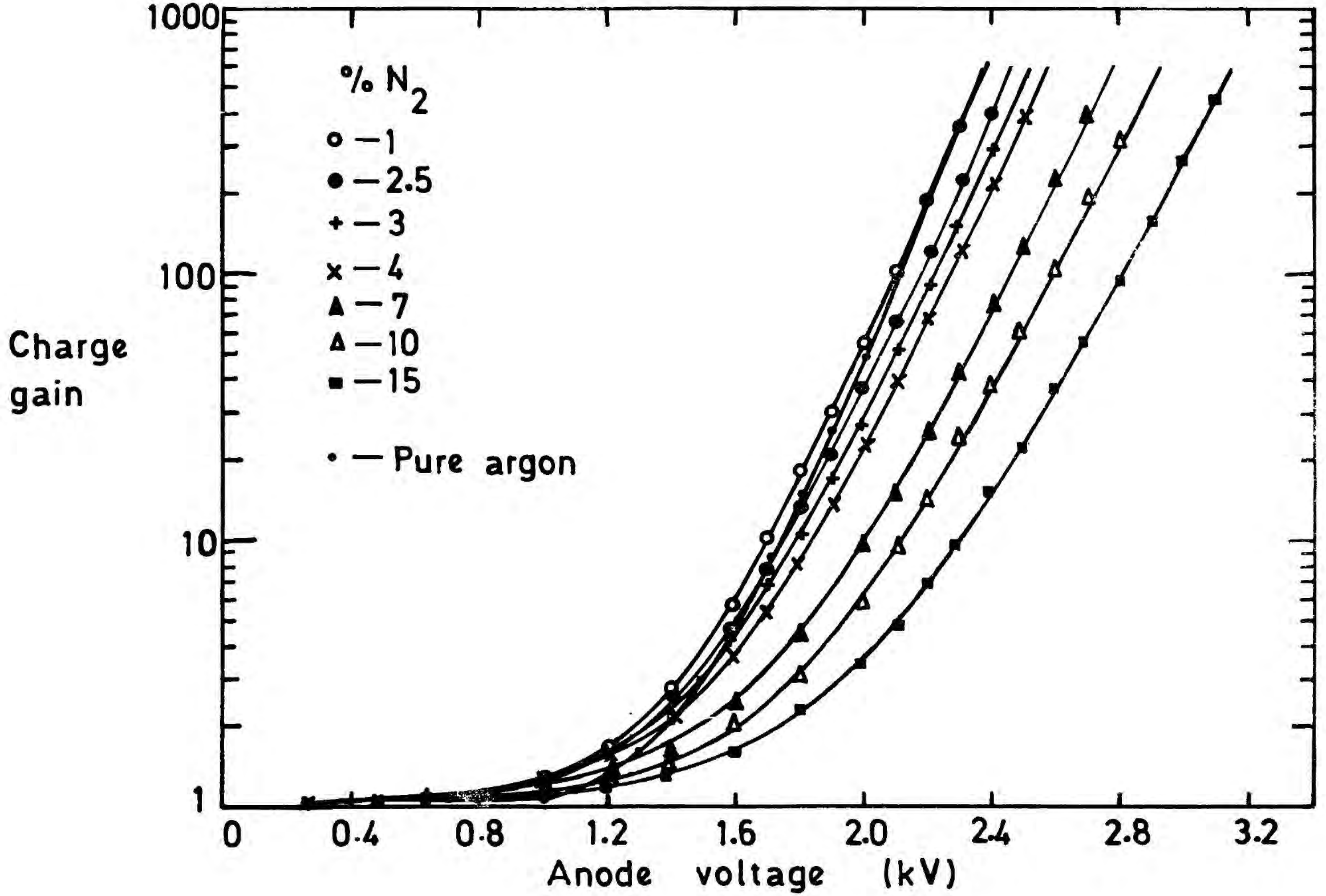

FIG. 21 Charge gain around the anode wire as a function of anode voltage for different concentrations of nitrogen in the mixture.

concentration for a fixed anode voltage (2000 V). A small reduction in the charge gain is apparent at small nitrogen concentrations. This can be explained as being due to loss of some of the primary electrons created close to the cathode planes, through diffusion effects since the electric field near the cathodes is generally small and the diffusion coefficient of electrons in pure argon is high. The maximum in the light gain curve (Fig 17) is also a direct consequence of this effect.

Several authors$^{(4,17,18)}$ have shown experimentally as well as theoretically that the energy distribution of electrons in argon can be shifted to low energies by adding a small amount of molecular gas to argon (also see Fig (10)). In particular, Uman$^{(17)}$ has solved the Boltzmann equation for the electrons immersed in binary gas mixtures such as Ar-H_2 and Ar-CO_2 in the presence of a static electric field to show this effect. As an example, the effect on the electron energy distribution upon addition of a small amount of CO_2 to argon is shown in Fig (22). A similar behaviour is expected with the argon-nitrogen gas mixture.

According to the findings mentioned in the preceding paragraph, the charge gain for a fixed anode voltage should decrease with the nitrogen concentration since more and more primary electrons fail to ionise argon atoms. In fact this is exactly the situation as can be seen from the charge gain measurements in Fig (21).

As a consequence of the reduction in charge gain, the light gain also decreases with nitrogen concentration for anode voltages which correspond to charge gains greater than 1. This apparent reduction in the light gain can be compensated by increasing the anode voltage with nitrogen concentration so that the charge gain is independent of the nitrogen concentration or alternatively, the light gain can be obtained for a fixed charge gain using light and charge gain curves in Figs (16) and (21) respectively.

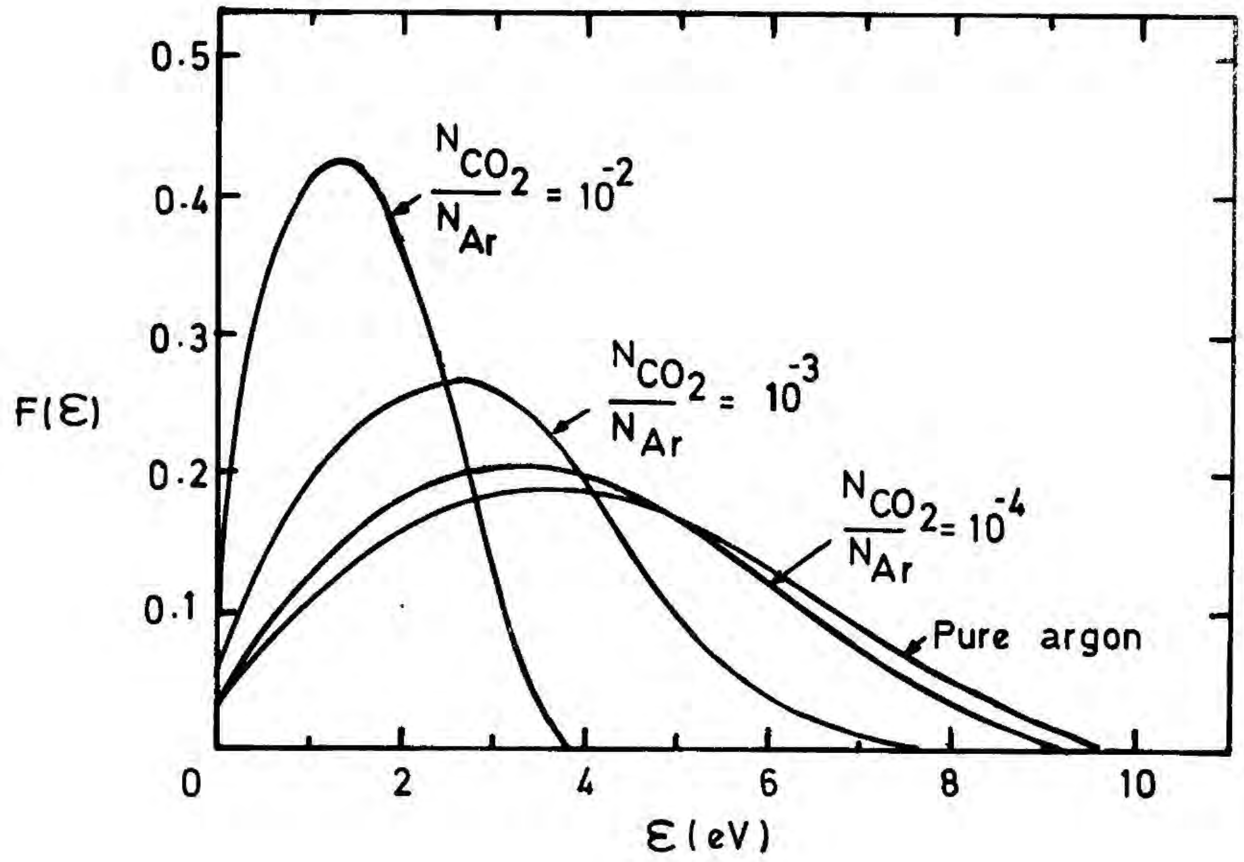

FIG. 22 Electron energy distribution function, F(ε), vs electron energy (ε) for several values of CO_2 density to Ar density ratio with E/p = 1.0 V/cm/Torr.

Fig (23) shows the behaviour of the 'corrected' light gain with nitrogen concentration. Corrections were made using the second method mentioned in the preceding paragraph. The light gain is found to be practically constant up to the maximum nitrogen concentration (15%) used in the tests, though some of the points are slightly scattered. One of the deductions that can be made from this result is that the variation of the amplitude of the secondary scintillation pulses with nitrogen concentration is similar to that of the primary scintillation. Drop in the light gain at small nitrogen concentrations is again due to the loss of primary electrons through diffusion.

4.4 CHOICE OF THE OPERATING PARAMETERS

4.4.1(a) The Optimum Value for Nitrogen Concentration in the Gas Mixture

In order to ensure the successful operation of the C.S.D.C's at high rate the percentages of the constituents of the gas mixture must be chosen such that the resulting mixture fulfils the following requirements.

(i) The gas mixture must possess a high drift velocity for electrons.

(ii) The scintillation light output must be large.

(iii) It must produce light pulses with small width.

The dependence of the first two parameters on the nitrogen percentage has already been discussed in this chapter. The drift velocity measurements show that nitrogen concentration of $\sim$ 2% gives maximum drift velocity for a given drift field - in fact concentrations of more than 1% are acceptable. Regardless of this, nitrogen concentrations greater than 2% are more convenient since much higher drift velocities can be achieved by increasing the drift field. However, very high drift fields are

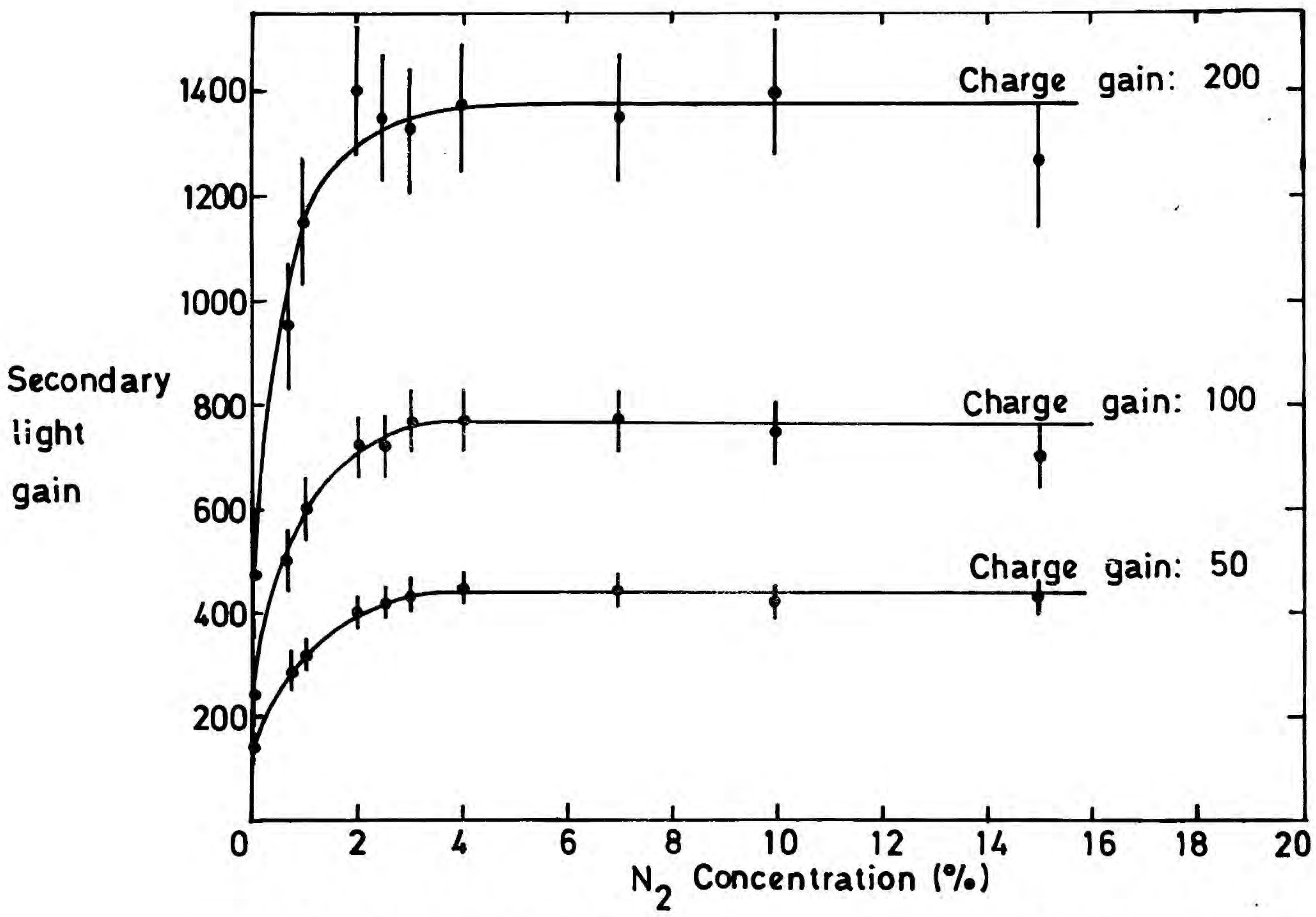

FIG. 23 Corrected light gain as a function of nitrogen concentration in the mixture for three different charge gains.

undesirable because they produce very high electric fields in the gap between the drift cathode plane and the earthed plane causing noise or discharges across the planes.

According to the light gain measurements maximum light amplitude can be obtained with a nitrogen concentration around 8.5%. Large nitrogen concentrations are not suitable because of their high quenching power.

As mentioned in chapter two the addition of nitrogen to argon has a great effect on the width of the light output. In order to investigate this effect the same scintillation drift chamber system used in the drift velocity measurements was used with a collimated X-ray source (Fe^{55}, 5.9 keV). The X-ray source was placed in the slot so that its beam traversed normal to the drift planes 8 mm away from the anode wire, and the amplified pulse widths (using a Nuclear Enterprise NE.4634 fast amplifier) were measured on the Tektronix 475 oscilloscope for different nitrogen concentrations under constant drift velocity (2.2 cm μsec) and constant pulse amplitude (80 mV). The results are shown in Fig (24). As expected the pulse width drops with the nitrogen concentration. The widths given in the figure are the full widths of the pulses. The maximum pulse width was obtained when there was no nitrogen (i.e. pure argon) in the mixture and its length was mainly due to a long tail formed by the long lived excited states. The addition of nitrogen greatly reduces the tail of the pulses with some improvements in the rise time as well. These effects are clearly seen in Fig (25).

The results from the pulse width measurements together with the drift velocity and light gain measurements suggest a gas mixture with 10% nitrogen as a reasonable compromise which satisfy all the requirements mentioned at the beginning of this section to a greater extent.

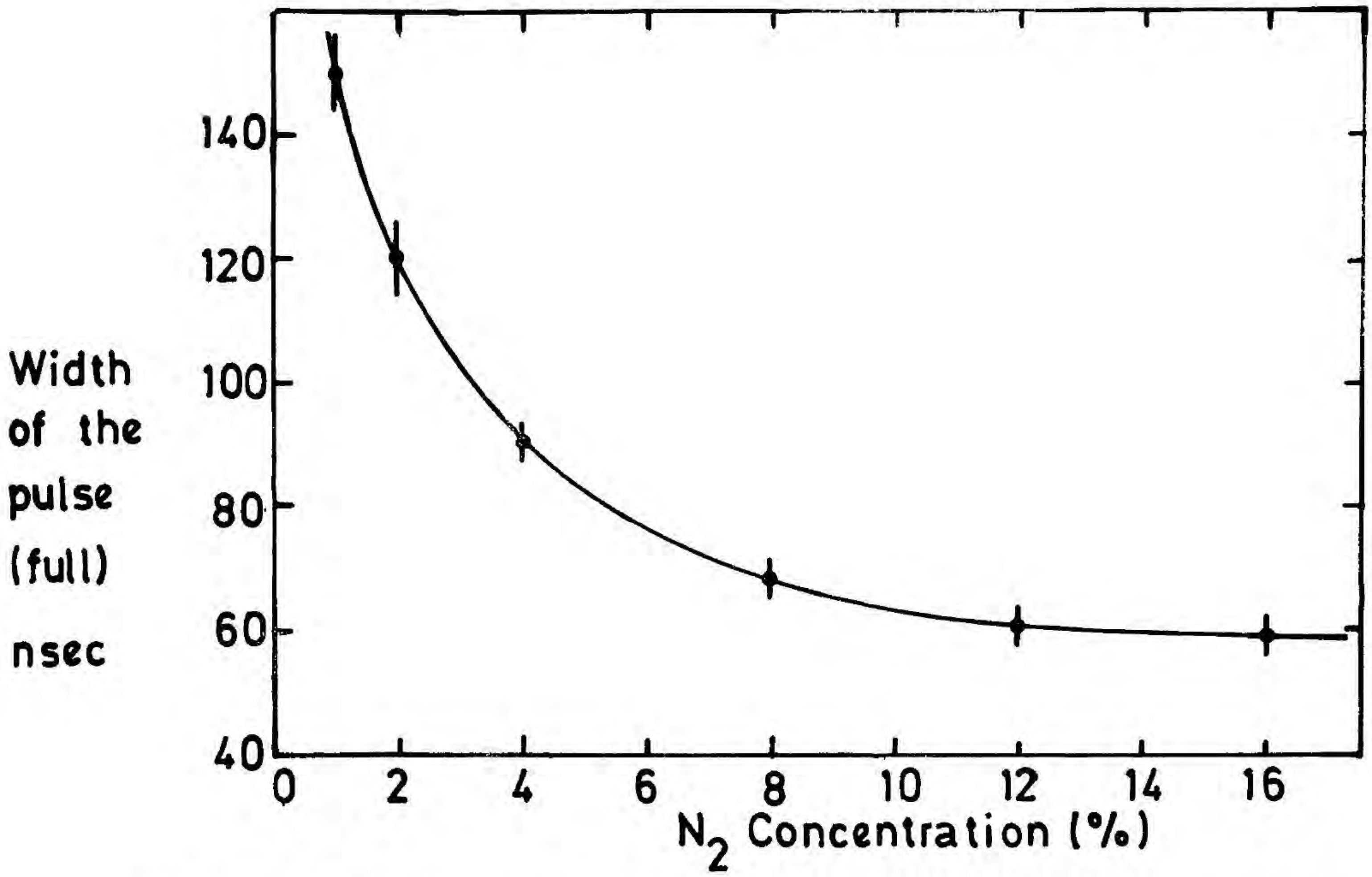

FIG.24 Variation of secondary scintillation pulse width with nitrogen concentration.

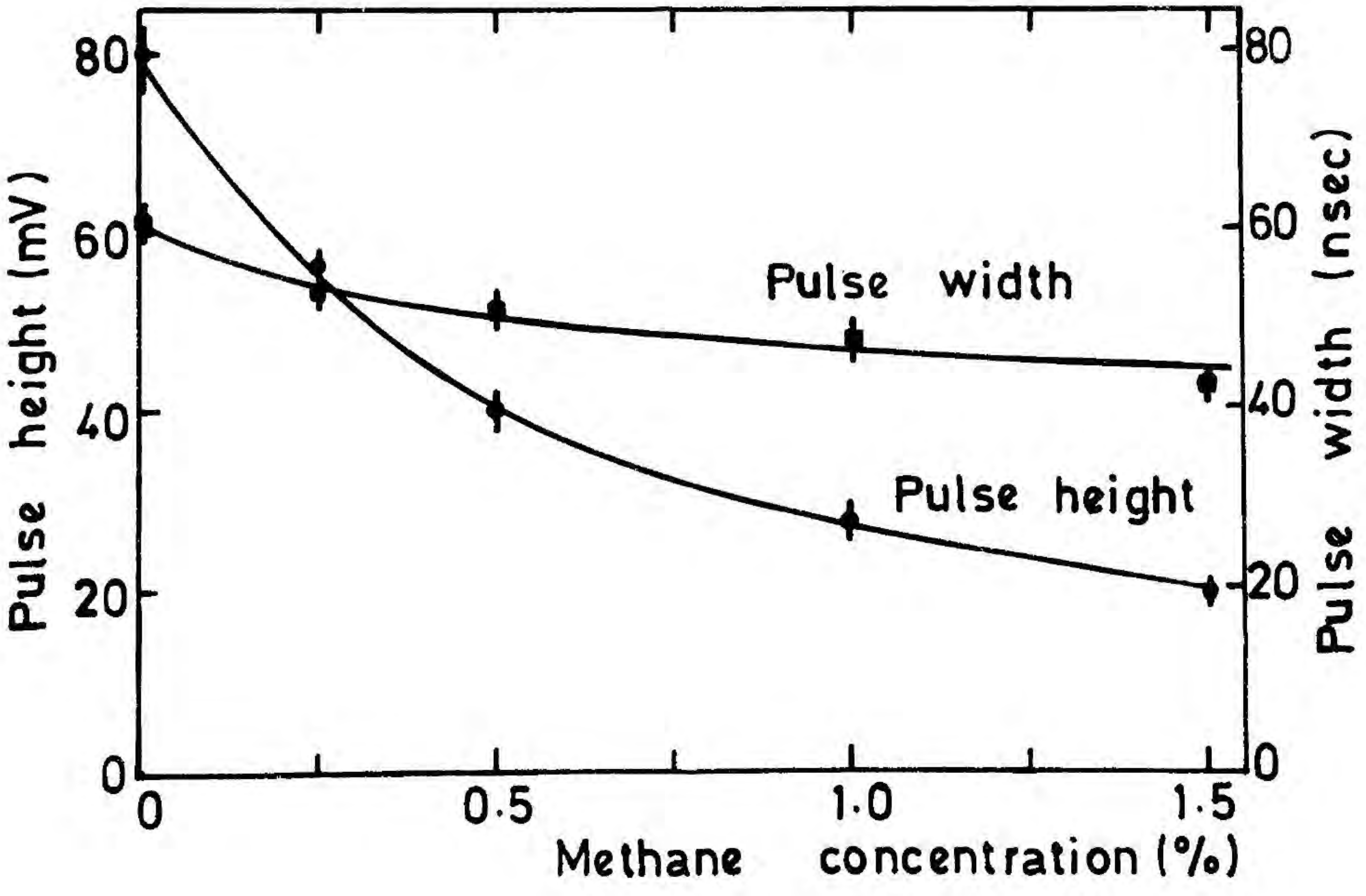

FIG.26 Variation of height and width of the scintillation pulse with methane concentration in argon–10% nitrogen mixture.

FIG. 25 Variation of the width of scintillation pulses with nitrogen concentration.

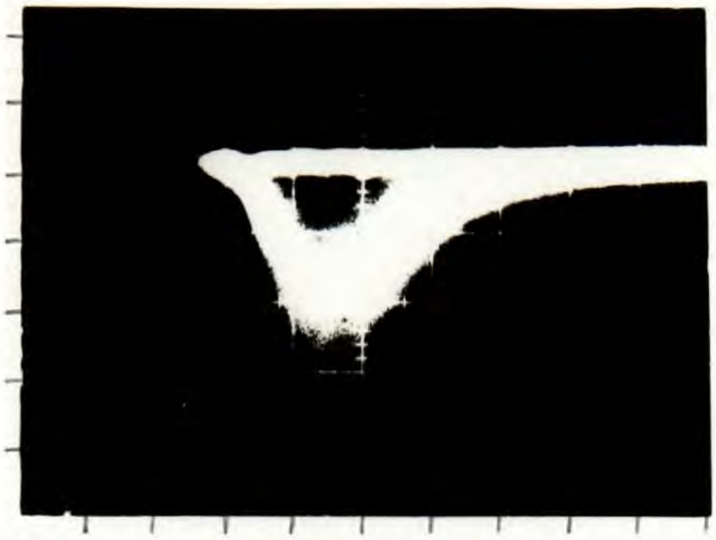

Pure argon
Horizontal 50 ns/div
Vertical 20 mV/div

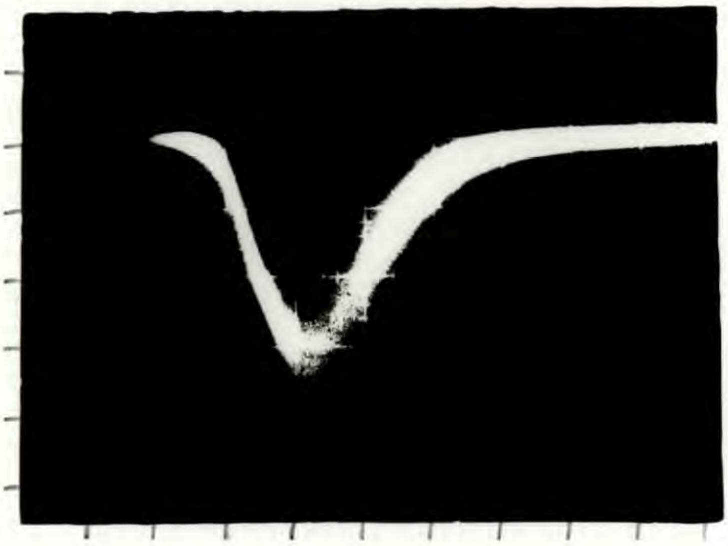

Ar – 3% N_2
Horizontal 20 ns/div
Vertical 20 mV/div

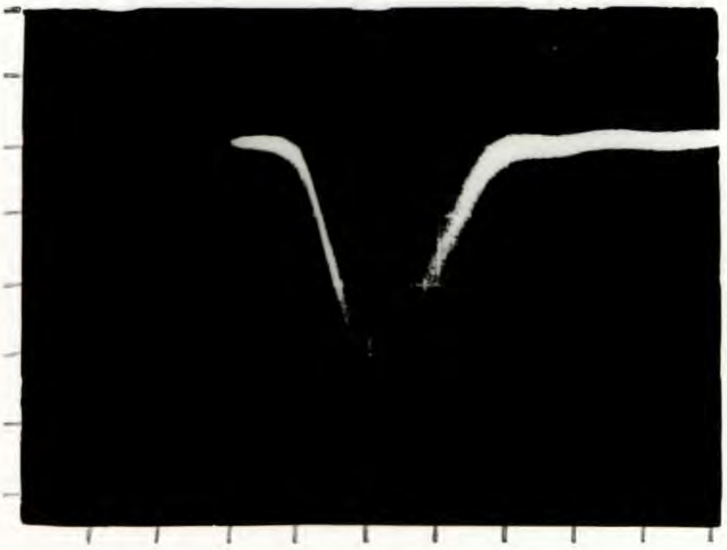

Ar – 10% N_2
Horizontal 20 ns/div
Vertical 20 mV/div

FIG 25

4.4.1(b) Effect of Other Molecular Gases on the Pulse Width

The addition of molecular gases such as carbon dioxide or methane to the argon-nitrogen mixture has a considerable effect on the pulse width. Charpak et al (19) using a mixture of 48% Ar - 48% N_2 - 4% CO_2 at a drift field of 1.2 kV/cm obtained a pulse width close to 30 nS for 5.9 keV photons, but they had to increase the charge gain up to 300 in order to obtain a reasonable light amplitude from their system. The necessity of such a high charge gain around the anode wire is clearly a direct consequence of the excessive collisional quenching of the excited states by nitrogen and carbon dioxide molecules.

To study the effect on the pulse width of the addition of methane to Ar-10% N_2 mixture, the same drift chamber, X-ray source and the electronics described in section 4.4.1 a were used. Argon-nitrogen mixtures with small percentages of methane were obtained by mixing correct amounts of pure argon, pure nitrogen and pre-mixed Ar-10% CH_4 mixture. The pulse width and the amplitude of the scintillation pulse were measured as a function of methane concentration and the results are shown in Fig (26). A sharp fall in the amplitude of the pulses was observed with some reduction in widths with increase in methane concentration. The charge gain measurements with these mixtures indicated no changes on the charge amplification process around the anode wire with addition of methane (see Fig (27)). The reduction in amplitude of the scintillation pulses is therefore mainly due to the quenching of the argon and nitrogen excited states by methane. The argon metastable quenching rate constants of various molecular gases (20) are given in Table (4.1) which also indicates that most of the polyatomic molecular gases including CO_2 and CH_4 have very much higher quenching powers than nitrogen.

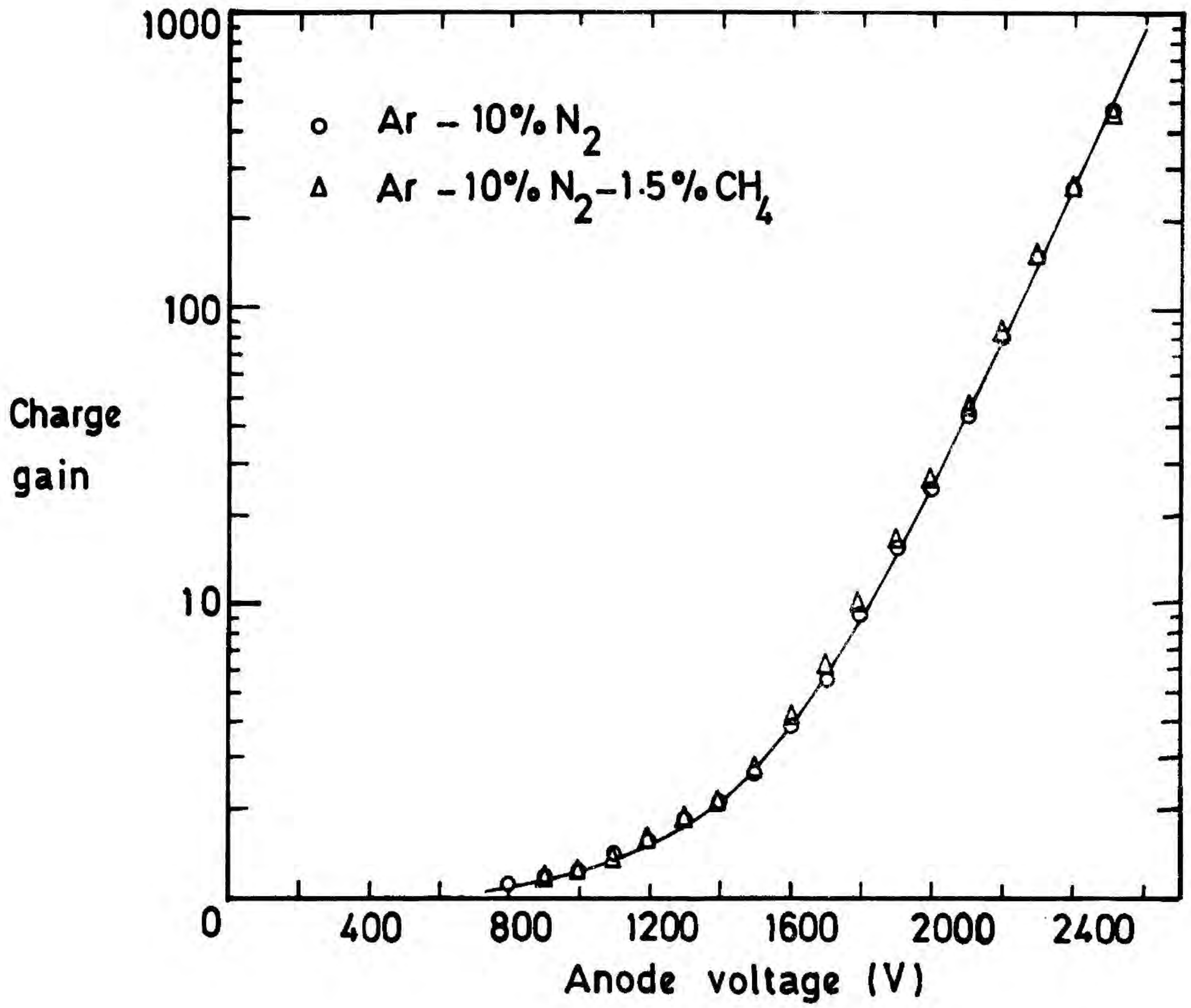

FIG. 27 Charge gain as a function of anode voltage for Ar - 10% N_2 and Ar - 10% N_2 - 1.5% CH_4 gas mixtures.

Quenching Molecule	Ar^* $(3p_2)$		Ar^* $(3p_0)$	
	k_Q	σ_Q (Å^2)	k_Q	σ_Q (Å^2)
N_2	3.6	5.8	1.6	2.5
O_2	21	35	24	41
Cl_2	47	95	-	-
CO_2	53	97	59	108
CS_2	106	218	-	-
CH_4	33	45	55	74
C_2H_6	66	109		
C_3H_8	73	134		
C_4H_{10}	76	149		

k_Q has units of 10^{-11} cm^3.molecule^{-1}.sec^{-1} ; $\sigma_Q = \frac{k_Q}{\nu}$

TABLE 4.1 Metastable argon quenching rate constants and cross-sections$^{(20)}$

4.4.2 Anode Wire Diameter

The diameter of the anode wire in a G.S.D.C. is an important parameter especially when using the latter as a high rate counter since it can affect the performance of the counter in a number of ways. The diameter of the anode wire must therefore be selected to fulfil certain requirements.

(1) Light gain around the anode wire for a fixed charge gain must be high in order to attain high counting rates before the space charge effects become appreciable.

(2) It must provide a good efficiency plateau.

(3) The depth of the scintillation region, which determines the width of the secondary scintillation pulse, must be small.

Light gains and charge gains for different wire diameters were measured using an α-particle source and the system described in section 4.3.1, and the results are presented in Fig (28). Three wire diameters were used in the test and, as expected the light gain for a fixed charge gain was found to increase with diameter of the wire. For example a charge gain of 10 yields a light gain of 80 (±7%) with 205 μm diameter wires where as it yields 135 (± 7%) with 410 μm wires. The efficiency plateaus were also obtained for different wire diameters using an Fe^{55} X-ray source and a G.S.D.C. The output from the G.S.D.C. was amplified and discriminated at a fixed threshold level, by means of a N.E. fast amplifier (NE 4634) and a N.E. fast discriminator (NE 8684) respectively and fed to a fast scaler (20 MHz, Borer Type 512). Pulse widths were also measured on a Tektronix 475 oscilloscope and the change in pulse width with the wire diameter was found to be negligibly small up to the largest diameter (410 μm) used in the test. The efficiency plateaus

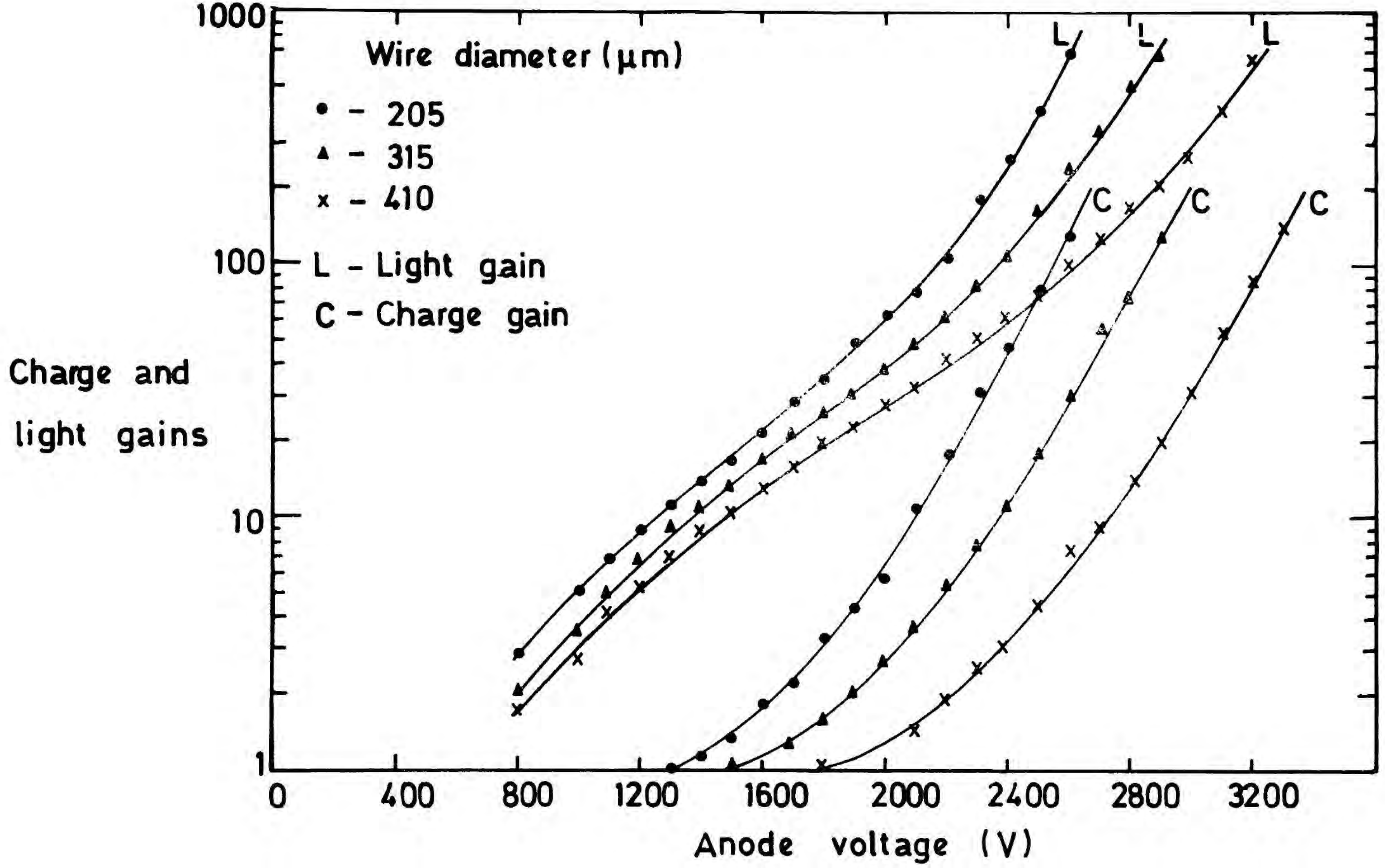

FIG. 28 Charge and light gains as a function of anode voltage for different wire diameters.

(count rate as a function of anode voltage) for a constant drift field (700 V/cm) are shown in Fig (29). Ar-10% N_2 was used both in light gain and the plateau measurements. As seen in Fig (29) the width of the plateau increases with the wire diameter and for smaller diameter wires the plateaus are virtually non-existent because of the formation of secondary avalanches. However, in the case of smaller diameter wires the amplitude of the pulses reaches the threshold level set by the discriminator for smaller anode wire voltages, since the electric field which causes excitation and ionisation around them is higher than that around larger diameter wires. Marel et al(21) investigated the variation of width of the efficiency plateau with sense wire diameter in a conventional drift chamber. Their results (see Fig (30)) show that a larger diameter wire requires a higher voltage than that required for smaller diameter wires to produce the same charge amplification. Also, the width of the plateaus decrease with the wire diameter since the breakdown voltage (ends of plateaus) which is mainly determined by the production of uv photons (light), is nearly the same for all three diameters. This clearly shows that although the largest diameter wire is the most inefficient one in producing secondary electrons for a given electric field around the wire, its light production efficiency is higher than the other two, and this fact confirms the results in Table 4.2 and Fig 28.

It is clear from Figs (28) and (29) that for a G.S.D.C. larger diameter wires are more suitable than smaller diameter wires. However, it was decided to use 410 μm diameter wire, since extremely large diameter wires are mechanically inconvenient and may also produce broad pulses.

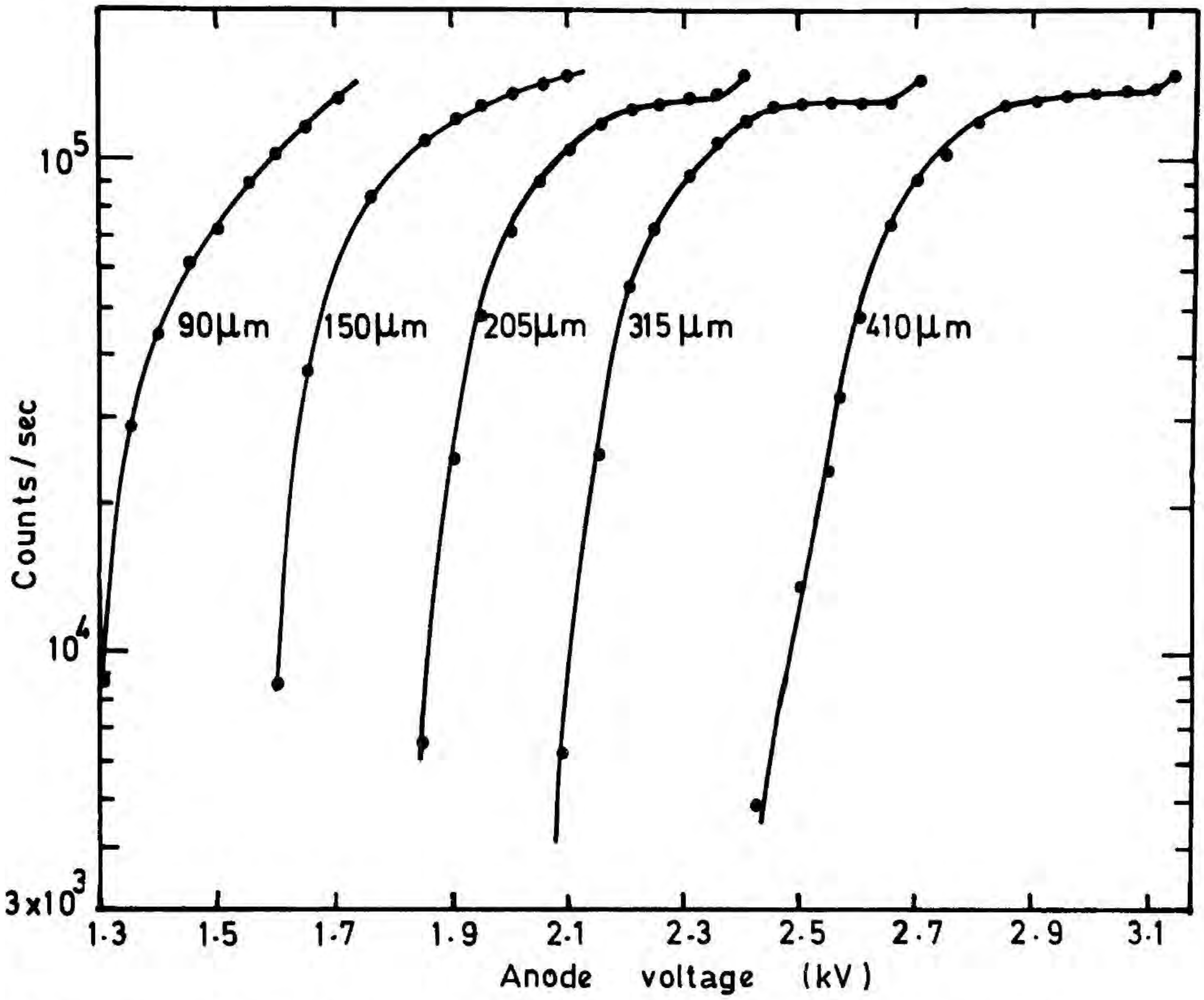

FIG. 29 Efficiency plateaus for different anode wire diameters.

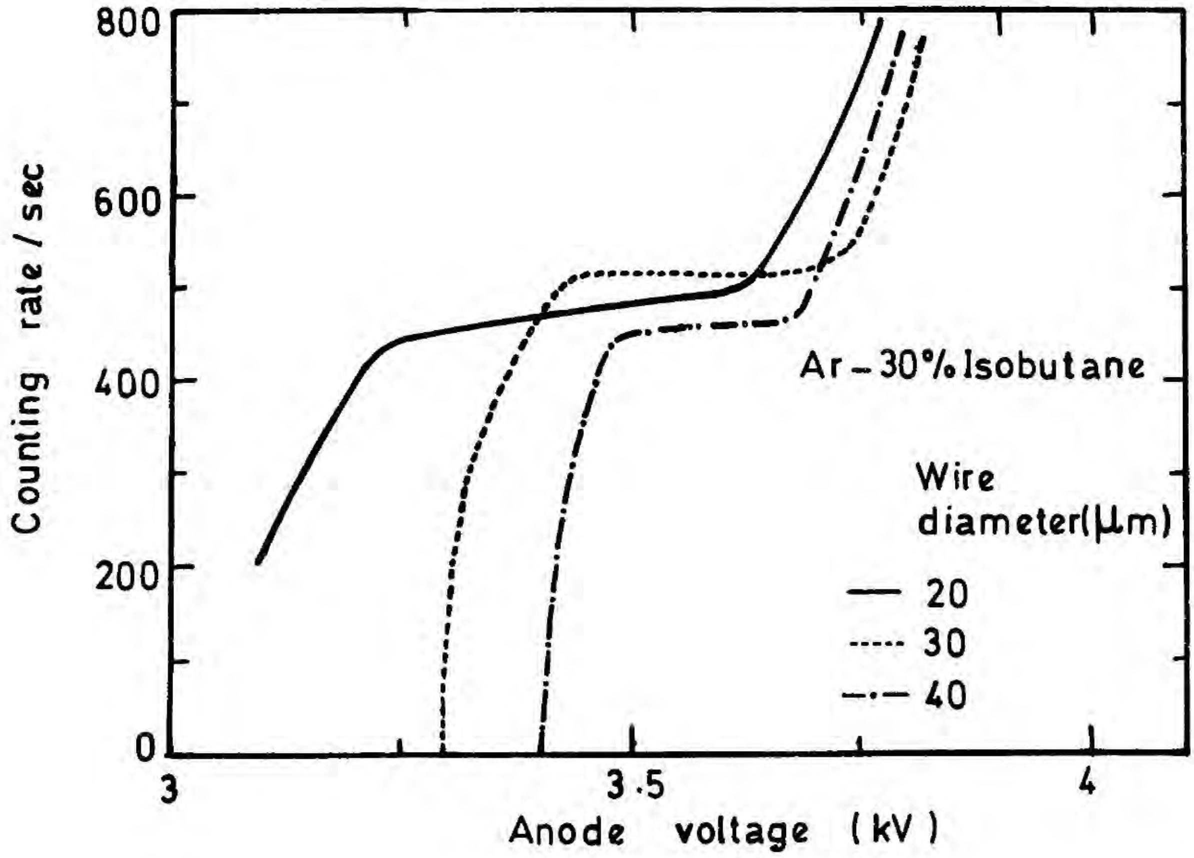

FIG. 30 Dependence of efficiency plateau on the diameter of anode wire of a proportional counter.

Chapter 4 - References

1. G. Charpak, F. Sauli and W. Duinker, Nucl. Instr. and Meth. 108 (1973) 413.
2. L. Colli and U. Facchini, Rev. Sci. Instr. 23 (1952) 39.
3. E.D. Klema and J.S. Allen, Phys.Rev. 77 (1950) 661.
4. W.N.English and G.C. Hanna, Can. J. Phys. 31 (1953) 768.
5. J. Townsend, 1947, Electrons in Gases, Hutchinson's Scientific and Technical Publications (London).
6. R.W. Crompton and D.J.Sutton, Proc.Roy.Soc. (London) A215 (1952) 467.
7. R.A.Nielsen, Phys.Rev. 50 (1936) 950.
8. L.G.H. Huxley, R.W. Crompton, The Diffusion and Drift of Electrons in Gases, John Wiley & Sons, 1974.
9. H.S.W.Massey and E.H.S.Burhop, Electronic and Ionic Impact Phenomena, Oxford Univ. Press (1952).
10. A.G.Engelhardt, A.V.Phelps and C.G.Risk, Phys.Rev. 135 (1964) A 1566.
11. W.P.Jesse and J.Sadauskis, Phys. Rev. 78 (1950) 1.
12. A.J.P.L. Policarpo, M.A.F. Alves and C.A.N. Conde, Nucl. Instr. and Meth. 55 (1967) 105.
13. M.A.F. Alves and A.J.P.L. Policarpo, Nucl. Inst. and Meth. 57 (1967) 321.
14. J.L. Teyssier, D. Blanc and H.Brunet, C.R. Acad. Sci. (France) 260 (1965) 1614.
15. C. Eggler and C.M.Huddleston, Nucleonics 14 No.4 (1956) 34.
16. A.E.Grun and E.Schopper, Z. Naturforsch 9a (1954) 134.
17. M.A.Uman, Phys. Rev. 123 (1961) 399.
18. M.A.Uman, Phys. Rev. 133 (1964) A 1266.

19. G. Charpak, S. Majewski and F. Sauli, IEEE Trans.Nucl.Sci. NS23 (1976) 202.

20. L.G.Piper, J.E.Velazco and D.W.Setser, J.Chem. Phys. 59 (1973) 3323.

21. G. Marel, P. Bloch, S. Brehin, B. Devaux, A.M. Diamant-Berger, C.Leschevein, J.Maillard, Y. Malbequi, H. Martin, A. Patoux, J. Plancoulaine, G. Tarte and R. Turlay, Nucl. Instr. and Meth. 141 (1977) 43.

CHAPTER FIVE

OPERATION OF PHOTOMULTIPLIERS AT HIGH COUNT RATE

5.1 INTRODUCTION

The rate capability of the photomultiplier is one of the most important factors which determine the performance of G.S.D.C's at high counting rates. Among the different types of photomultiplier (PM), one with a focused dynode structure is most suitable for this kind of operation since it delivers a fast and narrow electron pulse at the output. However, the performance of PMs is complicated by the fact that the formation of the electron avalanche (pulse) is always accompanied by a number of parasitic effects which lead to a deterioration of both the counting rate ability and the gain stability of the tube. Because of these variations it is necessary to test the phototubes intended for use in a G.S.D.C. at high rates in order to ensure that their performances are adequate. This chapter describes some of the effects which are important in the operation of G.S.D.C's at high rate and in particular the performance of an RCA 8575 PM tube in connection with these effects.

5.2 FACTORS AFFECTING THE PERFORMANCE OF A PHOTOMULTIPLIER

5.2.1 Dark Currents

If a photomultiplier is operated in total darkness, some current will be collected at the anode. This current, which is known as the dark current, arises from a number of causes and varies from one tube to another, even in a batch of tubes bearing the same type number. One source of dark current is thermionic emission from the photocathode and first few dynodes. The magnitude of the current is an exponential function of the temperature at which the tube electrodes are operated, and is given by the well known Richardson equation

$$i = \frac{4\pi mek^2T^2}{h^3} e^{-\phi_T/kT} \tag{5.1}$$

where i = thermionic current density (A/cm^2)

T = absolute temperature and all the other constants have their usual meanings.

Another component of dark current is caused by particles of stray ionising radiations such as cosmic rays, high energy β-particles and small amounts of natural radio-active materials in the glass of the PM tubes, producing photoelectrons at the photocathode and dynodes. However, the results of Birks et al(1) on luminescence of glass and quartz show that the production of photons for which the glass is transparent, by γ-rays incident on glass PM tube windows are negligibly small. In addition another component of dark current appears when operating PMs which have been exposed to light for a long time. This dark current, which lasts for one or two days, arises from some electrons in the photoemissive material of the dynodes and the photocathode which have absorbed the light and jumped into trap levels and later leave the material after gaining energy from thermal sources.

5.2.2 Feedback Effects and After-Pulses

Feedback effects are important when operating a photomultiplier at high gains. With this situation ionisation of residual gas in the tube (mainly Caesium vapour) can take place and if the resulting positive ions and photons strike the photocathode, the latter will emit more electrons. If the gain is very high the resulting current can even damage the tube. Feedback effects tend to be reduced if the tube is cooled, since the cooling reduces the vapour density of caesium in the tube.

In pulsed operation of photomultipliers, the ionic and optical feedback effects can give rise to after pulses which produce spurious counts in scintillation counters and affect its energy resolution. These pulses are very likely to occur especially when the pulse of current at the anode is high. The after pulses which occur a few microseconds after the main pulses are caused by positive ions while the pulses which occur some nanoseconds after the main pulses are a result of optical feedback.

5.2.3 Saturation Effects

There are two mechanisms which cause saturation of a photomultiplier tube in the pulsed mode. The most commonly known effect is the space charge limitation at the last few dynodes and is generally considered as the ultimate limitation, though an increased voltage between the last few dynodes can improve the situation to some extent. The most prominent consequences of this limitation are the non-linearity in response to incident light and the broadening of the width of the output pulse. The other effect is the creation of a radial voltage drop at the photocathode caused by large cathode current densities. This effect occurs only with semitransparent photocathodes (2) which have a relatively low resistance and once it occurs it can deteriorate the cathode to the first dynode electron collection efficiency by changing the electric field in this region. In the case of the RCA 8575 phototube, the peak cathode current at which this effect begins to cause a non-linear response is 10^{-9} amperes at a tube temperature of 22° C.

5.2.4 Fatigue

The performance of PM tubes can be affected by fatigue at the photocathode and dynodes if the respective currents are high. Because of this effect the sensitivity of the tube decreases over a short period of time and is believed to be due to the heating of the electrodes by the flow of current and the resulting evaporation of some of the caesium from the surface. Recovery or partial recovery is possible when the light source is removed. Although the fatigue is generally negligible in pulsed operations it may affect the performance of the PM tube if pulsing rate and the average anode current are extremely high.

5.2.5 Grain Variation with Count Rate

As far as the G.S.D.C's are concerned, the most undesirable effect is the variation of the gain of the photomultiplier with count rate. This effect not only degrades the counting ability of the counter but also adversely affects the energy resolution(3) of the X-rays which are being detected. Two types of gain variations have been observed by a number of workers(3-8). One type of variation is caused by a change in potential at the last few dynodes resulting from large diversions of current from the potential distribution network to the tube.(3) The other type of variation is due to changesoccurring inside the photomultiplier itself. Both of these effects will be discussed in detail in later sections.

Most of the effects described in this section are hard to control when large currents flow through the tube. The stability in the operation of photomultipliers therefore can only be achieved by operating them at anode currents which are well below the maximum recommended anode current of the photomultiplier.

5.3 EVALUATION OF AN RCA 8575 PHOTOTUBE

The RCA 8575(9) (35 CT) is a 50.8 mm diameter, twelve-stage, linear focused type of photomultiplier with a semi-transparent caesium-potassium-antimony (Bialkali)photocathode. It features high quantum efficiency, low dark current, good time resolution characteristics and is intended primarily for use in pulse counting and high current applications. Some of the important characteristics and the spectral response of the tube are shown in Table 5.1 and Fig (14) of Chapter two. The transmission properties of pyrex (Corning glass, No.7740) extends the blue response of the tube (window) even below 3000 Å and therefore it is suitable for viewing the emission from argon-nitrogen mixtures, which lies principally between 3000-4000 Å.

TABLE 5.1 Characteristics and Ratings of R.C.A. 8575 Photomultiplier

Spectral Response	see Fig (14) of Chapter two.
Cathode, Semitransparent	Caesium-Potassium-Antimony (Bialkali).
Window	Pyrex Corning No.7740.
Dynodes: Substrate	Copper-Beryllium
Secondary-Emitting Surface	Beryllium Oxide
Direct Inter-electrode Capacitances	
(Approx): Anode to dynode No.12	5 pF
Anode to all other electrodes	6 pF
DC Supply Voltage	
With voltage distribution shown in Table 5.2	3500 max V 800 min V
Between anode and dynode No.12	800 max V
Between dynode No.12 and dynode No.11	800 max V
Between consecutive dynodes	400 max V
Between dynode No.1 and cathode	1000 max V 300 min V
Between focusing electrode and cathode	1000 max V
Average anode current	0.2 max mA
Ambient Temperature Range	-100 to 85° C
Characteristic Range Values:	Typical
Anode pulse rise time	2.1×10^{-9} s
Electron Transit time at 3000 V	3.1×10^{-8} s
Mean Gain Deviation:	
With count rate change of 1000-10000 cps	1%
For a period of 16 hrs at a rate of 1000 cps.	1%
With voltage distribution shown in Table 5.2 and DC supply voltage=3000 V	
Pulse current:	
Linear	0.15 A
Space charge limited (saturated)	0.50 A

5.3.1 Dynode Potential Distribution Network

An R.C.A.8575 phototube with a resistive dynode potential divider was used in the initial tests. A negative H.T. power supply was used to power the photomultiplier in order to avoid the anode being a.c. coupled to the counting electronics. At high counting rates capacitors across the signal path are undesirable since they cause pile-up problems and therefore shifts in the base line of the pulses. Potentials applied to the dynodes were those recommended by the tube manufacturers(9) for high peak current and fast applications. The potentials on the last three dynodes were in ascending order to suppress the space charges being formed in the regions between those dynodes - (see Fig (1)). The resistance values for the potential divider have been calculated on the basis that the current through the resistor chain is at least 10 times larger than the largest value of the anticipated anode current ($\sim$150 μA). The choice of resistance values for the voltage divider chain is usually a compromise. If low values of resistance per stage are used, the power drawn from the supply increases and as a result the phototube noise may increase due to heating if the divider is mounted close to the tube. On the other hand, the use of high values of resistance per stage may cause deviation from linearity if the divider chain current is not maintained at a value which is much higher than the tube current. Table 5.2 shows the ratios of the potentials(9) to be provided by a potential divider and Fig (1) represents the nearest preferred values to the calculated resistance values. In order to minimise the non-linearity effects due to diversion of electron current from the potential divider to the tube, large capacitors (ceramic) were connected across the latter stages of the tube.

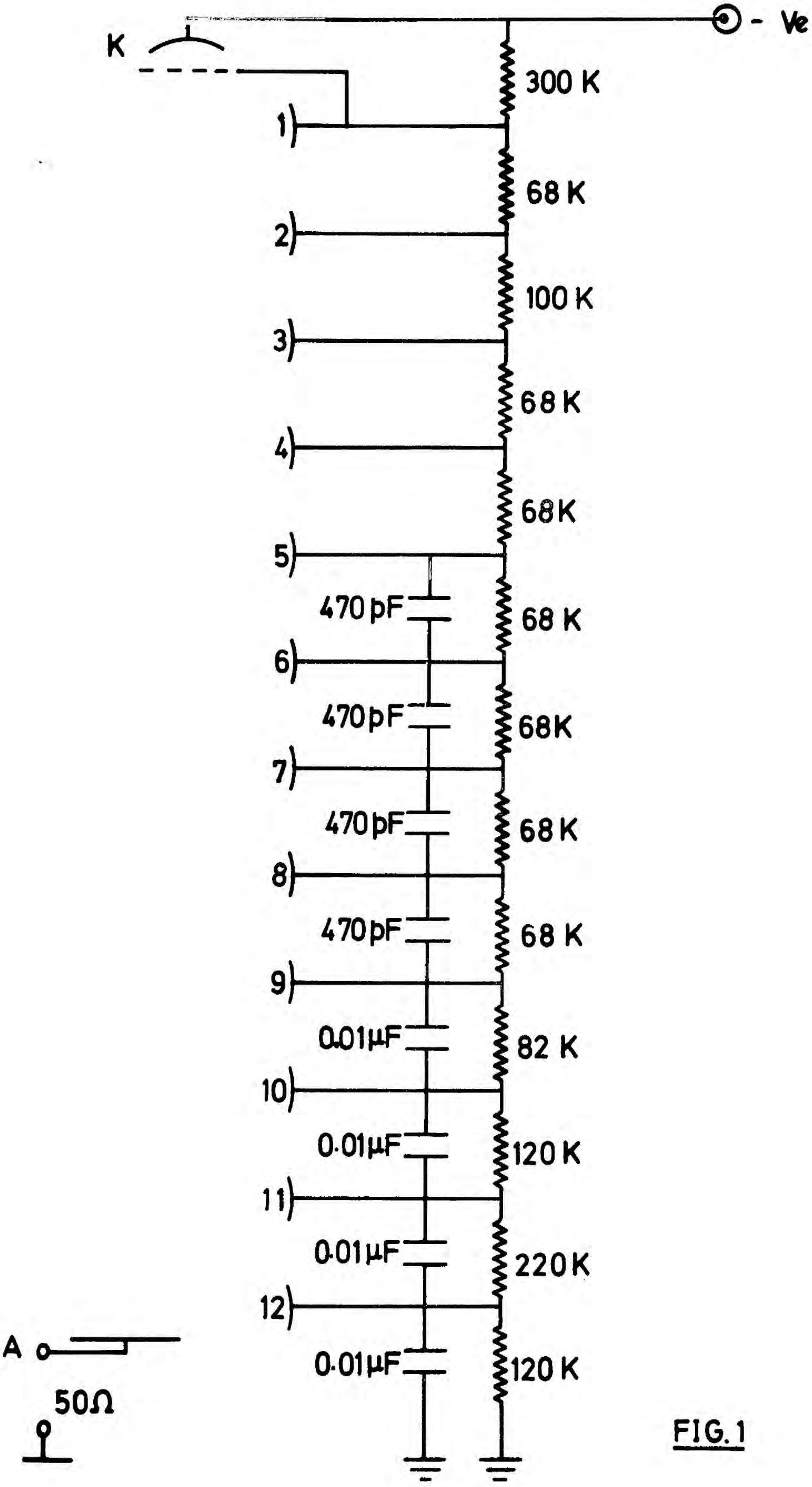
K
- Ve
300 K
1)
68 K
2)
100 K
3)
68 K
4)
68K
5)
470 pF
68 K
6)
470 pF
68K
7)
470 pF
68 K
8)
470 pF
68 K
9)
0.01µF
82 K
10)
0.01µF
120 K
11)
0.01µF
220K
12)
0.01µF
120 K
A
50Ω

FIG. 1

Value of the capacitors are given by the formula

$$C = 100 \frac{q}{V} \tag{5.2}$$

where C is in farads, q is the charge per pulse in coulombs and V is the voltage across the capacitor in volts. This formula applies for the anode to final dynode and the factor 100 is used to limit the voltage change across the capacitor to 1% maximum during a pulse.

TABLE 5.2 Voltages to be provided by Divider (from R.C.A. manual)

Between the following electrodes: Cathode (K) Dynode (Dy) and Anode (A)	4.6% of Supply Voltage (E) multiplied by
K - Dy^1	4.0
Dy_1 - Dy_2	1.0
Dy_2 - Dy_3	1.4
Dy_3 - Dy_4	1.0
Dy_4 - Dy_5	1.0
Dy_5 - Dy_6	1.0
Dy_6 - Dy_7	1.0
Dy_7 - Dy_8	1.0
Dy_8 - Dy_9	1.0
Dy_9 - Dy_{10}	1.5
Dy_{10} - Dy_{11}	2.0
Dy_{11} - Dy_{12}	4.0
Dy_{12} - A	2.0

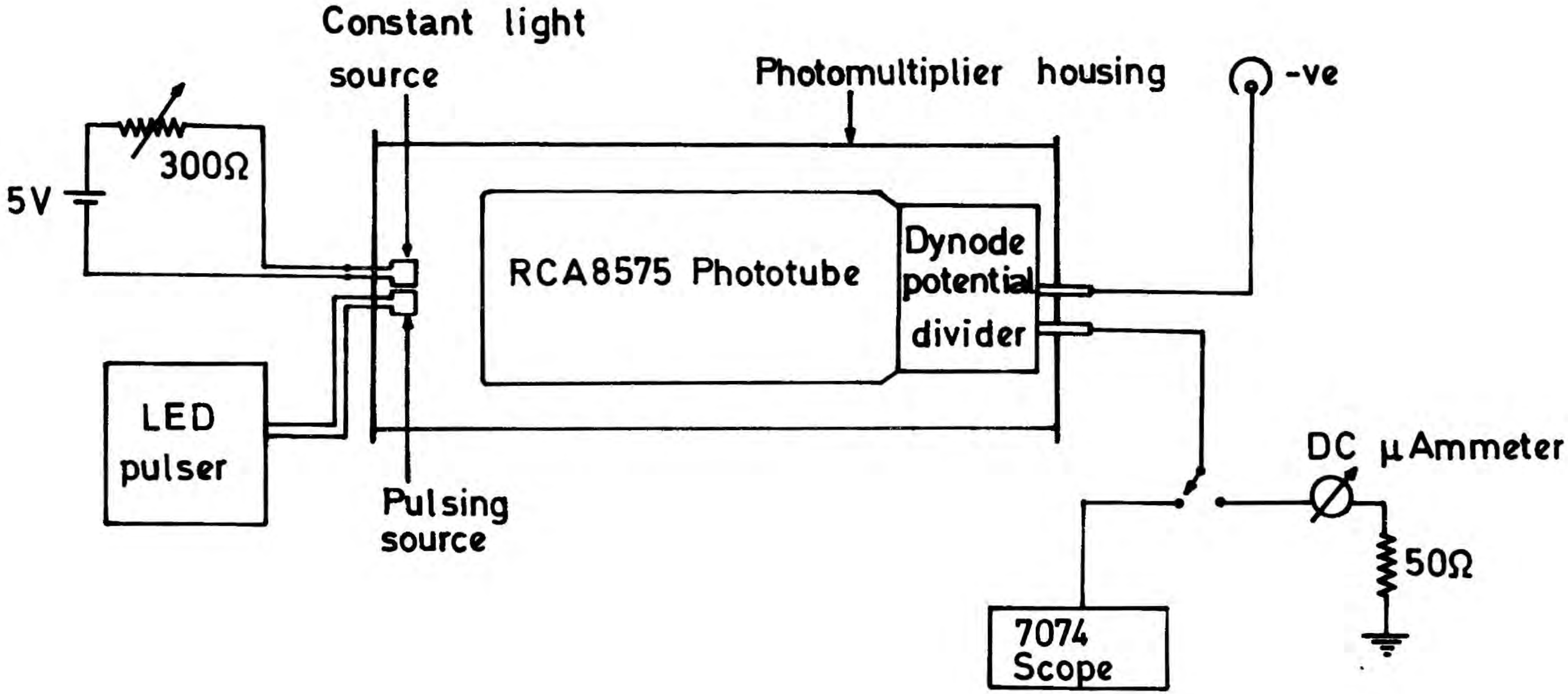

FIG.2 Experimental arrangement used for evaluation of the RCA 8575 phototube.

5.3.2 Experimental Set-up

The experimental arrangement used in the tests is shown in Fig (2). A constant light source and a pulsing light source were used to test the performance of the photomultiplier. The constant light source was a small yellow indicator lamp the intensity of which could be adjusted to produce different average anode currents thus simulating various count rates to which the phototube may be exposed(10). The pulsing source was a yellow light emitting diode (LED) driven by means of a TTL Nand gate, a stabilised power supply and a pulse generator(11) (see Fig (3)). The only variables measured in the tests were pulse amplitudes, average anode currents and pulsing rates. Pulse amplitudes and pulsing rates were measured on a Tektronix 7704 oscilloscope with a 7A16 amplifier and the average anode currents with a d.c. micro-ammeter.

5.3.3 Results

In order to justify the use of a constant light source to simulate different count rates, the following tests were carried out. The photomultiplier was pulsed with the LED pulser and the pulsing anode current was measured as a function of pulsing rate. A plot of the anode current versus pulsing rate is shown in Fig (4). The pulsing source was then switched off and the anode current was set at 2 μA by illuminating the photocathode with the constant light source. Then in addition to the constant light, pulsing was again introduced and the total anode current was measured as a function of pulsing rate. The 'exact count rate' corresponding to the total currents were deduced from the above measurements on the assumption that the equivalent count rate corresponding to a constant light current of 2 μA is identical to the count rate that can be obtained with a pulsing current of 2 μA. The exact count rates were then plotted against the pulsing rates and the results are shown in Fig (4).

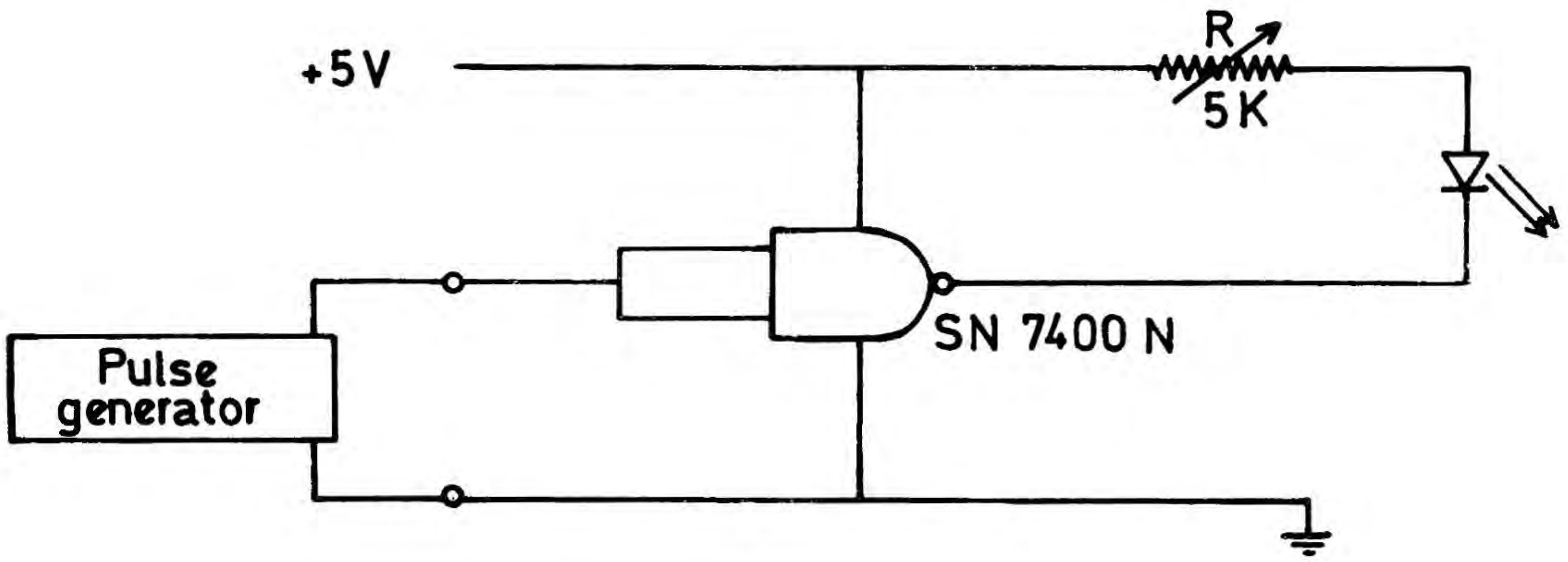

FIG.3 LED Pulser

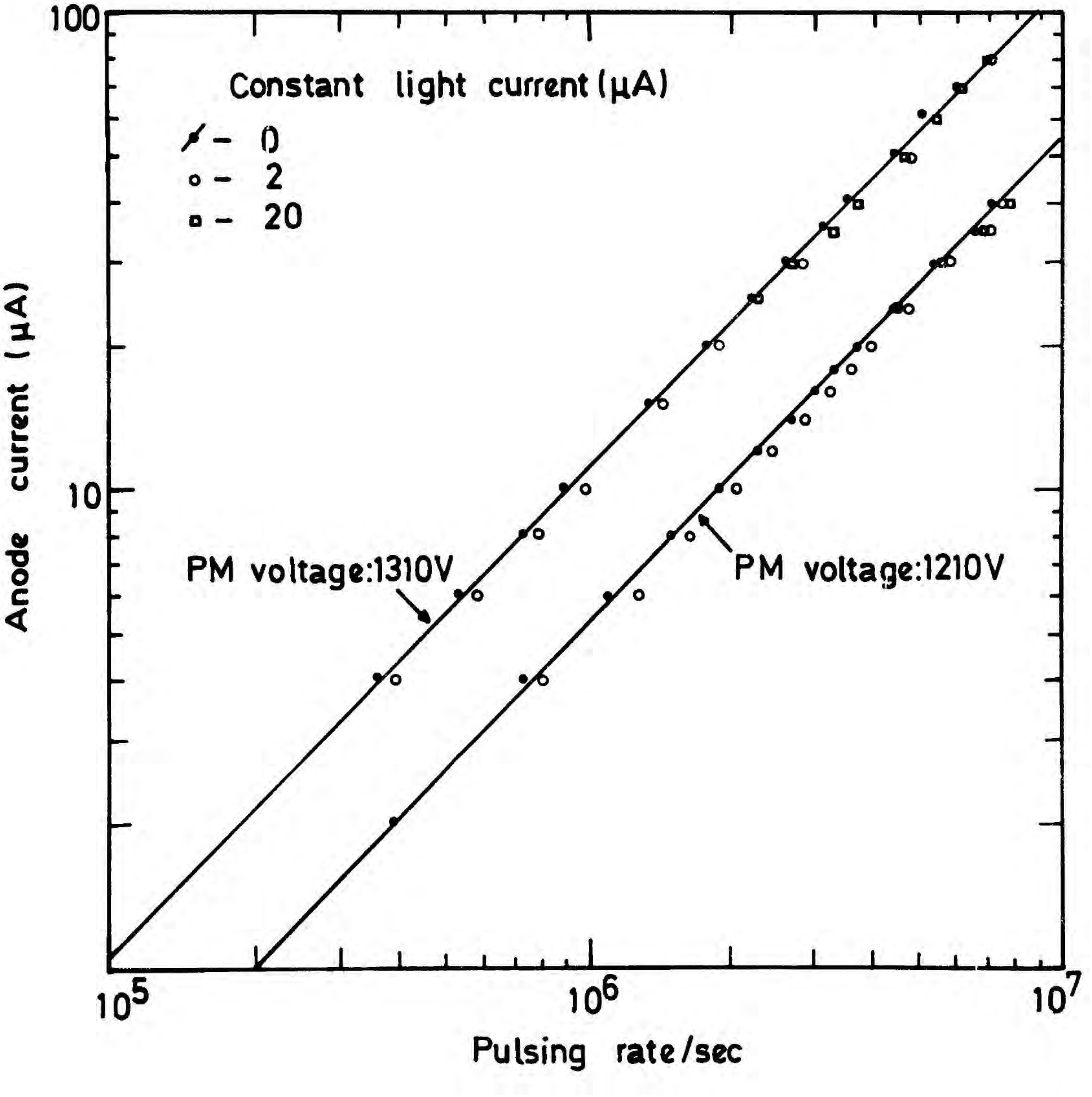

FIG.4 Correlation between constant light current and pulsing current.

The comparison of results obtained with the constant light source plus pulsing with those obtained only by pulsing showed (within 2%) that as far as the current through the phototube is concerned various count rates can be simulated by biasing the photomultiplier with a 'calibrated' constant light current. Fig (4) also shows that relationship between the anode current and the pulsing rate is linear (slope of the curve in the log-log plot is unity). It must be mentioned here that when measuring the amplitude of the pulses in the presence of a constant light current, the constant current part of the pulses were always subtracted from the total pulse amplitudes. This method has been adopted throughout the remaining part of the tests to obtain high pulsing rates ($> 10^7$ Hz).

The amplitude of the photomultiplier pulses (across 50 Ω) and the average anode current were measured as a function of the pulsing rate for different photomultiplier voltages and the results are shown in Figs(5) and (6). The pulse height, and hence the gain of the photomultiplier, has been found to increase with the pulsing rate. The shift in gain is more pronounced at higher PM voltages, i.e. at higher anode currents. Previous measurements which have been done with the same photomultiplier in conjunction with a GSDC showed a similar behaviour with pulses formed by 5.9 keV X-rays (see Fig (7)).

In order to investigate the variation of interdynode voltage supplied by the potential divider network with anode current, the interdynode voltages were measured using a valve voltmeter of input impedance 200 MΩ at two different pulsing rates corresponding to anode currents of 50 μA and 100 μA and the results are shown in Table 5.3. It shows an increase in most of the interdynode voltages and a considerable drop in voltage between last dynode and the anode. The same effect has been observed by Gupta and Nath(3).

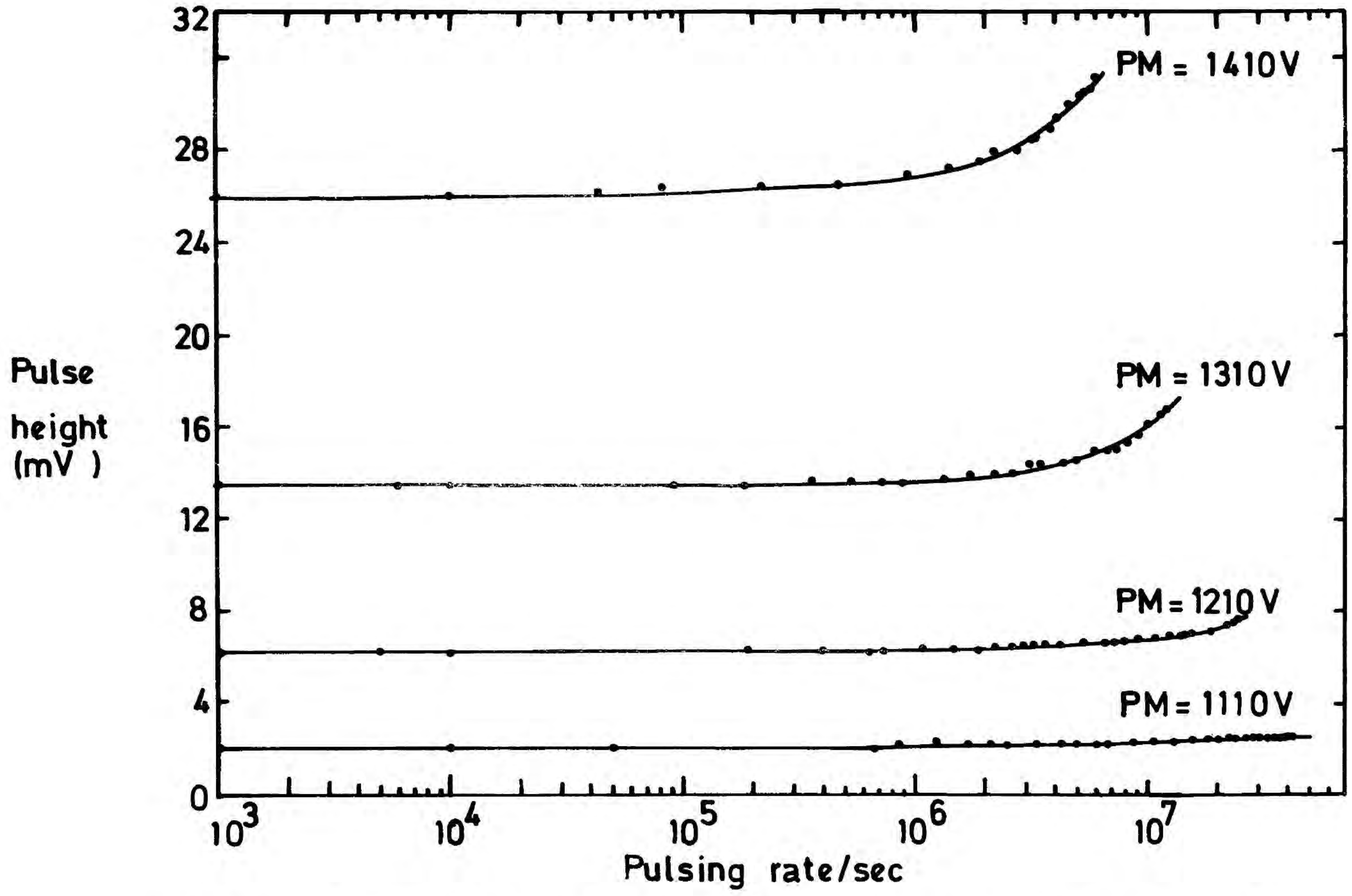

FIG.5 Amplitude of photomultiplier pulses as a function of pulsing rate.

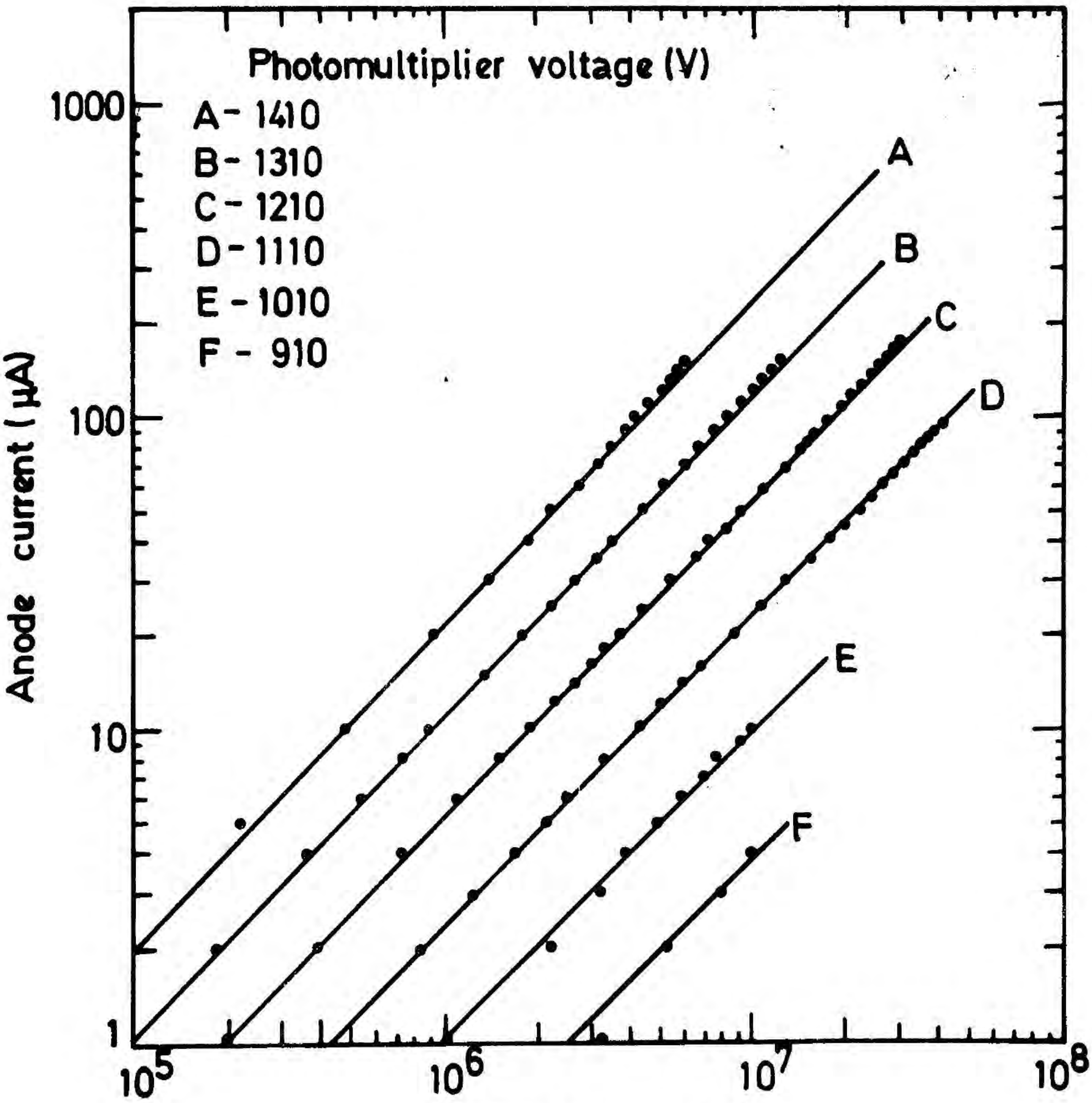

FIG.6 Photomultiplier anode current as a function of pulsing rate.

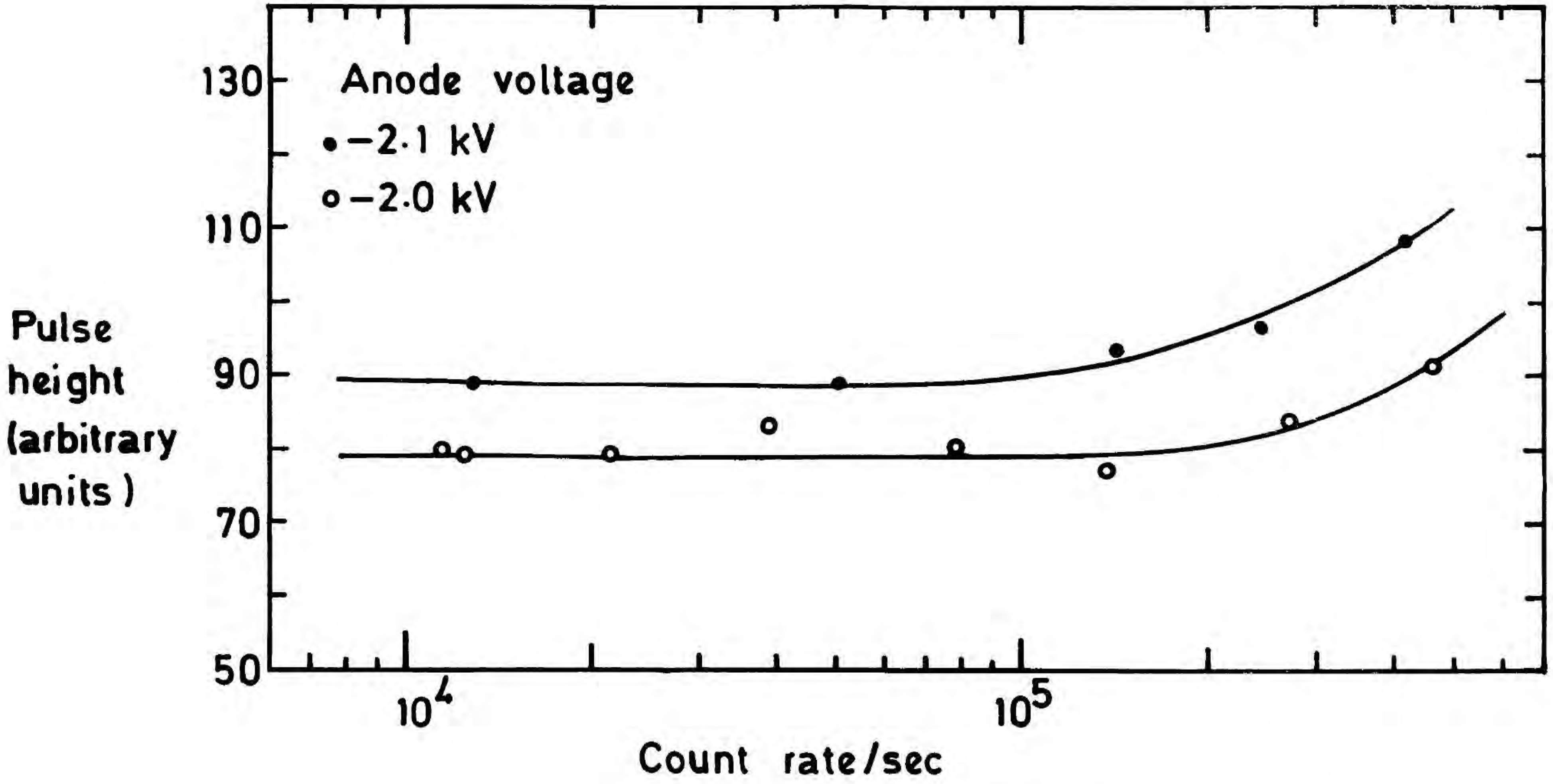

FIG.7 Variation of the amplitude of GSDC pulses (5·9 keV X-rays) as a function of count rate.

The electron current collected at the anode of a photomultiplier essentially comes from the potential divider chain to which the dynodes are being connected. The diversion of electron current from the chain mostly occurs through the last few dynodes, especially through the last dynode,and if these diversion currents are large, the potential difference between the last dynode through all the stages back to the cathode, will increase considerably.

TABLE 5.3 Variation of interdynode voltage with anode current

	Interdynode voltage (V) when		
	anode current = 0	anode current=50μA	anode current=100μA
$K - Dy_1$	310	310	315
$Dy_1 - Dy_2$	65	68	65
$Dy_2 - Dy_3$	95	97	100
$Dy_3 - Dy_4$	65	65	60
$Dy_4 - Dy_5$	65	65	70
$Dy_5 - Dy_6$	65	65	70
$Dy_6 - Dy_7$	60	63	60
$Dy_7 - Dy_8$	65	67	67
$Dy_8 - Dy_9$	65	70	68
$Dy_9 - Dy_{10}$	75	77	75
$Dy_{10} - Dy_{11}$	110	109	108
$Dy_{11} - Dy_{12}$	205	202	198
$Dy_{12} - A$	115	105	104
	$\Sigma = 1360$V	$\Sigma = 1363$V	$\Sigma = 1360$V

This increase in potential is mainly due to the large drop in voltage across the anode and the last dynode. The gain of a photomultiplier increases therefore with the anode current. At extremely high pulsing rates the smoothing action of capacitors become less effective because of pile-up effects. The small difference (3V) in total A-K voltages given in Table 5.3 is due to the errors caused during the measurement of individual voltages.

5.4 STABILISATION OF DYNODE POTENTIALS USING AN ACTIVE POTENTIAL DIVIDER

It is clear from the above discussion that a potential divider chain with a very high current compared to the anode current would be needed to stabilise the potentials of the last few dynodes. In the present study, this condition has been achieved by replacing the last seven resistors in the existing resistor chain with an emitter follower circuit chain(12) as shown in Fig (8). The current gain property (β) of the emitter followers enables the dynodes to contribute large currents to the anode current while drawing small currents, smaller by a factor of β, from the potential divider (resistor) chain. It is clear that success of this method depends on the value of β and therefore transistors with high β value should be employed in the divider.

5.4.1 Calculation of Resistance Values

The potential divider has been designed to draw a current of 1.5 mA from the power supply at 2000 V. The values for the resistances from R_1 to R_6 can be calculated from the information given in Table 5.2 and considering the total chain current (1.5 mA). Values for resistances from R_7 onwards have been calculated as follows.

Suppose the total current flowing through the divider chain is I and the potential divider is to be designed so that the emitter current

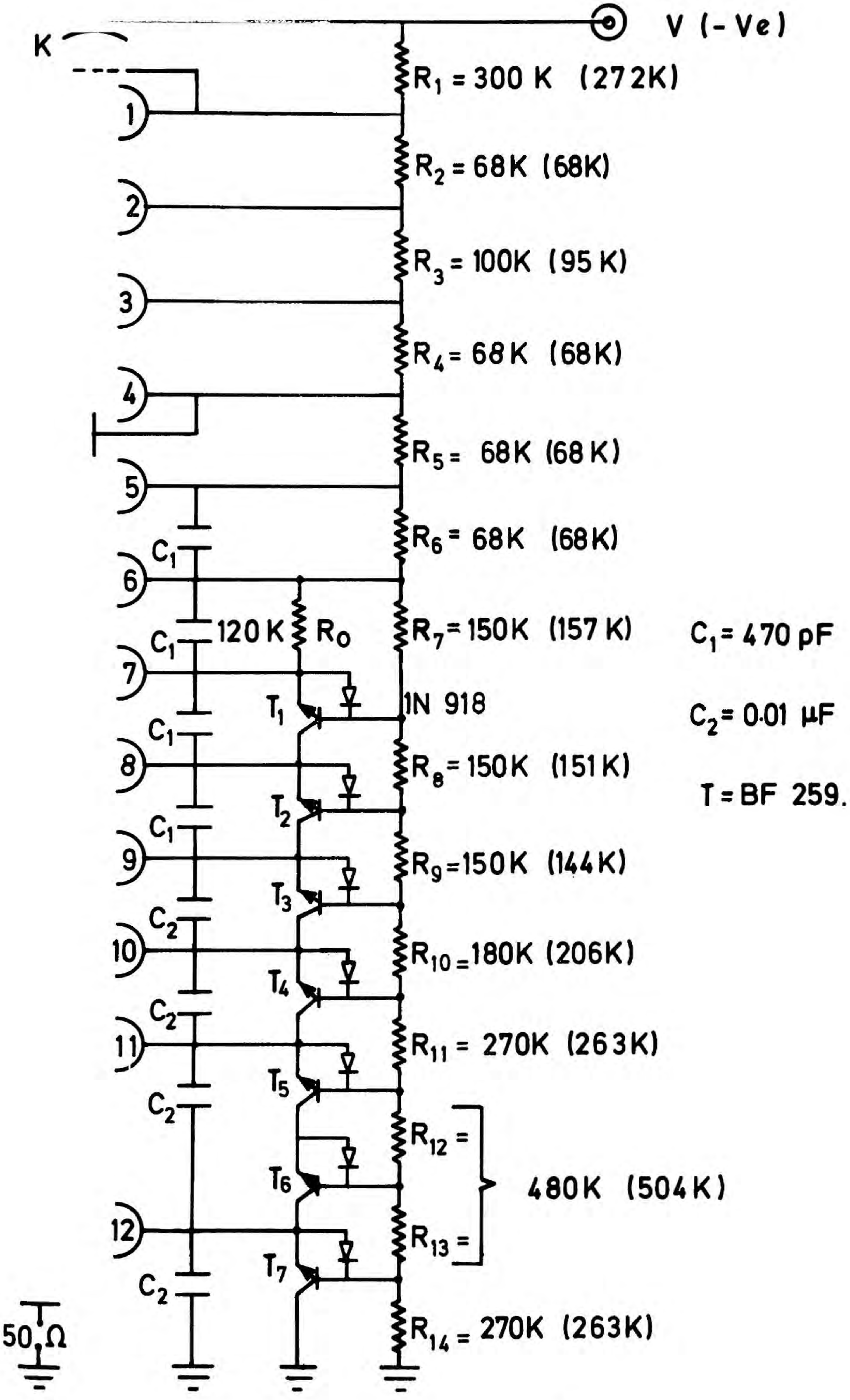
V (-Ve)
K
1
2
3
4
5
6
7
8
9
10
11
12
R1 = 300 K (272K)
R2 = 68K (68K)
R3 = 100K (95 K)
R4 = 68 K (68K)
R5 = 68K (68 K)
R6 = 68K (68K)
R7 = 150K (157 K)
1N 918
R8 = 150K (151 K)
R9 = 150K (144K)
R10 = 180K (206K)
R11 = 270K (263K)
R12 =
R13 =
480K (504K)
R14 = 270K (263K)
120 K
Ro
C1
C2
T1
T2
T3
T4
T5
T6
T7
C1 = 470 pF
C2 = 0.01 μF
T = BF 259.
50 Ω

FIG. 8

of the first transistor (Tr_1) is I_E (see Fig (9)).

Considering the closed loop containing R_o, Tr_1 and ~~R_6~~ R_7

$$I_E R_o + V_{EB} = (I - I_E) R_7 \tag{5.3}$$

Since $V_{EB} << I_E R_o$

$$I_E R_o \approx (I - I_E) R_7 \tag{5.4}$$

and the R.H.S. of equation (5.4) represents the potential across Dy_6 and Dy_7, which is known from Table 5.2, and hence R_o can be calculated. Since the voltages across the other resistances (R_7-R_{14}) are also known, the following relations can be used to calculate all the R values.

$$V_{R_8} = (I - \alpha I_E) R_8 \tag{5.5}$$

$$V_{R_9} = (I - \alpha^2 I_E) R_9 \tag{5.6}$$

$$\vdots \qquad\qquad \vdots$$

$$V_{R_{14}} = (I - \alpha^7 I_E) R_{14} \tag{5.7}$$

where $\alpha = \dfrac{\beta}{1+\beta}$

In order to evaluate the values of R, a numerical value must be substituted for I_E and it should not be too small since β is an increasing function of the collector current (αI_E).

5.4.2 Design of the Potential Divider

Transistors used in the divider were npn, high voltage, high β, video transistors ; BF 259. According to the manufacturers data ,the BF 259 has the following characteristics

P_T(max)	I_C(max)	V_{CEO}(max)	V_{CBO}(max)	h_{fe}(typ)	f_t(typ)
800 mW	100 mA	300 V	300 V	25	90 MHz

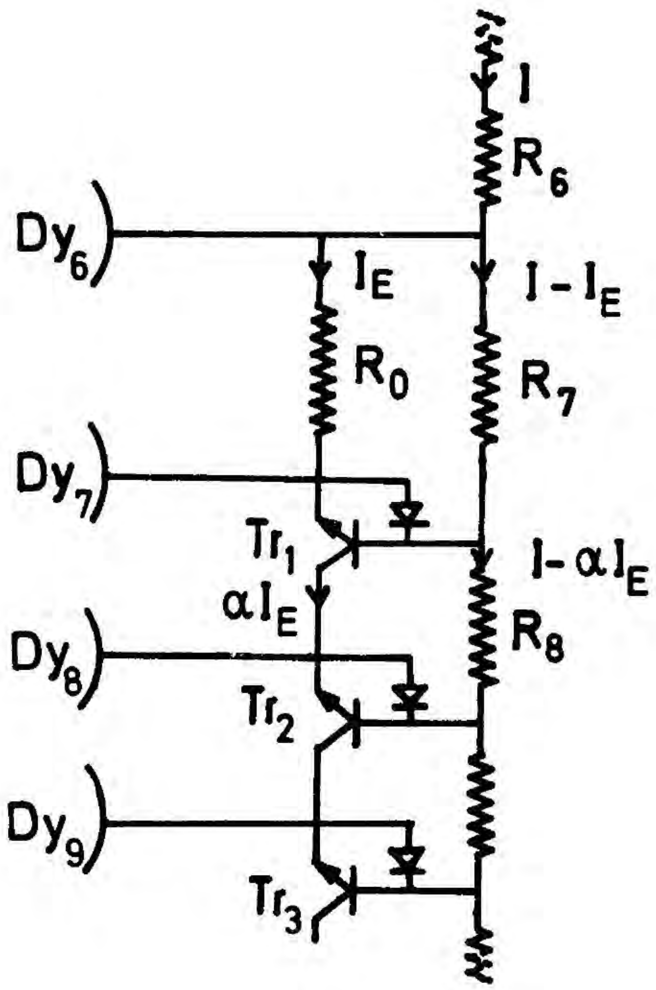

FIG. 9 Section of the potential divider chain showing the currents through various components.

A batch of transistors was purchased and after measuring their individual β values by means of a transistor meter, seven transistors with highest β values were selected. Resistor values were calculated assuming an emitter current of 0.75 mA through the first transistor (Tr_1). All the calculated values (in brackets) and the nearest preferred values of the resistances are shown in Fig (8). Two emitter follower stages were used across Dy_{11} and Dy_{12} since the interstage voltage was too high for one transistor. Transistors and resistors were separately mounted on two printed circuit boards and clamped to the phototube assembly as shown in Fig (10). The assembly itself consists of four thin wooden bars fitted to a metal disc and carrying a perspex ring to which the phototube socket was fitted at the other end. All the connections between components and the pins in the phototube socket were made with short wires in order to minimise stray capacitances. To obtain the best overall performance of the divider, transistors were connected down the chain in such a way that their β's were in ascending order. Diodes, 1N 918, were connected between emitters and bases of the transistors to prevent accidental over-voltaging of emitter base junctions in the reverse direction. Although such a situation does not normally occur, it could happen under fault conditions or during the transient turn-on or turn-off periods. Values of the capacitors used in the circuit were similar to those used in the resistive potential divider. Output from the anode was taken through a coaxial cable.

5.5 PERFORMANCE OF THE PM WITH AN ACTIVE POTENTIAL DIVIDER

5.5.1 Variation of Interdynode Voltages with Anode Current

Interdynode voltages of the PM were measured with a value voltmeter under two conditions:

FIG.10 Photograph of the phototube base.

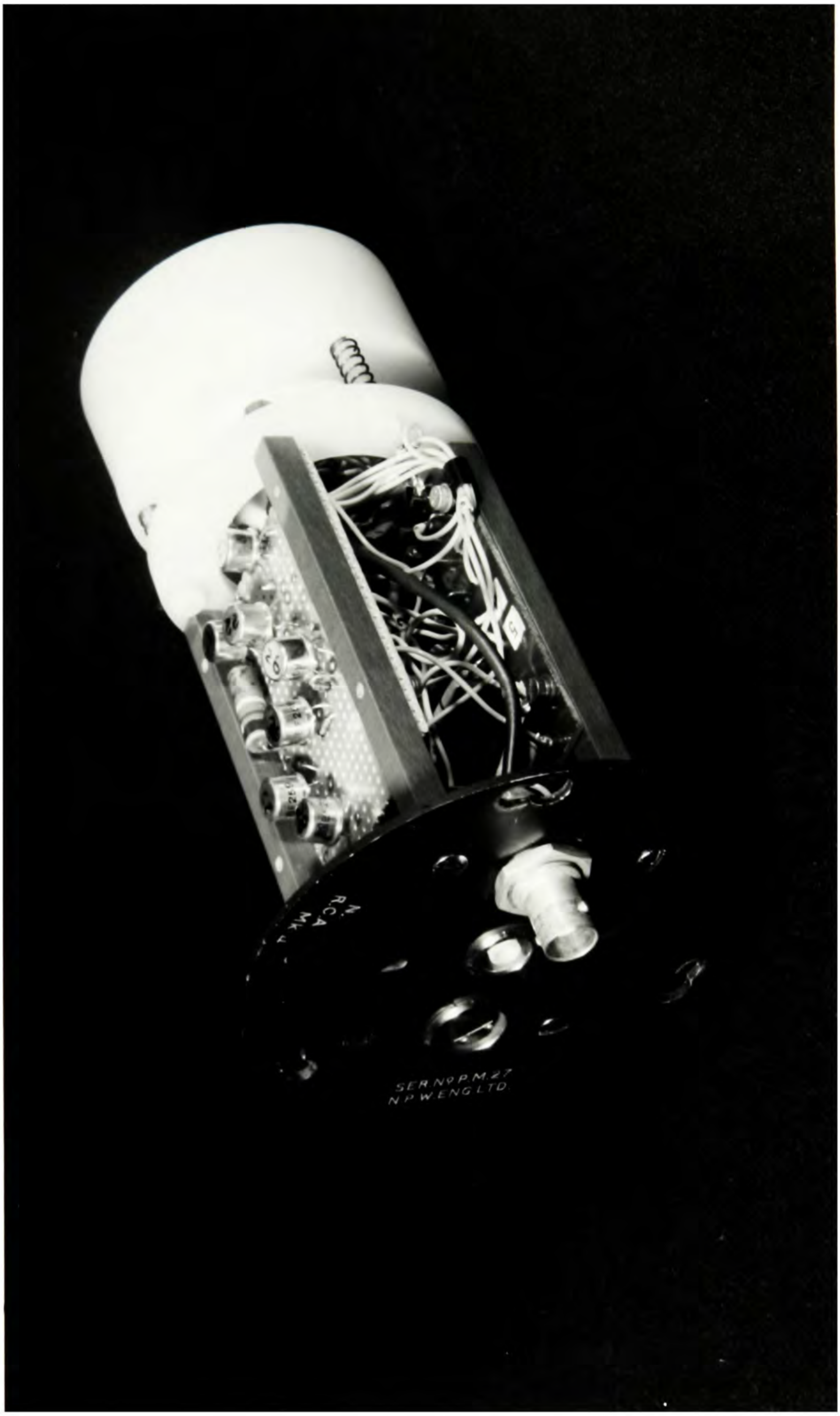
N.
R.C.A.
Mk 4
SER. No P.M.27
N.P.W. ENG. LTD.

(1) when the anode current is zero,

and (2) when the anode current is about 180 μA (out of which 100 μA was due to the pulsing and the rest was due to the constant light source)

Results of the measurements are shown in Table 5.4.

TABLE 5.4 Interdynode voltages at two anode currents.

	Interdynode voltage (V) when	
	anode current = 0	anode current =180μA
K - Dy_1	305	306
Dy_1 - Dy_2	71	71
Dy_2 - Dy_3	104	104
Dy_3 - Dy_4	71	71
Dy_4 - Dy_5	71	71
Dy_5 - Dy_6	71	71
Dy_6 - Dy_7	70	70
Dy_7 - Dy_8	70	70
Dy_8 - Dy_9	71	71
Dy_9 - Dy_{10}	81	81
Dy_{10} - Dy_{11}	132	132
Dy_{11} - Dy_{12}	215	215
Dy_{12} - A	134	134

The interdynode voltages were found to remain constant within 1% with the anode current.

Oscillogram of photomultiplier output pulse without constant light current (positive trigger pulse is also shown).

Photomultiplier output when the anode current is 180 μA out of which 100 μA is due to the pulsing.

FIG. 11

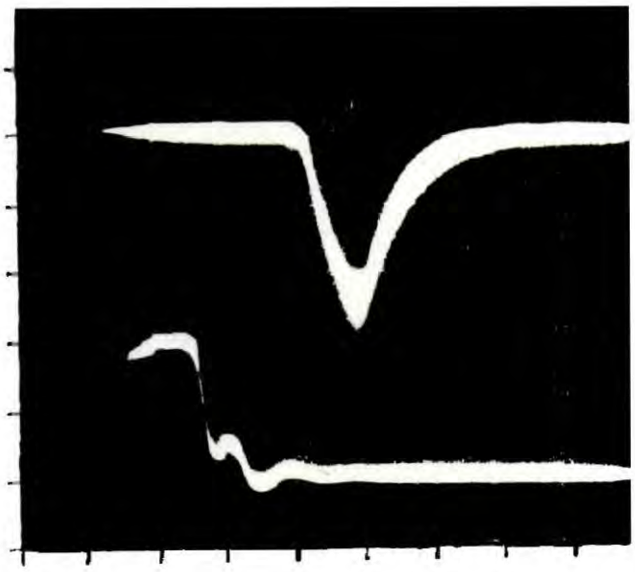

Horizontal: 20 ns/div

Vertical 5mV/div(upper trace)

1V/div (lower trace)

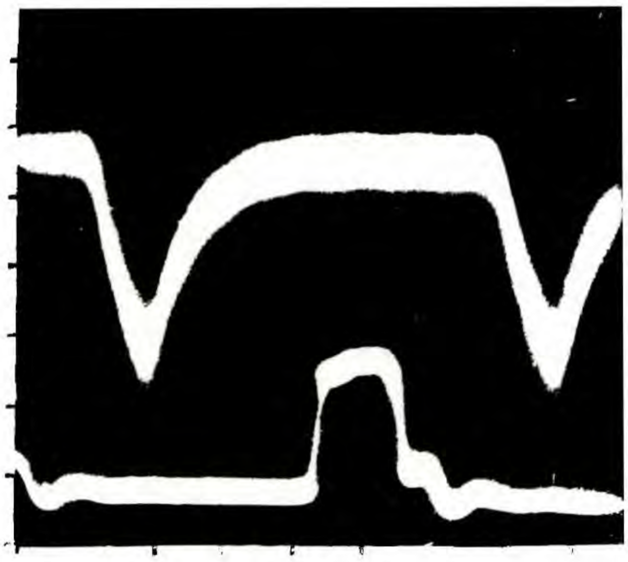

Horizontal: 20ns/div

Vertical. 5mV/div(upper trace)

1V/div (lower trace)

FIG. 11

5.5.2 Variation of Pulse Height with Pulsing Rate

The performance of the photomultiplier with the new potential divider was investigated using the same procedure discussed in Section 5.3. Fig (11) shows the PM output pulses at a very small and a very large anode currents. It is apparent from Fig (11) that although the shape and amplitude of pulses are the same under both conditions, the base line of pulses under the latter condition is much thicker than that of the former because of the constant light current. The amplitude of anode pulses and the anode current were also measured as a function of pulsing rate for different photomultiplier voltages and the results are shown in Figs (12) and (13). No appreciable change in amplitude (within 3%) with pulsing rate have been observed up to an anode current very near to the maximum permissible anode current of the tube.

In order to ensure successful operation of the photomultiplier with random pulses at very high rate ($> 10^7$ pulses per second), it was decided to improve the existing divider further by increasing the total divider current to a few milliamperes and by employing transistors of the same type but with β values higher than those used in the existing divider network. Transistors were selected out of a large batch and the new potential divider was made so that when the applied voltage was 2000 V the total current (I) through the chain and the emitter current (I_E) through the first transistor were 3.4 mA and 1.12 mA respectively. Calculated resistance values of the new chain are given in Appendix 1. The variation of pulse height and the anode current with pulsing rate for this potential divider are also given in Figs(12) and (13). When the tube was in operation, the temperature inside the housing near the potential divider network was found to be about 3-4° C above room temperature ; this

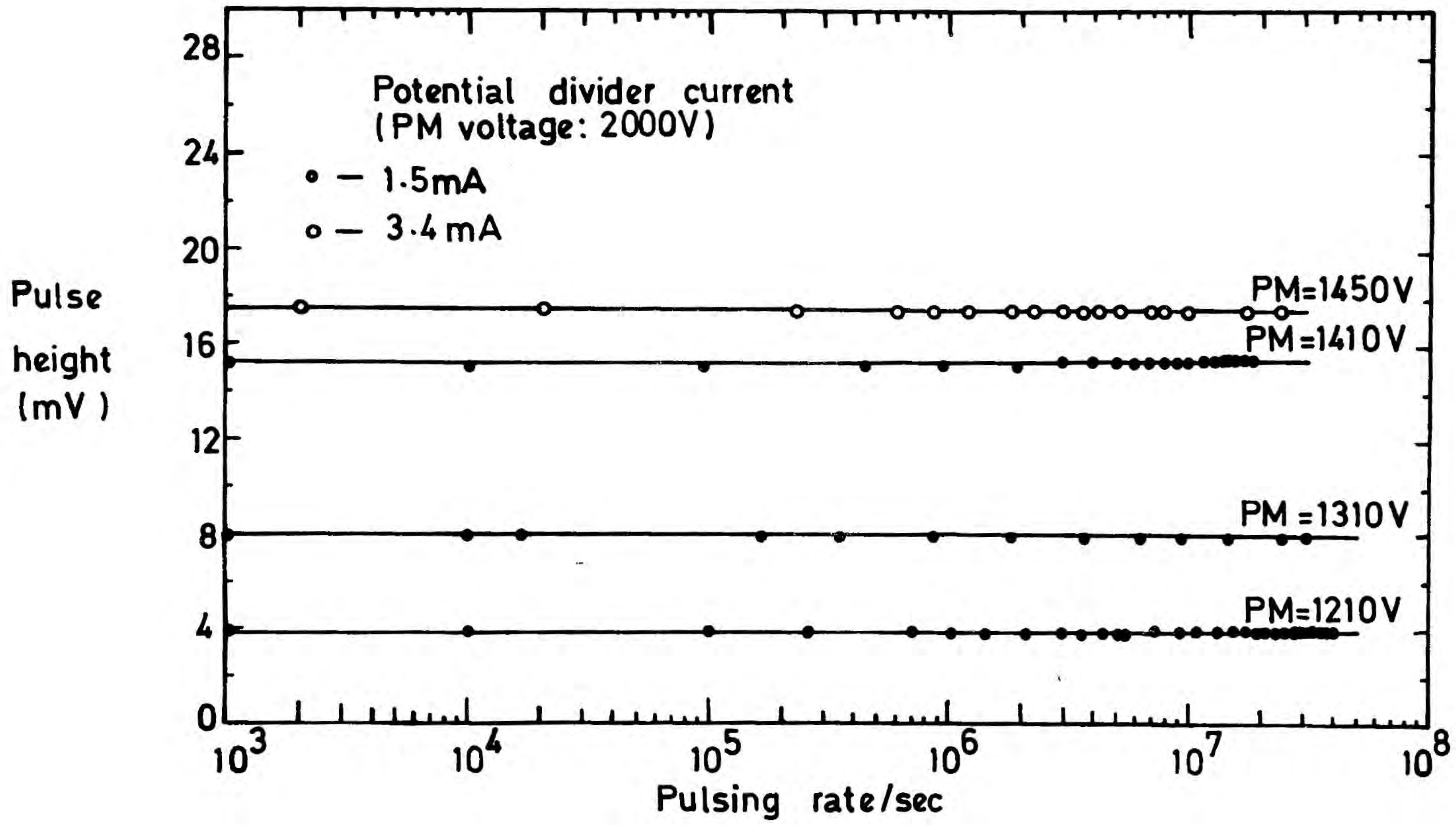

FIG.12 Variation of the amplitude of photomultiplier pulses as a function of pulsing rate.

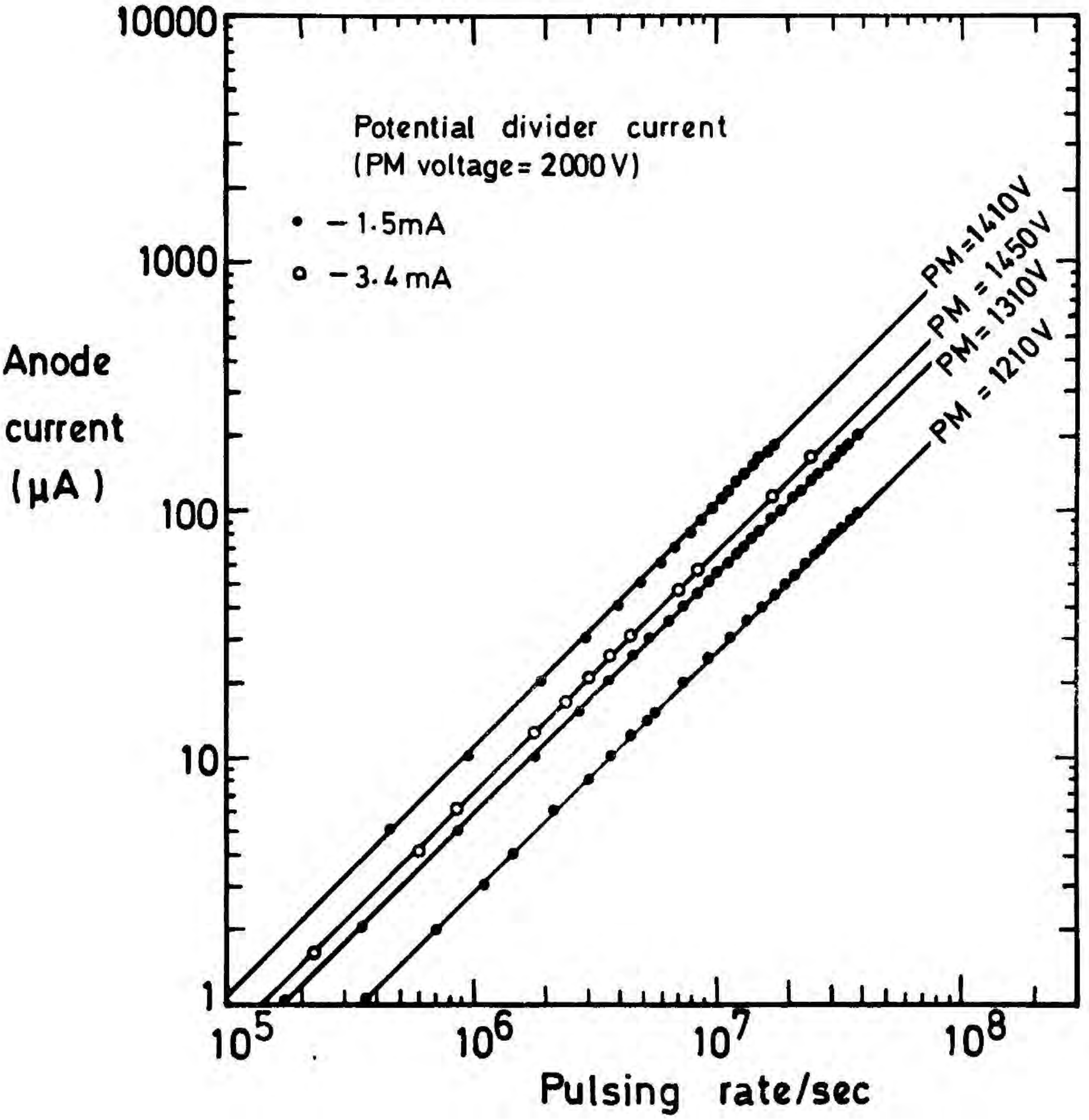

FIG. 13 Variation of photomultiplier anode current as a function of pulsing rate.

increase in temperature was believed to be too small to affect the performance of the phototube.

Anomalous variations in gain with abrupt changes in pulsing rate have been reported(5,7,8) for certain types of photomultiplier. In the case of the RCA 8575 phototube, these variations were found to occur only at low temperatures (∿ 10^{o} C) and one of the anomalies reported(8) is shown in Fig (14). In order to see if this type of variation occurs in the RCA 8575 phototube employed in this study, pulse heights were measured by changing the pulsing rate from 500 per sec to 5×10^{6} per sec in four equal steps. Once a change in pulsing rate was made, pulse amplitude was recorded for a duration of 150 minutes before the second change in the rate was made, in order to investigate slow variations in pulse height. The pulse height was found to remain constant within 2% against all the sudden variations in pulsing rate and furthermore, no slow variations were observed throughout the test which lasted for about seven hours.

5.6 MEASUREMENTS ON AFTER-PULSING

Spurious pulses originating from the photocathode after a real pulse can cause errors in counting experiments and degrade the pulse height resolution of the photomultiplier. Gulari et al(13) have measured the after pulsing rate as a function of delay time after a real pulse for several RCA photomultipliers and found that the pulsing rate was negligibly small in RCA photomultipliers for delay times between 10-1000 nS. In order to investigate this effect in the RCA 8575 phototube, narrow light pulses corresponding to a photomultiplier output of 20 nS (half-width) and height 35 mV, a fast discriminator (NE 8684, pulse pair resolution ∿ 9 nS) and a 100 MHz scaler were used. Light pulses were obtained from a yellow LED driven directly by a fast pulse generator

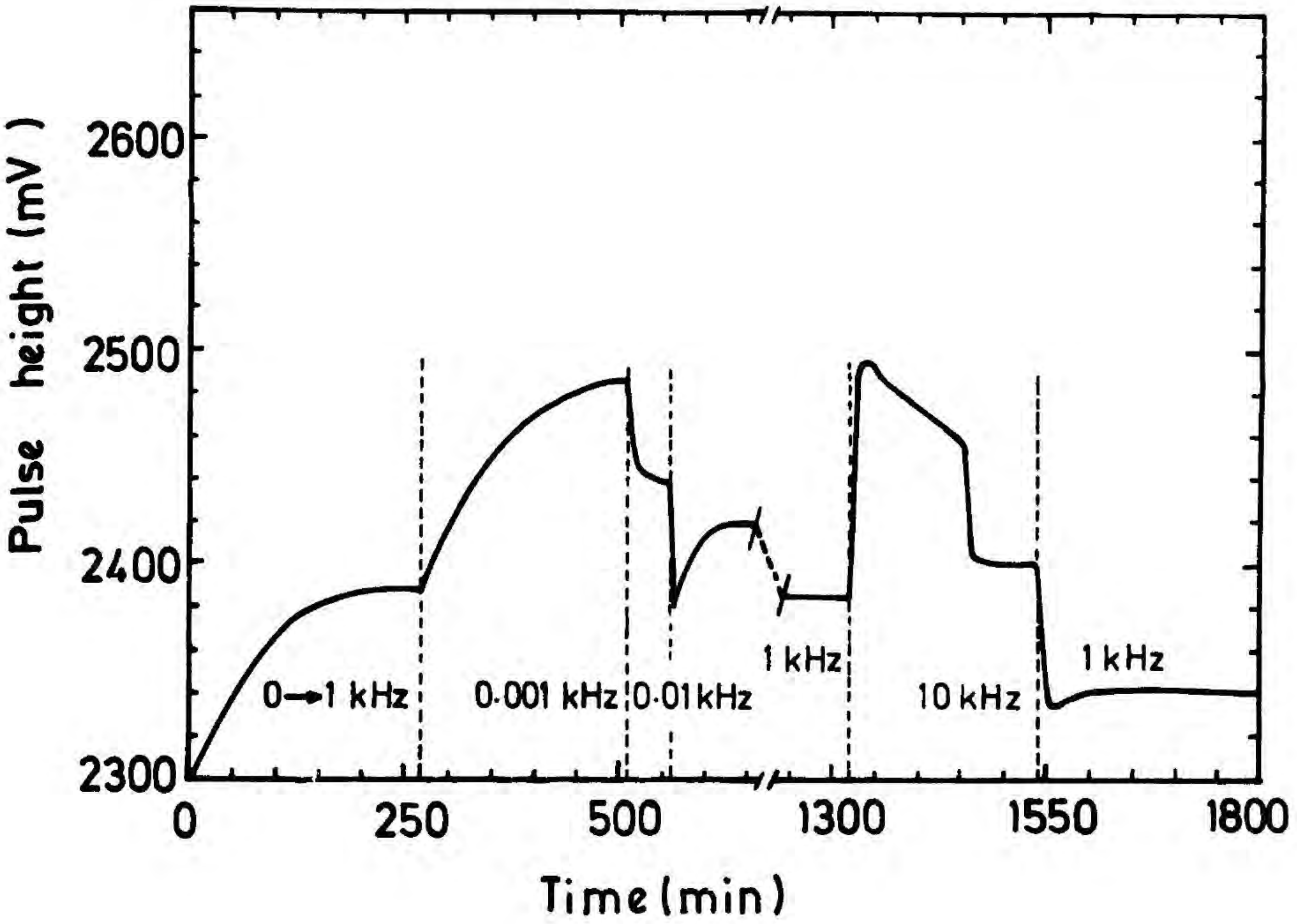

FIG. 14 Time behavior of pulse height during the period when the count rate is altered in such a manner as 0→1→0.001→0.01→1→10→1 kHz at 10°C, measured in an RCA 8575 tube.

(HP 8004A) and the PM output after being discriminated at 25 mV was fed into the scaler via a Tektronix 475 oscilloscope. Count rates were measured on the scaler as well as being observed on the oscilloscope for different pulsing rates from 10 kHz to 1 MHz. The values obtained for pulsing rates in each case agreed within the statistical error. This clearly shows that the after pulsing is negligibly small for the RCA 8575 phototube (between 25 nS - 100 μsec) since the measurements obtained using the oscilloscope do not include the after pulsing rates while the other method does.

5.7 PHOTOMULTIPLIER PULSE RESPONSE

The fast time response of a photomultiplier is of prime importance in high counting rate applications. When a photomultiplier is illuminated by a very short light pulse, the resulting current pulse at the anode is not of the same width as the original light pulse but has a slightly larger width due to fluctuations in the electron transit time between the cathode and the anode. Another reason for broadening of the pulse response is the imperfect electrical matching of the anode to the external circuit. In general the form of the pulse response is characterised by the rise time and the full width at half maximum (FWHM) value of the output pulse, and depends on the level of illumination of the photocathode. However, in most cases the rise time and FWHM of a pulse corresponding to an emission of a single photoelectron from the cathode are used to specify the pulse response of a photomultiplier. The single photoelectron rise time and FWHM are the smallest values that can be obtained for these two parameters since in this case, variations in electron transit time between photocathode and first dynode do not interfere with these values. However, when studying anode pulses which are formed from a number of photoelectrons ejected from the cathode, these broadening effects are usually not of much importance since the FWHM of the single photon response is probably very small compared to the duration of the emission of photoelectrons from the cathode.

5.8 MEASUREMENT OF PULSE RESPONSE

In general, measurements on single electron rise time and FWHM of pulses do not require a fast pulsed light source. This work can be done by means of a steady light source which is so weak that the probability of a single photoelectron per pulse from the photocathode is much greater than the probability of the emission of two, three or more photoelectrons and that the average time interval between emission of photoelectrons by the photocathode is very much greater than the time resolution of the photomultiplier-measuring equipment combination.

The test arrangement was similar to the one described in section 5.3.2. The constant light source was the yellow indicator lamp which has been used in previous tests and the intensity of emission from the light source was reduced by decreasing the current through filament by means of a potentiometer. Output pulses were observed on a Tektronix 475 oscilloscope whose fastest calibration time per division is 2 nsec. Fig (15a) shows the oscillogram of the single photoelectron response of the photomultiplier. The estimated rise time and FWHM of the pulse were 2 nsec and $\sim$3.5-4 nsec respectively. The pulse response of the photomultiplier to multi-photoelectron pulses was also investigated using a light pulse from a yellow LED triggered by a short pulse from a fast pulse generator (HP 8004 A). Fig (15b) shows the oscillogram representing both trigger pulse and the PM output pulse and Table 5.5 shows some of the characteristics of both pulses.

FIG. 15a Single photoelectron pulse response of an RCA 8575 phototube.

FIG. 15b Multi photoelectron pulse response. (lower trace shows the trigger pulse)

FIG. 15c Primary scintillation pulse response of the phototube for 6.9 keV X-rays.

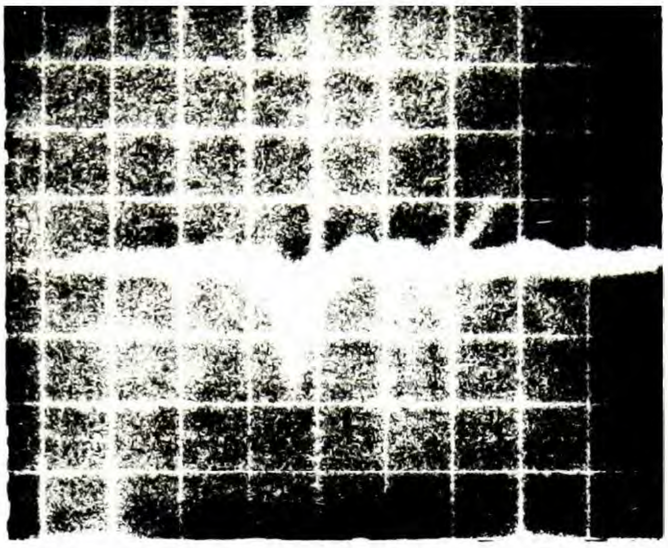

FIG. 15a

Horizontal: 10ns/div

Vertical: 2mV/div

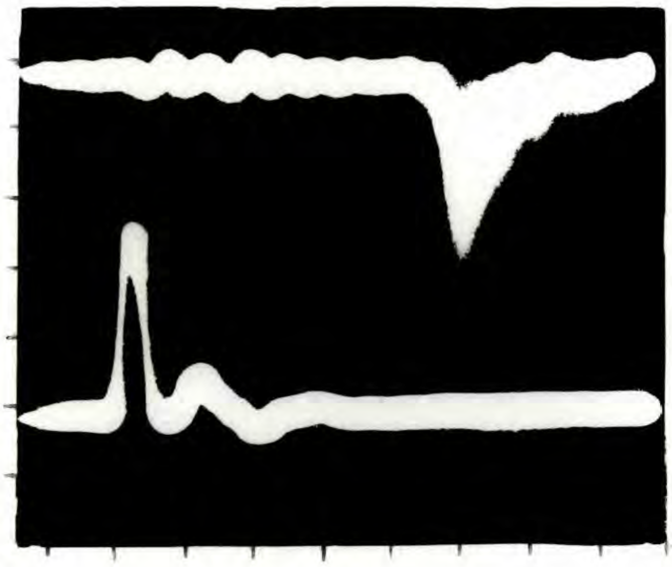

FIG 15b

Horizontal: 10 ns/div

Vertical: 2mV/div
(upper trace)
1 V/div
(lower trace)

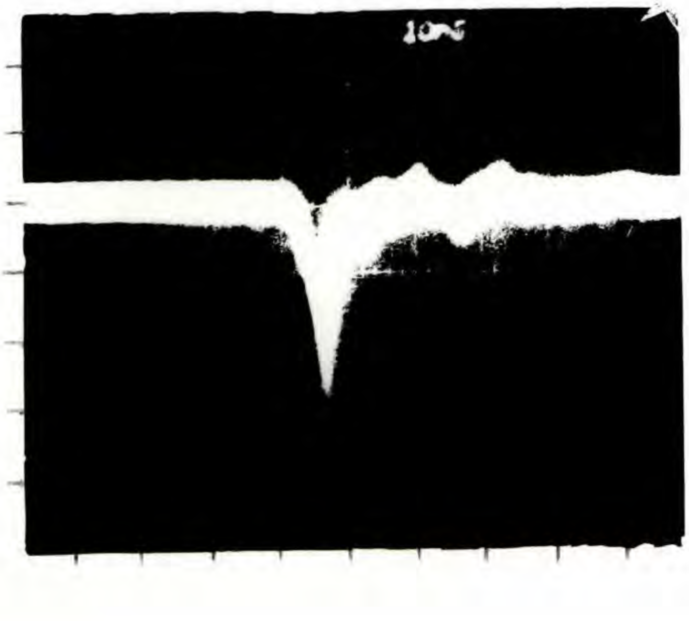

FIG.15c

Horizontal : 10ns/div

Vertical : 20 mV/div

TABLE 5.5 Some of the characteristics of the trigger pulse and the photomultiplier output

		Trigger Pulse	PM output pulse
Rise time (10-90%)	nS	2.1	3.2
Fall time "	nS	2.2	9
FWHM	nS	3.7	5

It is clear from Fig (15b) and Table 5.5 that the photomultiplier contribution to the width of the output pulse is small. The dispersion and relatively long fall time of the PM output was believed to be due to light emission properties of the LED. The pulse response of the RCA 8575 photomultiplier is also demonstrated in Fig (15c) which shows the primary scintillation output from a GSDC for 6.9 keV X-rays (from a X-ray machine). Narrow width of the pulses obtained again indicate the 'fastness' of the photomultiplier. It is clear from these results that the RCA 8575 photomultiplier is suitable for high rate applications.

Chapter 5 - References

1. J.B. Birks and J.W.King, Proc.Phys.Soc. B66 (1953) 81.

2. D.H.Hartman, Rev.Sci.Instrum. 49 (1978) 1130.

3. A.K.Gupta and N.Nath, Nucl.Instr. & Meth. 53 (1967) 352.

4. R.D. Connor and M.K.Husain, Nucl.Instr. & Meth. 6 (1960) 121.

5. C. Weitkemp, G.G.Slaughter, W.Michaelis and H.Schmidt, Nucl.Instr. & Meth. 61 (1968) 122.

6. R.B. Galloway and D.G.Vass, Nucl.Instr. & Meth. 49 (1967) 55.

7. M. Yamashita, Nucl.Instr. & Meth. 142 (1977) 435,
Rev.Sci.Instrum. 49 (1978) 1336.

8. M. Yamashita, Rev. Sci. Instrum. 49 (1978) 499.

9. RCA 8575, Instruction Manual.

10. C. R. Kerns, Proceedings of the Calorimeter Workshop, Fermi Lab. Batavia, Illinois, May 1975.

11. Optoelectronic Data Book, Texas Instruments Inc.

12. C. R. Kerns, IEEE Trans. Nucl. Sc. NS 24 (1977) 353.

13. E. Gulari and B. Chu, Rev. Sci. Instrum. 48 (1977) 1560.

CHAPTER SIX

TESTS ON ENERGY RESOLUTION AND COUNTING CAPABILITY OF THE G.S.D.C.

6.1 INTRODUCTION

This chapter describes the results of the tests which have been carried out with 5.9 keV X-rays from an Fe^{55} radioactive source and 6.9 keV X-rays from a machine in order to investigate the rate characteristics and energy resolution of the GSDC. In particular it investigates the dependence of energy resolution on various counter parameters and limitations set by processing electronics and the counter itself on the performance of GSDC's at high counting rates. A statistical analysis of the counter data and a method of correcting the observed data at high counting rates are also presented.

6.2 BASIC IDEAS OF ENERGY RESOLUTION

One of the most important parameters characterising a scintillation spectrometer is the line width associated with the peak arising from an absorption of monoenergetic radiation. This property is generally described in terms of a quantity $\frac{\Delta V}{V}$ where ΔV is the full width at half maximum (FWHM) of the pulse height distribution obtained from a scintillation spectrometer upon the absorption of monoenergetic radiation and V is the mean height of the pulses. This ratio is called the pulse height resolution or energy resolution of the counter. It is assumed when referring to the energy resolution that V is proportional to the energy absorbed. In a GSDC the width, ΔV arises as a result of statistical fluctuations in several processes which are responsible for forming the scintillation pulse. They can be listed as follows :

fluctuations in

(1) the number of primary electrons produced in a scintillation event,

(2) the number of secondary electrons produced around the anode wire,

(3) the number of photons emitted per secondary scintillation event,

(4) the number of photons that are incident on the photocathode of the photomultiplier,

(5) the number of photons emitted by the photocathode per incident photon,

(6) the number of photoelectrons collected by the first dynode and,

(7) the secondary emission ratio at each dynode.

The overall contribution of these factors to the final energy resolution can be obtained by extending the method used by Garlick et al(1) and also Birks(2) to obtain the corresponding value for gaseous scintillation detectors. Suppose a photon of energy E dissipates all its energy in a gas producing N primary electrons which upon charge multiplaction around the wire produce NM secondary electrons. These electrons produce NMK photons from excitation processes, and a fraction G of these impinge on the photocathode. These are converted with an efficiency f into electrons which are collected with an efficiency h by the first dynode, so that the number of electrons arriving at first dynode is

$$T = N.M.K.G.f.h \qquad (6.1)$$

These electrons are multiplied at the dynodes which have an overall gain of R, so that the total number of electrons collected at the photomultiplier anode is

$$Q = N.M.\kappa p.R \qquad (6.2)$$

where p = Gfh is the photon transfer efficiency of the drift chamber and the photomultiplier.

Since Q is proportional to the amplitude (V) of the charge pulses, statistical fluctuations in N,M,κ,p and R produce variations in V. Using the results derived by Shockley et al$^{(3)}$ for a cascade of events, the mean value of Q, $\bar{Q}$,and the fractional variance v(Q) of Q (i.e. $\frac{\mathrm{Var}(Q)}{\bar{Q}^2}$) can be written as

$$\bar{Q} = \bar{N}\,\bar{M}\,\bar{\kappa}\,\bar{p}\,\bar{R} \qquad (6.3)$$

and

$$v(Q) = \frac{\mathrm{Var}(Q)}{\bar{Q}^2} = v(N) + \frac{v(M)}{\bar{N}} + \frac{v(\kappa)}{\bar{N}\,\bar{M}} + \frac{v(p)}{\bar{N}\bar{M}\bar{\kappa}} + \frac{v(R)}{\bar{N}\,\bar{M}\,\bar{\kappa}\,\bar{p}} \qquad (6.4)$$

If the number of photons per scintillation pulse incident on the photocathode is large, the observed distribution of pulse amplitudes due to monoenergetic X-rays approximates to a Gaussian distribution and the energy (pulse height) resolution for such a distribution is related to v(Q) by

$$(\text{energy res.})^2 = 5.54\ v(Q) \qquad (6.5)$$

Equation (6.4) can therefore be used to estimate the energy resolution of the GSDC.

The fluctuation in the number of ion pairs (N) created by an ionising particle in a volume of gas has been analysed by Fano$^{(4)}$. For the case in which the energy dissipated is fixed (E_o), thus implying that the expected number of ion pairs is $\bar{N} = \frac{E_o}{W}$, W being the energy required to create an ion pair, Fano has shown that the fluctuations in N can be written as

$$v(N) = \frac{F}{\bar{N}} \tag{6.6}$$

where F is the Fano factor and is equal to 0.19 for argon$^{(5)}$. Curran et al$^{(6)}$ have investigated the fluctuation in the size of the electron avalanches around an anode wire of a cylindrical proportional counter and obtained an average value of 0.68 for the fractional variance of the multiplication process. Theoretical justification of Curran's results were made later by Byrne$^{(7)}$. Theoretical investigations$^{(8)}$ of the gas amplification process show that the fractional variance of fluctuations in the charge multiplication process is independent of M even for small M values. Curran's value can therefore be used to represent the fractional variance of the charge multiplication process in a GSDC even when the multiplication is less than 10. Substituting Fano's and Curran's values for fractional variances in equation (6.4), and using equation (6.5), the energy resolution (η) of a GSDC can be written as

$$\eta^2 = 5.54 \left[\frac{0.19}{\bar{N}} + \frac{0.68}{\bar{N}} + \frac{v(K)}{\overline{NM}} + \frac{v(p)}{\overline{NMK}} + \frac{v(R)}{\overline{NMKp}} \right] \tag{6.7}$$

Equation (6.7) shows that the theoretical limit (η_o) of the energy resolution, which can be achieved from this counter is given by the equation

$$\eta_o^2 = 5.54 \cdot \frac{0.19}{\bar{N}} \tag{6.8}$$

In the case of 5.9 keV X-rays, the mean number of primary ion pairs produced by a photon is approximately 200 in most gases and therefore η_o = 7.25% (apart from the contribution due to K of course). However, in real situations, the contribution from other terms will degrade the energy resolution of the counter, in fact introduction of charge amplification alone will degrade the resolution to 15.5%. In most cases the last term in equation (6.7) is negligibly small since R is generally large (10^6-10^7). Contributions due to the third and fourth terms mainly depend on the anode voltage which determines the number of photons being produced around the wire. As far as the high counting studies with GSDC's are concerned, the contributions from these two terms may also be appreciable due to the following reasons.

(1) Imperfect light collection:

The number of photons per scintillation pulse reaching the photocathode of the photomultiplier is affected by imperfect transmission of photons through wire planes (cathodes and mesh) and reflection losses at the counter walls.

(2) Limitations imposed on the anode voltage by space charge effects (at high rates).

(3) Reduction of the photon yield due to collisional quenching of argon and nitrogen excited states.

The lack of sensitivity of the photomultiplier to UV light will also affect the energy resolution of the counter.

6.3 PERFORMANCE OF THE GSDC AT MODERATE COUNTING RATES

Before investigating the counting ability of the counter, its operating conditions including the distance of the X-ray beam from the anode wire must be chosen so as to give a reasonable value for energy resolution. This is essential because the conditions under which the smallest value of the pulse width (i.e. optimum condition for counting purposes) can be obtained may not be suitable for measurements of the energy of incident photons.

In order to investigate the dependence of energy resolution of the counter on its operating parameters a collimated source of 5.9 keV X-rays, a fast amplifier (LeCroy 612 AM) and a pulse height analyser (NS 900) with its built-in charge sensitive amplifier were used.

The X-ray beam was allowed to pass through the counter normal to its cathode planes and the output pulses obtained from the photomultiplier, after being amplified by using fast amplifier and charge sensitive amplifier were recorded on the PHA.

6.3.1 Dependence of the Energy Resolution on the Distance of the X-ray Beam from the Anode Wire

The variation of the energy resolution of the counter with the distance of the X-ray beam from the anode wire was measured by moving the X-ray source perpendicular to the direction of the cathode wires, towards the potential wires in each half cell. As expected two peaks appeared on the PHA when the passage of the beam was very close to the anode wire and as the source was moved away from the wire one peak gradually disappeared leaving the main peak and the escape peak. The energy resolution of the counter was deduced from the position of the main peak and the FWHM of the pulse height distribution. In Fig (1) the result is plotted against the distance from the anode wire. A sharp rise in the resolution is apparent when the passage of the beam is close to the anode wire. This increase in the energy resolution is due to the delocalisation of the production of secondary light around the anode wire which shadows the photocathode for some of the secondary photons. However,

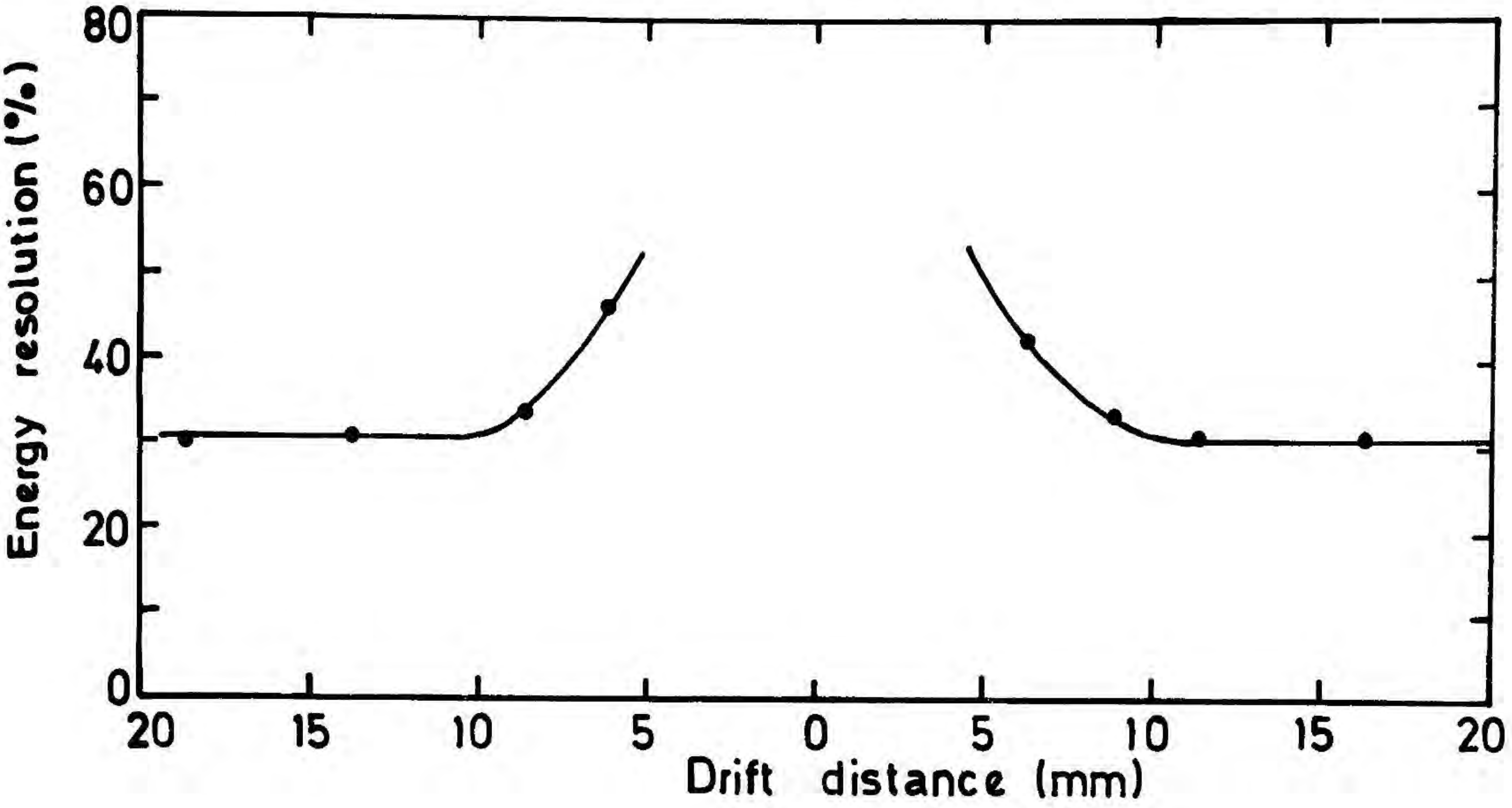

FIG. 1 Variation of energy resolution as a function of distance of the passage of x-ray beam from the anode wire.

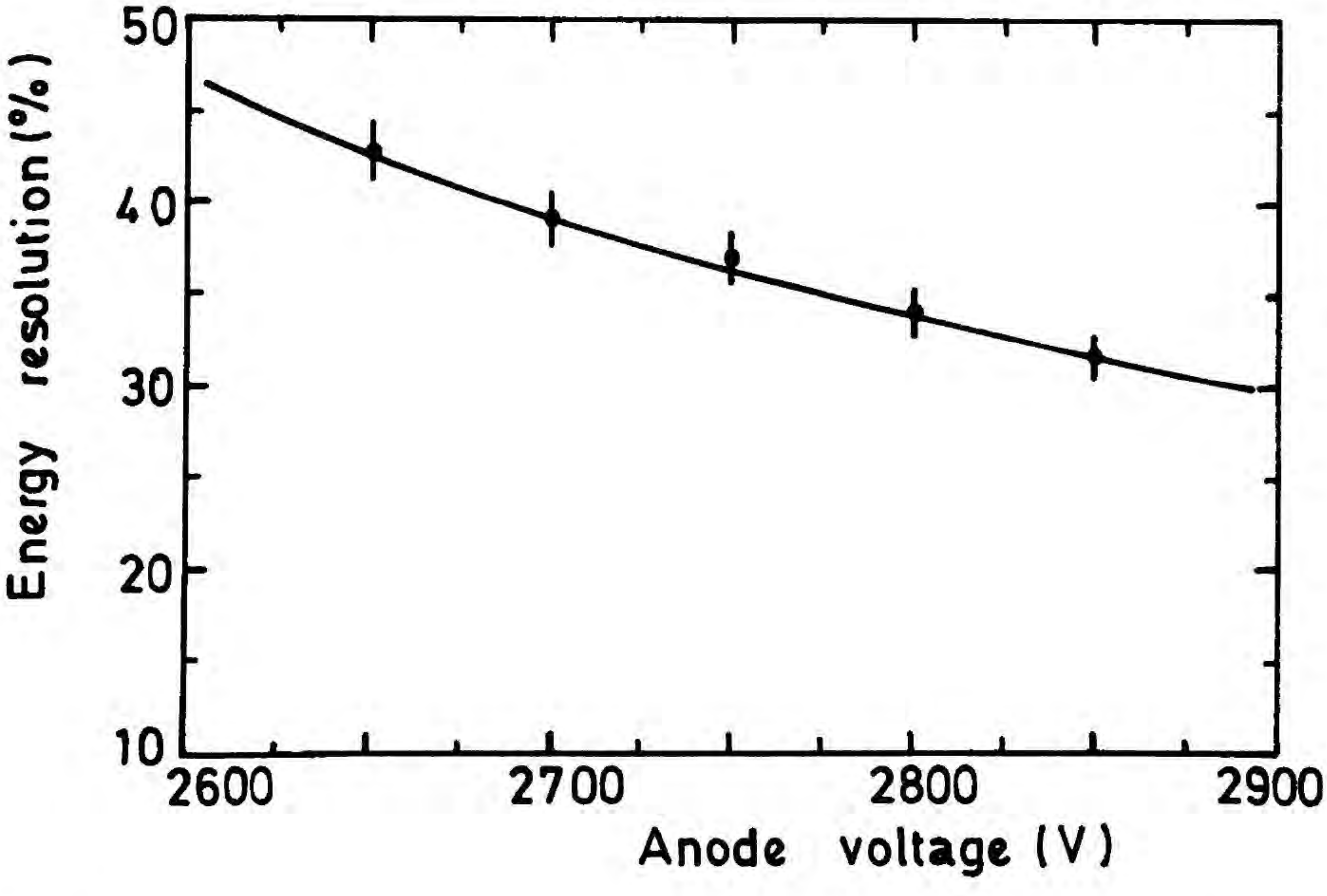

FIG. 2 Energy resolution of the counter for 5.9 keV x-rays as a function of anode voltage.

the resolution remained constant at 31% in most of the counter. It is clear from these results that a small gap must be allowed between the passage of the X-ray beam and the anode wire in order to retain the energy resolution of the counter at a suitable value. Unless otherwise mentioned this gap length was kept fixed at 9 mm in all the subsequent measurements.

6.3.2 Variation of the Energy Resolution with Anode Voltage

The energy resolution of a GSDC is obviously a function of the anode voltage since the production of secondary photons depends strongly on the latter. However, when employing this counter in applications involving high counting rates, the anode voltage must be kept at the smallest possible value to avoid space charge effects. Fig (2) shows the energy resolution of the counter as a function of anode voltage. The drift field and the photomultiplier voltage were kept fixed at 500 V/cm and 1500 V respectively. An improvement in energy resolution was observed with increase in the anode voltage of the chamber. This improvement is obviously due to the increase in the number of photons resulting from the electron collision processes.

Policarpo et al(9) have shown that for a given photomultiplier voltage (gain), the variation of energy resolution of a GSPC with the amplitude (charge) of the output pulse satisfies the equation

$$\eta^2 = A + \frac{B}{V} \qquad (6.9)$$

Where V is the pulse amplitude, A is a function of the fractional variance of primary and secondary ionisation processes and B is related to the fractional variance of the photomultiplier gain. Fig (3) shows their results which have been obtained using a GSPC and a 5.9 keV X-ray source.

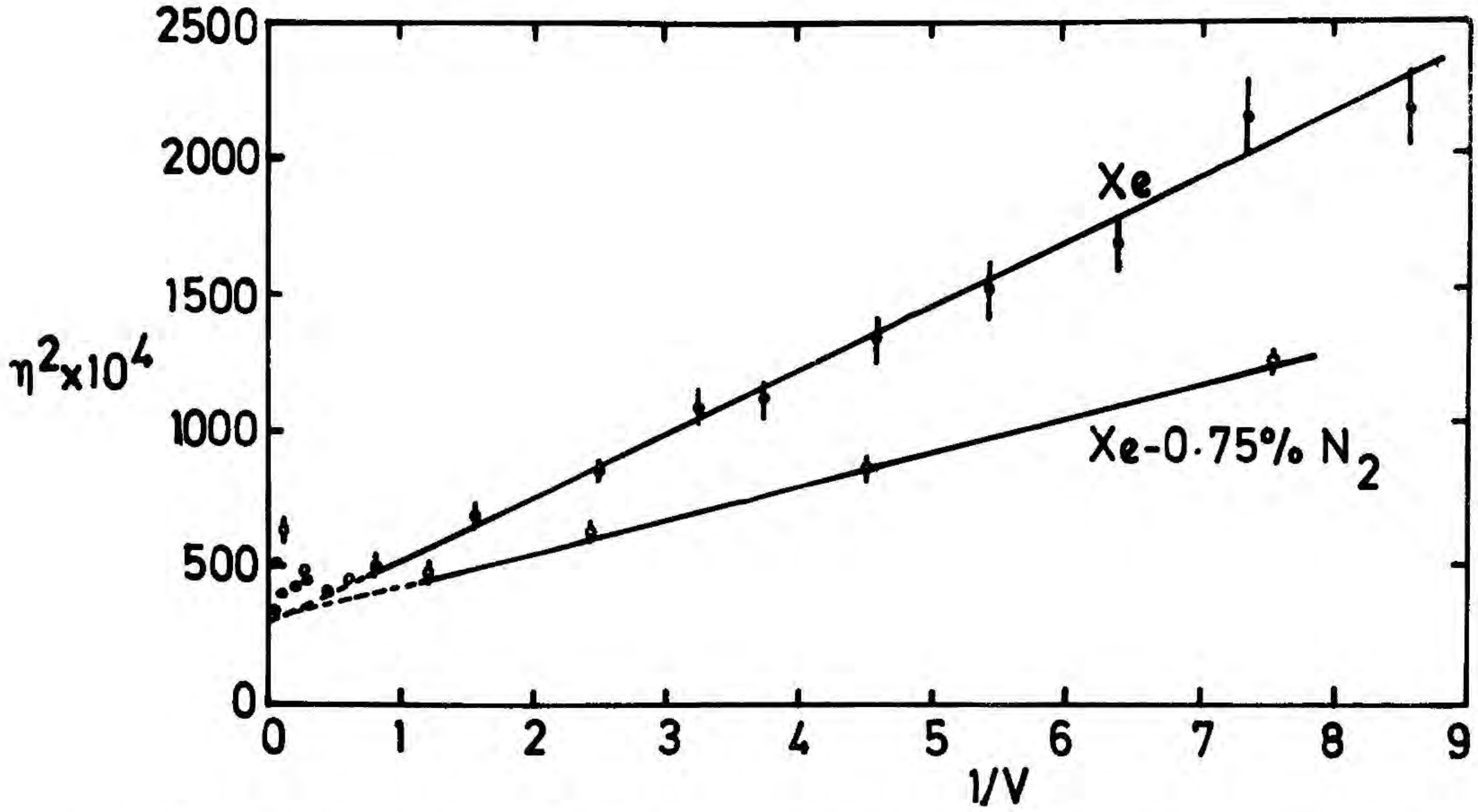

FIG.3 Variation of η^2 as a function of the inverse of the normalized light pulse amplitudes for Xe and for Xe-0.75% N_2, for 5.9 keV x-rays.

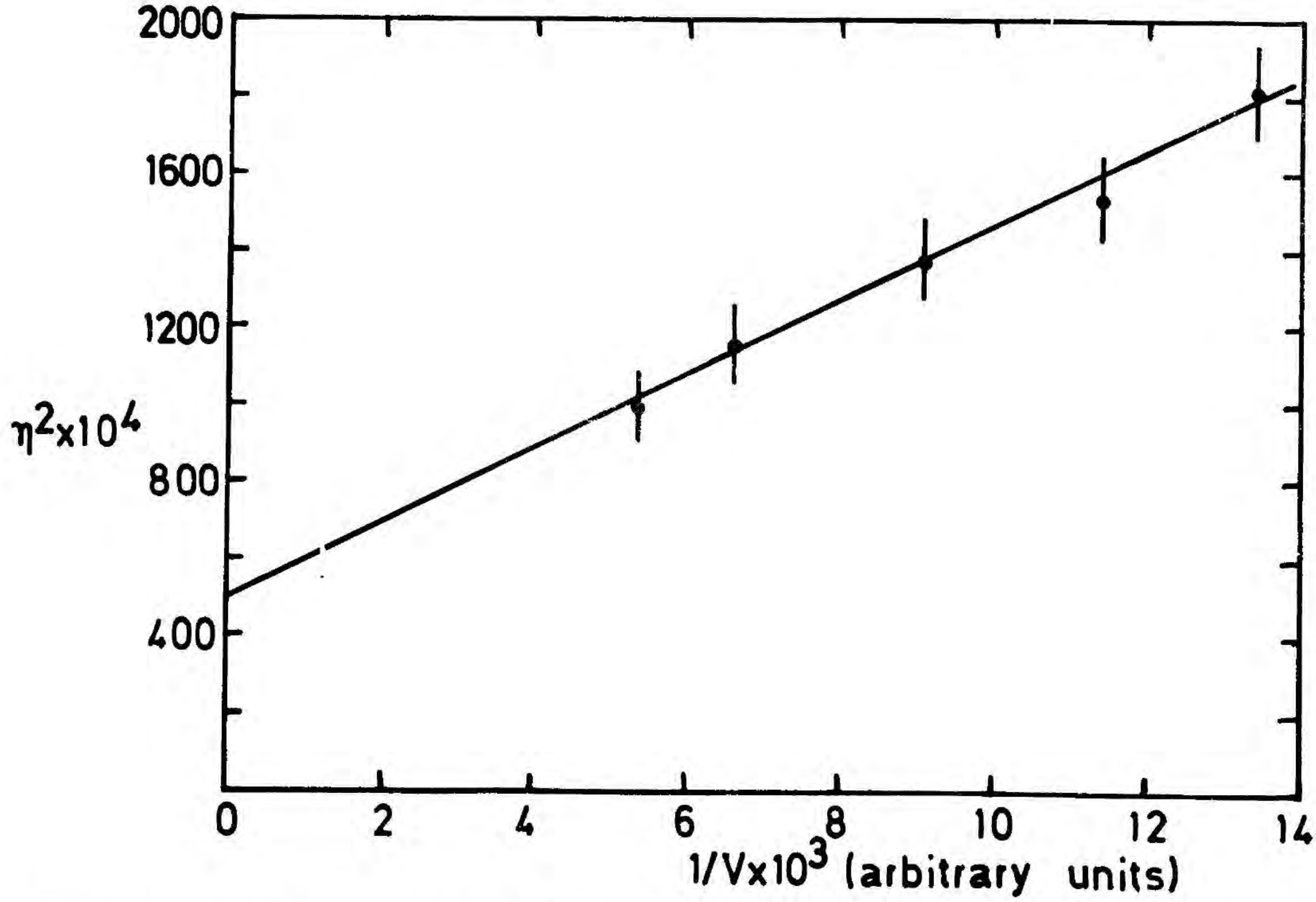

FIG. 4 Variation of η^2 (η-energy resolution) as a function of inverse amplitude for 5.9 keV x-rays.

The equation (6.9) is merely a simplified representation of equation (6.7) with

$$A = 5.4 \left\{ \frac{0.19}{\bar{N}} + \frac{0.68}{\bar{N}} \right\} \qquad (6.10)$$

and

$$B = 5.54 \frac{eR}{C} \left\{ Kpv(K) + pv(p) + V(R) \right\} \qquad (6.11)$$

where e is the electronic charge and C is the effective integrating capacitance of the charge sensitive amplifier.

Although K is dependent on the anode voltage, and hence on V, Policarpo's results, which imply that B is a constant, suggest that the first term in equation (6.11) is either negligibly small compared to other terms or is a constant similar to the terms in equation (6.10) under their operational conditions. Fig (4) shows the variation of η^2 with the inverse of the pulse amplitude obtained with the GSDC for 5.9 keV X-rays. The linear behvaiour of η^2 with $\frac{1}{V}$ confirms equation (6.9), and the best straight line fit through the experimental points shows that, in the limit $V \longrightarrow \infty$, thus eliminating the photomultiplier intrinsic resolution and the contributions due to imperfect light collection, the intrinsic resolution of GSDC for 5.9 keV X-rays is 22.4%. The value obtained by Policarpo et al with Xe - 0.75% N_2 was 17.7%. This value is higher than the value estimated using the first two terms in equation (6.7) and it may be that under the operating conditions in which the secondary light amplification is large, the secondary light production process also adds a fixed contribution to A instead of to B. Another factor which may have contributed to the measured intrinsic resolution is the electronic noise of the amplifiers used with the GSDC.

6.3.3 Variation of the Energy Resoltuion with Photomultiplier Voltage

The dependence of the energy resolution of the GSDC on the photomultiplier voltage was investigated using the same experimental arrangement discussed at the beginning of this section. The anode voltage and the drift voltage were kept constant and the energy resolution was measured as a function of PM voltage. The results are shown in Fig (5). The improvement in resolution obtained as the anode voltage is increased is due to two main factors.

(1) At low photomultiplier voltages, collection of photoelectrons at the first dynode is not efficient due to insufficient electric field across the photocathode and the first dynode. As a result considerable fluctuations in the number of photoelectrons reaching the first dynode can be expected. According to the manufacturers(10) data the voltage applied between the cathode and the first dynode should be at least 300 V (corresponding to a PM voltage of 1600 V) to ensure high quantum and collection efficiencies.

(2) Statistical fluctuations in the overall gain of the PM are reduced with increase in the PM voltage giving rise to a better resolution.

6.3.4 Variation of Energy Resolution with Drift Field

The energy resolution was measured as a function of drift field for fixed anode and photomultiplier voltages and the results are presented in Fig (6). The resolution was found to deteriorate with increase in the drift field. This can be explained as being due to a modification of the electric field inside the counter by the applied drift field. As the drift field increases circular equipotentials around the anode wire gradually become normal to the cathode planes (see Fig (7)). They

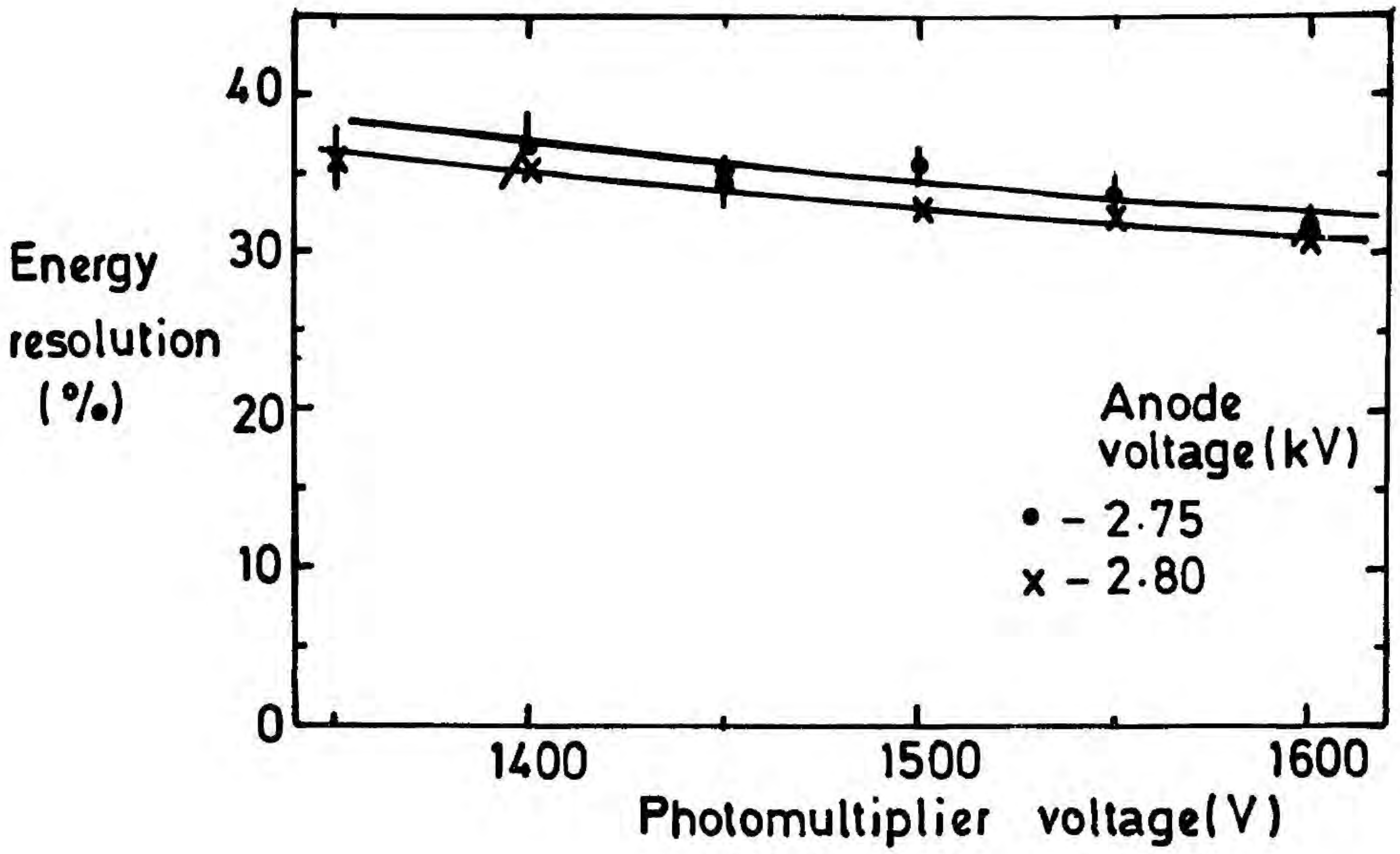

FIG. 5 Variation of energy resolution with photomultiplier voltage.

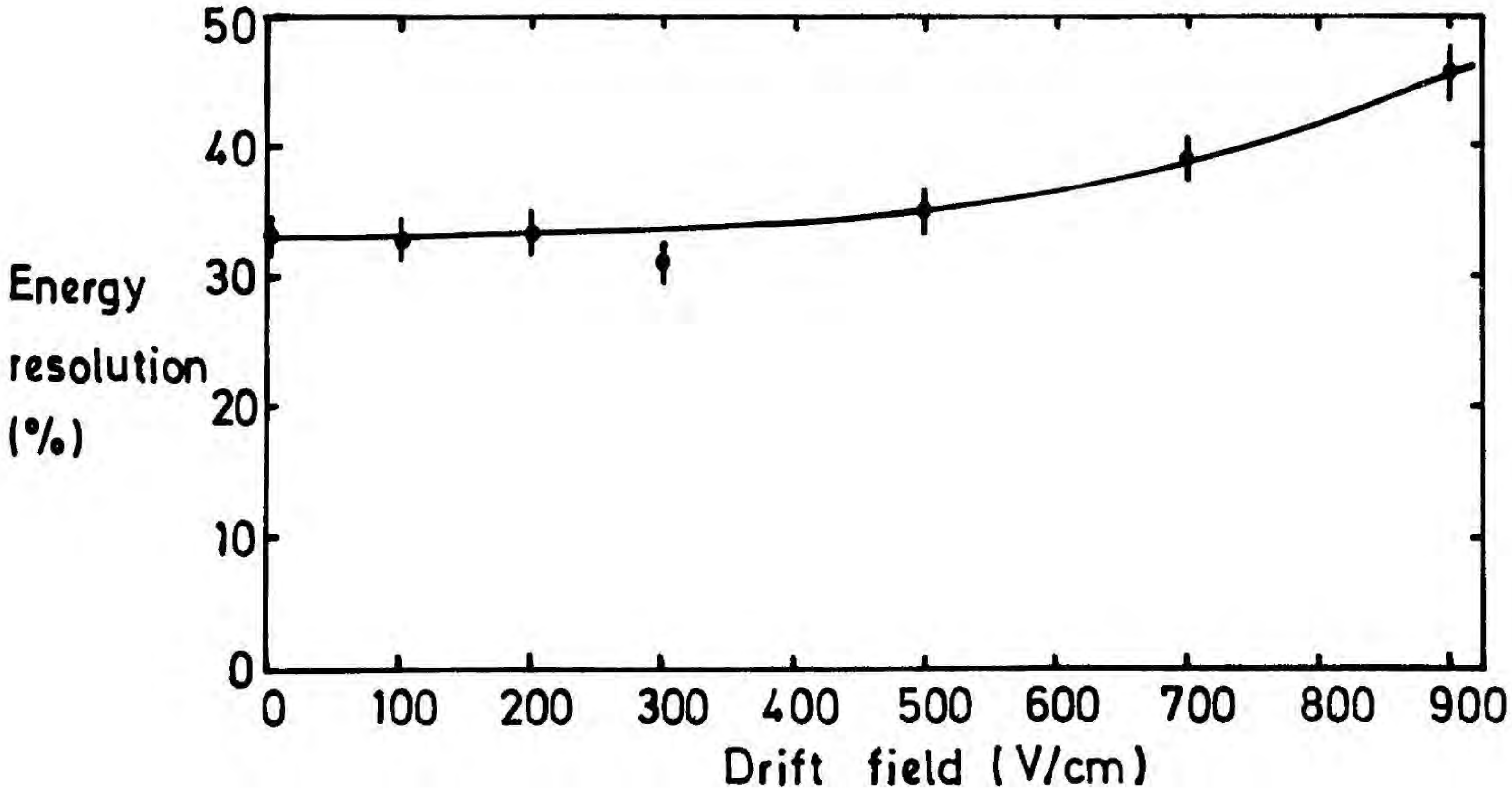

FIG. 6 Variation of energy resolution as a function of drift voltage.

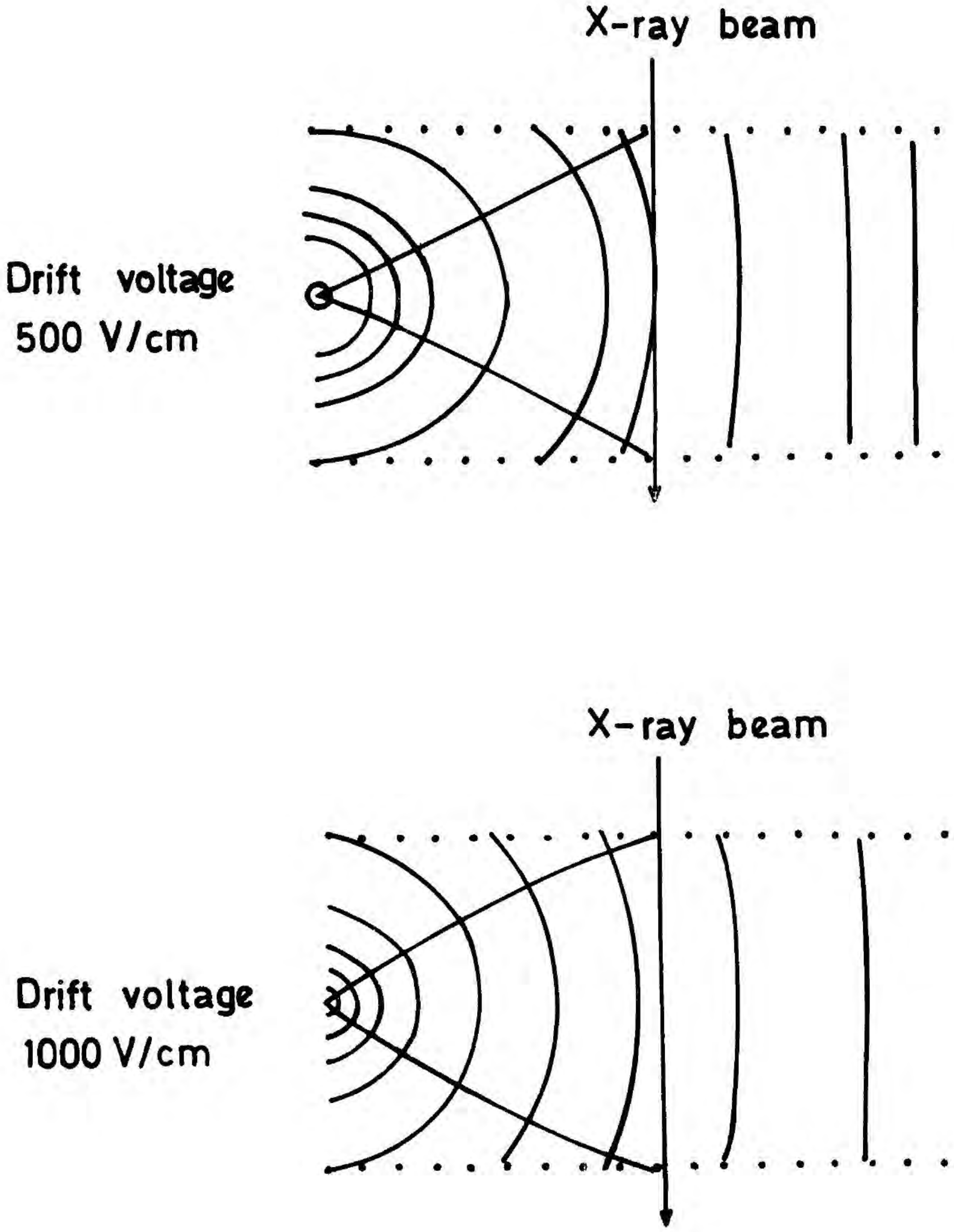

FIG. 7 Dependence of the angle subtended by incoming primary electron at the anode wire on the drift field.

thereby increase the angle subtended by the incoming primary electrons at the anode wire degrading the localisation of secondary light production. Increasing the drift voltage thus has the same effect as moving the X-ray beam towards the anode wire. Another phenomenon which affects the resolution of the counter at high drift fields is the production of spurious photons in the region between the cathode planes and screening electrodes. This occurs since high cathode voltages can produce very large electric fields in this gap.

6.4 DATA ACQUISITION AT HIGH COUNTING RATES

In general the data acquisition at high rates is limited by the bandwidth of the processing electronics. Apart from that,the measurements are further complicated due to the lack of a pulse height analyser which can analyse and record data at counting rates greater than 1 MHz which are anticipated from a GSDC. Modern pulse height analysers can cope with pulsing rates only up to few hundreds of kilo herts. This problem however, can be overcome by gating the PHA in such a way that it receives pulses at considerably lower rates.

6.4.1 Electronic Scheme for Pulse Height Measurements at High Rate

The experimental set-up including the gating circuitry is shown in Fig (8). Pulses from the photomultiplier were amplified by means of a fast amplifier with a built-in fan-out of two. One of the outputs was then fed into a linear gate. Pulses from the other output of the amplifier, after being discriminated and shaped to fast narrow NIM standard pulses, were used to open the linear gate for a certain duration sufficient to pass either the 10th, 100th or 1000th pulse as necessary. Selection of required pulses were done by means of decade scalers and a trigger was used to provide the gate opening pulse. The output of the linear gate,after being amplified, integrated and stretched using a

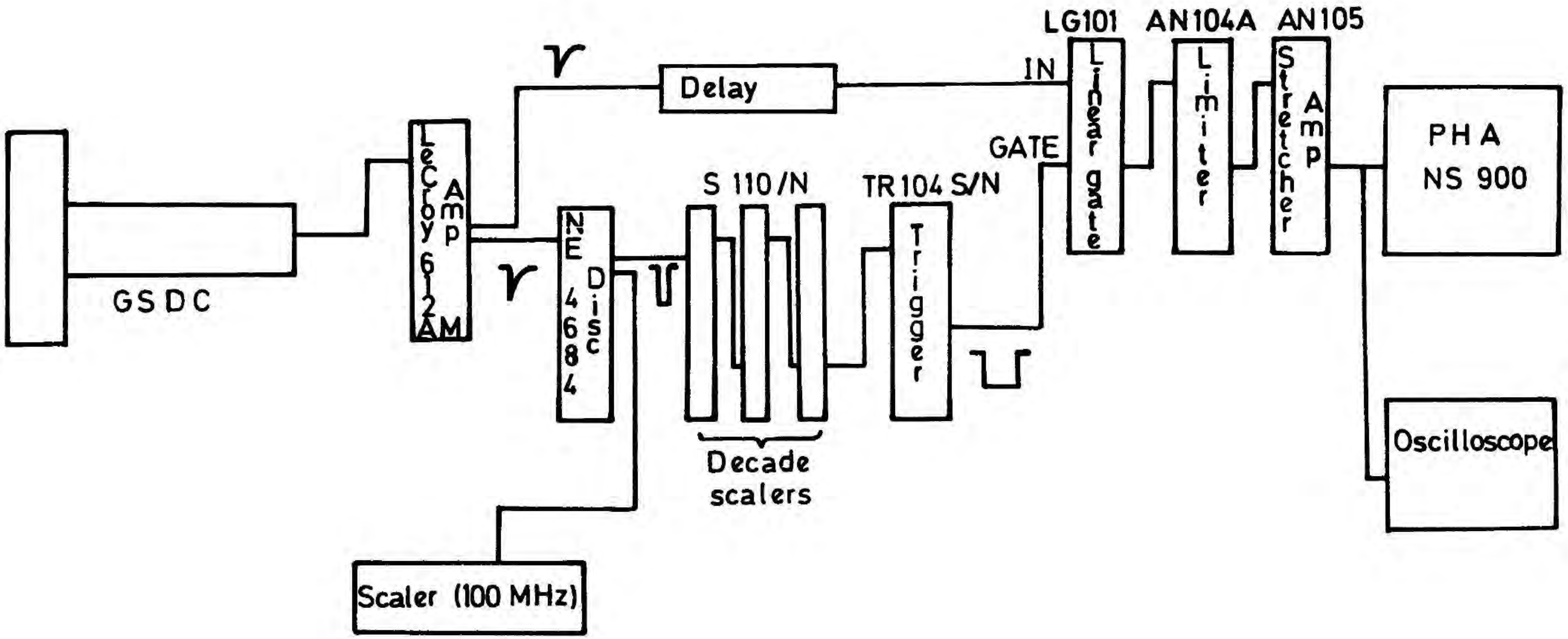

FIG. 8 Electronic scheme for pulse height measurements.

stretcher amplifier was fed into a pulse height analyser.

One of the most important requirements for all the modules in such a circuit is d c coupling, in order to eliminate base line shifts which would result in smaller pulses and smearing of the lower side of the pulse height spectrum at high counting rates. They must also have a bandwidth greater than 100 MHz, large enough not to degrade the information contained in the pulses. The preamplifier used in this circuit was a LeCroy NIM model 612AM photomultiplier amplifier. This unit, which is direct coupled, features a bandwidth of D C to 140 MHz, within 0.2% integral linearity and a maximum gain of 40. The rise time of the amplifier output in response to a step edge input is better than 3 nS. A fast discriminator (Nuclear Enterprises NE 4684) was employed to convert amplifier output signals to NIM standard signals. The pulse pair resolution and minimum threshold level of this discriminator were measured and found to be 9 nS and 25 mV respectively. The discriminator output provides three simultaneous fast outputs of variable width (6 nS → 50 nS) suitable to run fast scalers without limiting their counting ability. Decade scalers used to control the gating rate of the linear gate were EG & G S110/N, whose counting capability extends to 200 MHz. The linear gate which was an EG & G type LG 101 is a direct coupled device which can handle gating rates from D C to greater than 75 MHz and has a typical bandwidth of D C to 175 MHz.

In general when there is no signal at the input of the linear gate, the signal output level should remain at zero when switching the gate manually from the CLOSED state to the OPEN state and in the LG 101 this situation can be realised by making adjustments to the gate. However, once the gate is pulsed open, gating transients which occur during the opening and closing times of the gate, create unavoidable non-zero output pulses. The pulse height into 50 Ω termination of the gating transients of the linear gate which has been used in the present study was 20 mV. This value lies within the manufacturer's specified limit$^{(11)}$ of 30 mV. In the present study, since the pulses are being integrated after the gating, the above mentioned adjustments will not guarantee that the net charge per gating cylcle is zero because of these gating transients. However, the'zero net charge per gating cycle' condition was ensured by observing the integrated output from the stretcher amplifier with no signal applied to the linear gate and making adjustments on the latter for zero net integrated output. This ensures that the integrated charge during each gating cycle will be due entirely to the signal under investigation.

When connecting the linear gate output to a stretcher amplifier (AN 105), loading by the gate must also be considered since it presents an extremely high impedance$^{(11)}$ to the internal CR network of the stretcher amplifier when the gate is in closed state and relatively low impedance (500 Ω) when it is in open state. This small resistance shunts the integrating capacitance and causes fast decay of charge. This situation was avoided by buffering the LG 101 output with an AN 104A limiter module which presented a high impedance (100K Ω) to the stretcher amplifier input.

6.4.2 Effect of Gating on the Energy Resolution

In order to obtain an optimum value for the resolutions of the counter,the width of the gate must be large enough to pass the entire scintillation pulse with its long tail. However, the width of the gating pulse cannot be increased arbitrarily since it limits the repetition rate of the processing electronics. On the other hand, a gating pulse width smaller than the input pulse itself will allow only a portion of the pulse to pass through and consequently will degrade the observed energy resolution.

The effect of gating on the energy resolution was studied using a 5.9 keV X-ray source. The electronic circuitry described in the preceding section was used with a NS 900 pulse height analyser. Drift field, anode and PM voltages were kept at 500 V/cm, 2800 V and 1600 V respectively. The delay of the input signal to the linear gate was adjusted so that the leading edge of the input signal arrived at the linear gate 2 nS after the arrival of the leading edge of the gating pulse, 2 nS being the time required to fully open the gate. This adjustment was done by means of a fast oscilloscope. Keeping this adjustment fixed the peak of the pulse height distribution on the PHA was measured as a function of the width of the gating pulse. Fig (9) shows the variation of the pulse height and the energy resolution as a function of gate width. Variations in both parameters (pulse amplitude and energy resolution) were less pronounced for gate widths greater than 50 nS while a rapid reduction in the pulse height and deterioration in the energy resolution were apparent for gate widths less than 50 nS. The width of the input pulses used in this measurement was approximately 65 nS and the integrating time constant set on the input pulses was 0.9 μsec. Unless mentioned otherwise all the energy resolution measurements which will be presented in following sections were obtained with the processing electronics shown in Fig (8) and a gating pulse width of 50 nS. Use of a gating pulse of this width degraded the resolution, which can be obtained with gate fully opened, by ∿ 10%.

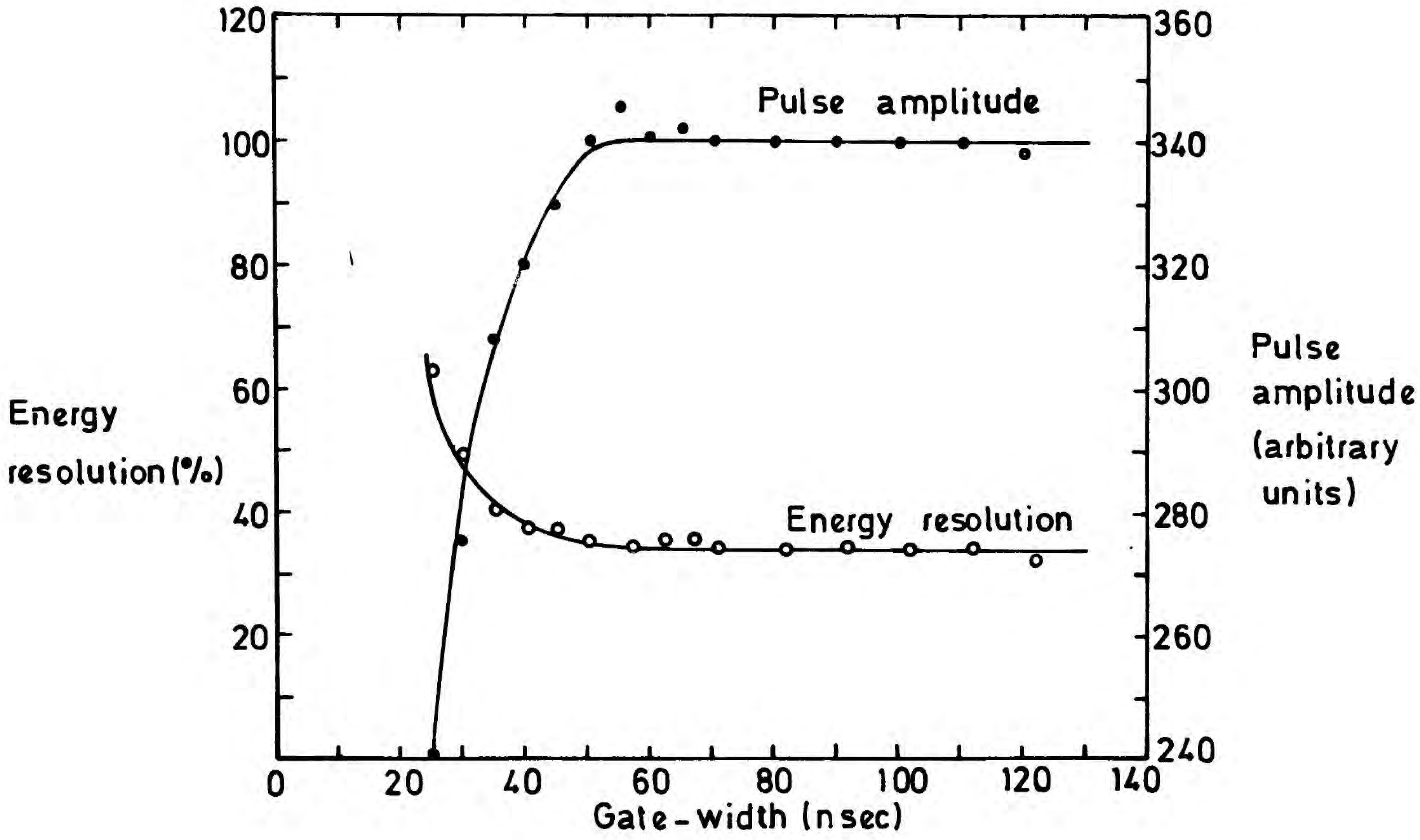

FIG.9 Variation of pulse amplitude and energy resolution with width of the gate.

6.5 PERFORMANCE OF THE COUNTER AT MODERATE PULSING RATES

6.5.1 Counting Characteristics

The performance of the GSDC at moderate X-ray intensities was investigated using a collimated 8 mCi, Fe^{55} 5.9 keV radioactive source. For counting purposes a Borer type 613, 100 MHz fast scaler was used with the fast amplifier and discriminator described in the previous section. The counting rate was measured as a function of the anode voltage for different X-ray intensities and the results are shown in Fig (10). X-ray beams of different intensities were obtained by varying the aperture of the collimator. The discrimination level was kept at 25 mV and the drift field used in the measurements was 500 V/cm. The set of curves thus obtained reveal a number of features of the counter regarding its counting capability. Firstly the plateaus of the curves imply that the counter records all the X-ray photons which have been absorbed in the active volume of the counter. Secondly the curves show that as far as counting is concerned the counter does not saturate up to a rate of at least 3 x 10^5 counts per second. Results also show that the counter was not affected by rate effects (space charge) up to the rate achieved with the radioactive source. This is indicated by the fact that the plateaus of all the three curves start at the same anode voltage. If there had been considerable space charge around the anode wire the charge would have shifted the plateaus to higher anode voltages as the rate was increased. Also shown in Fig (10) is the variation of the amplitude of the preamplifier output with the anode voltage. It indicates that an amplitude of at least 125 mV is necessary to make sure that all the pulses will be counted by the discriminator-scaler combination.

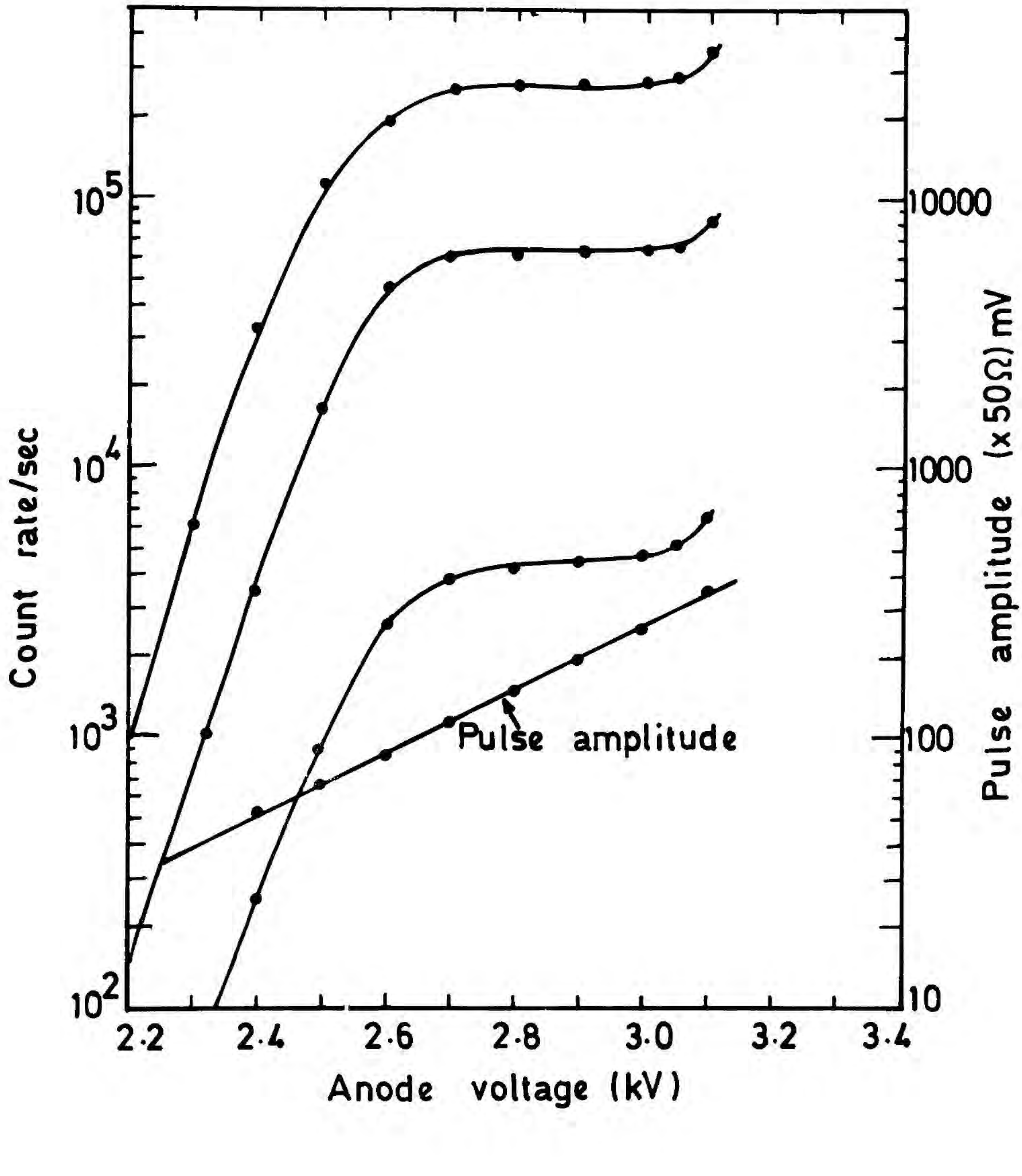

FIG. 10 Counting plateaus for different X-ray intensities, and variation of the pulse amplitude with anode voltage.

6.5.2 Variation of Pulse Height and Energy Resolution with Count Rate

As discussed in chapters one and three the formation of space charge around the anode wire causes a reduction in the local electric field which subsequently results in a smaller charge gain around the wire, (see Fig (3) of chapter one). Furthermore, the space charge effect degrades the proportionality of the pulse height to the amount of energy being deposited by a photon in the gas. This fact has been demonstrated with proportional chamber pulses whose energy resolution as a function of count rate is shown in Fig (11). Similarly, in a GSDC if the charge amplification is large enough to produce a dense space charge cloud around the anode wire, similar effects can be expected since the secondary light production is mainly governed by the space charge around the wire. In order to investigate these effects the peak of the pulse height spectrum and its width (FWHM) were measured as a function of counting rate. The variation of pulse height and energy resolution with the counting rate are shown in Figs (12) and (13). In contrast to the results obtained with conventional proportional counters (see Fig (3) of chapter one) the pulse height remained constant up to a rate of 3×10^5 per sec. The variation of the energy resolution with counting rate is also small. Slight deterioration of resolution at rates close to 3×10^5 per sec.was due to the poor collimation which resulted when increasing the intensity of the X-ray beam.

6.6 PERFORMANCE OF THE COUNTER AT HIGH RATES

6.6.1 The X-ray Source

It is apparent from previous sections that the collimation of the radiation beam is essential in order to obtain satisfactory performances from a DSDC. Since the collimated radioactive X-ray sources were unable

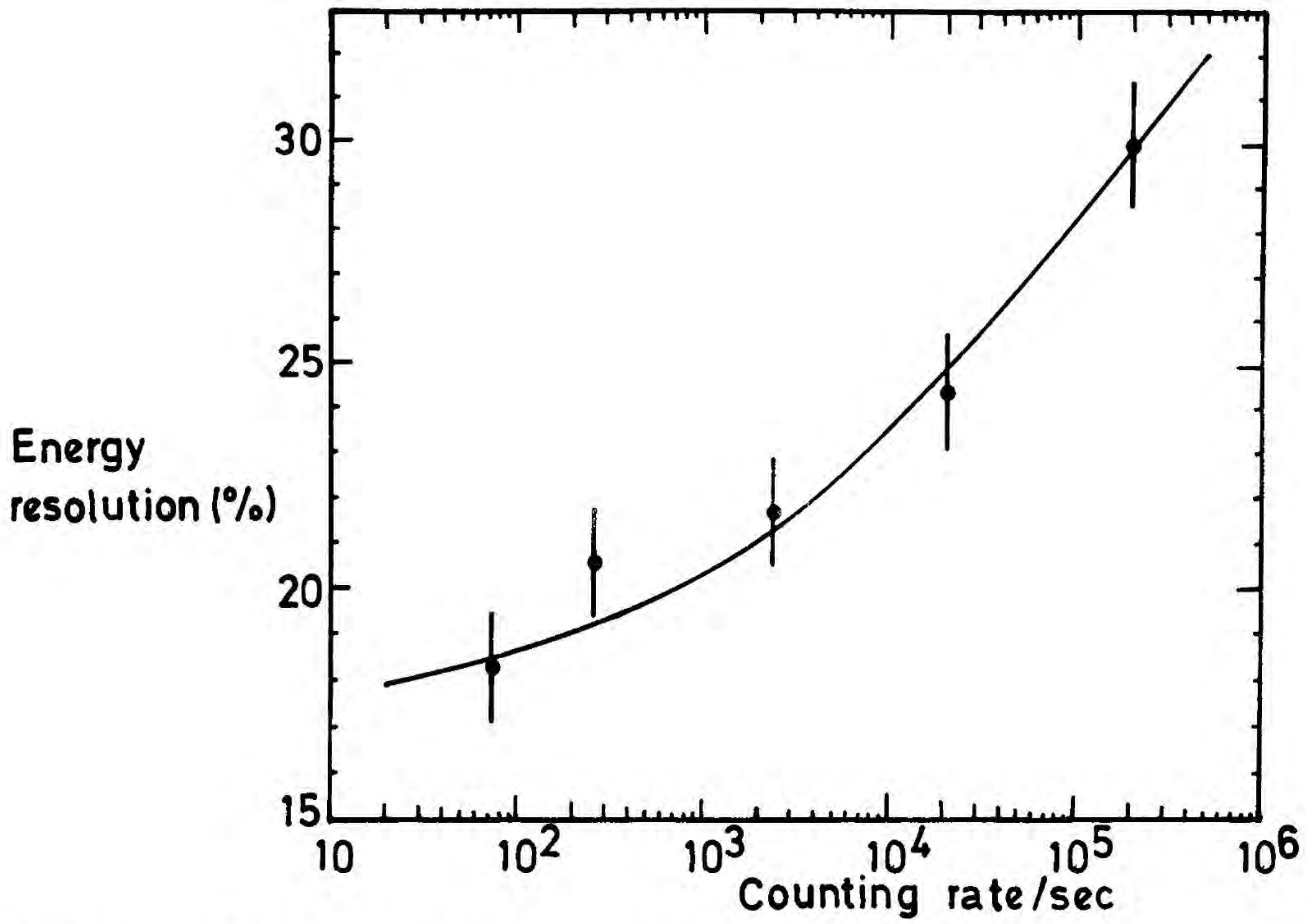

FIG. 11 Variation of energy resolution of a proportional counter as a function of counting rate for 5.9 keV x-rays.

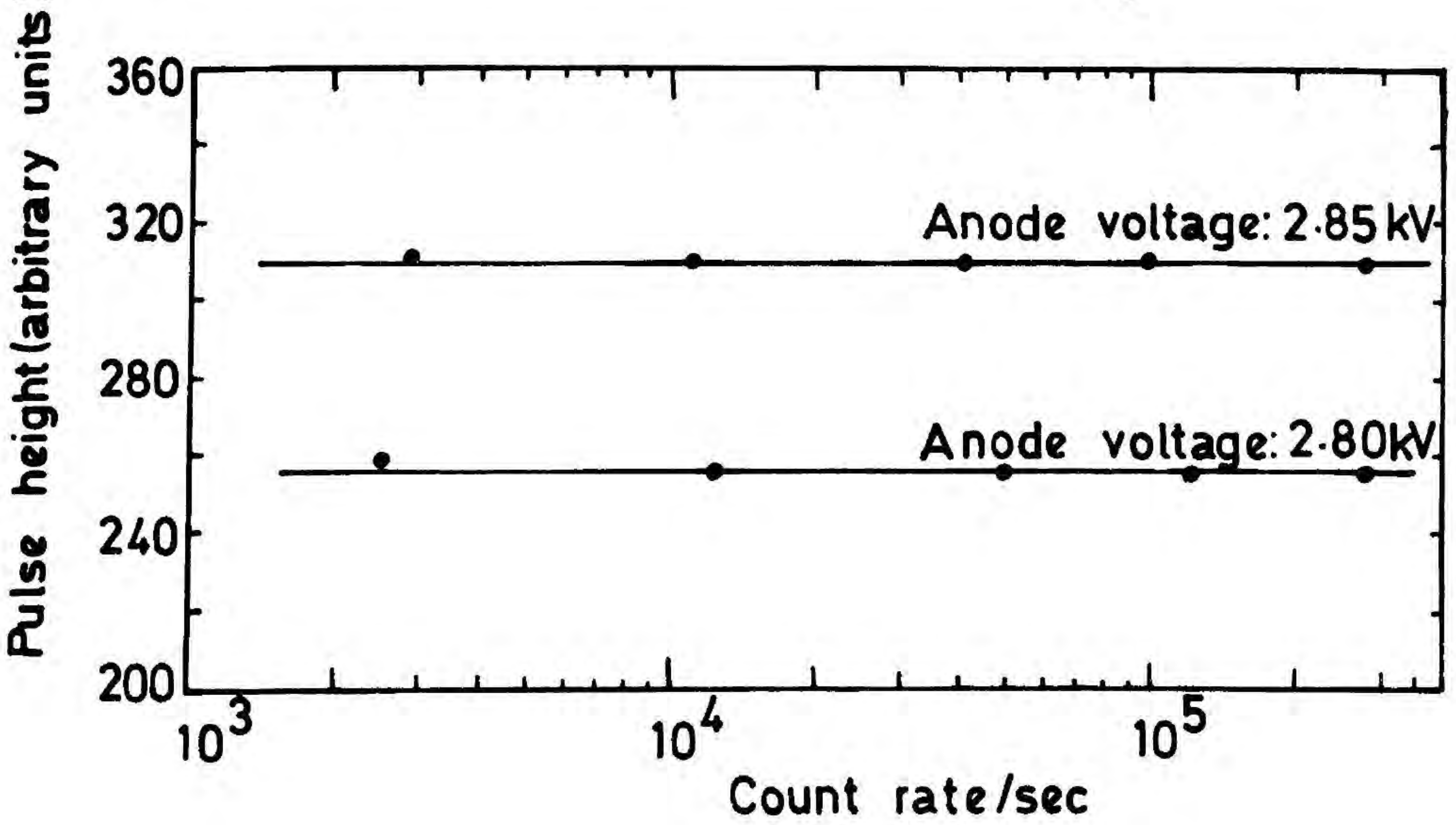

FIG.12 Variation of pulse height as a function of counting rate.

to provide high intensity beams, an X-ray machine with a fixed target was used in the following tests. A one kilo watt X-ray tube with a cobalt target was used to generate X-rays. Some of the important lines in the X-ray emission spectrum from cobalt are shown in Fig (14). In general the spectrum consists of two sets of intense characteristic lines, K_α and K_β, and a continuous spectrum caused by electron bremsstrahlung and some faint satellite lines. In order to separate K_α lines from K_β lines, an iron filter was inserted in the beam path, which absorbed most of the K_β emission. In addition to the large reduction of K_β, the filter reduced the portion of the continuous spectrum close to and above the Fe K absorption edge (see Fig (14)). Further refining of the spectrum was not attempted in order to save the intensity of the beam. In fact use of a combined silicon monochromator and Fe filter which gave rise to a much refined K_α line reduced the intensity of the beam to a level which was insufficient for this study(13).

6.6.2 Experimental Set-up

Fig (15) shows the experimental arrangement of the counter system placed in the X-ray beam line. An iron filter which was selected from a set of built-in filters, was placed at the exit of the X-ray beam. The beam was collimated by means of a collimator (1 mm diam. and 15 mm thick) one end of which was fitted to the filter and the other end to a light tight box which carried the counter system. The position of the counter was adjusted so that the X-ray beam passed 9 mm above the anode wire. The output from the photomultiplier was fed into a LeCroy 612AM amplifier and one of its outputs was connected to a fast scaler (Borer 100 MHz) via a discriminator (NE 4684) and the other output of the amplifier was connected to the processing electronics described in section 6.4.1, to measure the energy resolution of the counter.

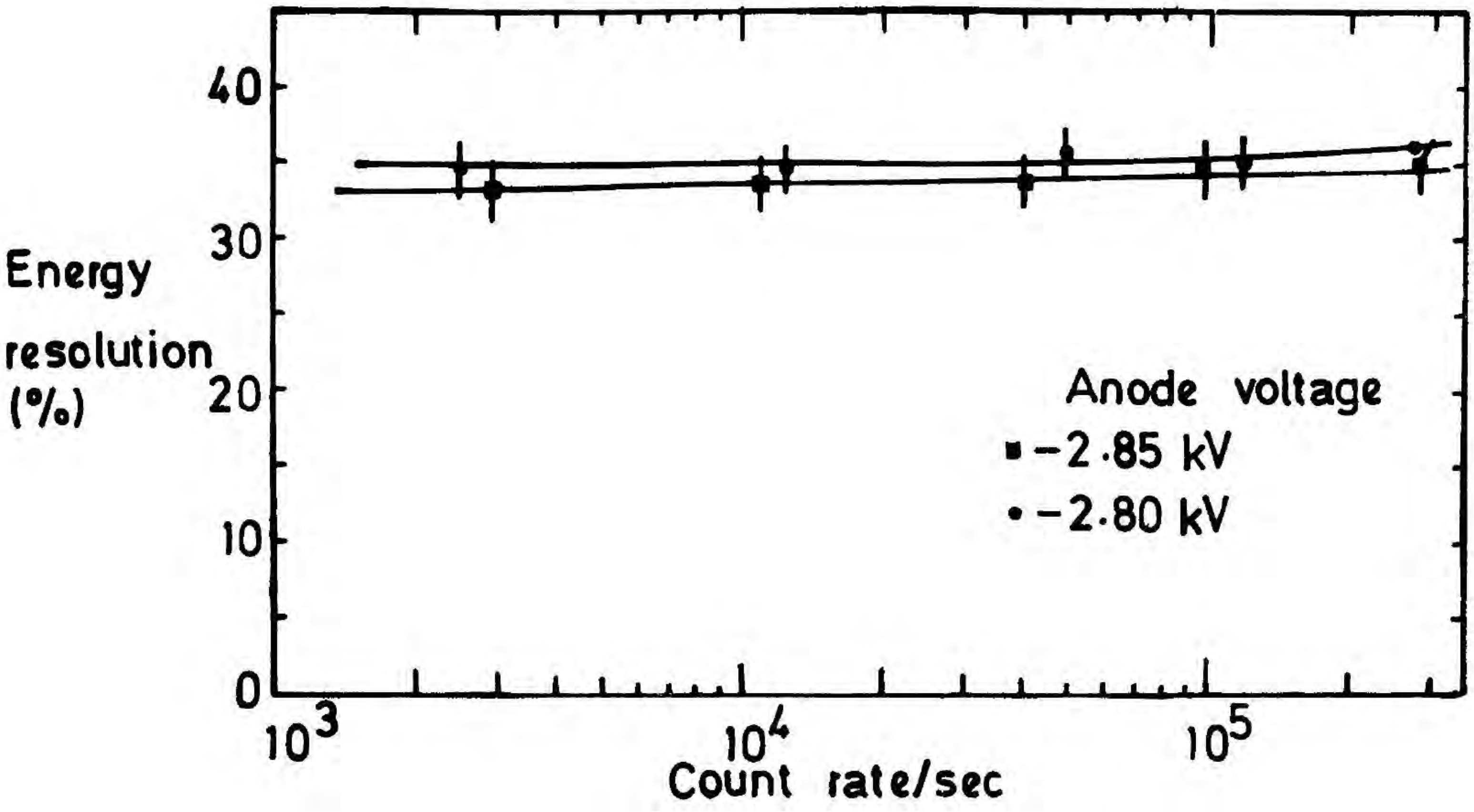

FIG.13 Variation of energy resolution as a function of counting rate.

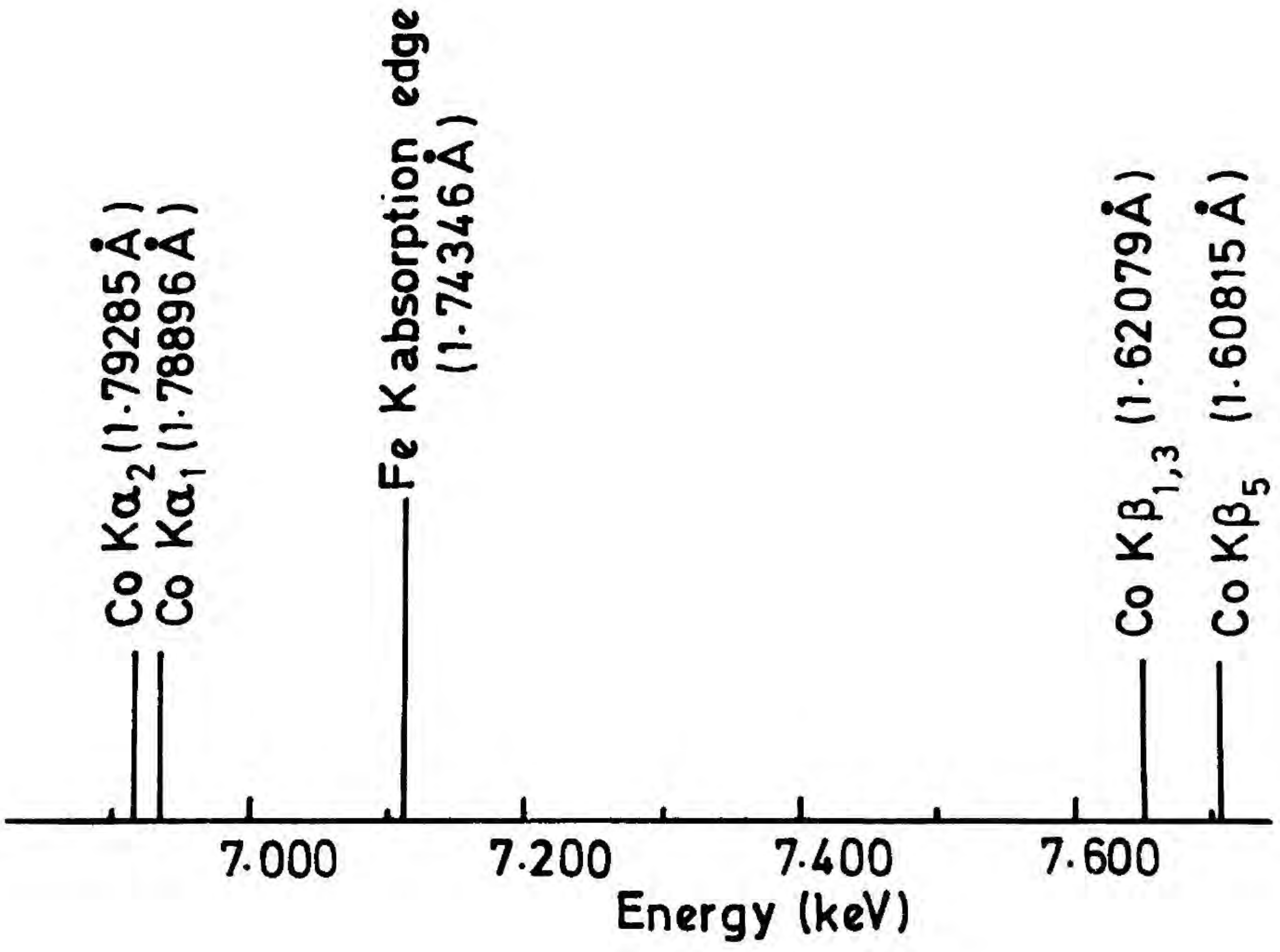

FIG.14 Some important emission lines from cobalt target (K absorption edge of iron filter is also shown).

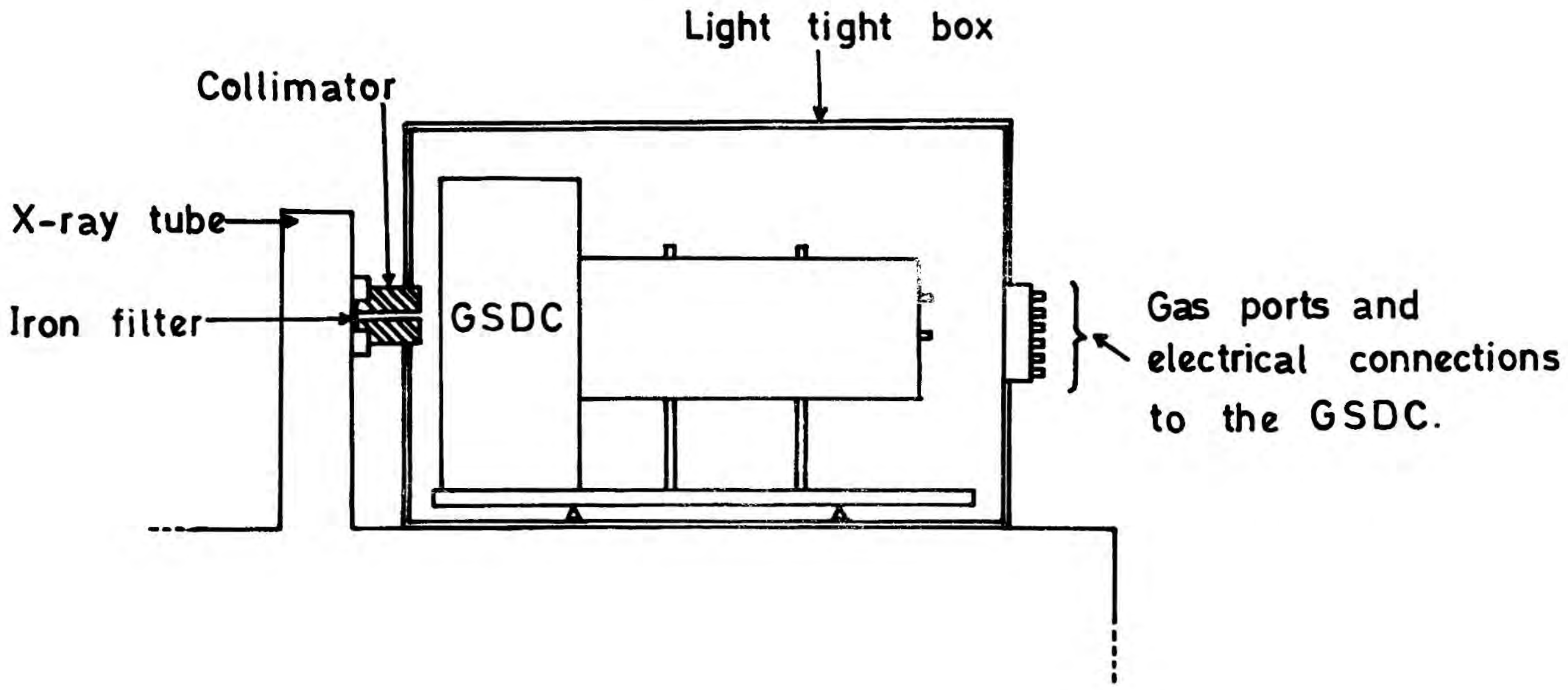

FIG.15 Experimental setup used to test the GSDC using an X-ray machine.

6.7 RESULTS

6.7.1 Counting Characteristics at High Rate

In order to investigate the counting characteristics of the system at high rate, the threshold level and the output-pulse-width of the discriminator were set at 25 mV and 6 nS and the counting rate was measured as a function of anode voltage for different intensities of the X-ray beam. The pulse height spectrum for the X-rays was constantly monitored on the PHA to ensure that the counts recorded were due to genuine pulses (without appreciable background). Fig (16) shows the counting rate as a function of the anode voltage. For rates less than 3×10^6 per sec. the behaviour of the curves was similar to those obtained for moderate counting rates (see Fig (10)). However, for X-ray intensities which correspond to counting rates greater than 3×10^6 per sec., the rate was found to decrease with increasing anode voltage. As seen in Fig (16) this effect was more pronounced at higher counting rates. This decrease can be explained as being due to the variation of the resolving time of the GSDC-discriminator combination with the anode voltage. The resolving time can be defined as the time between the leading edges (at full width half maximum) of the most closely-spaced scintillation pulse pair for which the GSDC-discriminator combination produces two distinct output pulses. Since the pulse pair resolution of the scaler used in this measurement was small ($<$ 5 nS) compared to that of the discriminator, resolution of the scaler did not affect the resolving time of the counting system (i.e. the GSDC-discriminator combination).

The resolving time of the counter for typical scintillation pulses is shown in Fig (17). The pulses shown in this figure have been traced from oscilloscope photographs. Pulse pair resolution of the discriminator

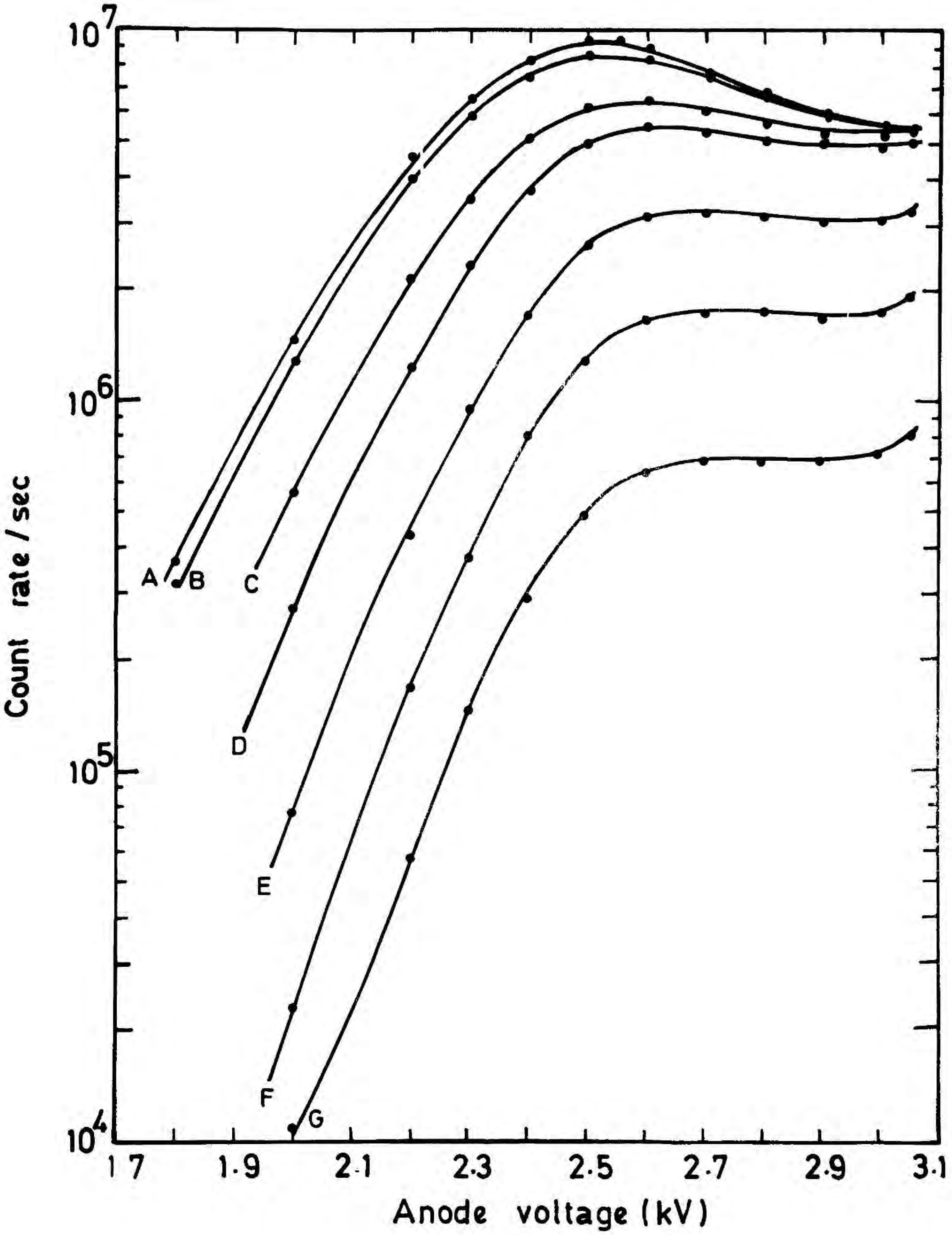

FIG. 16 Counting plateaus for different X-ray intensities. ($E_\gamma = 6{\cdot}9$ keV)

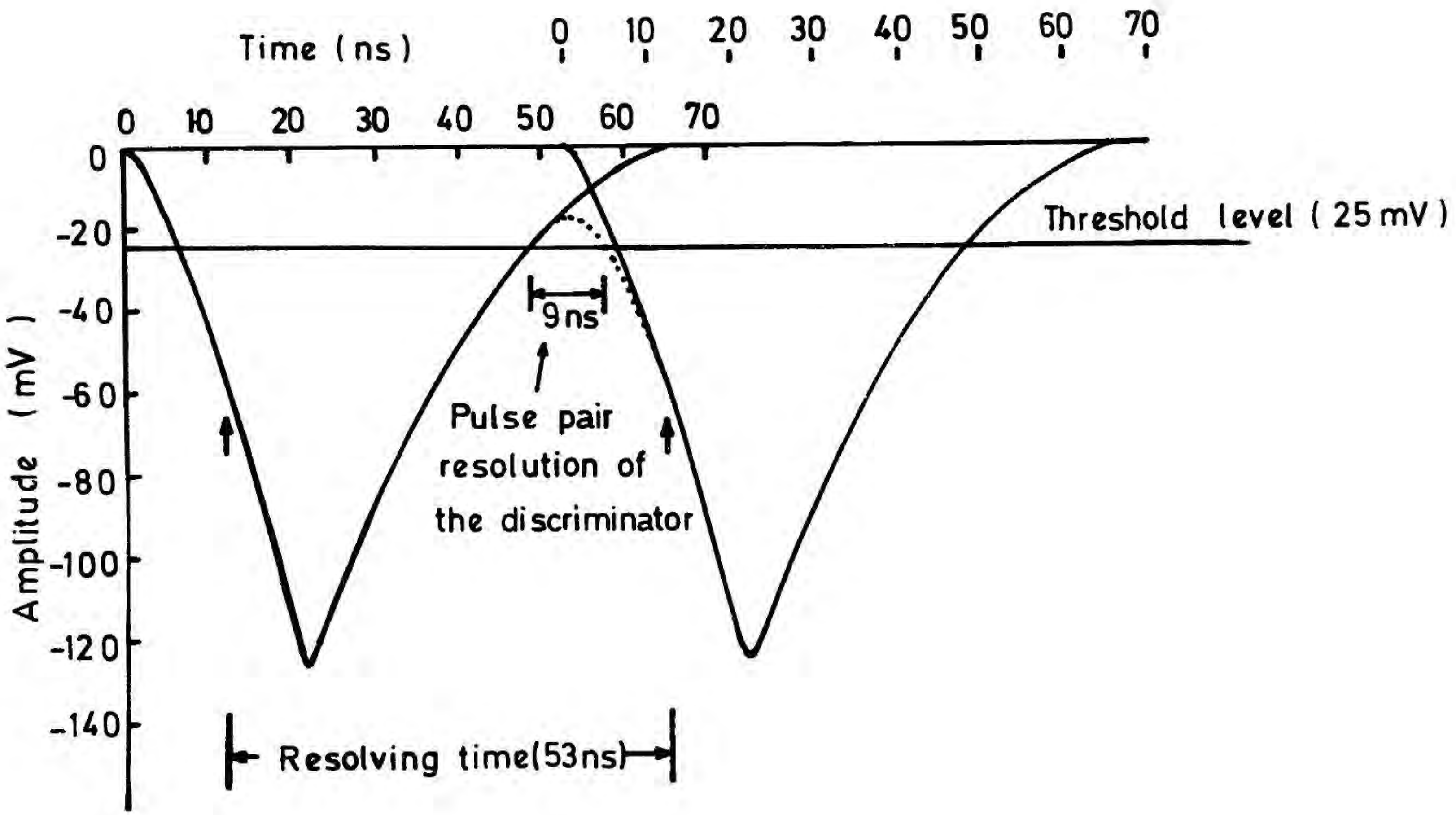

FIG.17 Resolving time of the GSDC-discriminator combination for typical scintillation pulses.

has also been considered when determining the resolving time of the counter. It is clear from Fig (17) that since the GSDC pulses are approximately triangular in shape, the discrimination level is one of the factors which determines the resolving time. In fact high discrimination levels reduce the resolving time of the counter and vice-versa. Alternatively for a fixed threshold level on the discriminator, pulses with smaller amplitudes give rise to smaller resolving times thus improving the counting capability of the counter. Increase in the anode voltage (and hence pulse amplitude) of a GSDC therefore has the effect of degrading the resolving time of the counter. At extremely high event rates, the observed counting rate therefore decreases with increase in the anode voltage. In order to investigate this fact the measurements corresponding to curve A in Fig (16) were repeated for different discriminator threshold and the results are presented in Fig (18). It clearly shows that the loss in counting rate with anode voltage can be regained by increasing the threshold level of the discriminator. It further proves that the decrease in observed counting rate is merely due to the deterioration of resolving time of the counter.

6.7.2 Counting Statistics

It is apparent from the results presented in the preceding section that the GSDC-discriminator combination counts only those pulses which are separated by a time interval greater than the resolving time, ρ, of the counter. The observed counting rate (n_{obs}) is therefore less than the true event rate (N).

The occurrence of scintillation events are random in nature and the frequency of occurrence of any particular number of events is expected to follow some probability distribution law or frequency distribution. The most appropriate frequency distribution which fits the sequence of

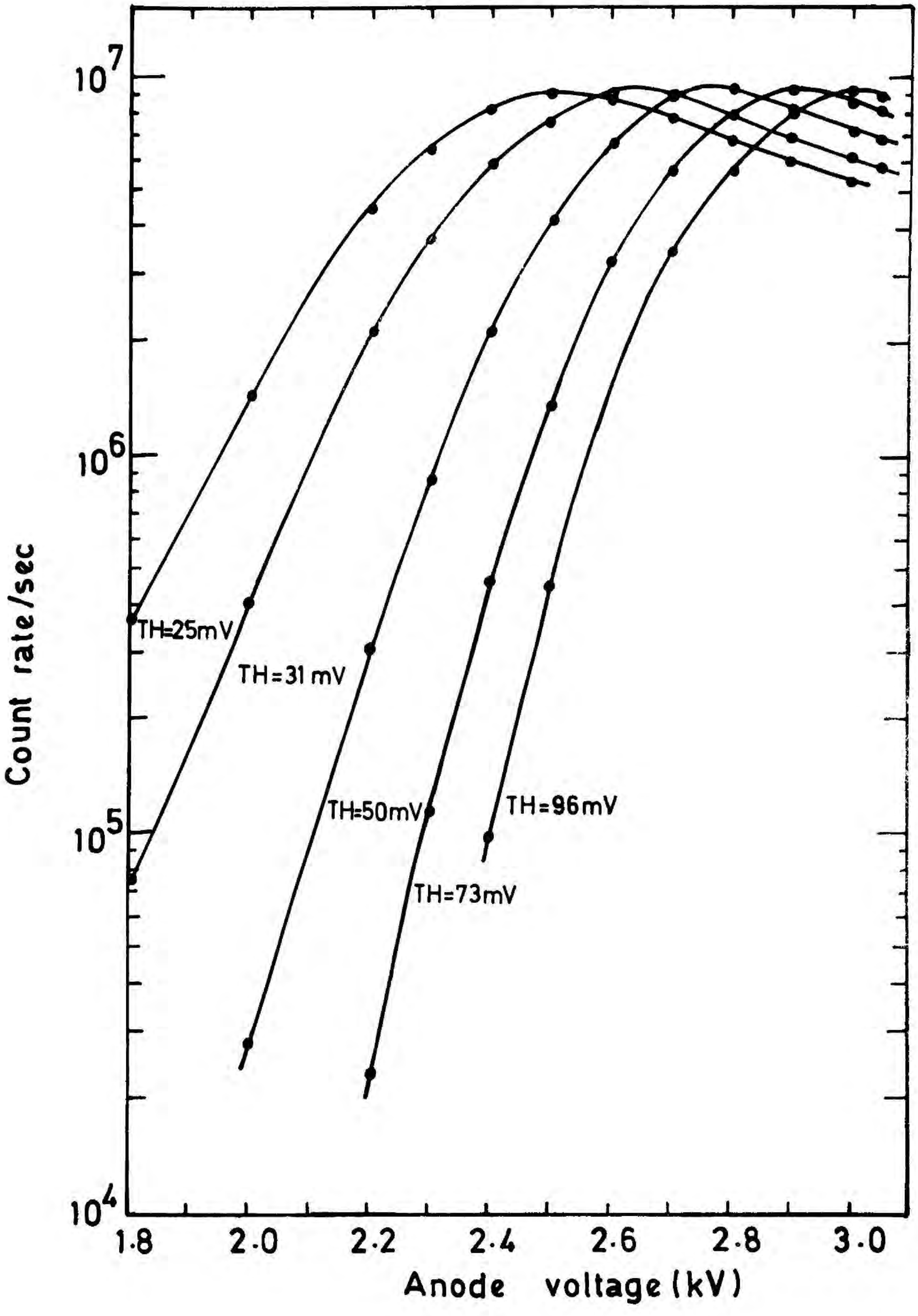

FIG.18 Variation of the counting capability of the GSDC discriminator combination with the threshold level (TH) of the discriminator.

such random events is the Poisson distribution which in its usual form

$$P_x = \frac{m^x}{x!} e^{-m} \tag{6.12}$$

gives the probability (P_x) of observing x events when the average for a large number of observation is m events. This distribution can be used to derive an interval distribution which describes the distribution in size of the time intervals between successive events in any random process in which the mean event rate has a constant value of 'a' per unit time.

According to expression (6.12) the probability that there will be no events in a time interval t ; during which there should be 'at' events on the average is

$$P_o = e^{-at} \tag{6.13}$$

The probability that there will be an event in the time interval dt is adt. The combined probability that there will be no events during the time interval t, but one event between time t and t + dt is

$$dP_t = a\, e^{-at} dt \tag{6.14}$$

and it gives the probability that the duration of a particular interval will be between t and t + dt. Equation (6.14) indicates that the smaller intervals have a higher probability than large time intervals between events and this obviously is an undesirable feature which limits the counting capability of a counting system at some rate depending on its resolving time. In other words those pulses which occur within a time interval equal to ρ, the resolving time of the counter merely increase the signal occupation time of the discriminator thus reducing the observed counting rate. Assuming a = N, the true event rate averaged over a large duration of time for which the n_{obs} is the observed counting rate, the number of intervals greater than ρ can be written as

$$n_{obs} = N \int_{\rho}^{\infty} N e^{-Nt} dt \qquad (6.15)$$

i.e. $$n_{obs} = N e^{-N\rho} \qquad (6.16)$$

If ρ is known, the observed counting rates can be corrected using equation (6.16) to obtain the true event rates. As the true event rate is increased, differentiation of equation (6.16) with respect to N shows that, when $N\rho = 1$ the observed counting rate n_{obs} passes through a maximum given by

$$n_{max} = \frac{N}{2.72} = \frac{1}{2.72\rho} \qquad (6.17)$$

It can be seen from equation (6.17) that the maximum counting rate which can be obtained with random events is less than that which can be achieved with equally spaced events by the factor of 2.72. Furthermore equation (6.17) shows that n_{max} varies inversely with the resolving time of the counter. As the true event rate approaches infinity the observed rate, n_{obs} approaches zero resulting in complete paralysis of the system.

6.7.3 Correction of the Observed Counting Rates

For any counting system which counts random events, it is essential that the observed counting rate satisfies the equation (6.16) for all true event rates. Provided that no saturation occurs and above equation is satisfied, the true event rate can easily be evaluated if ρ is known for the particular situation. The relationship between the true event rate and the observed counting rate was investigated using the same counting electronics described in section (6.6.2). The true event rate was assumed to be proportional to the anode current of the photomultiplier and it was further assumed that the anode current due to primary scintillation events was negligible compared to that of the secondary events. The former assumption has been justified in chapter five for pulsed anode currents. Suppose the photomultiplier current i is related to the true event rate by the relation

$$N = Bi$$

where B is the constant of proportionality

Then using equation (6.16)

$$n_{obs} = Bi\ e^{-Bi\rho}$$

$$\text{or } \ell n\ (n_{obs/i}) - \ell n\ B = -Bi\rho$$

The photomultiplier current was measured as a function of n_{obs} for different intensities of the X-ray beam (event rate) and $\ell n(n_{obs/i})$ was plotted as a function of i. The photomultiplier voltage and the drift field employed for this measurement were 2750 V and 500 V/cm respectively. Fig (19) shows the results for two anode voltages 2600 and 2750 V. Linear behaviour of the curves indicates that n_{obs} does satisfy equation (6.16) at least up to the rate (n_{obs}) 8.9×10^6 counts per sec. for an anode voltage of 2600 V and up to 6.9×10^6 counts per second for an anode voltage of 2750 V. According to Fig (19) the resolving times (ρ) of the counter system for these two anode voltages are 43 and 52 nS respectively. Results presented in Fig (19) further

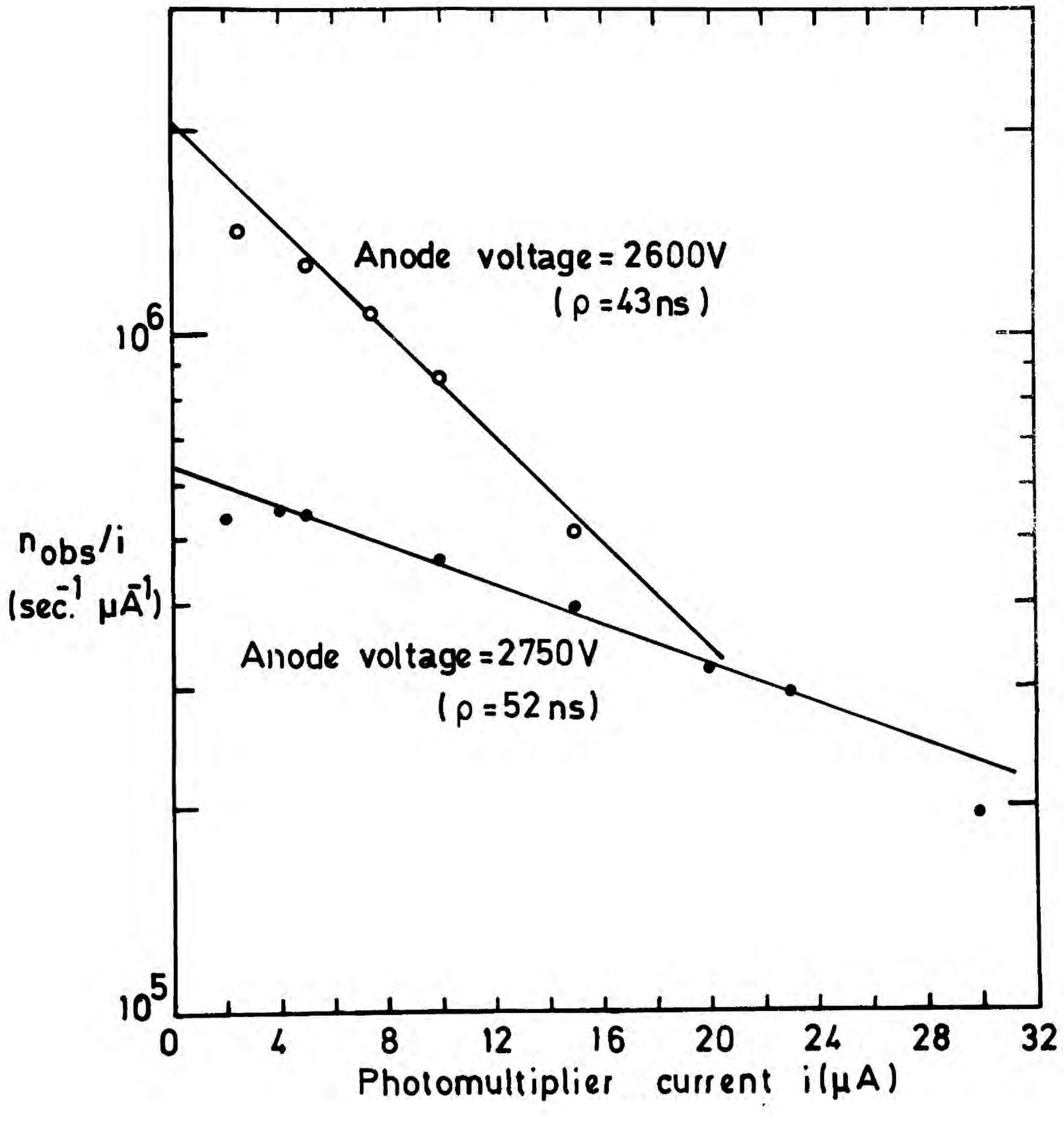

FIG.19 Variation of n_{obs}/i with photomultiplier anode current(i).

show that the resolving time of the system for a particular anode voltage is a constant. This is expected since the shape and the amplitude of individual scintillation pulses do not vary with the counting rate.

Before the corrections can be made it is necessary to consider the variation of the resolving time of the counter system with anode voltage. As mentioned in section (6.7.1) the resolving time ρ increases with the anode voltage and therefore the corrections for the observed counting rates in Fig (16) must be done individually by using appropriate ρ values. The ρ values for different anode voltages can, however, be calculated by using equation (6.16) and the two ρ values obtained from Fig (19), in fact these two values can be used to evaluate N for curves such as A and B in Fig (16). For example curve B in Fig (16) gives N as 1.825×10^7 counts/sec. The N value can now be used together with n_{obs} values in curve B for different anode voltages to calculate ρ as a function of anode voltage. Fig (20) shows the calculated ρ values as a function of anode voltage for the counter system. It must be mentioned that this particular set of results is applicable only when the photomultiplier voltage and the drift field are 1750 and 500 V/cm respectively.

6.7.4 Peak Shift and Energy Resolution at High Rate

Variation of the pulse amplitude (peak shift) and the energy resolution with counting rate were also investigated using 6.9 keV X-rays. Three decade scalers were used in the circuit (see Fig (8)) to reduce the pulsing rate in order to perform the pulse height analysis on the PHA. The position of the Co K_α peak and its half width were measured for different intensities of the X-ray beam. The X-ray peak position as a function of counting rate (n_{obs}) for three different

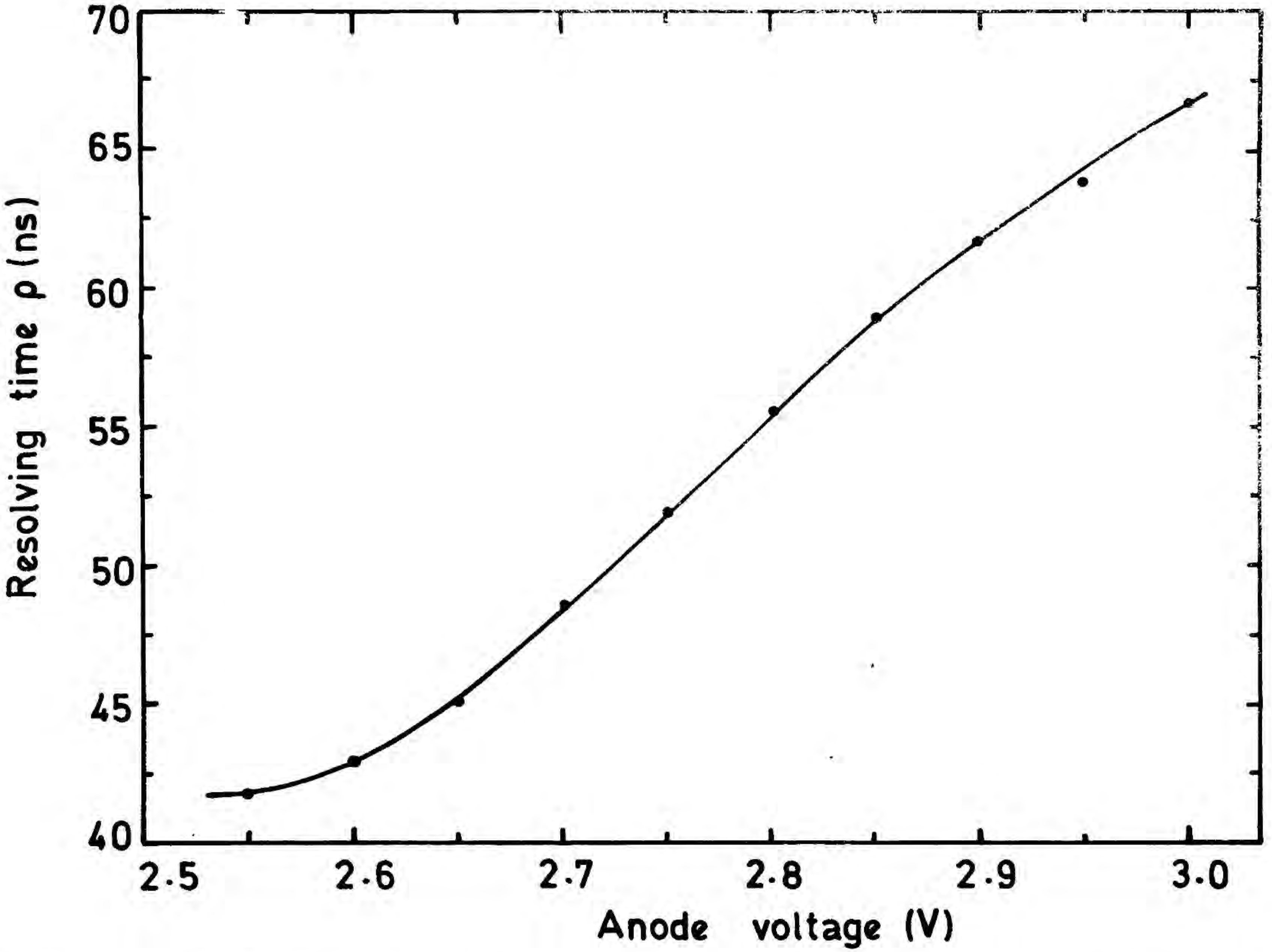

FIG. 20 Calculated resolving time ρ as a function of anode voltage.

anode voltages is shown in Fig (21). The change in the position of the peak with counting rate was found to be negligible up to a rate close to 6×10^6 counts/sec. However, a small peak shift towards the lower channels was observed with counting rate when the anode voltage was at 2800 V and this can be attributed to space charge effects. On the other hand a very small shift towards the higher channels was also observed with anode voltages, 2700 and 2750 V. This increase may be due to the overlapping of pulses at high counting rates and thereby shifting the lower side of the spectrum to the higher side.

Pulse height spectra obtained with 6.9 keV cobalt X-rays at different counting rates for an anode voltage of 2750 V are shown in Fig (22). The argon escape peak is also visible in all spectra. The energy resolution of the counter (calculated using these spectra) as a function of counting rate (n_{obs}) is shown in Fig (23). As expected an improvement in the resolution was observed for higher anode voltages. An improvement in resolution was also apparent with increasing counting rate for an anode voltage of 2800 V. However, the reason for this improvement is hard to explain. It is apparent that the energy resolution obtained at high rate with the Co K_α line is not as good as the values obtained at low rate with the Fe^{55} source. This is mainly due to the pile-up effects at high rate and poor monochromatisation of the X-ray beam.

As shown in Fig (22) the number of pulses with amplitudes larger than those corresponding to the main peak was also found to increase with the counting rate, distorting the pulse height spectrum at the high amplitude end. Formation of these large pulses at high rates is due to the pile-up of scintillation pulses which occur within a short duration (i.e. within the resolving time, ρ). This effect was

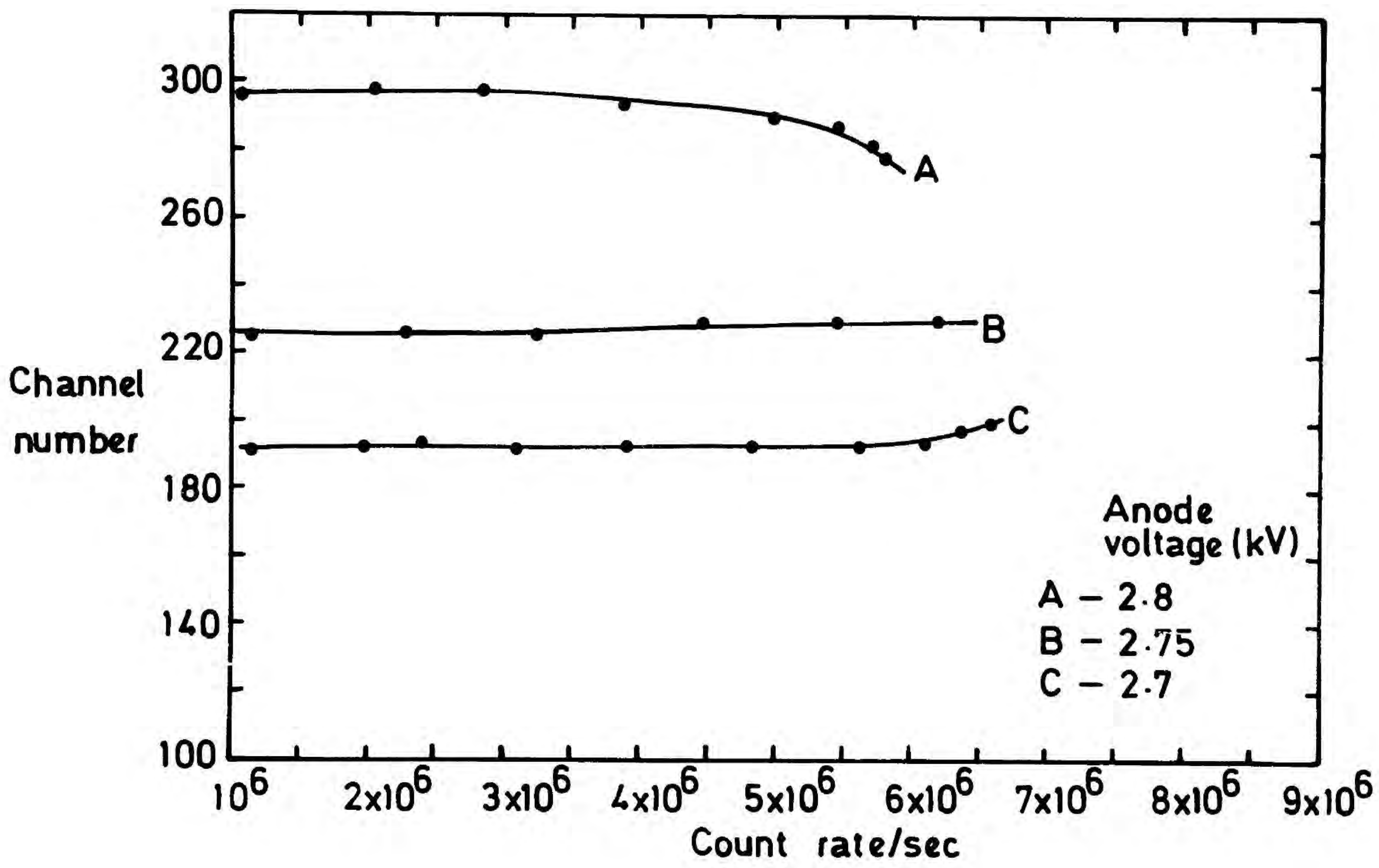

FIG. 21 Position of the cobalt X-ray peak vs counting rate.

FIG. 22 Pulse height spectra of cobalt K_{α} line for different counting rates.

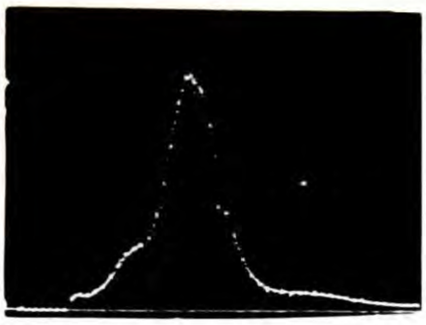

Count rate: 2·283 x 10^6/sec

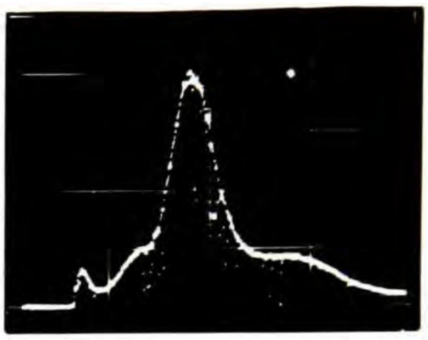

Count rate: 5·499 x 10^6/sec

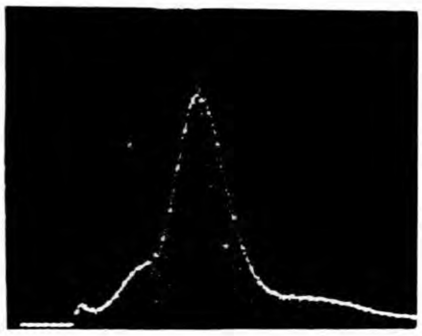

Count rate: 3·349 x 10^6/sec

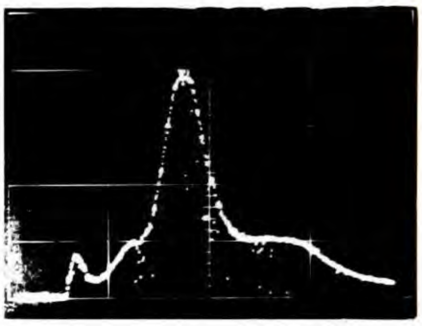

Count rate: 5·930 x 10^6/sec

Count rate: 4·480 x 10^6/sec

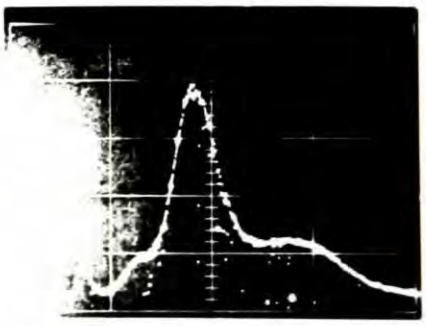

Count rate: 6·194 x 10^6/sec

FIG 22

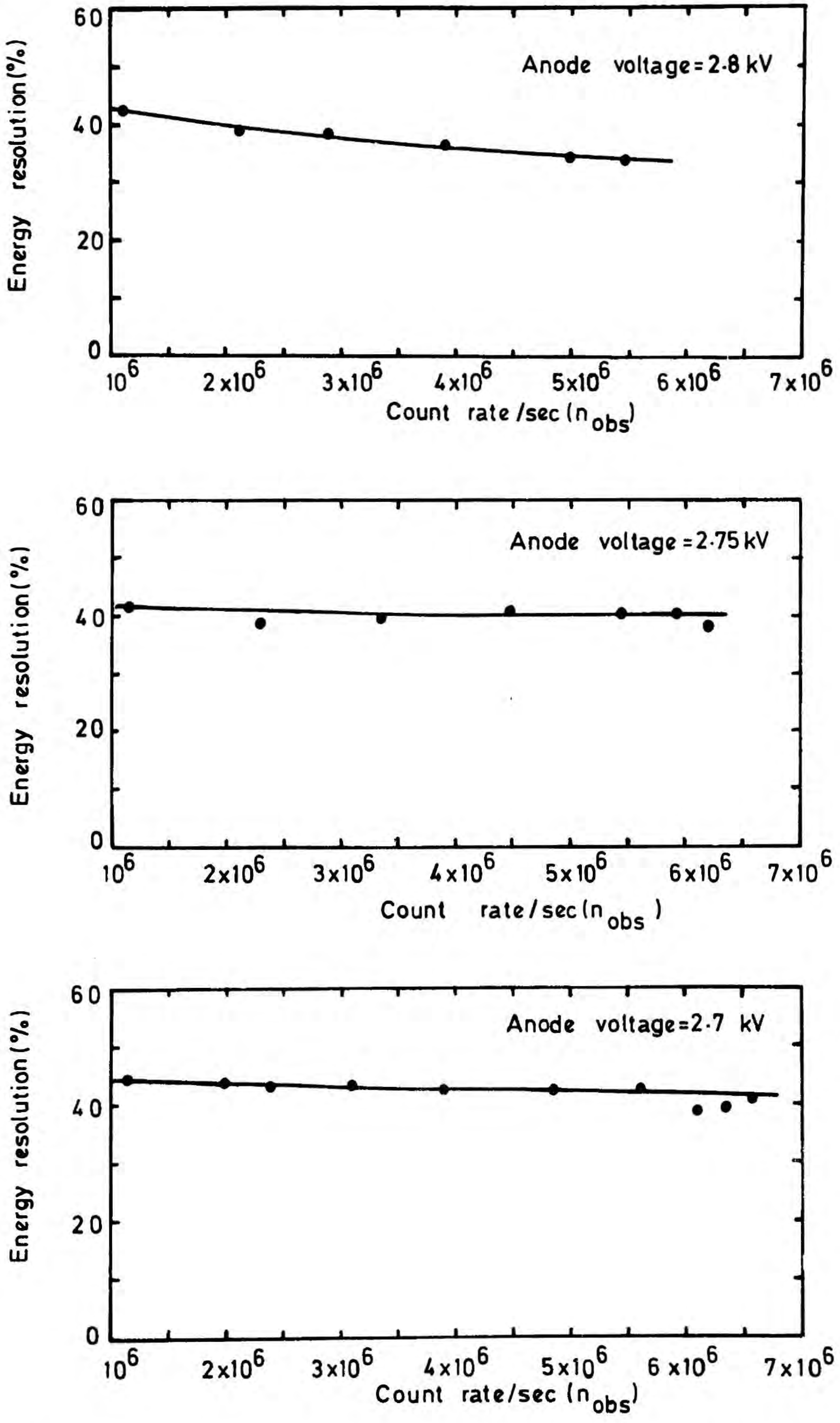

FIG. 23 Energy resolution of the GSDC as a function of counting rate for different anode voltages.

further investigated by analysing the pulse height spectra for different linear gate widths. If the width of the gate is increased excessively, more than one pulse will pass through the gate during a single opening and a large integrated pulse will result at the input of the PHA. Pulse height spectra obtained for different gate widths are shown in Fig (24). Smaller gate widths produced less distortion on the pulse height spectrum. However, as expected the small gate widths degraded the energy resolution of the counter (see Fig (25)).

In order to estimate the percentage pile-up as a function of counting rate, number of pulses which falls beyond the K_α peak was measured by operating the PHA in single channel analyser mode. First the total counting rate was measured by keeping the low level discriminator at a level which discriminates the noise from real pulses and the upper level discriminator at its maximum value. Then the same measurement was repeated after setting the upper level at the high amplitude end of the Co K_α peak (i.e. setting it at a channel whose accumulated pulse height corresponds to 5% of the height of the K_α peak), thus discriminating the piled up pulses. The difference between these two measurements is an approximate measure of the number of pile-up pulses at that rate. The percentage pile-up was then obtained by dividing this difference by the total counting rate. Following the above procedure,the pile-up percentage of the counter system (counter plus electronics) was measured as a function of counting rate for different gate widths. All the counting rates were measured by connecting the PHA signal output to a fast scaler. During the counting periods the PHA was operated in stop mode in which PHA offers smallest resolving time (3 μsec) to incoming pulses, and the PHA input pulsing rates were much smaller than its maximum counting speed. Counting rates were also monitored on a fast

FIG. 24 Pulse height spectra obtained with different gate widths.

Gate width: 90 ns

Count rate: 5·864 x 10^6/sec

Gate width: 70 ns

Count rate: 5·922 x 10^6/sec

Gate width: 50 ns

Count rate: 5·837 x 10^6/sec

Gate width: 35 ns

Count rate: 5·982 x 10^6/sec

FIG. 24

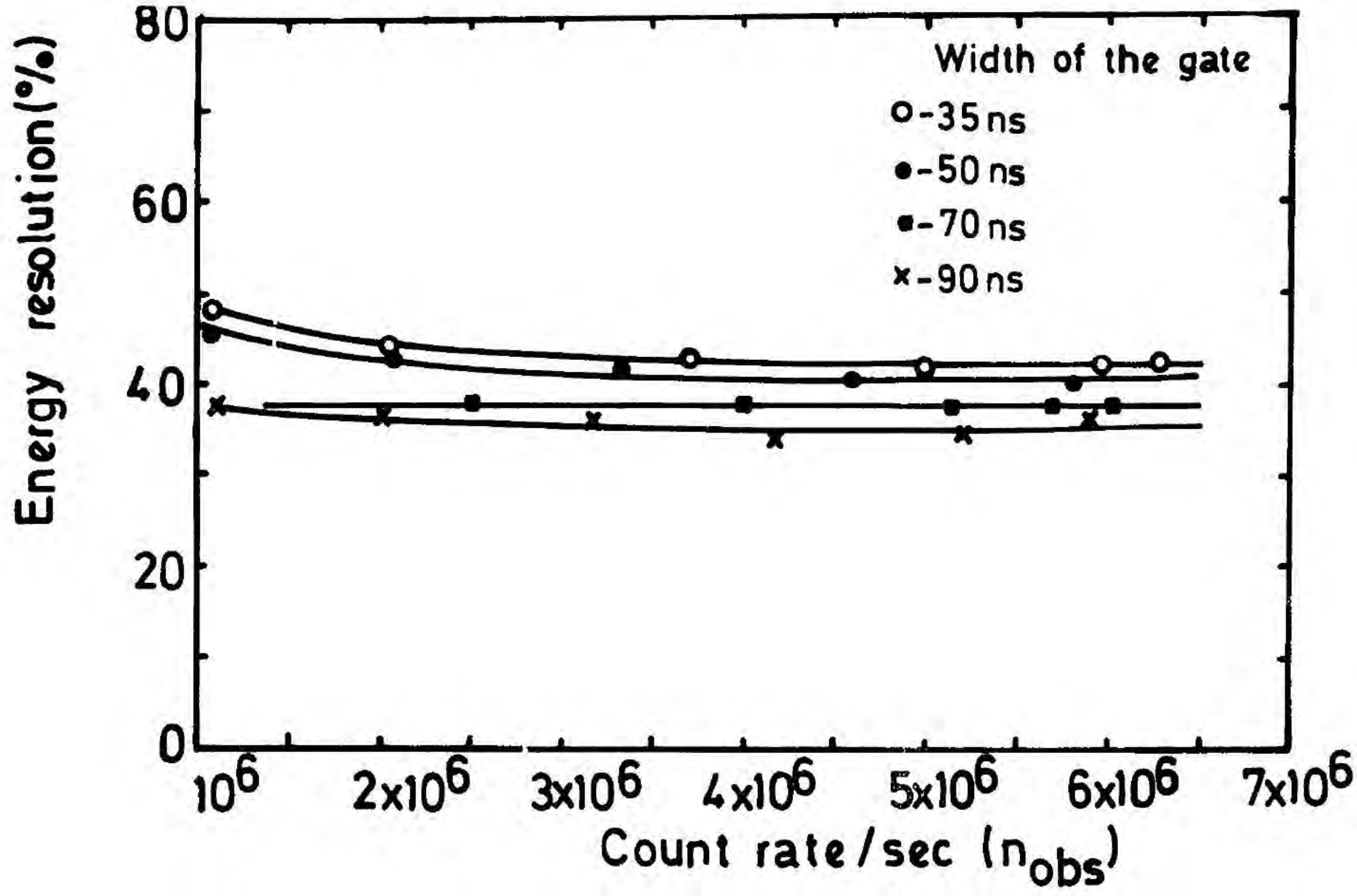

FIG. 25 Dependence of energy resolution on the width of the gate.

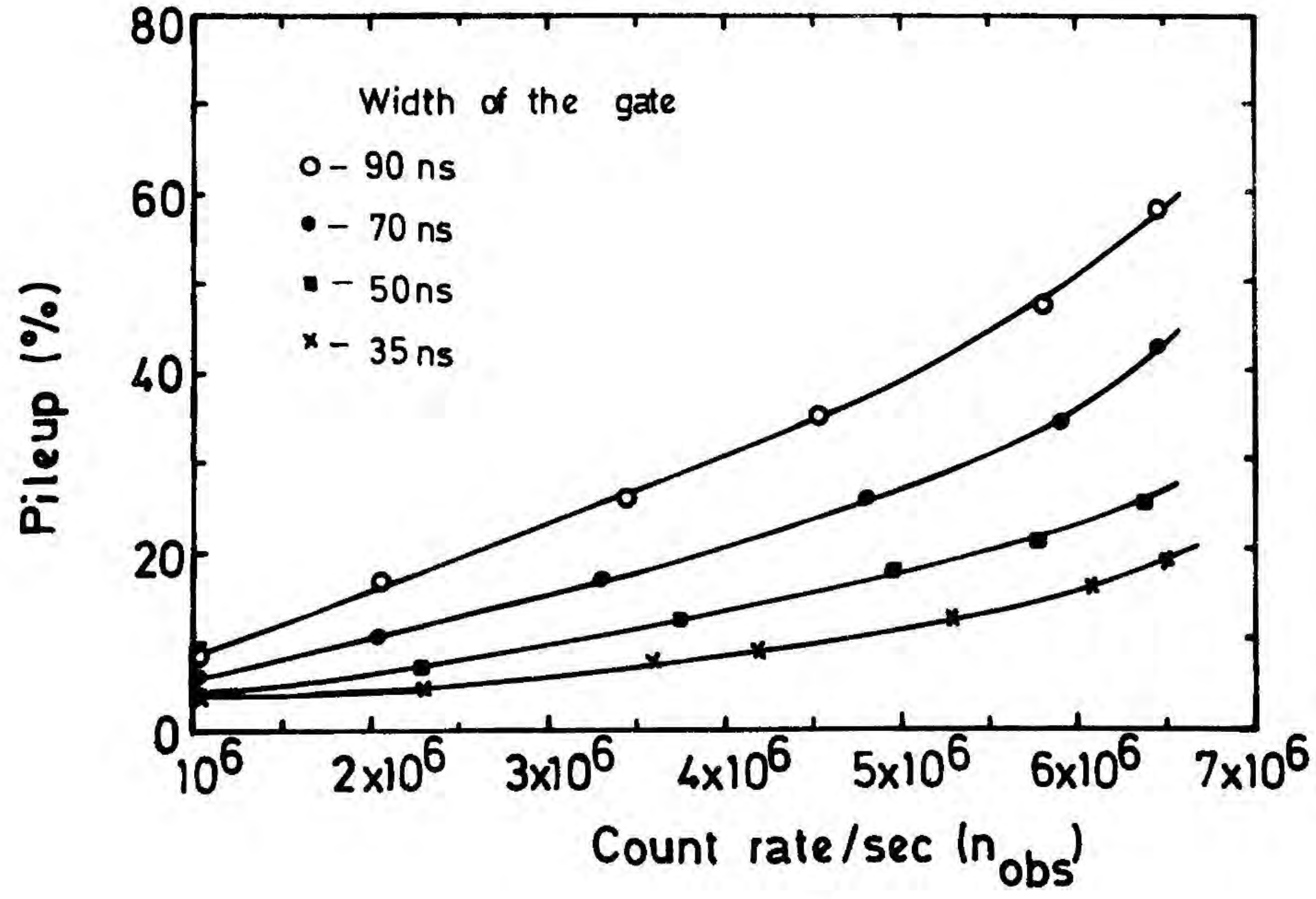

FIG. 26 Pileup percentage vs count rate for different gate widths.

scaler (100 MHz) which was directly connected to the fast discriminator (NE 4684) output. Results of the measurements are shown in Fig (26). The percentage pile-up was found to increase with the width of the gate as well as with the counting rate. Use of a 50 nS gate, for example, produced 25 per cent pile-up at a counting rate of 6.25 MHz. In high rate studies however, the pile-up pulses cannot totally be eliminated since their existence is a consequence of the statistical nature of the length of the time interval between pulses. But this effect can be minimised by reducing the width of scintillation pulses.

6.8 CONCLUSION

The results presented in this chapter have shown that the GSDC can be operated successfully with X-rays (6.9 keV) up to the counting rate of 6 MHz with an energy resolution around 40%. This value of resolution which is larger than the value obtained with 5.9 keV radioactive X-ray source is mainly due to insufficient monochromatisation of the incoming X-ray beam and the electronicsused in data acquisition. However, better energy resolution can be obtained by increasing the anode voltage of the GSDC thus producing more photons (and also more secondary electrons) at the expense of its counting capability and gain stability with counting rate.

The resolving time of the counter system has been found to vary with the anode voltage of the GSDC, in fact under the operating conditions stated in this chapter, the resolving time has varied from 43 nS to 67 nS when increasing the anode voltage from 2600 V to 3000 V. At high counting rates the performance of the counter was found to degrade due to piling up of scintillation pulses, and the results presented in this chapter has shown that the pile-up effects on the pulse height spectrum can be reduced by means of proper gating electronics. However, at extremely high counting rates the counting capability and the energy resolution of the counter are limited by the statistical nature and the width of the scintillation pulses.

Chapter 6 - References

1. G.F.J. Garlick, G.T.Wright, Proc. Phys.Soc. B65 (1952) 415.
2. J.B.Birks, The theory and practice of scintillation counting Pergamon Press, 1964, page 150.
3. W. Shockley and J.R.Pierce, Porc. I.R.E. 26 (1938) 321.
4. U. Fano , Phys. Rev. 72 (1947) 26.
5. G.D.Alkhazov, A.P.Komar and A.A.Vorobev, Nucl.Instr. and Meth. 48 (1967) 1.
6. S.C.Curran, A.L.Cockroft and J.Angus, Phil. Mag. 40 (1949) 929.
7. See S.C.Curran and H.W.Wilson, α,β,γ Spectroscopy, ' K. Siegbahn, Vol. 1, page 303, North Holland Publ. 1965.
8. H. Snell, Nuclear Instruments and their uses, Vol.1, Wiley & Sons, 1962, Page 67.
9. A.J.P.L. Policarpo, M.A.F. Alves, M.J.T. Carvalho and M.A.G. Da Rocha, Nucl. Instr. and Meth. 77 (1970) 309.
10. Instruction Manual for R.C.A. 8575 phototube.
11. Instruction Manual for LG 101 Liner Gate, E.G. & G.Inc. B-3285.
12. S.S.Al-Dargazelli, T.R. Ariyaratne, J.M. Breare, B.C. Nandi and M.V. Verrells, Nucl. Instr. Meth. 156 (1978) 63.
13. M.V. Verrells, Durham University, Private communications.

CHAPTER SEVEN

CONCLUSION AND FUTURE WORK

7.1 CONCLUSION

The work described in this thesis has served two main purposes. Firstly it developed a fast X-ray counter which can count up to 5-6 MHz with a reasonable energy resolution. Secondly it provided a comprehensive study of the scintillation properties and one of the important transport properties, the drift velocity, of argon-nitrogen which is a cheap and extremely useful gas mixture.

The design and operation of drift chambers in the scintillation mode needs careful attention since these factors can give rise to a poor energy resolution through improper localisation of the secondary scintillation. Sufficient localisation can be obtained however, by passing the X-ray beam normal to the cathode planes of a drift chamber and shifting the passage of the beam away from the anode wire so that the angle formed by the paths of primary electrons created close to the cathode planes is small. Large pulse widths which would have resulted from such a design can be successfully avoided on the application of a lateral drift field, but the strength of the drift field must be carefully controlled since very large drift fields can again give rise to poor localisation of the secondary scintillation process. This kind of operation eliminates the possibility of formation of two sets of pulses for X-rays converting in the upper and lower halves of the active volume of the counter. However, because of the formation of these two sets of pulses, the width of the scintillation pulses, which decrease with ~~the~~ decrease of the distance of the X-ray beam from the anode wire, cannot be reduced arbitrarily by moving the passage of the X-ray beam towards the anode wire. The dependence of the width of the scintillation pulse on drift distance and the formation of two sets of pulses also unable one to use the counter when the beam passes parallel to the cathode planes.

It is apparent from chapter six that the limitations on the counting capability of the counter arise from the width of the scintillation pulses. However, as shown in the preceding chapter, this is expected when counting randomly spaced pulses at high rates. The width of the scintillation pulses can be reduced in two ways ;

(1) by increasing the electron drift velocity

and (2) by reducing the life time of metastable states.

The drift velocity measurements given in chapter four indicate that argon-nitrogen mixtures with small nitrogen concentrations are not suitable, since the drift velocity of electrons in such mixtures reaches saturation levels at small velocities. On the otherhand, addition of more nitrogen to argon reduces the scintillation emission from the mixture despite the creation of narrow pulses. Results presented in chapter four indicate that Ar-10% N_2 is a satisfactory compromise which produces a scintillation pulse of about 65 nS full width. However, the addition of other molecular gases such as methane also reduces the width of the pulse, thus improving the rate capability of the counter, but at the expense of the amplitude of the scintillation pulses. Results presented in that chapter also show that the minimum concentration of nitrogen necessary to transform most of the argon excited states to nitrogen $C^3\pi_u$ states is approximately 4%. The nitrogen concentration in the mixture must not be less than this value in order to obtain a satisfactory emission in the spectral region to which the pyrex window photomultipliers are sensitive.

Another parameter which determines the width of the scintillation pulses is the thickness of the scintillation region. Although the width of the pulse is expected to vary with the anode wire diameter, no such variation has been observed up to a diameter of 410 μm. This enables one to use larger diameter wires (up to probably 500 μm) which provide better light gains for a given charge gain.

Gain variation in the photomultiplier at high counting rate has been successfully eliminated by replacing a part of the resistive potential divider chain (which supplies potentials to the dynodes) with emitter follower circuits. Results presented in chapter six also confirm its unchangeable behaviour towards random current pulses occurring at extremely high rates (10^7/sec). Although it is not sensitive to U V radiation below 3000 Å , the R C A 8575 photomultiplier proves itself a reliable and stable photomultiplier for high counting rate applications. Furthermore the operation of this photomultiplier with the photocathode at a high negative potential in the vicinity of an earthed plane did not show any noticeable deterioration in performance.

According to the results, the energy resolution of the counter for 5.9 keV X-rays at moderate counting rates is about 30%. This value, which is nearly four times as large as the value obtained by Policarpo et al(1) using a GSPC (8.4%),is a result of the limited charge amplification around the anode wire and the photon loss due to imperfect light collection and collisional quenching of argon excited states by nitrogen molecules. Although some improvement can be made by increasing the charge amplification around the wire thus producing more photons to compensate the loss, the space charges created by such an action shift the amplitudes of the scintillation pulses to lower values. The intrinsic energy resolution of the counter for 5.9 keV X-rays has also been found to be 22.4%.

The analysis done on the counting characteristics obtained with 6.9 keV X-rays, shows that the resolving time of the counter at a fixed discrimination level of 25 mV, varies from 43 nS at an anode voltage of 2600 V to 67 nS at 3000 V. This variation is due to the change in width of the scintillation pulse above the discriminator threshold level with anode voltage. Thus the smallest possible anode voltage which gives satisfactory energy resolution and counting efficiency must be used as the operating voltage of the counter. Use of a low anode voltage has the added advantage that it keeps the space charge density of positive ions around the anode at a low level. However, even at 2800 V on the anode wire and an X-ray flux corresponding to an event rate of 2.5×10^7 per sec, the space charge ~~density~~ around the anode is less than 2×10^8 electr which is the value$^{(2)}$ required to produce appreciable space charge effects. The space charge density corresponding to the above mentioned anode voltage has been calculated using the expression given in chapter three.

The following values have also been used for parameters in the expression
$M = 15$ $N = 230$ ion pairs $a = 205$ µm, $b = 4.5$ mm, $L = 0.2$ mm, $p = 1$ atm, and $\mu_{Ar} = 1.6 \text{ cm}^2 \text{V}^{-1} \text{s}^{-1}$. The gas amplification factor of the GSDC at an anode voltage of 2800 V and drift field of 500 V/cm has been derived by using the corresponding value obtained for the GSPC (see Fig (28) of chapter four) and correcting it for the drift field using Fig (22) of chapter three.

During the course of tests the counting electronics have not shown any limitations in their performances up to the counting rates reached with this detector. This is expected since the resolving time of the detector is larger than the pulse pair resolution of all the electronic modules used in the counting circuitry. Results also indicate the successful operation of the electronic system employed to obtain the energy resolution of the counter at high counting rates. However, the gating system degraded the energy resolution to a small extent depending on the width of the gating pulse. This is due to the setting of a gate width, which is less than the width of the scintillation pulse.

Results of the present study also revealed a number of important scintillation properties of argon-nitrogen mixtures. Most of the scintillation emission from pure argon occurs in the UV region for which the spectral response of pyrex window-photomultipliers is poor. Once nitrogen is added to argon some of the argon excited states transfer their energy to nitrogen molecules to produce the $N_2(C)$ states some of which subsequently decay to the ground state, emitting photons in the visible region. The rest decay through collisional deactivation processes. The fraction of the excited states which de-excite through collisional deactivation processes increases with increase in nitrogen concentration, resulting in a drop in the scintillation pulse amplitude. This phenomenon occurs both in primary and secondary scintillation processes. However, during the secondary scintillation process the number of secondary electrons produced around the anode wire also reduces with increase in nitrogen concentration, resulting in a further drop in the amplitude of scintillation pulses. This drop can be compensated for by increasing the anode voltage and once this has been done the results (presented in chapter four) indicate similar variations in both primary and secondary scintillation pulse amplitudes with nitrogen concentration.

7.2 FURTHER DEVELOPMENTS

Further developments of the counter are possible in many areas. According to the results of the present study, the major limitation to the counting capability of GSDC's arises from the width of the scintillation pulse. One of the methods with which a reduction in the width of the scintillation pulse can be made is to use argon-nitrogen mixture with a small percentage of another powerful quenching gas. Some of these quenching gases are listed in Table 4.1 of chapter four. For example the metastable argon quenching rate constants of CO_2 and CH_4 are of the order of magnitude greater than that of the nitrogen and therefore a small quantity of these gases would be sufficient to reduce the width of scintillation pulses to some extent. Loss of pulse height resulting from such an addition can partially be compensated for by increasing the efficiency of light detection using a fast wavelength shifter such as para-quaterphenyl. Use of a wavelength shifter has the additional advantage that it can convert the UV resonance radiation emitted by excited argon atoms into visible light. Though expensive, the use of xenon, which provides the largest light output per unit energy loss of an ionizing particle (see table 2.1 of chapter two) in a GSDC, with a molecular gas may be advantageous for high counting studies since narrow scintillation pulses can be obtained from such a gas mixture by sacrificing a considerable fraction of its light amplitude. However, the width of the scintillation pulses cannot be reduced arbitrarily only by adding molecular gases. This is because the width of the scintillation pulse is not only a function of the life times of the excited states but also depends on the thickness of the secondary scintillation region. The latter itself provides a major contribution to the resolving time of the GSDC, which determines the ultimate counting rate of the counter (see equation 6.17 of chapter six). It is also worth investigating different counter geometries especially ones in which the axis of the photomultiplier is perpendicular to the direction of the ionisation beam. Although the present structure is the simplest of all possible designs, counters with the proposed geometry can be used as track locating detectors in high energy physics experiments. The geometry also prevents accidental exposure of PM tube to extremely high intense and energetic ionising beams.

7.3 APPLICATIONS OF THE GSDC

The main motivation behind the development of this counter is to provide a fast counting device for the 'extended X-ray absorption fine structure' (EXAFS) studies. With the recent availability of synchrotron radiation, there has been a renewed interest in the use of X-ray absorption studies to determine interatomic distances. A 2 GeV electron storage ring is being built at the Daresbury Laboratory to provide a dedicated source of synchrotron radiation. This facility, the commissioning of which is programmed for April 1980, is expected to produce a continuous spectrum extending from infrared through the ultraviolet into the X-ray region. The intensity of the beam in X-ray region will be around 10^{13} photons/sec/m rad (horizontal) in 0.1% bandwidth (see Fig 1 of chapter one).

The extended X-ray absorption fine structures which appear on the high energy side of the absorption edges is believed to be the result of the interference between the outgoing photoelectron and the component back scattered from neighbouring atoms. Such a spectrum showing fine structure on the copper K absorption edge is shown in Fig 1. The amplitudes of these oscillatory structures seem to be small and therefore the main experimental difficulty in an EXAFS experiment is that the total

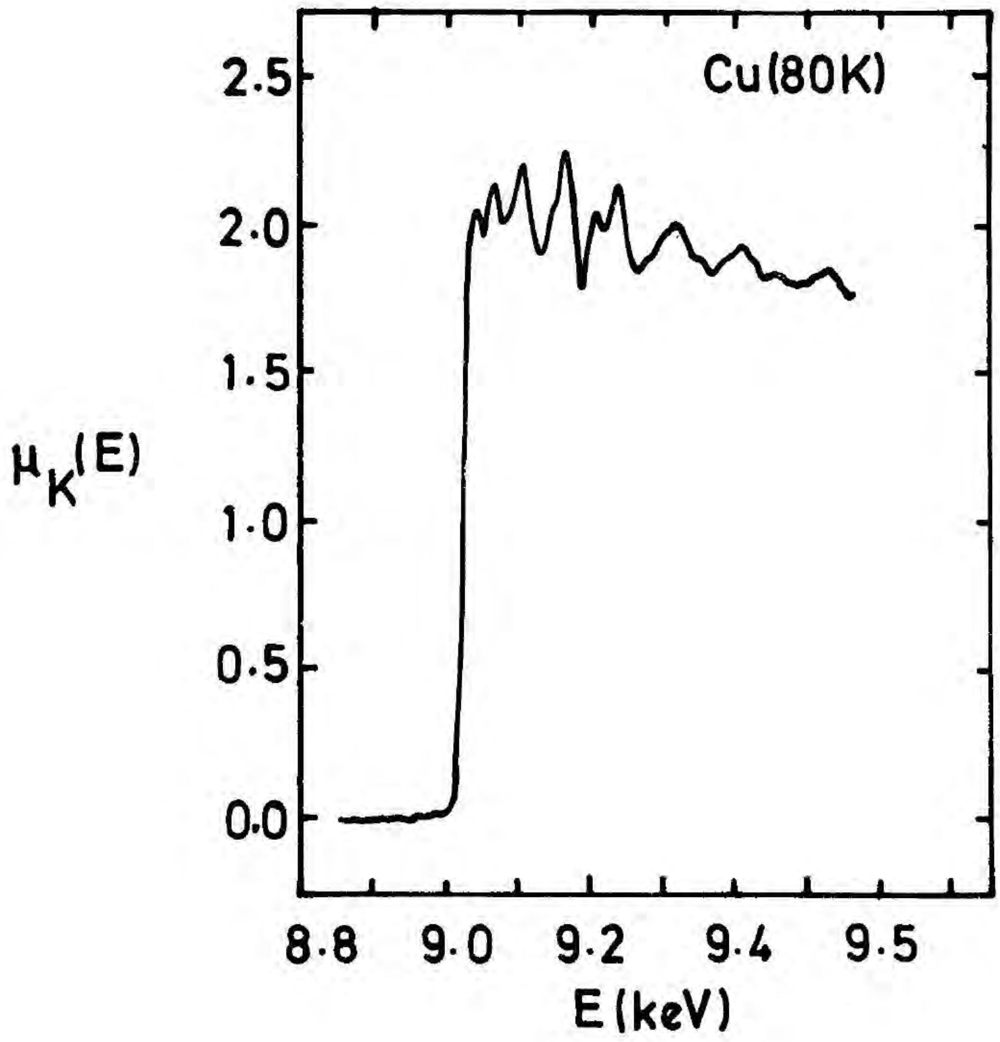

FIG. 1 Measured K-shell absorption coefficient, $\mu_K(E)$, is plotted versus x-ray energy, E, for copper at 80K.

absorption coefficient must be measured to very high accuracy. This would require both the random and systematic errors in counting to be less than 0.1% of the total absorption coefficient for some experiments(3). Therefore it is necessary to count at least 10^6 photons to achieve adequte accuracy. However, an even larger number of counts are necessary in order to obtain the fine structure at a distance of a few hundreds of eV from the absorption edge where the variations are very small indeed.

Monochromatisation of the radiation beam creates another difficulty especially when using synchrotron radiation for EXAFS studies. The monochromators such as double crystal arrangements used in the energy selection generally transmit not only the fundamental wavelength (λ) but also the harmonics ($\frac{\lambda}{2}$, $\frac{\lambda}{3}$ - - -). In order to eliminate these harmonics in an EXAFS experiment, the detector used to collect transmitted photons must have either an energy resolution better than 50% or some other property such as 'poor absorption coefficient for high energy photons'. Although proportional counters and solid scintillation counters have both of these properties, because of counting rate limitations, they need considerable collection times before acquiring the accuracy demanded by such studies.

At present solid scintillation counters(3,4) ionisation chambers(5,6) and proportional counters(3) are used in EXAFS studies. Although ionisation chambers have no energy resolution for X-rays and cannot provide a digital output, they are the only detector so far which can be used efficiently to measure fine structures in dilute samples such as aqueous solutions in which the absorption of X-rays is small. In the case of solids, the count rates used by Martens et al(4) and Knapp et al(3) in their EXAFS investigations with a NaI (Tℓ) scintillation detector were of the order of 10^5 counts/sec. Results of the present study show that the counting ability of a GSDC with a reasonable energy resolution is at least 50 times better than those which can be obtained from proportional and solid (NaI) scintillation counters. Use of this new device in an EXAFS experiment should therefore be more advantageous than other detectors which could provide a digital output.

Possible EXAFS work using the GSDC should include metals and solid metallic compounds whose K shell electron energies are such that the ranges of the photoelectrons ejected from the K shell of the absorbing gas are small, preferably less than 1 mm, since larger ranges produce wider secondary scintillation pulses.

TABLE 7.1

X-ray energy (keV)	5.9	8.64	11.22	14.16	22.6	24.47
Photoelectron mean range $\bar{R}$ (mm)	0.059	0.23	0.51	0.97	3.35	4.73

For example, table(7) 7.1 shows the variation in range of photoelectrons in argon with energy of the incident X-rays. The GSDC with an argon-nitrogen gas mixture can therefore be used satisfactorily up to a incident X-ray energy of 15 keV. This enables one to study the fine structures of metals such as iron and copper up to chromium (K_{abs}=14.32keV) in the perodic table, using the GSDC.

Chapter 7 - References

1. A.J.P.L. Policarpo, M.A.F. Alves, M.C.M. Dos Santos and M.J.T. Carvalho, Nucl.Instr. and Meth. 102 (1972) 337.
2. R. Browell, Ph.D. thesis, Durham University (1975).
3. G.S.Knapp, H.Chen, and T.E.Klippert, Rev.Sci.Instrum. 49 (1978) 1658.
4. G.Martens, P. Rabe, N.Schwentner and A. Werner, Phys.Rev. B17 (1978) 1481.
5. P. Eisenberger and B.M.Kincaid, Chem.Phys. Lett. 36 (1975) 134.
6. E.A.Stern, D.A. Sayers, and F.W.Lythe, Phys.Rev. B11 (1975) 4836.
7. T.J.Harris and E. Matthieson, Nucl.Instr. and Meth. 96 (1971) 397.

Appendix 1

Operating parameters and resistance values of the potential divider chain.

Total current through the chain = 3.4 mA

Emitter current through T_{r_1} = 1.12 mA

R_1	108 K	(all 2 Watts)
R_2	38 K	
R_3	53 K	
R_4	38 K	
R_5	38 K	
R_6	38 K	
R_0	82 K	
R_7	40 K	
R_8	39.5 K	
R_9	39.0 K	
R_{10}	57 K	
R_{11}	75 K	
R_{12}	74 K	
R_{13}	73 K	
R_{14}	72 K	

ACKNOWLEDGEMENTS

The author would like to thank Professor A.W.Wolfendale,F.R.S., and Professor B.H.Bransden, for their interest in the work and for the use of laboratory facilities. The Association of Commonwealth Universities and the Commonwealth Scholarship Commission in the U.K. are thanked for the provision of a Commonwealth Scholarship Award and so are the British Council for the welfare of the author and his wife throughout their stay in the U.K. Thanks are also due to the Colombo Campus of the University of Sri Lanka for granting study leave to achieve the completion of this thesis and the Paul Instrument Fund for their financial support towards this project.

The author is deeply indebted to his supervisor, Dr.J.M.Breare, for his invaluable guidance, encouragement and assistance throughout this work.

Dr.B.C.Nandi is thanked for his collaboration in part of this work. The author is also grateful to Dr.M.Comyn for his support and to Miss S.Al-Dargazelli for her collaboration in the work. Mr.M.Verrells is thanked for his useful comments and discussions. All the past and present members of the Nuclear Instrumentation Group are thanked for their assistance and friendship.

Technical assistance from Mr.J.Webster and Mr.R.McDermott are gratefully acknowledged. Mrs. S.Mellanby is thanked for the excellence of her typing. Mr.M.Lee and co-workers in the Audio-Visual Section are thanked for the photographs. The author's wife, Sanda, is thanked for diagrams in the thesis.

Finally, the author would like to pay his gratitude towards his wife, parents and relations for their support, sacrifices and encouragement.